CHAPTER ONE

INTRODUCTION

1.1 Background.

Chemotherapy remains the best means of treatment of metastatic cancer (Choi *et al*., 2007; Ullah, 2008). Its effectiveness, however, is greatly compromised by the multidrug resistance (MDR) phenomenon whereby cancer cells evade the cytotoxic effects of anticancer agents of divergent chemical structures and mechanisms of action. MDR is, in most cases, acquired sequel to the exposure of tumour cells to one cytotoxic agent or another, but can nevertheless occur intrinsically in the cells without previous exposure to any chemotherapeutic agent. (Fardel *et al.*, 1996; Ambudkar *et. al*., 1999; Gottesman *et al.*, 2002). And though its aetiology may be multifactorial (Gottesman *et.al.*, 2002), the overexpression of P-glycoprotein (P-gp), a 170- KDa transmembrane efflux transporter belonging to the ATP Binding Cassette (ABC) protein superfamily, is by far the most important MDR mechanism (Gottesman and Pastan, 1993; Gottesman *et al.*, 2002). Discovering drug leads that could be developed into clinical P-gp inhibitors for cancer MDR inhibition, therefore, is both logical and highly required.

By and large, there are two major chemical sources from which drug leads can be sourced, i.e., combinatorial synthesis and nature (Silverman, 2004; Buttler, 2004, 2005; Newman and Cragg, 2007). The antecedents of these two "lead pools" show that while combinatorial synthesis is capable of generating large number of leads in a relatively short period of time, traditional drug discovery from nature is a very slow process (Silverman, 2004). Moreover the thrusts of traditional natural drug discovery necessitating the screening of extracts and fractions of extracts do not always make it compatible with the automated mechanism-based

techniques of bioassay known as High Throughput Screenings (HTS) which comprise the mainstay of biological assays in the industry in this genomics era (Posner, 2005). These notwithstanding, the structural novelties that accompany natural compounds tend to put them at an advantage over their combinatorial synthesis-derived counterparts as these confer on them intrinsic drug-likeness (Silverman, 2004). Such structural novelties are evidenced by the dioxygen bond and endoperoxide linkage in artemisinin (**1**), the intricate stereochemistry in erythromycin A (**2**), and the complex ring system in paclitaxel (**3**), all being structural features that no combinatorial chemist would have ordinarily imagined. Furthermore, the assertion of the superiority of nature to combinatorial synthesis as far as novel drug lead discovery is concerned is corroborated by the revelation that after about three decades of extensive investments in combinatorial synthesis at the expense of natural drug discovery the pharmaceutical industry succeeded in putting only one combinatorial synthesis-derived drug in the market, while many natural product derived drugs were launched in the same period, the neglect of natural drug research notwithstanding (Newman and Cragg, 2007). Nature should therefore be the best source of cancer MDR inhibitors.

Natural discovery of cancer MDR inhibitors, however, would require adopting methods or approaches that would address the two afore-mentioned ills of traditional natural drug discovery, i.e., its HTS-incompatibility and elements of extensive empiricism that makes it not only time involving, but also capital intensive.

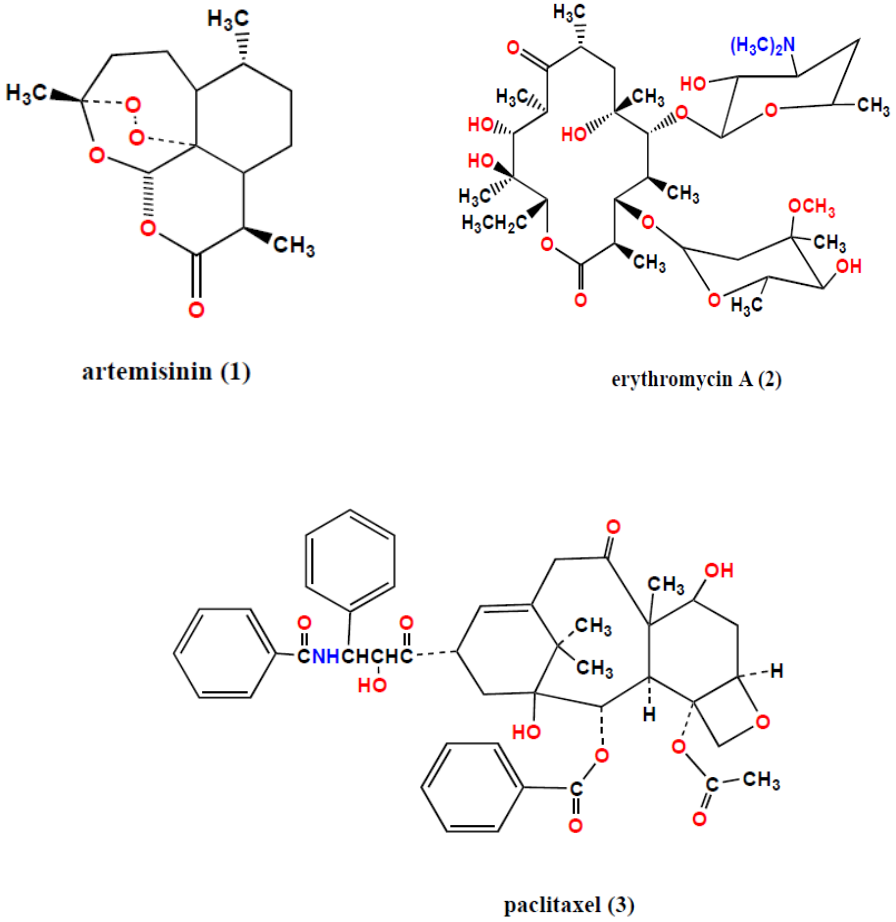

Fig. 1: Some natural products with unique structural novelties (Olaniyi, 1989; Remers, 1998).

A structure-guided isolation approach focused on natural products that have high propensity for interacting with multiple macromolecular targets, otherwise described as privileged structures (Silverman, 2004) – the rationales for possible interactions with P-gp of which are either obvious or not – is hypothesised here as a bridging intermediate that could ensure the discovery of potential clinically applicable cancer MDR inhibitors, while, at the same time, taking care of the ills inherent in natural drug discovery.

1.2 Statement of the Problems.

Cancer chemotherapy is bedevilled by the phenomenon of multidrug resistance (MDR) whereby cancer cells evade the cytotoxic effects of structurally and functionally dissimilar chemotherapeutic agents including the new "targeted" drugs (Lage, 2008). The major cancer MDR mechanism is the over-expression, by cancer cells, of efflux transporter proteins of the ATP- Binding Cassette (ABC) superfamily, of which P-gp is the most important member (Gottesman and Pastan, 1993; Fardel *et al.*, 1996; Ambudkar *et. al*., 1999; Gottesman, 2002; Gottesman *et al.*, 2002). Definite attempts at the discovery of P-gp inhibitors have therefore been made to solve the problem of cancer MDR (Tsuruo *et al.*, 1981; Ferry *et al.*, 1996, Takara and Okumura, 2006). Disappointingly, however, there is yet a paucity of cancer MDR inhibitors in clinical oncology mainly for toxicity and pharmacokinetic interactions reasons (Ferry *et al.*, 1996; Sonneveld and Wiemer, 1997; Van Zuylen *et al*., 2000; Lage, 2008).

Hence, the dire need for the discovery of P-gp inhibitor drug leads from natural products, which remains the unequivocal most probable source of molecules with structural novelties often required for drug likeness and high therapeutic indices or safety margins (Silverman, 2004, Newman and Cragg, 2007). As a matter of fact, the paucity of clinical cancer MDR inhibitors is not unconnected with the unadvised neglect of natural drug research for combinatorial synthesis by the pharmaceutical industry for a period of about three decades which coincidentally included the period of the fruitless search for clinical cancer MDR inhibitors (Newman and Cragg, 2007). And though the industry is trying to make a comeback to nature by adapting the tools of combinatorial synthesis and computational drug design to discovering natural product-like molecules (Morrell, 1996; Nicolaoaou *et al*., 2000; Newman and Cragg, 2007), these are not likely to supply the novelties with which real natural products

are associated, more or less necessitating, once again, the discovery (by isolation) of cancer MDR inhibitor drug leads from nature.

On another hand, the natural discovery of cancer MDR inhibitors cannot be done without addressing the inherent problems that necessitated the afore-mentioned abandonment of natural drug research, i.e., incompatibility with High Throughput Screening (HTS) techniques of bioassay, which comprise the mainstay of biological assays in the industry in this genomics era (Posner, 2005), and its associated extensive empiricism that makes it both time involving and capital intensive (Silverman, 2004; Newman and Cragg, 2007).

Essentially therefore, an HTS-compatible natural drug discovery approach, that can readily be equipped with elements of rationality, is highly required to discover highly probable clinically applicable cancer MDR inhibitor drug leads.

1.3 Aim and Objectives.

1.3.1 Aim

To discover molecular leads for clinically applicable cancer MDR inhibitors.

1.3.2 Objectives

(1) To fractionate methanolic crude extracts of the seed, leaf and stem bark materials of the plant *Hunteria umbellata* based on pH differentials and media polarity.

(2) To identify fractions rich in iridoid, monoterpenoid indolealkaloids, and triterpenoid privileged structures.

(3) To isolate pure compounds from the identified iridoid-, MTIA- and terpenoid-rich fractions.

(4) To chemically characterize all isolated compounds using spectroscopic techniques.

(5) To evaluate the P-gp inhibitory activities of the chemically characterized isolates.

1.4 Significance of the Study

Cancer is a killer disease of global concern: It has been estimated that worldwide, 9 million people die of cancer yearly, and the WHO anticipates that this figure will increase to 20 million by the year 2020 (Adebamowo and Ajayi, 2000; Parkin *et al.*, 2002; Sweeney, 2005). Given this background, and the fact that cancer mortality is (in most cases) a direct fall out of metastasis (Karp, 1996): The main effective therapeutic mode against metastasis is chemotherapy, therefore a research like this–ultimately aimed at making chemotherapy effective – has very great potentials of addressing the increasing trend of cancer mortality rates; and this is highly welcome (if not most required) in clinical medicine.

1.5 Hypothesis

Serotonin is a multipurpose chemical mediator whose diverse transduction signallings include being a substrate of an ATP-dependent transmembrane transporter (Ganong, 1999), although not an ABC type this time around. An extention of comparative biochemistry principles of rational drug discovery (Cohen, 1979) to this fact implies that serotonin and its analogues are highly probable interactives, and hence, possible inhibitors of the ABC protein transporters, the P-gp inclusive.

Monoterpenoid indolealkaloids (MTIAs), which are structurally and biogenetically related to serotonin, are naturally occurring serotonin analogues widely distributed in the Apocynaceae, Loganiaceae and Rubiaceae plant families (Herbert, 1983). Exploring plants in any of these families for their MTIA contents, therefore, is a right step towards discovering natural P-gp inhibitors.

On another hand, the putative P-gp-interactive abilities of MTIAs could, on the basis of their possession of the indole organic moiety, be alluded to their being privileged structures (Evans *et al*., 1988; DeSimone *et al.*, 2004; Constanlino and Barlocco, 2006), which, by definition, have the inherent ability to interact with multiple macromolecular targets – the P-gp, once again, inclusive.

If the latter (i.e. privileged structure) theory of the putative P-gp-interactive ability of the MTIAs were anything to rely upon, then the revelation from their biosynthetic pathway that MTIA sources should also be rich in triterpenoid and iridoid privileged structures is simply fortuitous (section 2.2.3), as it more or less deductively broadens the scope of potential P-gp interactives obtainable from one single MTIAs source.

This rational search for natural P-gp inhibitors from the plant, *Hunteria umbellata* (apocynaceae), therefore, is based on a pharmacodynamic hypothesis that its chemotaxonomy-established MTIA contents are transmembrane protein pumps interactives, and on the fact that both its established MTIAs and its biosynthetic permutation-conjectured triterpenoids and iridoids are by definition (as privileged structures) endowed to interact with multiple macromolecular targets–P-gp inclusive.

1.6. OPERATIONAL DEFINITION OF TERMS/ABBREVIATIONS

Downfield	Left side of the chemical shift scale of an NMR spectrum. It corresponds to high frequency which in turn indicates lack of electron density.
Upfield	Right side of the chemical shift scale of an NMR spectrum. It corresponds to lower frequency and hence high electron density.
Drug lead	A prototype molecule with an interesting biological activity, its toxicity and pharmacokinetic profiles notwithstanding.
Phase cycling	Method of signal selection in some 2 dimentional NMR experiments involving alternation of the phase of applied RF pulses and /or receiver detection on successive passes through a pulse sequence without variation of pulse lengths or delays.
Privileged Structures	These, in medicinal chemistry parlance, are molecules with inherent abilities to interact with multiple macromolecular targets.
Pulse Field Gradient	Method of signal selection in some 2 dimentional NMR experiments involving alteration of the strength of applied magnetic field as a function of position.
Metastasis	The phenomenon whereby cancer cells easily break away from the parent mass, enter the lymphatic or vascular circulation, and spread to distant sites in the body where they establish lethal secondary tumours that are no longer amenable to surgery.

Therapeutic index (Plural: Therapeutic indices)	It is a measure of the safety of a drug as determined from the ratio of its concentration that gives undesirable effects to that which gives desirable effects.

ABBREVIATIONS

ABC	ATP-Binding Cassette
COSY	Correlation Spectroscopy
DEPT	Distortionless Enhancement by Polarization Transfer
HTS	Highthroughput Screening
HMBC	Heteronuclear Multiple Bond Coherence
HRESIMS	High Resolution ElectroSpray Ionization Mass Spectrometry
HSQC	Heteronuclear Single Quantum Coherence
LRESIMS	Low Resolution ElectroSpray Ionization Mass Spectrometry
MTIA	Monoterpenoid indolealkaloid
NMR	Nuclear Magnetic Resonance
P-gp	Permeability glycoprotein
ROESY	Rotational Nuclear Overhauser Effect Spectroscopy

CHAPTER TWO

LITERATURE REVIEW

2.1 Cancer

Cancer is the generic name used to describe all diseases associated with aberrant cell division. It is genetic in aetiology as it can always be traced to alterations within specific genes. In most cases, however, it is not inherited because the genetic alterations that lead to most cancers arise in the DNA of a somatic cell during the lifetime of the affected individual (Karp, 1996). It is therefore more of an environmentally mediated genetic disorder.

2.1.1 Causes of Cancer

The first environmental factors to be correlated to cancer development are carcinogenic chemicals such as those present in soot and cigarette smoke (Siemiatycki *et al.*, 1995). They have all been shown either to be directly mutagenic or to be converted to mutagenic compounds by cellular enzymes, e.g. nitro-based compounds. Similarly, ultraviolet radiation, which is the leading cause of skin cancer, is also strongly mutagenic. In addition, a number of viruses can infect vertebrate cells, transforming them into cancer cells. These viruses are broadly divided into two large groups: DNA tumour viruses and RNA tumour viruses, depending on the type of nucleic acid found within the mature virus particle. Important tumour viruses capable of transforming cells and in the process causing cancers in humans include the hepatitis B virus which causes liver cancer, human papiloma virus which causes cervical and penile cancer, Epstein-Barr virus which causes Burkitt's lymphoma, herpes virus which causes Kaposi's sarcoma and the retrovirus (i.e RNA virus) HTLV-1 which causes adult T-cell leukemia. (Karp, 1996).

Tumour viruses can transform cells because they carry genes whose products interfere with cell's normal growth-regulating activities.

2.1.2 Cancer Treatment

2.1.2.1 Surgery

Surgery continues to play a vital role in the diagnosis and treatment of cancers. There are in general six applications of surgery in neoplasia namely: Prevention, diagnosis, staging, surgical palliation, cytoreduction/debulking, surgical cure (or complete excision). Surgical excision of cancerous tissues/glands is a major means of cancer cure. It is however largely limited by the fact that malignant cells almost always metastasize, spreading to other tissues and organs distant from the primary site of the malignancy. This necessitates the incorporation of other means of therapy as adjuvants to surgery (Sasako, 2003).

The benefits of surgery compared to other treatment modalities include the fact that it is non-carcinogenic, less immunosuppressive and offers the best chance for local cure. Disadvantages of surgery include mortality and morbidity associated with the procedure, and potential for decreased function and possible disfigurement (Cuschieri *et al*., 1996).

2.1.2.2 Radiation Therapy

This involves the use of high energy radiation like X-rays, γ-rays and charged particles to shrink tumours and destroy cancer cells by damaging their DNA. Radiation may be localised or systemic. While localised radation is aimed at a particular anatomical site, systemic radiation therapy uses radioactive isotopes like radioactive iodine carried in the general circulation to kill cancer cells. Moreover, localised radiation can be delivered by a machine

from outside the body (external beam radiation therapy) or may come from a radioactive material implanted in or near the cancerous tissue (i.e. Internal radiation therapy, also known as brachytherapy) (Taylor and Powell, 2004; Lawrence *et al.*, 2008; Gaspar and Ding, 2008).

Radiation works by either directly damaging DNA molecules or by inducing the formation of free radicals which in turn react with DNA molecules to damage them. Radiotherapy has the major draw-back of non-selectivity as normal cells in the neighbourhood of the tissue or organ irradiated are equally susceptible.

2.1.2.3 Chemotherapy

This is the use of chemical agents in the selective killing of cancer cells. The fact that chemotherapeutic agents are almost always administered systemically gives chemotherapy an edge over other means of therapy in the prospects of handling or preventing metastasis (Choi *et al*., 2007; Ullah, 2008).

Chemotherapy in its strictest sense refers to the use of small molecule chemical agents in killing cancer cells. This, by far, remains the best means of treating and controlling metastatic cancers, the recent introduction of antibodies and antibody-based small molecule chemotherapies notwithstanding (Remers, 1998; Ross *et al.*, 2004).

Chemotherapeutic agents can be broadly classified into Classical chemotherapeutic agents and the relatively new targeted drugs (Ross *et al.*, 2004). While the classical agents are quantitatively, rather than qualitatively selective, relying largely on their special affinity for rapidly dividing cells, the targeted chemotherapeutic agents are designed to selectively target the rather rare structural and/ or functional differences between cancer cells and normal cells. They are expected by all standards to be less toxic than the classical agents which target

macromolecular structures (usually DNA) that are more or less the same in both cancer and normal cells (Silverman, 2004).

2.1.3 The Medicinal Chemistry of Small Molecule Anticancer Chemotherapeutic Agents.

2.1.3.1 Alkylating Agents

Alkylating agents are DNA interactive agents; they disrupt mitosis by covalently alkylating nucleophilic sites in the DNA molecule, most often the N-7 position of guanines in the DNA molecule causing intra- or inter-strand crosslinks. They essentially provide a carbon electrophile, usually as a carbonium ion, that reacts covalently with the nucleophilic site in a S_N1 or S_N2 fashion depending on their structure (Remers, 1998).

The prototype of the alkylating agents is mechlorethamine (**4**), an example of nitrogen mustards which are essentially nitrogen isosteres of the sulphur mustard, mustard gas or nerve gas (**5**). Autopsy on the victims of mustard gas during World War 1 showed it to have a profound effect against rapidly dividing cells like cells of the bone marrow and of the gastrointestinal epithelium. Mustard gas proved too toxic to be used clinically, it nevertheless formed the template for the development of its nitrogen analogues commonly referred to as nitrogen mustards, many of which have found specific use in the treatment of lymphomas (Remers, 1998). Other important clinical nitrogen mustards include chlorambucil (**6**) and melphalan (**7**).

The formation of an aziridinium ion as an intermediate in the course of action of the nitrogen mustards formed the basis for the employment of ethylenimines as alkylating agents (Remers, 1998). They however do not readily react as the aziridinium ions with nucleophiles.

Examples are triethylenemelanine (**8**) and thiotepa (**9**). Another group of alkylating agents are the N-alkyl-N-nitrosoureas which decompose under physiological conditions to produce carbonium ions that can alkylate. A typical example is methylnitrosourea (**10**) which decomposes initially to form isocyanic acid and methyldiazohydroxide. The latter species decomposes further to methyldiazonium ion and finally to methyl carbonium ion, an alkylating species.

Other important alkylating agents require biotransformation to yield the akylating electrophilic species. The leading example in this category is cyclophosphamide (**11**) which is converted by hepatic cytochrome p450 into the corresponding 4-hydroxy derivative by way of 4-hydroperoxy intermediate. The 4-hydroxy derivative is a carbinolamine in equilibrium with the open chair aminoaldehyde form. Decomposition of the latter generates phosphoramide mustard which has been shown to cyclise to an aziridinium ion, a principal cross-linking alkylating species (Remers and Iyengar, 1995; Remers, 1998)

Methanesulphonates are another group of alkylating agents. They particularly make use of the fact that methanesulphonate is an excellent leaving group, thereby fascilitating the alkylation process which essentially is a nucleophilic substitution reaction. The most prominent of this group of alkylating agents is the bifunctional anticancer drug busulfan (**12**) (Silverman, 2004).

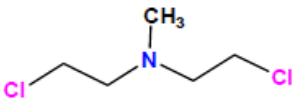

mechlorethamine (4)

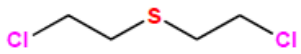

sulphur mustard (mustard gas) (5)

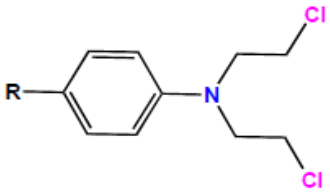

chlorambucil (6) R = $(CH_2)_3CO_2H$

melphalan (7) R= $CH_2CH(NH_2)CO_2H$

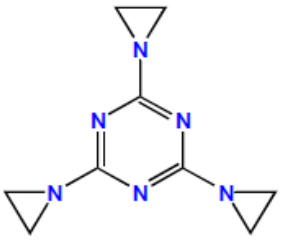

triethylenemelanine (8)

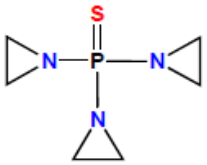

thiotepa (9)

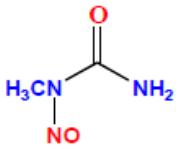

methylnitrosourea (10)

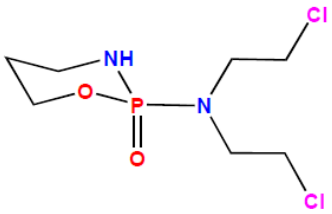

cyclophosphamide (11)

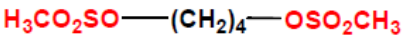

busulphan (12)

Fig. 2: Structures of some alkylating anticancer agents (Remers, 1998).

2.1.3.2 Antimetabolites

Antimetabolites are compounds that prevent the biosynthesis or utilization of normal cellular metabolites. The first anticancer antimetabolites are purine and pyrimidine analogues. Their structural relationship with the normal bases confers on them the ability to inhibit enzymes in the biosynthesis of the corresponding nucleotides as well as substitute the latter in the biosynthesis of DNA, more or less resulting in the generation of defective or "fraudulent" DNA molecules (Remers, 1998). Important examples of purine analogues are 8-azaguanine (**13**), 6-mercaptopurine (**14**) and azathioprine (**15**). 6-mercaptopurine has been shown to be very active against human leukemia (Remers, 1998).

5-fluorouracil (**16**) is a pyrimidine analogue. Its discovery as an antimetabolite of uracil (**17**) provided one of foremost examples of rational drug design. Starting with the observation that certain tumours use uracil more than orotic acid, the major precursor nucleic acid pyrimidine biosynthesis in normal tissue, 5-fluorouracil, was synthesised as an antimetabolite of uracil (Heidelberger, 1975).

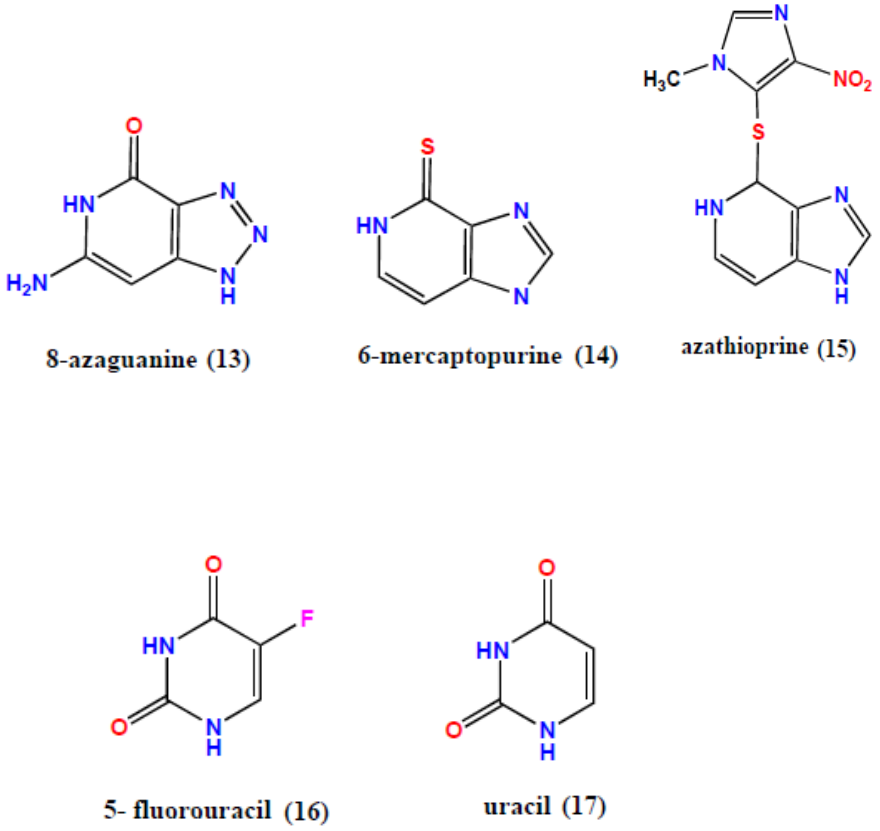

Fig.3: Structures of uracil and some Purine/Pyrimidine-based antimetabolites (Remers, 1998).

Nucleosides of purine and pyrimidine bases having altered sugar units with respect to the sugar units in nucleic acids have also been employed as antimetabolites. The first purine nucleoside analogue is adenine arabinose (vidarabine) (**18**). It has the sugar, D-arabinose that is epimeric with D-ribose at the 2' position. This structural change makes it a competitive inhibitor of DNA polymerase. Examples of pyrimidine nucleosides include the tetrahydrofuranyl derivative of 5-fluorouracil, known as tegafur (**19**), cytosine arabinose (cytarabine) (**20**) and cyclocytidine (ancitabine) (**21**). Other pyrimidine nucleoside analogues have one more or less nitrogen in the heterocyclic ring. They are known as azapyrimidine or deazapyrimidine nucleosides, e.g., 5-azacytidine (**22**).

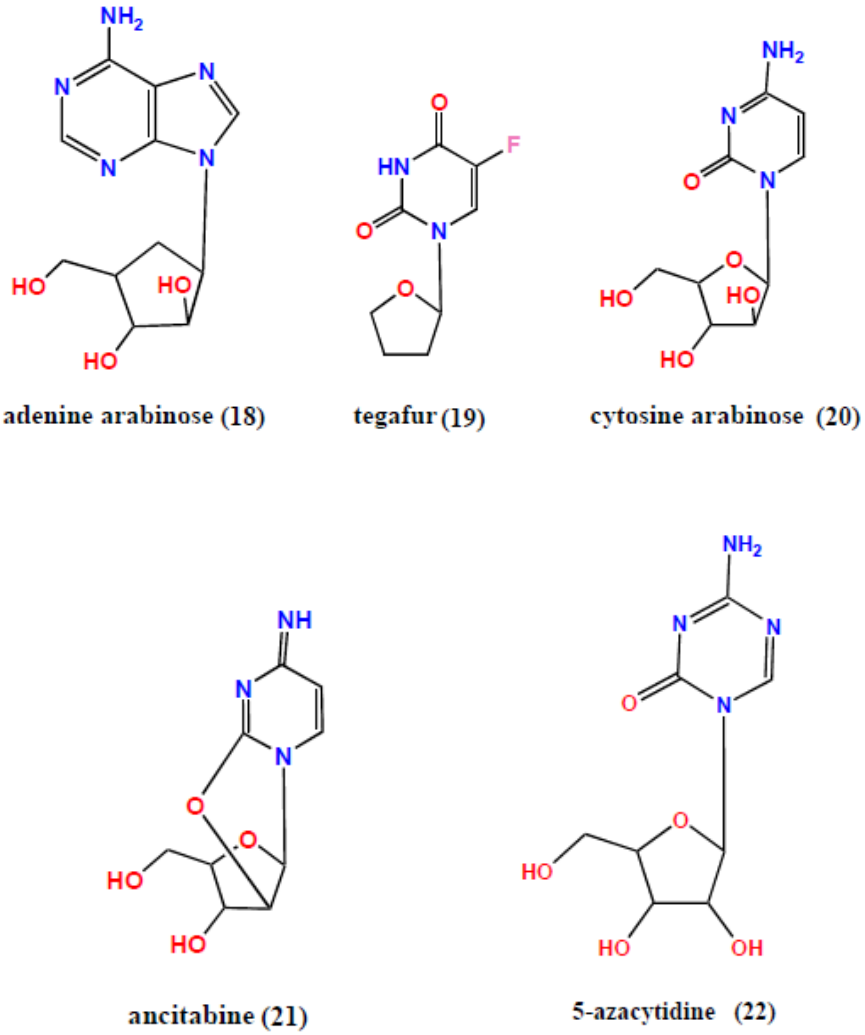

Fig.4: Structures of some nucleoside antimetabolites (Remers, 1998).

In addition to analogues of purine and pyrimidine bases and their nucleosides, analogues of important cofactors in the biosynthesis of these bases have also been tried as antimetabolites. Folic acid (**23**) is such a cofactor: Its discovery as a cofactor in the biosynthesis of the purine nucleotides led to the synthesis and evaluation of its structural analogues as possible antimetabolites. Active ones amongst them include aminopterin (**24**) and its N^{10}-methyl homologue, methotrexate (**25**).

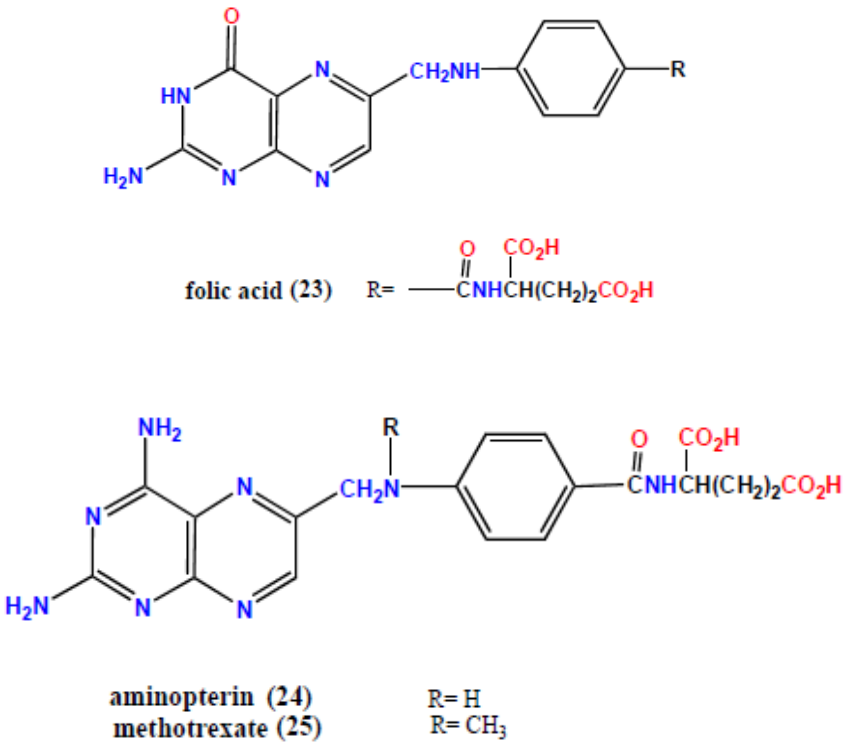

Fig. 5: Structures of folic acid and some folic acid analogue antifolate antimetabolites (Remers, 1998).

2.1.3.3 Antineoplatic Antibiotics

The penicillin-inspired era of screening microbial fermentation cultures for anti-infective agents (i.e. antibiotics) led to the discovery of certain compounds that were initially rejected as antibacterial agents because of their cytotoxicity. Only later was it found that this toxicity could be turned to an advantage in the chemotherapy of cancer. The discovery of antitumor activity is much simpler today, and some laboratories routinely screen extracts of microorganisms cultures for antitumour activity in cell cultures. The search for antitumour

and other bioactive agents from microbial fermentation is receiving particular attention in the industry as the cultures are easily manipulated to yield novel analogues of the original metabolites (Umezawa, 1976).

Important antineoplastic antibiotic already in clinical oncology include the actinomycins and anthracyclines. The actinomycins comprise a large number of closely related structures containing the actinocin chromophore. Actinocin is 3-phenoxazone-1, 9-dicarboxylic acid. Each of the carboxyl group is bonded to a pentapeptide lactone at the amino end of the L-threonine unit of the pentapeptide. The hydroxyl group of the L-threonine forms part of the lactone along with L-methylvaline, the fifth amino acid from the chromophore. D-valine or D-alloisoleucine is the second amino acid and the fourth amino acid usually is sarcosine. The third amino acid is more of a variable, consisting of L-proline, L-hydroxyproline, L-oxoprolie or others produced by controlled biosynthesis (Remers, 1998).

Actinomycins that have two identical pentapeptide lactones are called isoactinomycins, whereas those with different pentapeptide lactones are called anisoactinomycins. The individual pentapeptides are designated α and β, depending on their attachment to the 9- or 1-carboxylic group respectively. A popular isoactinomycin is dactinomycin (**26**), also known as actinomycin D.

Anthracyclines are essentially glycosides, the aglycone of which is the anthracyclinone scaffold consisting of the anthraquinone chromophore within a hydrocarbon skeleton related to that of the tetracyclines (Dimarco, 1967). Examples are daunorubicin (**27**), doxorubicin (**28**) idarubicin (**29**) carminomycin (**30**) and aclarubicin (or aclacinomycin A) (**31**).

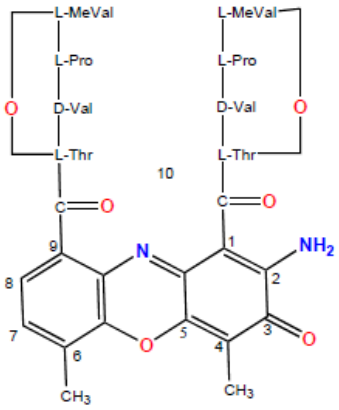

dactinomycin (26)

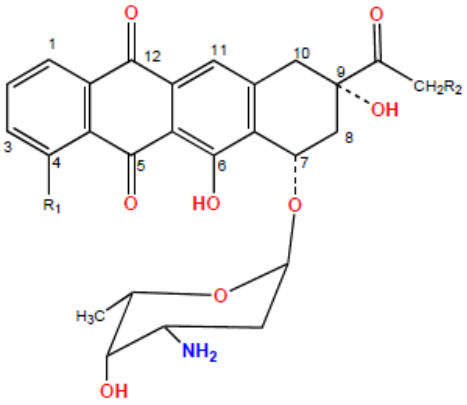

daunorubicin (27) $R_1 = OCH_3$, $R_2 = H$
doxorubicin (28) $R_1 = OCH_3$, $R_2 = OH$
idarubicin (29) $R_1 = H$ $R_2 = OH$
carminomycin (30) $R_1 = OH$ $R_2 = H$

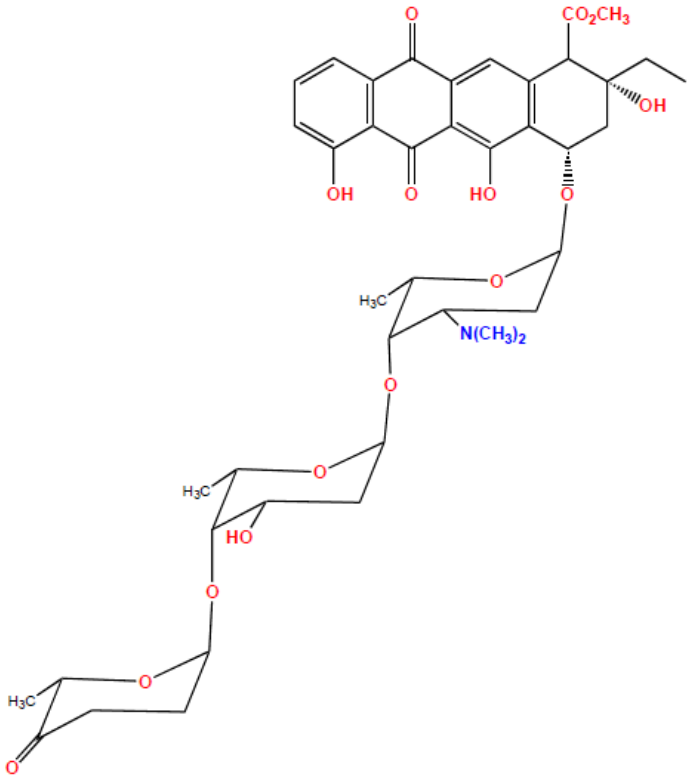

aclarubicin (31)

Fig. 6: Structures of some antineoplastic antibiotics (Remers, 1998).

The aforementioned anthracyclines differ from each other in the number and location of phenolic groups, the degree of oxidation of the two-carbon side chain at position 9, and the presence of carboxylic acid ester at position 10. Thus daunorubicin is a glycoside formed between daunomycinone and L-daunosamine, whereas doxorubicin is its 14 hydroxy analogue. In contrast, aclacinomycin A has aklavinone (Remers and Iyengar, 1995) in combination with a trisaccharide chain. A number of doxorubicin analogues with alteration in the sugar moiety have been prepared. They include 4'-deoxydoxorubicin (esorubicin) (**32**), 4'–epidoxorubicin (epirubicin) (**33**) and 4'-O-tetrahydropyranyl doxorubicin (pirarubicin) (**34**) (Dimarco, 1967).

Other but less common antineoplastic antibiotics include plicamycin, the bleomycins and the mitomycins (Umezawa, 1976; Remers and Iyengar, 1995).

Most antineoplastic antibiotics have been found to be DNA reactive: Some, like the actinomycins and anthracyclines, have been found to exert their antitumour activities by intercalating the DNA double heclical strands, and/or by inhibition of the enzymes DNA topoisomerases (topoisomerase I and II), enzymes which see to the topological integrity of the DNA molecule by unwinding and unlinking coils or kinks in the double helix (Remers, 1998; Silverman, 2004).

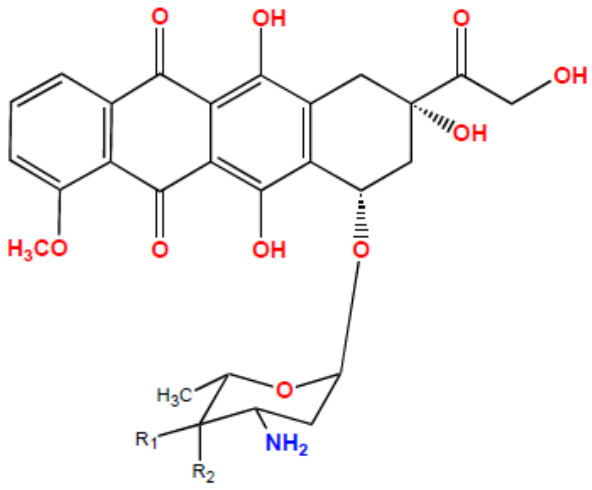

esorubicin (32) $R_1 = R_2 = H$

epirubicin (33) $R_1 = OH$, $R_2 = H$

pirarubicin (34) $R_1 = H$, $R_2 =$ 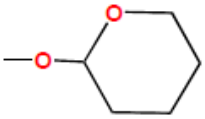

Fig. 7: Structures of some antineoplastic antibiotics continued

2.1.3.4 Antineoplastics Derived From Plants

The folkloric use of many higher plants in the treatment of cancer inspired the guided and random screening of many plant species for their possible anticancer activities. These efforts were not without their own rewards as a number of antineoplastic plant-based natural products now enjoy patronage in clinicall oncology (Clark, 1996). Notable among them are the vinca alkaloids–vincristine (**35**) and vinblastine (**36**) isolated from Madagascar periwinkle, *Catharanthus rosea*. They are used against different types of cancers despite similarities in their structures.

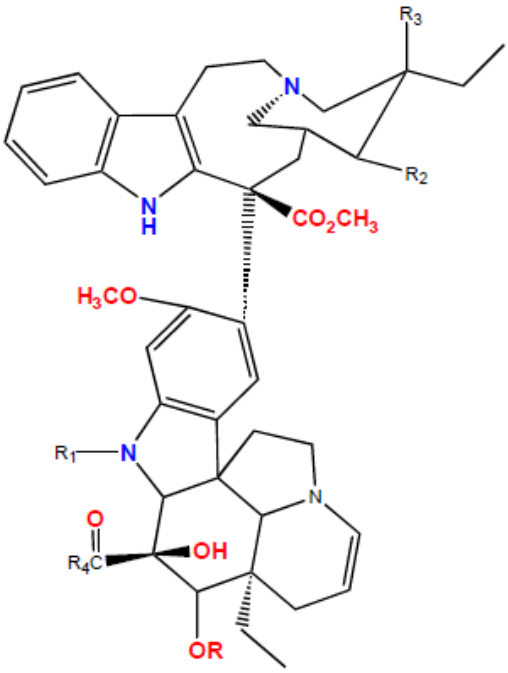

vincristine (35) R= CH_3CO R_1= CHO R_2= H R_3= OH R_4= OCH_3

vinblastine (36) R= CH_3CO R_1= CH_3 R_2= H R_3= OH R_4= OCH_3

Fig. 8: Structures of some plant-based anticancer angents (Remers, 1998).

Other examples of plant products are etoposide (**37**) and teniposide (**38**), which are derivatives of podophyllotoxin, an anticancer agent from the anti-warts resin from *Podophyllum peltatum*, paclitaxel (taxol) (**3**) from *Taxus brevifolia*, and camptothecin (**39**) from *Camptotheca acuminata* (Wall *et al.*, 1966; Wall, 1993).

The anticancer activities of most of the plant products have been found to revolve round interfering with the activities of the spindle apparatus essential in chromosome segregations in mitosis (Schiff, 1979; Clark, 1996).

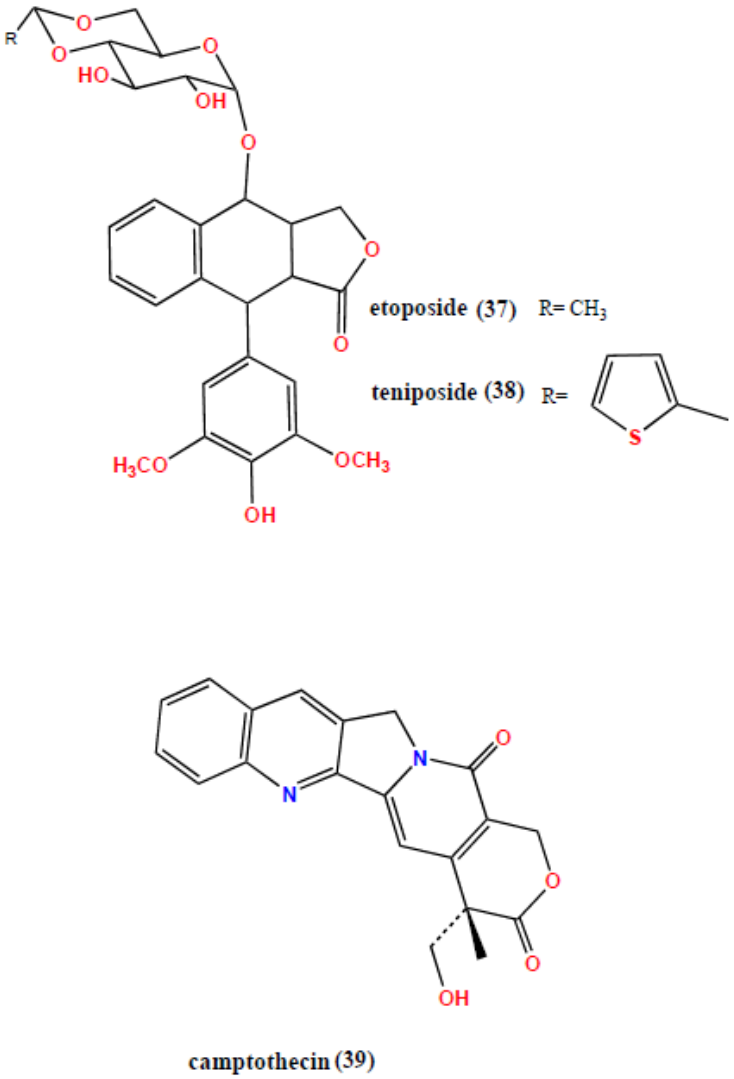

Fig. 9: Structures of some plant-based anticancer angents continued (Remers, 1998).

2.1.3.5 Hormones

Hormones were actually the first molecular agents ever employed in the possible treatment of cancer. The era of chemotherapy of malignant disease began in 1941, when Huggins demonstrated that the administration of oestrogens produced regression of metastatic prostate cancer (Boyd, 1993).

Though hormonal effects on cancers are complex and not completely understood, it is nevertheless appreciable that some cancers are stimulated by sex and other steroidal hormones. Examples are breast cancer in women which respond to tamoxifen (**40**), an antioestrogen, and prostate cancer in men in which diethylstilbestrol (**41**), a synthetic oestrogen agonist, has been found to be useful in more than 60% of patients (Remers, 1998).

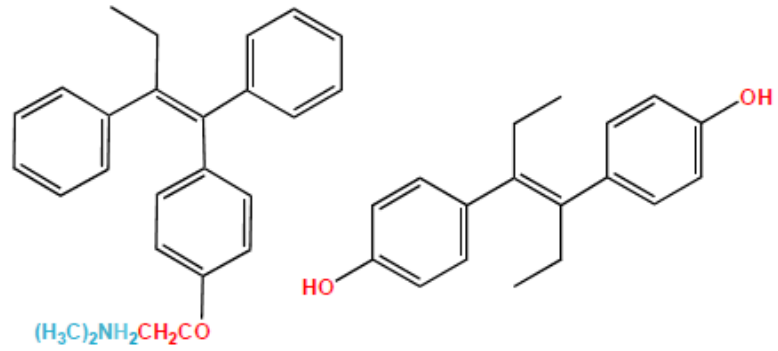

tamoxifen (40) diethylstilbestrol (41)

Fig. 10: Structures of some hormonal anticancer angents (Silverman, 2004).

2.1.4 Targeted Cancer Chemotherapeutic Agents

The indiscriminate pharmacodynamics of classical small molecule anticancer chemotherapeutic agents makes them highly toxic to the patient, their administration requiring extreme caution (Silverman, 2004). It has also necessitated researches targeted at discovering anticancer drugs with selective deleterious effects on macromolecular targets that are crucial to the malignant phenotype but not expressed significantly in vital organs and tissues. Such targeted anticancer therapeutic endeavours have yielded both small molecules as well as antibodies, some of which have been licensed and a number of others still under clinical trials. Some Anti-body based targeted therapies already licensed include rituximab, Zevalin, gemtuzumab, atemtuzumab and Daclizumab (Dillman, 2001; Grillo-Lopez, *et al.*, 2002; Coiffeier, 2002; Gordon *et al.*, 2002), while small molecules already approved as targeted therapies include erlotinib and the antiangiogenesis drugs angiostatin and thalidomide **(42)** (Thomas and Kantarjian, 2000; Mendel *et al.*, 2000; Zogakis and Libutti, 2001; Dell'Eva *et al.*, 2002).

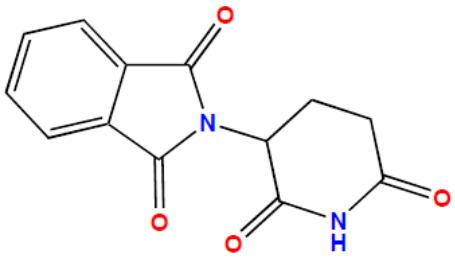

thalidomide (42)

Fig. 11: An antiangiogenetic targeted cancer chemotherapeutic agent (Slilverman, 2004).

The main drawback of targeted anticancer chemotherapy lies in the fact that most of the targeted macromolecules are expressed in a few cancers thereby limiting therapeutic applications. This necessitates search for targets that are expressed in virtually all cancers and not in normal cells. In addition, small molecule targeted drugs also suffer the same fate of multidrug resistance as their classical chemotherapeutic counterparts (Lage, 2008).

Telomerase is a highly promising potential cancer target that would most probably yield targeted anticancer drugs with wide applicability. It is the enzyme that synthesise telomeres which are terminal DNA at chromosome ends and which together with telomere-binding proteins confer stability on chromosomes (Greider and Blackburn, 1985; Liu *et al.*, 2004; De Lange, 2005). In the absence of telomerase, telomeres gradually shorten owing to the inability of polymerases to fully replicate the ends of duplex DNA and chromosomes termini processing ultimately leading to cell-cycle arrest and death (De Lange, 2005; Goldkorn and Blackburn, 2006). The key advantages of targeting telomerase in comparison to most other cancer targets are its relative universality, criticality and specificity for cancer cells (Harley, 2008).

2.1.5 Cancer Multidrug Resistance (MDR)

The term multidrug resistance (MDR) is the phenomenon used to describe the ability of disease-causing cells to resist the cytotoxic effects of chemical agents of wide variety of structure and function targeted at eradicating the cells (Gottesman et. al., 2002). Though it is a common occurrence in both deleterious prokaryotes and malignant eukaryotes, attention will be concentrated on the latter in this review.

A number of mechanisms have been described for development of cancer MDR. They can be broadly divided into cellular and non-cellular mechanisms. Non-cellular mechanisms are commonly observed as important contributors in inherent cancer MDR. They include compromised angiogenesis, induced hypoxia and impairment of nutrition, all of which make tumour cells less rapidly dividing and thereby conferring resistance on them against typical anticancer drugs that act on actively dividing cells (Demant *et al.*, 1990).

Cellular mechanisms on the other hand can be further subdivided into classical (or transport-based) and non-classical (or non-transport-based) mechanisms. Non-transport-based cellular MDR mechanisms involve enzyme systems that limit the desired activity of the drug without altering its effective concentration inside the cell. Glutathione-S-transferase (GST), for instance is an important enzyme of xenobiotic metabolism which catalyses the biotransformation of organic molecules by conjugating them with polar molecules to facilitate their excretion. It is actually known to mediate biotransformation of various anticancer drugs and its elevated level has been reported in some resistant cancers. MDR in such cancer cells could therefore be attributed to the over-expression of GST (Batist *et al.*, 1996).

The transport-based cellular mechanism is the most implicated of all cancer MDR mechanisms as it is found to be a major MDR means in most chemoresistant cancers (Choi *et al*., 2007). It involves the efflux of drug from the cancer cell by various energy dependent membrane transport proteins, thereby inhibiting it from reaching the therapeutic concentration inside the cell (Gottesman, 2002). ATP- Binding Cassettes (ABC) are a family of proteins that mediate MDR via ATP-dependent drug efflux pumps (Leonard *et al.*, 2003; Choi, 2005). Various transport proteins of the ABC superfamily have been characterized and include the permeability glycoprotein P-gp, the multidrug resistance-associated protein

(MRP1), its homologue MRP2-6 and the breast cancer protein (BCRP) (Riordan *et al.*, 1985). These are found to be overexpressed in malignant cells, resulting in lack of intracellular levels of the drug necessary for effective therapy.

The best-studied, well characterized and incidentally the most implicated of the ABC transporters is the P-gp. (Chen *et. al.*, 1986). Encoded by the MDR1 gene, P-gp overexpression has been correlated to the chemotherapeutic failures of important anticancer drugs that include the anthracyclines (e.g. daunorubicin) (**27**), vinca alkaloids (e.g.Vincristine) (**35**), Podophylotoxins (e.g.etoposide) (**37**), and the taxanes (e.g. paclitaxel) (**2**). Targeted anticancer drugs, as mentioned earlier, are also not spared of the spell of the P-gp - mediated cancer MDR (Lage, 2008).

The P-gp molecule is composed of two halves, each consisting of transmembrane α helices and the cytoplasmic ATP binding domain. The two half molecules are separated by a highly charged linker region which is phosphorylated at several sites by protein kinase C. Each half contains a highly hydrophobic domain with 6-transmembrane α helices (TMDs) and a hydrophilic domain located at the cytoplasmic face of the molecule; nucleotide binding domain (NBD). The protein molecule also contains the substrates binding domains. The transmembrane regions form the drug translocating pathway, while the ATP-binding sites, exhibiting ATPase activity provide the metabolic energy upon ATP hydrolysis enabling the active drug efflux. After binding the substrate, ATP hydrolysis induces conformational changes in the protein molecule that open the central pore and allows transportation of hydrophobic drugs directly from the lipid bilayer into the central pore of the transporter expelling the substrates out of the cell (Higgins, 1992; Rosenberg et al., 1997; Loo and Clarke, 2001).

2.1.6 Cancer MDR Inhibitors Discovery

Most of the efforts towards the discovery of cancer MDR inhibitors otherwise referred to chemosensitizers have been centred on the discovery of inhibitors of MDR –associated ABC transpoters especially P-gp, for reasons not unconnected with the fact that they mediate the most implicated mechanisms of cancer MDR (section 1.2.). Though the search for P-gp inhibitors is almost as old as the first discovery of P-gp itself (Juliano and Ling, 1976), there is yet a palpable paucity of P-gp inhibitors in clinical oncology. This may be attributed to the complexity and versatility of P-gp mediated cellular MDR mechanisms (Simon and Schindler, 1994).

Initial efforts at the discovery of P-gp inhibitors were concentrated at the discovery of small molecules for the direct inhibition of P-gp. All the small molecule P-gp inhibitors so far have one problem or the other trailing their clinical application, thereby engendering the exploration of several alternative approaches to MDR therapy, designed either to inhibit MDR in novel ways or to cleverly circumvent MDR mechanism altogether.

The small molecule P-gp inhibitors so far can be divided into three broad groups as first generation, second generation and third generation P-gp inhibitors. The discovery of the first generation drugs was inspired by the promiscuity of P-gp and of other MDR – associated transporters, suggesting the possiblilty of getting potent cancer MDR inhibitors from already existing drugs that are themselves non-cytotoxic. This led to the initial demonstration of the P-gp inhibitory activities of verapamil (**43**), a calcium channel antagonist (Tsuruo *et al.*, 1981), followed by the discovery of many other P-gp inhibitors of diverse structures and functions ranging from immunosuppressants, e.g., cyclosporine A (**44**), antibiotics e.g. erythromycin (**3**), antimalarials e.g. quinine (**45**), psychotropic phenothiazines, e.g.,

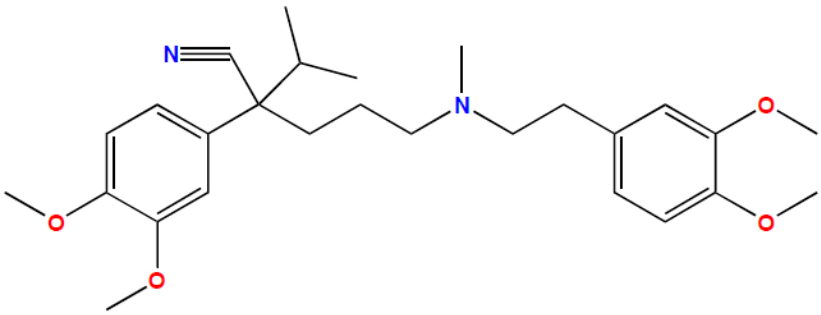

verapamil (43)

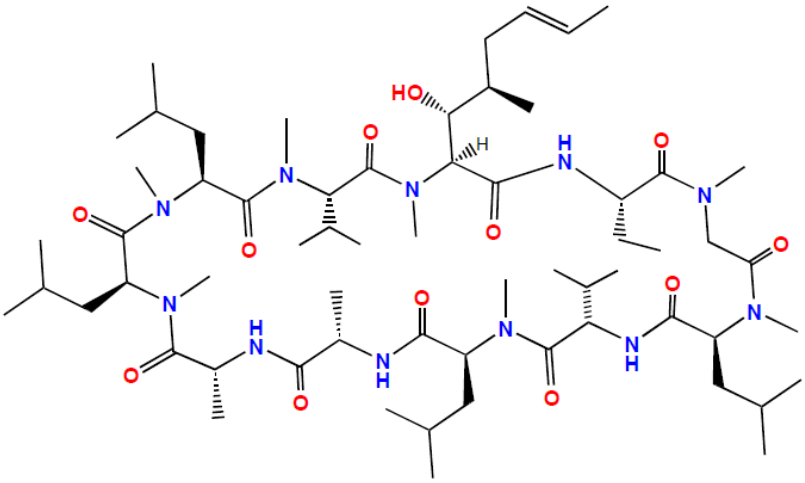

cyclosporine A (44)

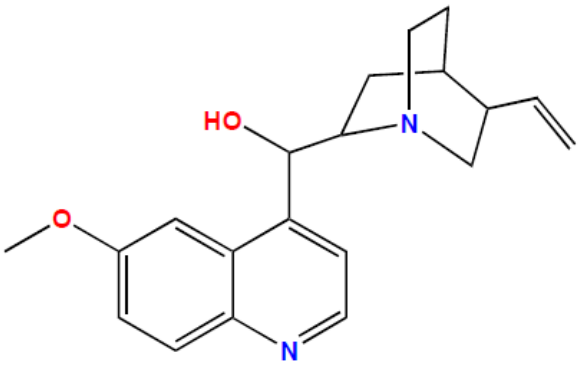

quinine (45)

Fig. 12: First generation P-gp inhibitors (Tsuruo *et. al.*, 1981).

fluphenazine (**46)** and indolealkaloids e.g. reserpine (**47**), steroid hormones and antisteroids e.g. tamoxifen (**40**).

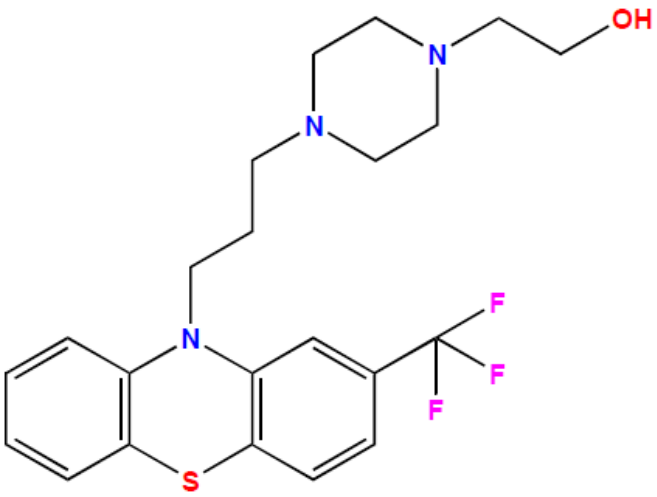

fluphenazine (46)

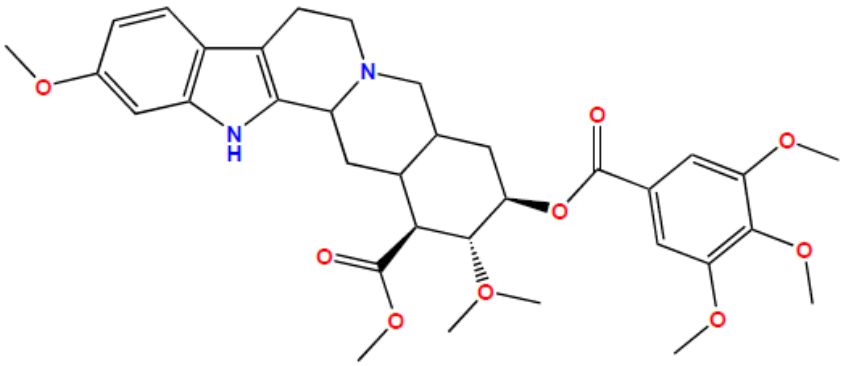

reserpine (47)

Fig. 13: First generation P-gp inhibitors continued (Tsuruo *et. al.*, 1981).

All the first generation drugs failed clinical trials for toxicity reasons traceable to the pharmacological basis of the therapeutic activities for which the drugs were originally marketed (Ferry *et al.*, 1996). The second generation drugs were based on the first generation drugs but were designed specially to reduce the side effects of the latter by eliminating their non-MDR pharmacological activities. Notable in this category is the R-enantiomer of verapamil, R- verapamil, a much weaker calcium channel blocker but nearly equally effective as the L-isomer in blocking P-gp. Unfortunately however, these drugs also suffered the same fate as their first generation counterparts. The third generation drugs were developed specifically to have high affinity for P-gp, allowing effective inhibition at nanomolar concentrations in *in vitro* P-gp models. Though several such compounds have passed through clinical trials while a number of them are still at different levels of the same, results so far have shown that they have inherent problems of pharmacokinetic interactions with anticancer agents, and inhibition of several non-MDR transporters (Sonneveld and Wiemer, 1997; Van Zuylen *et al*., 2000).

One of the non-conventional approaches being explored to inhibit MDR transporters is the suppression or downregulation of P-gp and other MDR transporters expression using antisense oligonucleotides (Bouffard *et al.*, 1996). Other novel approaches being tried include the development of anticancer agents that are poor substrates of MDR transporters; and the development of angiogenetic therapeutic strategies which targets vascular endothelia cells rather than tumour cells themselves, believing that this would be able to control both MDR and non-MDR cancers.(Folkman, 1995; Pierre *et al.*, 1998; Folkman, 2001).

2.2 Privileged Structures.

The phenomenon whereby certain organic structural moieties demonstrate inherent ability to interact with diverse macromolecular entities (mostly proteins and nucleic acids) was first noted and reported by Ariens and co-workers (1979). However, it was Evans and co-workers, working with benzodiazepines (**48**) which Ariens and co-workers earlier worked with, that first coined the term privileged structures to describe molecular species exibiting this phenomenon (Evans *et al*., 1998; DeSimone *et al.*, 2004; Constanlino and Barlocco, 2006).

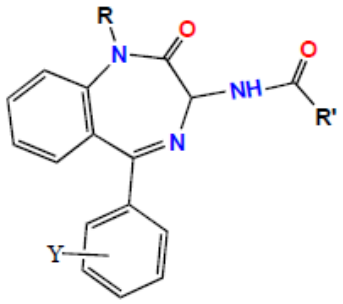

benzodiazepines (48)

Fig. 14: Benzodiazepine privileged structure (Silverman, 2004).

This phenomenon which, in its own rights, is a whole concept of rational drug discovery, led to the observation of the commonality of molecular features in a variety of drugs, giving a shocking revelation that only 32 scaffolds describe half of all known drugs (Bemis and Murcko, 1996). Similar studies carried out on side chains also revealed that a small number of moieties account for a large majority of the side chains found in drugs (Bemis and Murcko, 1999). These observations formed the template giving rise to the same phenomenon that led to the evolution of the concept of *drug-likeness*, from which many data bases and structural parameters have emanated which can be used to compute which molecules should

be selected for screening in any discovery programme, akin to the early Cowin Hansch's analysis (Sadowski and Kubinyi, 1998).

2.2.1 Privileged Structures and Natural Drug Discovery

As lofty as the concept of privileged structures is, its applications so far in the area of natural product chemistry appear to be in the early stages. Three basic principles could be conjectured to govern the rational concept of privileged structures in natural drug discovery:

Firstly, natural compounds can be structurally examined for the presence of part or whole molecules of established privileged structures and on this basis classified as privileged. For instance the indole structural moiety (**49**) is an established privileged structure (Patchett and Nargund, 2000). Its presence therefore in a lot of naturally occurring compounds cutting across plants, animals, microbial, terrestrial and marine biodiversities, is enough bases for classifying such natural compounds as privileged.

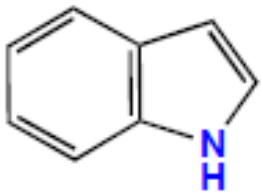

indole (49)

Fig. 15: Indole privileged structure (Silverman, 2004).

Secondly, natural compounds can be structurally examined for similarities with part or whole structures of endogenous chemical mediators that have been pharmacologically established to be involved in mediating multiple physiological and/or behavioural activities usually via multiple receptor- and/or enzyme-interactive activities. Such compounds would most likely have some binding affinities with most if not all of such receptors and enzymes eliciting diverse kinds of biological activities that would be interpretable as modulating the activities of the endogenous chemical mediator in question.

Based on these principles, the privileged attributes of the indole group could in part be attributed to its being the main pharmacophoric group of serotonin (**50**), a structurally simple endogenous indole-containing chemical mediator regulating a diverse array of physiological and behavioural activities in man and other mammals via its multiple receptor subtypes. The structural similarity of indoles (i.e. indole-containing compounds) with serotonin exemplifies natural compounds with similar biogenetic ancestry, meaning they have passed through and interacted with similar enzymes and other macromolecular structures during the course of their biosyntheses. On the basis of this biochemical background, one expects indole-containing structures to be capable of interacting with one or more of the diverse serotonin (also known as 5-hydroxytryptamine or 5-HT) receptors and other 5-HT – interacting macromolecules, especially enzymes involved in 5-HT metabolism and protein – pumps associated with serotonin's active transport across cell membranes. Moreover, while serotonergic transmission has not been confirmed in microbial homeostasis, the recent observation of the interference of some 5-HT targets – interactive agents with microbial metabolism and the discovery that some typical 4-aminoquinolines are 5-HT_3 antagonists provide ample evidence for using this principles in rationalizing the chemotherapeutic properties of indoles (Munoz-Bellido *et al.*, 2000; Thompson *et al.*, 2009). These submissions

are indeed supported by the fact that indole-based natural products have demonstrated a diverse range of biological activities including antihypertensive, antihelminthic, anticancer, etc., activities (Wang and Ng, 1999; Oh *et al.*, 2006). The non-steroidal anti-inflammatory (NSAID) drug, indomethacin (**51**) is an indole acetic acid derivative and it is not impossible that its anti-inflammatory activity is predicated on the serotonin/indole template (Silverman, 2004).

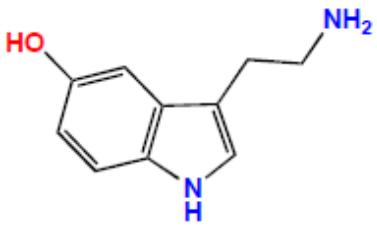

serotonin (50)

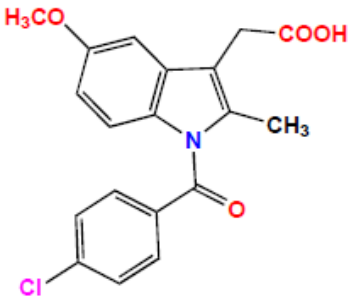

indomethacin (51)

Fig. 16: Indole privileged structure in an endogenous chemical mediator and a xenobiotic (Silverman, 2004).

Triterpenoids are another example of natural products sharing similar structural characteristics with endogenous chemical mediators, i.e., Steroidal hormones. They are biogenetically and structurally related to endogenous steroidal hormones, having rigid tetracyclic or pentacyclic skeletons similar to the steroidal nucleus common to all natural steroidal hormones and thus suitably positioning them to interact with steroidal hormone targets. They tend to modulate any signalling system where steroidal hormones also play pivotal roles as modulators including cancer cell signalling systems (Karp, 1996). Given myriad signalling systems that endogenous steroidal hormones mediate either directly or indirectly, the enormous biological activities available to triterpenoids cannot just be fully

imagined. The diverse biological activities reported for triterpenoids are thus not a surprise (Dzubak *et al*, 2006).

The third possible principle of extending the rational concept of privileged structures to natural drug discovery is by merely targeting natural products that have been reported to have diverse biological activities. Such natural products might not necessarily have structural moieties alludable to established privileged structures or structural features in any chemical mediator or enzyme substrates. This is because the only way such bioactivity diversity can be rationalized is their interaction with diverse macromolecular targets, which by definition makes them privileged structures. Iridoids are a group of phytochemicals with such attributes (Tundis *et al.*, 2008).

2.2.2 Monoterpenoid Indolealkaloids (MTIAs) As Privileged Structures of Potential Cancer MDR Inhibitory Activities.

One of the transduction signallings of serotonin is its interaction with a membrane transporter protein which ensures its ATP-dependent reuptake into pre-synaptic serotonergic neuronal endings after a release into the synaptic cleft following an action potential (Ganong, 1999). By all standards, this is an indication that indole-based compounds like serotonin have the potential to bind or interact with membrane transporters and modulate their activities. The fact that some fundamental functional differences and hence structural differences would exist between serotonin membrane transporters and MDR-associated transporters is well known: For instance serotonin transporters are influx transporters while MDR–associated transporters are basically efflux transporters. This notwithstanding, the fact that both are ATP-dependent membrane transporters indicates the presence of common structural features and hence ability to interact with similar ligands. Now the fact that MDR-associated

membrane transporters are also found in deleterious prokaryotes and are by no means exclusive to malignant eukaryotes (Levy, 1992), and probably because microbes are much easier to work with than cancer cells, studies on bacterial and protozoal MDR-associated transporters and their possible modulation by selective serotonine reuptake inhibitors (SSRIs) have been undertaken: For instance it has been found that fluoxetine (an SSRI) potentiated the activities of Chloroquine and Mefloquine against MDR-*Plasmodium falciparum,* on the food vacuole of which earlier research had shown the presence of a P-gp homologue, Pgh1(Price *et al.*, 2004). This and other similar researches (Mahamoud *et al.*, 2007; Kristiansen *et al.*, 2007) investigating serotonin reuptake pump inhibitors as possible modulators of MDR-associated protein targets in prokaryotes can be extrapolated to the possible cancer MDR inhibition by potential serotonin reuptake pump interactives, amongst which MTIAs are a notable group based on the indole moiety (**49**) they share with serotonin (**50**). Searching for cancer MDR-associated membrane transporter inhibitors from MTIA-containing plant species is thus not out-of-place. MTIAs are widely distributed in plant species of the Apocynaceae, Loganiaceae and Rubiaceae families (Herbert, 1983).

2.2.3 Triterpenoids and Iridoids – Putative Privileged Structures in MTIAs Sources.

A careful consideration of the biosynthetic pathway of the MTIAs fortuitously reveals the possible presence of at least two potential natural privileged structure groups in addition to the MTIAs as follows: The biosynthesis of MTIAs involves the condensation of two structural subunits, an indole moiety derived from tryptamine (**52**) and a C_9 or C_{10} unit derived from the secoiridoid secologanin (**53**), to form the universal MTIA precursor – strictosidine (**54**). Rearrangements in the C_9/C_{10} unit give rise to the structural diversity seen in MTIAs.

Secologanin **(53)** is an example of irregular monoterpenoids known as of iridoids: Iridoids are formed by the fusion of two isoprene units in a fashion which, though not yet fully understood, is quite different from the conventional head-to-tail fashion to form a characteristic cyclopentano[c]pyran ring system known as the iridane skeleton (**55**) that is more or less common to all iridoids (Dewick, 2001). The presence of one iridoid is an indication of the presence of many more as it is contrary in nature's antecedence to annex biosynthetic intermediates to produce just one member of a rather large chemical group.

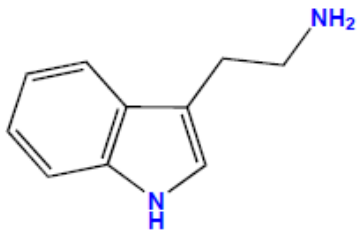

tryptamine (52)

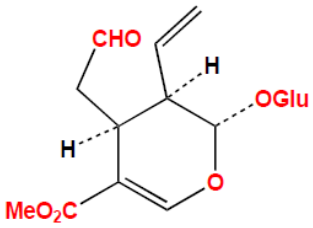

secologanin (53)

Fig. 17: Key intermediates of the monoterpenoid indolealkaloid biosynthetic pathway (Herbert, 1983).

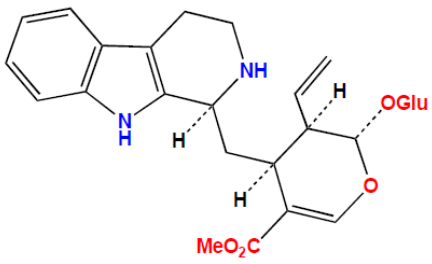

strictosidine (54)

Fig. 18: Monoterpenoid indolealkaloids universal precursor (Herbert, 1983).

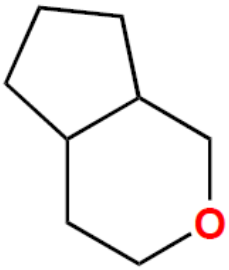

iridane (55)

Fig. 19: The heterocyclic backbone of iridoids (Dewick, 2001).

In the same vein, the presence of iridoids, though irregular monoterpenes, is an indication of the presence of the terpene building unit i.e. isoprene (Bhart *et. al.*, 2005). Now if irregular terpenoid products of the isoprene units condensation can be present how much more should the regular ones of varying complexity including monoterpenoids, diterpenoids, sesquiterpenoids, triterpenoids, etc., be expected? Therefore, MTIA-containing plant species should be expected to be rich in iridoids and triterpenoids, literature documentations notwithstanding. The advantage of this awareness is the ability to simultaneously explore a source for these three privileged structure groups, more or less increasing the scope of potential bioactive compounds realisable from any biological assay.

2.3 The Plant *Hunteria umbellata*

Hunteria umbellata is a small glabrous tree measuring about 12m and 1m in height and girth repectively. It shares phylogenetic similarities with *Picralima nitida*, Stapf. Picralima *elliotii* Stapf., *Hunteria eburnea* Pichon and *Hunteria elliotii* Pichon, but has the distinguishing features of having smaller flowers and fruits (Falodun *et al* ., 2006). In South West Nigeria, where the plant is commonly refered to as *abere*, it is reputed for ethnomedicinal uses ranging from antihelminthic, antiimflammatory, antidiabetic, antilipidaemic, antimicrobial and uterotonic uses (Falodun *et al.*, 2006; Adeneye and Adeyemi, 2009).

Fig. 20: Herbarium sample of the Leaves and seeds of *Hunteria umbellata.*

Previous phytochemical investigations have shown *H. umbellata* to be rich in alkaloids, tannins, phlobatanins, anthraquinones, cardiac glycosides and saponins (Adeneye and Adeyemi, 2009). Definitive isolation have given some 20 indole alkaloids from the plant and these include: Corymine (**56**), acetylcorymine (**57**) eburnamine (**58**), eburnamonine (**59**), vincamine (**60**) and the abereamines **(61)** (Bevan *et al.*, 1967; Adegoke and Alo, 1986; Adeneye *et al.*, 2010). To the best of our knowledge there are no specific records of isolation of triterpenoids and iridoids from *H. umbellata*.

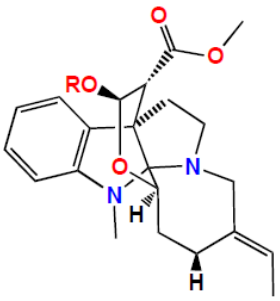

R = H corymine (56)

R = Ac acetylcorymine (57)

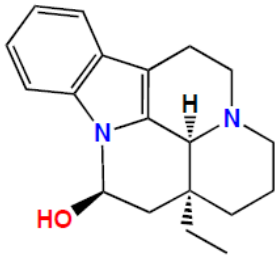

eburnamine (58)

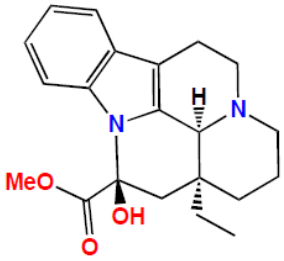

eburnamonine (59)

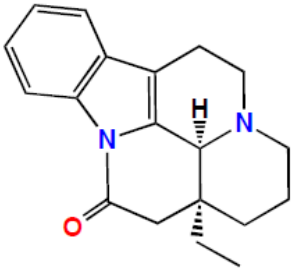

vincamine (60)

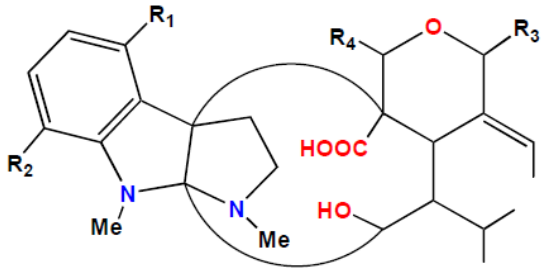

1 $R_1 = R_2 =$ OH, $R_3 = R_4 =$ H
2 $R_1 = R_2 =$ H, $R_3 = R_4 =$ OH
3 $R_1 = R_2 =$ H, $R_2 = R_4 =$ OH
4 $R_1 = R_4 =$ H, $R_2 = R_3 =$ OH

four isomeric abereamines (61)

Fig. 21: Structures of some indolealkaloids from *Hunteria umbellata* (Bevan *et al.*, 1967; Adegoke and Alo,1986).

Though *Hunteria umbellata* is not known for iridoids and triterpenoids, the establishment of its monoterpenoid indolealkaloid content is an indication that *Hunteria umbellata* is also a possible source of iridoids and triterpenoids based on the ealier-shown interdependency of the biosynthetic routes of the three phytochemical groups (section 2.2.3.).

2.4 Concluding Remarks

The adoption of a structure-guided approach to natural drug discovery, as opposed to the traditional activity-guided approach, would not only remove the problem of HTS-incompatibility, it would also enable the incorporation of elements of rationality to the discovery process as compounds of particular structure and hence of predictable biological activities can be targeted.

In this experiment, ^{1}H NMR profiling is adopted as the main structural guide to the isolation of indole, iridoid and triterpenoid phytochemical groups as putative P-gp interactives. This is, to a large extent, aided by the extraction procedure which enabled the preconcentration of the targeted chemical groups to particular fractions, indoles to the organic subfractions of the basified aqueous acid fraction, terpenoids to the aqueous acid insolubles fraction and iridoids to the alkaline aqueous left- over subfraction of the extracted basified aqueous acid fraction (section 3.4).

CHAPTER THREE

METHODOLOGY

3.1 General Experimental Procedures

Optical rotations were measured on a JASCO P-1010 polarimeter with a 10 cm length cell. UV spectra were obtained on a Cary 50 UV – Visible spectrometer with 1cm pathway cell. NMR experiments were performed on a Bruker Avance DR 600 spectrometer and referenced to residual ^{1}H signals in the deuterated solvents. ESIMS experiments were carried out on an Agilent 1100 series LC/MSD instrument. HR-ESIMS data were acquired on a Bruker micrOTOF mass spectrometer by direct infusion on MeCN at 3µl/min using sodium formate clusters as an internal standard. All HPLC analyses and purifications were performed on Agilent 1100 series LC instruments with corresponding detectors, collectors and software inclusively.

Human colon carcinoma parental cell line (SW620) was obtained from the United States of America's National Cancer institute (NCI) and a MDR subline (SW620 AD300), selected at 300ng/ml adriamycin (Lai *et al.*, 1991), obtained from it and maintained in a customised tissue culture medium accompanying the parental line kit.

All chemicals were purchased from Merck, Sigma-Aldrich or Fluka. Solvents used for general purposes were of at least analytical grade, and solvents used for HPLC were of HPLC grade. Agilent Zorbax SB-C18 (5µm, 4.6 x 150mm (analytical) and 9.4 x 250mm (semipreparative) columns were used for HPLC analyses and separations. Altech SPE catridges were also used in some of the separations.

3.2 Plant Collection and Taxonomy

The seed, leaf, and stem bark materials of the plant *Hunteria umbellata* were collected from a cocoa plantation in Odofin Agbegi village, Ikire, under Irewole local government area of Osun state, Nigeria, in July 2007. Authentication of plant materials was done at the Forest Reserves Institute of Nigeria (FRIN), Aleshinloye, Ibadan, Oyo state, Nigeria, where a herbarium sample was also deposited with the registration number FHI 107776.

3.3 Crude Extracts Preparation.

The leaf, stem bark and seed materials were air – dried at room temperature and pulverised. 1Kg each of the powdered materials was extracted with MeOH using a sohxlet extractor, yielding 65 g, 45 g and 78 g of the leaf, seed and stem bark crude extracts respectively.

3.4 General Fractionation

65g crude leaf extract was extracted with aqueous HCl (1N) yielding an aqueous acidic extract (fraction A) and an aqueous acid-insoluble fraction B (25g). Fraction A was basified with drop-wise addition of 5N NaOH and thereafter extracted with $CHCl_3$ to give fractions C (1.5 g) and D (2.0 g) obtained at pH 6.0 and pH10.0 respectively. The alkaline fractions from the $CHCl_3$ extractions were neutralized to pH 7 by acidification and freeze dried to yield fraction E (15 g). Each of the fractions C and D was triturated in succession with CH_2Cl_2 and MeOH. C gave fractions F (372 mg) and G (675 mg) while D gave H (54 mg) and I (1.8 g). Fraction E was triturated with *n* - butanol and H_2O in succession to afford fractions J (0.1 g) and K (3.5 g). Fraction B was triturated with n-hexane, CH_2Cl_2, and MeOH in succession to yield fractions L (3.1 g), M (1.2 g) and N (3.8 g). These procedures were repeated for the methanolic crude extracts of the seed (45 g) and stem bark (78 g), yielding fractions A, B

(4.0g), C (6.0g), D (5.0g), E (18.0g), F (100mg), G (3.4g), H (2.8g), I (1.8g), J (700mg), K (5.9g), L (784mg), M (665mg) and N (2.4g) for the seed extract and fractions A, B (33.0g), C(5.0g), D(0), E(20g), F(623mg), G(1.7g), H(0), I(0), J(600mg), K(5.5g), L (1.4g), M(455mg) and N(7.3g) for the stem bark extract.

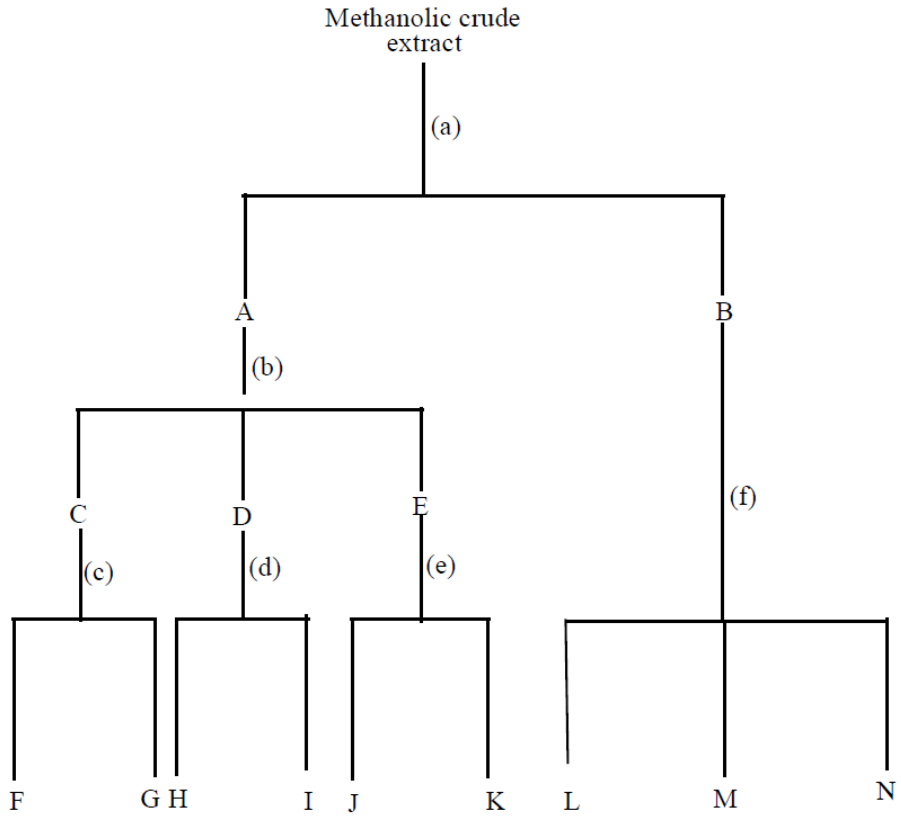

(a) -- aqueous acid extraction
(b) -- basification and $CHCl_3$ extraction at pH 6 and pH 10
(c), (d) -- successive trituration with CH_2Cl_2 and MeOH
(e) -- successive trituration with n-butanol and H_2O
(f) -- successive trituration with n-hexane, CH_2Cl_2 and MeOH

Scheme 1: General fractionation scheme.

3.5 ^{1}H NMR Profiling

10mg of each of the fractions of the seed, leaf and stem bark extracts was subjected to ^{1}H NMR spectroscopy at 600MHz using $CDCl_3$ as solvent for CH_2Cl_2 and n-hexane fractions, and CD_3OD for MeOH fractions.

3.6 Isolation of Compounds

3.6.1 Isolation of Compounds 2, 4 and 7 and 9 from the Leaf Extract.

Compound 2: The leaf fraction M was left standing for 30 minutes to afford compound 2 (20mg) by precipitation.

Compounds 4 and 9: A 15mg portion of the leaf fraction G was triturated in acetonirile. The acetonitrile insoluble fraction (8.2mg) taken up in MeOH was subjected to HPLC purification using a Zorbax C_{18}, 9.4mm x 250mm semipreparative column, 5µm; 10% MeOH/H_2O - 100% MeOH (0.01% TFA) in 15 min, at 3.5ml /min. to afford compounds 4 (3.5mg) and 9 (2.6 mg) .

Compound 7: In the same vein, a 15mg portion of the leaf fraction I was triturated with acetonitrile, and the acetonitrile-insoluble fraction (7mg), taken up in MeOH was subjected to HPLC purification, using a Zorbax C18 9.4 x 250mm column 5µm; 30% - 70%MeOH/H_2O (0.01%TFA) in 15 min at 3ml/min to yield compound 7(1.2mg).

3.6.2 Isolation of Compounds 1and 3 from the Crude Seed Extract.

Compound 1: 10.0mg of the seed fraction J was washed through a C_{18} SPE (5g) with water and 50% MeOH in succession. The 50% MeOH fraction was concentrated and further cleaned up by CH_2Cl_2 trituration leaving compound 1 (7mg) as CH_2Cl_2 – insoluble solid.

Compound 3: The seed fraction H (50mg) was recrystallized in MeOH/H_2O (3:7). The mother liqueur (dry mass 42mg) was washed through a diol SPE (2g) cartridge with CH_2Cl_2 and MeOH in succession to yield a MeOH-soluble fraction (35mg), 5mg of which was then purified using a Zorbax C_8 XBD 9.4 x 250mm, 5µm; 30 -70% MeOH/H_2O in 15 at 3ml/min to afford compound 3 (2.0mg).

3.6.3 Isolation of Compounds 5, 6 and 8 from the Crude Stem Bark Extract.

Compound 5:

The stem bark fraction G (5mg) was purified using a Zorbax C_8 column 9.4mm x 250mm, 5µm; 30 – 70% MeOH/H_2O (0.01%TFA) in 15 min at 3ml/min to afford compound 5 (2.4mg).

Compounds 6 and 8: 10mg of the stem bark fraction J was washed through a diol SPE (2g) cartridge with CH_2Cl_2 and MeOH in succession. The MeOH elution was further purified using a Zorbax SB Aqua 9.4mm x 150mm column, 5µm; 10 – 50% MeOH/H_2O (0.01%TFA) in 10min at 3.5ml/min to afford compound 6 (2.8mg) and compound 8 (2.0mg).

3.7 Chemical Characterization of Compounds

UV scan of each compound was taken and absorption maxima and logε values carefully examined to determine the nature of the absorbing chromophore. Two 1D (^{1}H and ^{13}C) NMR data and three 2D NMR data namely DEPT-edited ^{1}H-^{13}C HSQC, ^{1}H-^{1}H gCOSY and ^{1}H-^{13}C gHMBC were acquired on a Bruker 600MHz spectrometer, processed with Topspin 2.0 and interpreted to give the gross structure of each compound. CD_3OD was used as solvent in each case with the exception of compound 2 for which pyridine-d_5 was the solvent used. Coupling constant analysis in conjunction with the analysis of the cross peaks of an additional 2D (^{1}H-^{1}H ROESY) NMR spectrum was used to assign relative configurations about chiral centres and/or geometry about isolated double bonds except with compound 1 which has no such stereochemical issues.

3.8 P-gp Inhibition Assay

Standard P-gp inhibition assay procedures (Polli *et al.*, 2001; Schwab *et al*., 2003; Rautio *et al.*, 2006) were adopted with little modifications: 25µl of each of 1 µg/ml, 10 µg/ml, and 100µg/ml solutions of each of the pure compounds in DMSO was put in a well in a 96-well u-bottom microplate. 25µl each of Phosphate buffer solution, (PBS), an MDR cell line culture (25 x 10^5 cells/ml) and DMSO were set as negative controls in separate wells just as 25µl 800µM verapamil was as positive control. 50µl of the MDR cell line culture (25 x 10^5 cells/ml) was then seeded in each of the wells already containing either a test compound or a control. This procedure was repeated using three additional plates followed by the incubation of the four ensuing plates at 37^0C for 15 minutes. Following this incubation, 25µl of 1µM calcein AM was dispensed into each well in the four plates and mixed well (making the effective concentration of each compound in the final mileu one-quarter of its initial

concentration) followed by further incubation at 37^0C for 15 minutes. After incubation, the microplates were centriguged for 5 minuites at 200 x g, the supernatants removed and the cells resuspended and washed in 100µl of cold (4^0C) tissue culture medium four times before being transferred to four 96-well flat bottom well plates.

Fluoresence associated with calcein accumulation in the cells was then detected using a POLARstar omega plate reader at an excitation wavelength of 490nm and emission wavelength of 517nm. Modifications involved in setting conditions for hits selection included configuring the plate reader to set the highest RFU as pivot and the RFUs less than 50% of the difference between the pivot and RFU of the least-value negative control at values close to the latter. Hits were thus selected as samples (at particular concentrations) producing RFUs greater than 50% of the afore-mentioned difference, and the statistical significance of these values analysed with student-t test (Colton, 1974; McHugh, 2008).

CHAPTER FOUR

RESULTS

4.1. Results of ^{1}H NMR Profiling of Fractions (Section 3.5.)

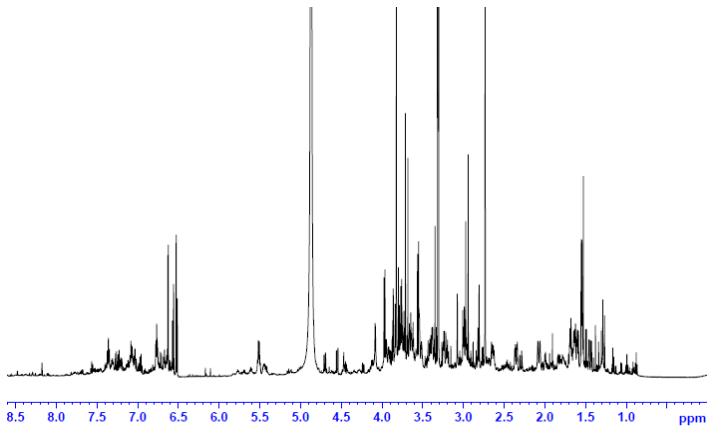

Fig. 22: Representative ^{1}H NMR spectrum (600MHz, CD_3OD) of indole-containing fractions.

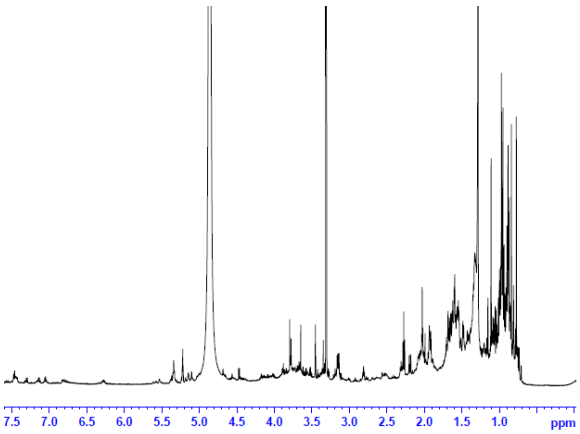

Fig. 23: Representative ^{1}H NMR (600MHz, CD_3OD) spectrum of triterpenoid-containing fractions.

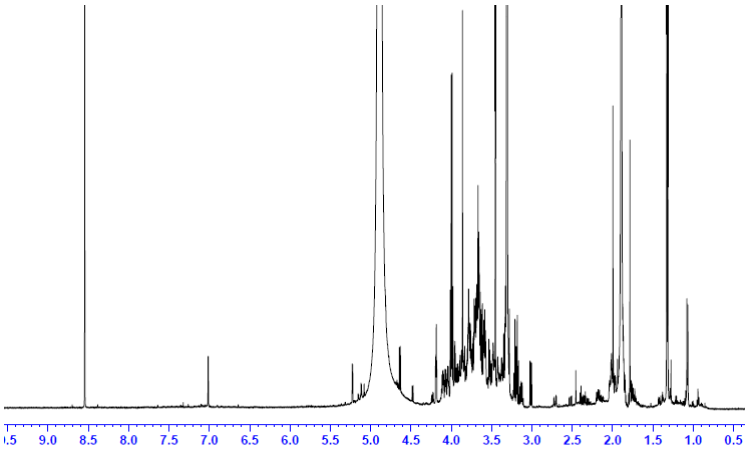

Fig. 24: Representative ^{1}H NMR spectrum (600MHz, CD_3OD) of iridoid-containing fractions

4.2. Results of Chemical Charactirization of Compounds (section 3.7).

4.2.1 Summary of Chemical Characterization Data

Compound 1: Yellow crystalline solid; UV (MeOH) λ_{max} (logε) 204nm (4.45), 223nm (4.39) 263nm (4.05), appendix 7; ^{1}H, ^{13}C and other NMR data (CD_3OD, 600MHz), appendices 2-6c, Table 1; ESI(+)MS m/z 309 M^+; HRESI(+)MS m/z 309.1607 M^+ (calcd for $C_{19}H_{21}N_2O_2$, 309.1598), appendix 1.

Compound 2: Greyish amorphous solid; $[\alpha]^{22}_D$ +64.9 (*c* 1.0, pyridine), UV (MeOH) λ_{max} (logε) 204 nm (4.30), 289 nm (3.40), appendix 15; ^{1}H, ^{13}C and other NMR data (pyridine-d_5, 600MHz), appendices 9-14b, Table 2; ESI(+)MS m/z479 $[M+Na]^+$, ESI(-)MS m/z 455 $[M-H]^-$; HRESI(+)MS m/z 479.3475 $[M+Na]^+$ (calcd for $C_{30}H_{48}NaO_3$, 479.3496), appendix 8.

Compound 3: Colourless amorphous solid; $[\alpha]^{22}_D$ -14.46 (*c* 0.1, MeOH); UV (MeOH) λ_{max} (logε) 203nm (4.40), 241nm (3.80) 310nm (3.40), appendix 23; ^{1}H, ^{13}C and other NMR data

(CD_3OD, 600 MHz), appendices 17-22, Table 3; ESI(+)MS m/z 431 M^+; HRESI(+)MS m/z 431.1740 M^+ (calcd for $C_{23}H_{28}ClN_2O_4$, 431.1732), appendix 16.

Compound 4: Yellow amorphous solid; $[\alpha]^{22}_D$ +93.1 (*c* 0.15, MeOH); UV (MeOH) λ_{max} (logε) 206 nm (4.480), 251nm (4.38), 308nm (4.21), 364nm (3.54), appendix 31; ^1H, ^{13}C NMR data (CD_3OD, 600MHz), appendices 25-30b, Table 4; ESI(+)MS m/z 349 M^+; HRESI(+)MS m/z 349.1557 M^+ (calcd for $C_{21}H_{21}N_2O_3$, 349.1547), appendix 24.

Compound 5: Light brown solid; $[\alpha]^{22}_D$ +30.1 (*c* 0.02, MeOH); UV (MeOH) λ_{max} (logε) 209 nm (4.84), 272nm (3.99), 308nm (3.54), appendix 39; ^1H, ^{13}C and other NMR NMR data (CD_3OD, 600MHz), appendices 33-38, Table 5; ESI(+)MS m/z 327 M^+; HRESI(+)MS m/z 327.2070 M^+ (calcd for $C_{20}H_{27}N_2O_2$, 327.2067), appendix 32.

Compound 6: Colourless amorphous solid; $[\alpha]^{22}_D$ -5.2 (*c* 0.05, MeOH); UV (MeOH) λ_{max} (logε) 207 nm (4.93), 250 nm (3.37) , 290 nm (3.34), appendix 47; ^1H, ^{13}C and other NMR data (CD_3OD, 600MHz), appendices 41-46b, Table 6; ESI(+)MS m/z 367 $[M+H]^+$, m/z 365 $[M-H]^-$; HRESI(+)MS m/z 367.2009 $[M+H]^+$ (calcd for $C_{22}H_{27}N_2O_3$, 367.2016), appendix 40.

Compound 7: Colourless amorphous solid; $[\alpha]^{22}_D$ -177.7 (*c* 0.067, MeOH); UV (MeOH) λ_{max} (logε) 208nm (4.96), 273nm (3.92), appendix 55; ^1H, ^{13}C and other NMR data (CD_3OD, 600MHz), appendices 49-54, Table 7; ESI(+)MS m/z 517 $[M+H]^+$, m/z 515 $[M-H]^-$; HRESI(+)MS m/z 517.2187 $[M+H]^+$ (calcd for $C_{26}H_{23}N_2O_9$, 517.2181), appendix 48.

Compound 8: Grey amourphous solid; $[\alpha]^{22}_D$ -60.86 (*c* 0.0350, MeOH); UV (MeOH) λ_{max} (logε) 235nm (3.59), appendix 64; ^1H , ^{13}C and other NMR data (CD_3OD, 600MHz),

Appendices 58-63, Table 8; LRESI(+)MS m/z 359 $[M+H]^+$, m/z 394 $[M+H+MeOH]^+$, appendix 56, HRESIMS, pseudomolecular ion conspicuously absent, appendix 57.

Compound 9: Yellow crystalline solid; $[\alpha]^{22}_{D}$ -11.88 (*c* 0.0160, MeOH); ^{1}H , ^{13}C and other NMR data (CD_3OD, 600MHz), appendices 66-69; HRESI(+)MS m/z 671.3248 $[M+H]^+$ (calcd. for $C_{41}H_{43}N_4O_5$, 671.3228), appendix 65.

4.2.2 NMR Assignment Tables

Table 1. NMR (CD_3OD, 600MHz) data for compound 1{N-[2-(2-carbomethoxy-3-indolyl)ethyl]-3-ethylpyridinium} (appendices 2- 6c)

No.	δ_C [a]	δ_H (mult., *J* in Hz)	COSY	HMBC[b] (^1H to ^{13}C
1	-	-	-	-
2	135.3	-	-	-
3	143.2	8.66 (d, 8.0)	H-14	C-5, C-14, C-21
4	-	-	-	-
5	63.2	4.83 (t, 5.9)	H-6	C-3, C-7
6	26.9	3.36 (t, 5.9)	H-5	C-2, C-5, C-7,C-8
7	105.9	-	-	-
8	130.0	-	-	-
9	116.7	6.60 (d, 7.9)	H-11	C-7, C-11, C-13
10	119.8	6.67 (t, 7.6)	H-11	C-8, C-12
11	121.9	6.91 (t, 7.4)	H-9, H-10, H-12	C-9, C-13
12	111.9	7.22 (d, 8.01)	H-11	C-8, C-10
13	136.6	-	-	-
14	128.2	7.68 (t, 6.8)	H-3, H-15	C-3, C-20
15	145.3	8.10 (d, 8.0)	H-14	C-3, C-19, C-20
16*	-	-	-	-
17*	-	-	-	-
18	14.3	0.88 (t, 7.6)	H-19	C-19, C-20
19	26.5	2.46 (q, 7.6)	H-18	C-18, C-20
20	145.7	-	-	-
21	145.6	8.47 (s)	-	C-3, C-5, C-19
2-$\underline{C}O_2Me$	177.8	-	-	-
2-$CO_2\underline{Me}$	36.5	3.60 (s)	-	C-2, C-7, C-22

[a] ^{13}C experiments run at 150MHz, and ^{13}CNMR assignments supported by HSQC experiment;
[b] HMBC correlations optimised for 8 Hz.
* missing with respect to the conventional numbering order of monoterpenoid indolealkaloids

Table 2. NMR (600MHz, pyridine-d_5) data for compound 2 (ursolic acid)(appendices 9-14b)

No.	δ_C[a]	δ_H (mult., *J* in Hz)	HMBC[b] (^{1}H to ^{13}C)	ROESY
1	39.4	a 1.56 (m)	C-2	
		b 0.98 (m)	C-9	
2	28.5	1.84 (m)	C-1	
3	78.4	3.48 (dd, 9.5, 5.8)	C-1, C-4,C-23, C-24	H-5, H-23, H-27, H-30
4	39.7	-	-	
5	56.2	0.88 (d, 11.8)	C-3, C-4, C-7	
6	19.1	a 1.62 (m)	C-4, C-10	
		b 1.49 (m)	C-4, C-5	
7	33.9	a 1.49 (m)	C-3, C-6	
		b 1.39 (m)	C-9, C-15	
8	40.3	-	-	
9	48.4	1.65 (m)	C-1, C-8C-10	
10	37.6	-	-	
11	24.0	1.95 (m)	C-8, C-9,C-14	
12	126.0	5.52 (br s)	C-8, C-11,C-14, C-18	H-11, H-18
13	139.6	-	-	
14	42.9	-	-	
15	29.0	a 2.35 (dt, 8.0, 4.3)	C-3, C-8,C-14, C-16, C-19	H-27, H-29
		b 1.25(overlapped)	-	
16	25.3	a 2.14 (m)	C-15, C-17, C-18, C-28	
		b 2.02 (m)	C-13, C-28	
17	48.4	-	-	
18	53.9	2.67 (m)	C-12, C-13, C-14, C-16, C-17, C-19,C-20	
19	39.8	1.48 (m)	C-21, C-30	
20	39.8	1.02 (overlapped)	C-18	
21	31.4	a 1.47 (m)	C-22, C-30	
		b 1.41 (m)	-	
22	37.8	2.02 (m)	C-16, C-20,C-21	
23	29.3	1.25 (s)	C-3, C-4,C-5	
24	16.3	1.05 (s)	C-3, C-4	
25	16.0	0.90 (s)	C-10	Ha-6, Hb-7
26	17.8	1.08 (s)	C-8, C-14	
27	24.3	1.25 (s)	C-8, C-16	
28	180.3	-	-	
29	17.9	1.02 (d, 6.3)	C-18, C-20	
30	21.8	0.91 (d, 6.1)	C-21, C-22	

[a] ^{13}C experiments run at 150MHz, and ^{13}CNMR assignments supported by HSQC experiment;
[b] HMBC correlations optimised for 8 Hz.

Table 3. NMR (CD_3OD,600MHz) data for compound 3:
4- chloromethylakuammineammonium ion (appendices 17- 22)

No.	δ_C[a]	δ_H (mult., *J* in Hz)	COSY	HMBC[b] (^1H to ^{13}C)	ROESY
1	-	-	-	-	
2	103.6	-	-	-	
3	64.9	4.79 (s)	Ha/b-14, H-15	C-2, C-14, C-15, (N-4)-$\underline{C}H_2$-	H-15
4	-	-	-	-	
5	58.1	a 4.42 (m)	Hb-5, Ha-6, Hb-6	C-6, C-21	
		b 3.40 (dd, 12.0, 5.4)	Ha-5, Ha-6	C-6, C-7, C-21 , (N-4)-$\underline{C}H_2$-	
6	28.4	a 3.73 (dd, 15.5, 5.8)	Ha/b-5, Hb-6	C-2, C-5, C-7, C-8, C-15	
		b 1.88 (dd, 15.5, 5.4)	Hb-5, Ha-6	C-7, C-8, C-16	
7	52.8	-	-	-	
8	138.9	-	-	-	
9	111.6	6.68 (br s)	-	C-8, C-10, C-13	
10	153.5	-	-	-	
11	115.6	6.65 (m)	-	C-10, C-13	
12	113.4	6.65 (m)	-	C-7, C-10, C-13	
13	144.6	-	-	-	
14	26.8	a 2.69 (br d, 15.3)	H-3, Hb-14, H-15	C-15, C-20	
		b 2.33 (br d, 15.3)	H-3, Ha-14, H15	C-2, C-3, C-20, C-21	
15	39.3	3.80 (br s)	H-3, Ha/b-14, H-18, H-19	C-3, C-7, C-14, C-19, C-20, C-21	H-3
16	58.3	-	-	-	
17	74.9	a 4.14 (d, 8.2)	Hb-17	C-2, C-7, C-15, C-16	
		b 3.67 (8.0)	Ha-17	C-2, C-7, C-16, C-20, 16-$\underline{C}$OOMe	
18	13.8	1.66 (d, 7.1)	H-15, H-19, Ha/b-21	C-19, C-20	16-COO$\underline{Me}$
19	127.2	5.83 (q, 7.1)	H-15, H-18, Ha-21	C-15, C-18, C-20, C-21	
20	131.1	-	-	-	
21	62.4	a 4.48 (d, 15.1)	H-18, H-19, Hb-21	C-5, C-20	
		b 4.06 (d,15.1)	H-18, Ha-21	C-3, C-5, C-14, C-15, C-19, C-20	
(N-1)-$\underline{C}H_3$	30.7	2.82 (s)	-	C-2, C-12, C-13	
(N-4)-$\underline{C}H_2$-	72.8	a 5.41 (d, 9.8)	Hb-(N-4)-CH2-	C-3, C-5, C-21	
		b 5.33 (d, 9.8)	Ha-(N-4)-CH2-	C-3, C-5, C-21	
16-COO$\underline{Me}$	53.1	3.89 (s)	-	16-$\underline{C}$OOMe	H-18
16-$\underline{C}$OOMe	171.9	-	-	-	

[a] ^{13}C experiments run at 150MHz, and ^{13}CNMR assignments supported by HSQC experiment;
[b] HMBC correlations optimised for 8 Hz.

Table 4. NMR (600 MHz, CD_3OD) data for compound 4: serpentine (appendices 25- 30b).

No.	δ_C[a]	δ_H (mult., *J* in Hz)	COSY	HMBC[b] (^1H to ^{13}C)	ROESY
1	-	-	-	-	
2	141.6	-	-	-	
3	133.6	-	-	-	
4	-	-	-	-	
5	117.1	8.53 (d, 6.5)	H-6	C-6	Ha/b-21
6	134.1	8.47 (d, 6.5)	H-5	C-2, C-3	
7	135.5	-	-	-	
8	121.7	-	-	-	
9	109.4	7.76 (ddd, 8.2, 2.0, 1.0)	H-10	C-8, C-10	
10	123.3	7.47 (ddd, 7.0, 5.8, 1.0)	H-11, H-12	C-11, C-12	
11	133.3	7.80, (ddd, 7.2, 5.8, 1.0)	H-10	C-12	
12	124.3	8.39 (ddd, (8.2, 2.0, 1.1)	H-11	C-11, C-13	
13	145.7	-	-	-	
14	30.2	a 4.17 (dd, 17.7, 6.3)	Hb-14, H-20	C-2, C-7, C-15, C-19	
		b 3.38 (dd, 17.7,9.3)	Ha-14, H-20	C-2, C-15, C-16	
15	27.8	3.22 (m)	Ha-14, Hb-14, H-20	C-14, C-16, C-17, C-19, C-20	
16	109.4	-	-	-	
17	157.3	7.74 (s)	-	16-$\underline{C}O_2Me$	
18	18.7	1.49 (d, 6.3)	H-19	C-19, C-20	
19	72.6	4.03 (qd, 6.0, 2.0)	H-20	-	H-20
20	37.3	2.57 (m)	H-15, H-19, Ha/b-21	-	H-19
21	55.8	a 5.04 (dd, 14.3, 5.9)	H-19, Hb-21	C-2, C-3, C-15, C-19, C-20	H-6, H-18, H-19, H-20
		b 4.70 (dd, 14.3, 10.3)	H-19, Ha-21	C-2, C-3, C-15, C-19, C-20	H-6, H-18, H-19, H-20
16-$CO_2\underline{Me}$	52.1	3.80 (s)	-	16-$\underline{C}O_2Me$	
16-$\underline{C}O_2Me$	169.0	-	-	-	

[a] ^{13}C experiments run at 150MHz, and ^{13}CNMR assignments supported by HSQC experiment;
[b] HMBC correlations optimised for 8 Hz.

Table 5. NMR (600 MHz, CD_3OD) data for compound 5: 4-Methylhuntrabrineammonium ion (appendices 33 - 38)

No.	δ_C[a]	δ_H (mult., *J* in Hz)	COSY	HMBC[b] (^1H to ^{13}C)	ROESY
1	-	-	-	-	
2	131.8	-	-	-	
3	29.7	4.65 (br s)	Ha-14	-	H-15
4	-	-	-	-	
5	59.6	a 3.88 (m)	Hb-5, Ha-6	C-3, C-6, C-7, (N-4)-$\underline{C}H_3$	
		b 3.86 (m)	Ha-5, Ha-6	C-3, C-7, C-21	
6	16.9	a 3.16 (m)	Ha-5, Hb-6	C-2, C-5, C-7, C-13, C-21	
		b 3.08 (m)	Ha-5, Ha-6	C-2, C-7	
7	103.4	-	-	-	
8	126.8	-	-	-	
9	112.4	6.88 (d, 2.3)	H-11, H-12	C-7, C-10, C-11, C-13	
10	150.8	-	-	-	
11	102.1	6.76 (dd, 8.7, 2.3)	H-9, H-12	C-9, C-13	
12	111.5	7.21 (d, 8.7)	H-9, H-11	C-8, C-10	
13	131.8	-	-	-	
14	29.7	a 2.64 (m)	H-3, Hb-14, H-15	-	
		b 2.30 (m)	H-3, Ha-14, H-15	C-15, C-16	
15	30.2	3.24 (dd, 14.5, 7.2)	Ha-16, Hb-16	C-14, C-16	H-3
16	35.3	a 1.60 (m)	H-15, Hb-16	C-14, C-17, C-20	
		b 1.43 (m)	H-15, Ha-16, H-17	C-14, C-17	
17	58.6	3.51 (m)	Ha/b-16	C-15, C-16	
18	12.3	1.84 (dd, 7.0, 1.4)	H-19, Ha-21	C-19, C-20	H-21
19	131.8	5.98 (q, 7.0)	H-18, Ha-21	C-15, C-18, C-21	
20	127.3	-	-	-	
21	62.5	a 4.36 (d, 12.8)	H-15, H-18, H-19, Hb-21	C-20, (N-4)-$\underline{C}H_3$	H-19
		b 3.69	Ha-21	C-2, C-3, C-15, C-20, (N-4)-$\underline{C}H_3$	
(N-4)-$\underline{C}H_3$	47.5	3.19	-	C-3, C-5, C-21	

[a] ^{13}C experiments run at 150MHz, and ^{13}CNMR assignments supported by HSQC experiment;
[b] HMBC correlations optimised for 8 Hz.
[c] overlapped by MeOH signal

Table 6. NM R (600 MHz, CD_3OD) data for compound 6: strictosidinic acid (appendices 41 - 46b)

No.	δ_C [a]	δ_H (mult., *J* in Hz)	COSY	HMBC[b] (^1H to ^{13}C)	ROESY
1	-	-	-	-	
2	109.5	-	-	-	
3	53.2	4.63 (br d, 11.8)	Hb-14	C-2	Hb-5, Hb-6
4	-	-	-	-	
5	42.9	a 3.75 (ddd(9.7, 5.6, 4.1)	Hb-5, Ha-6	-	
		b 3.41 (m)	Ha-5, Ha-6	-	
6	19.7	3.09 (m)	Ha-5, Hb-5, Hb-6	-	
		3.04 (m)	Ha-5, Hb-5, Ha-6	-	
7	107.3	-	-	-	
8	127.6	-	-	-	
9	112.4	7.32 (d, 7.0)	H10	C-10, C-11	
10	120.7	7.14 (dd, 8.0, 7.0)	H-9, H-11	C-12, C-13	
11	123.7	7.05 (dd, 8.0, 7.0)	H-10, H-12	C-8, C-9	
12	119.3	7.47 (d, 8.0)	H-8, H-13	C-10, C-13	
13	138.3	-	-	-	
14	35.0	a 2.36 (dddd, 17.7, 15.1, 12.5, 3.0)	H-3, Hb-14, H-15	-	
		b 2.22 (dddd, 18.4, 15.4, 12.1, 3.8)	H-3, Ha-14, H-15	-	
15	32.7	3.05 (m)	Ha/b-14, H-15, H-20	-	H-20
16	109.5	-	-	-	
17	157.3	7.84 (s)	-	C-15, C-16, C-21, C-22	
18	119.8	a 5.36 (ddd, 17.4, 2.7, 1.3)	Hb-18, H-19	C-19, C-20	
		b 5.27 (ddd, 17.5, 11.0, 7.0)	Ha-18, H-19		
19	135.6	5.86 (ddd(17.5, 11.0, 7.0)	Ha/b-18		
20	45.5	2.76 (m)	H-15, H-17, H-19	C-14, C-18, C-19, C-21	H-15
21	97.4	5.86 (d, 9.0)	H-16		
22	172.9	-	-		
1′	100.6	4.82 (m)	H-2′		
2′	71.9	3.22 (m)	H-1′, H-3′		
3′	78.9	3.38 (m)	H-2′, H-4′	C-2′, C-4′	
4′	74.8	3.24 (m)	H-3′, H-5′	C-5′	
5′	78.2	3.40 (m)	Ha/b-6′		
6′	63.2	a 3.99 (m)	H-5′, Hb-6′		
		b 3.65 (m)	H-5′, Ha-6′		

[a] ^{13}C experiments run at 150MHz, and ^{13}CNMR assignments supported by HSQC experiment;
[b] HMBC correlations optimised for 8 Hz.

Table 7. NMR (600 MHz, CD_3OD) data for compound **7:** Pseudoakuammigine (appendices 49- 54)

No.	δ_C[a]	δ_H (mult., *J* in Hz)	COSY	HMBC[b] (^1H to ^{13}C)	ROESY
1	-	-	-	-	-
2	99.0	-	-	-	
3	55.9	4.62 (br s)	Ha-14, Hb-14,H-15	-	
4	-	-	-	-	
5	53.2	a 3.95 (m)	Hb-5,Ha-6, Hb-6	C-3, C-21	
		b 3.22 (m)	Ha-6, Hb-21	-	
6	28.7	a 3.59 (d, 15.6)	Ha-5, Hb-5, Hb-6	-	
		b 1.77 (d, 15.9)	Ha-5, Ha-6	-	
7	54.5	-	-	-	
8	151.0	-	-	-	
9	123.7	7.14 (d, 7.7)	H-10	C-11, C-13	
10	122.6	6.86 (td, 7.8, 1.0)	H-9, H-11	C-8, C-12	
11	129.7	7.21 (td, 7.7, 1.2)	H-10, H-12	C-9, C-13	
12	112.5	6.81 (d, 7.9)	H-11	C-8, C-10	
13	153.0	-	-	-	
14	27.2	a 2.64 (dd16.8, 8.5)	H-3, Hb-14, H-15	H-15	
		b 2.31 (ddd, 16.5, 3.5,1.6)	H-3, Ha-14, H-15	-	H-3, H-15, Ha-21
15	40.4	3.8 (br s)	H-3, Ha/b-14, H18	-	
16	59.0	-	-	-	
17	75.5	a 4.13 (d, 7.8)	Hb-17		
		b 3.63 (d,7.5)	Ha-17		
18	13.8	1.66 (dd, 7.1, 2.7)	H-19, Ha-21, Hb-21	C-19	
19	132.0	5.81 (q, 7.0)	H-18, Ha/b-21,	C-15, C-21	
20	139.0	-	-	-	
21	54.5	a 4.37 (d, 15.6)	H-18, H-19, Hb-21	-	H-19
		b 3.70 (d, 15.6)	Ha-21	C-3, C-6, C-15, C-19, C-20	
(N-1)-Me	29.9	2.86 (s)	-	C-2, C-13	H-12
17-COOMe	172.3	-	-	-	
17-COOMe	51.2	3.80 (s)	-	17-COOMe	

[a] ^{13}C experiments run at 150MHz, and ^{13}CNMR assignments supported by HSQC experiment;
[b] HMBC correlations optimised for 8 Hz.

Table 8: NMR (600MHz, CD_3OD) data of compound 8: 1-glucopyranosyl-8-methyliridan-3-en-4, 7-carbolactone (appendices 58- 63).

No	δ_C [a]	δ_H m *J*Hz	COSY	HMBC [b] (^1H to ^{13}C)	ROESY(H-H)
1	79.8	5.28 d (3.0)	9	-	H-8, H-9, H-10, H-1'
2	-	-	-	-	
3	152.3	7.39 s	-	C-1, C-4, C-5, C-11	
4	114.3	-	-	-	
5	32.3	3.09 m	Ha/b-6 , H-9	C-3, C-4	Ha-6
		a 2.24	H-5, H-7	C-7, C-9	H-5
6	34.9	b 1.66	H-5, H-7	C-4	H-7
7	75.2	4.04	Ha/b-6, H-8		Hb-6, H-8
8	42.3	1.88	H-7, H-9, H-10		H-1, H-7
9	46.7	2.03	H-1, H-5, H-8		H-1
10	13.6	1.09	H-8	C-7, C-8, C-9	
11	171.1	-	-		
1'	100.2	4.85 d (9.8)	H-2'	C-1	
2'	74.9	3.20	H-Í', H-3'	C-Í', C-5'	
3'	78.5	3.37	H-2', H-4'	C-5'	
4'	71.7	3.28	H-3', H-5'		
5'	78.2	3.29	H-4', Ha-6' Hb-6'	C-3'	
		a 3.90	H-5', Hb-6'		
6'	62.9	b 3.66	H-5', Ha-6'		

[a] ^{13}C experiments run at 150MHz, and ^{13}CNMR assignments supported by HSQC experiment;
[b] HMBC correlations optimised for 8 Hz.

4.2.3 Structures of compounds.

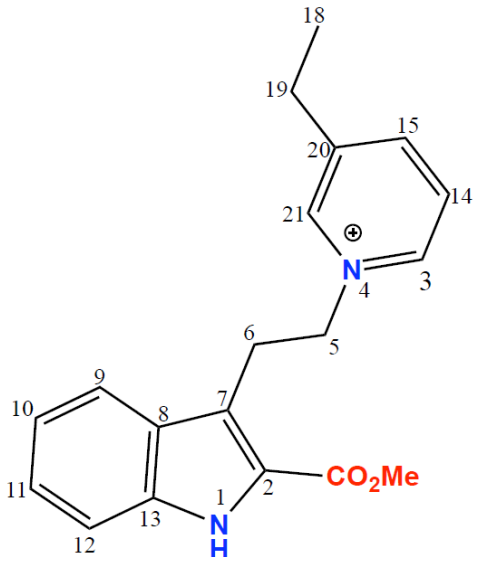

Fig. 25: **Compound 1: N- [2-(2-carbomethoxy-3-indolyl) ethyl]-3-ethylpyridinium, from the seed extract.**

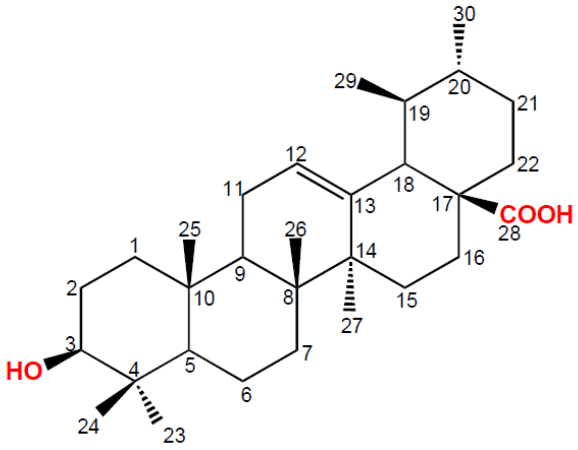

Fig. 26: **Compound 2: ursolic acid (Thanakicharoenpath and Theanphong, 2007), from the leaf extract.**

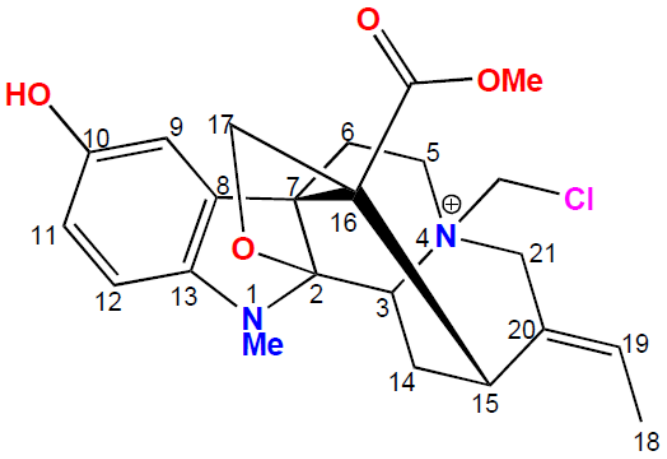

Fig. 27: Compound 3: 4-chloromethylakuammineammonium ion (Ramirez and Garcia-Rubio, 2003), from the seed extract.

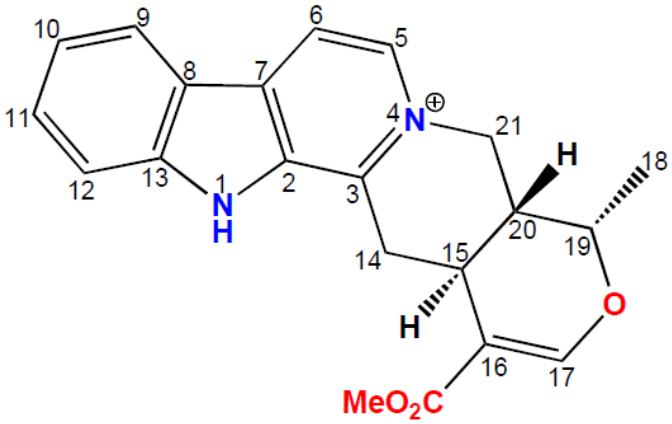

Fig. 28: Compound 4: Serpentine (Wachsmuth and Matusch, 2002), from the leaf extract.

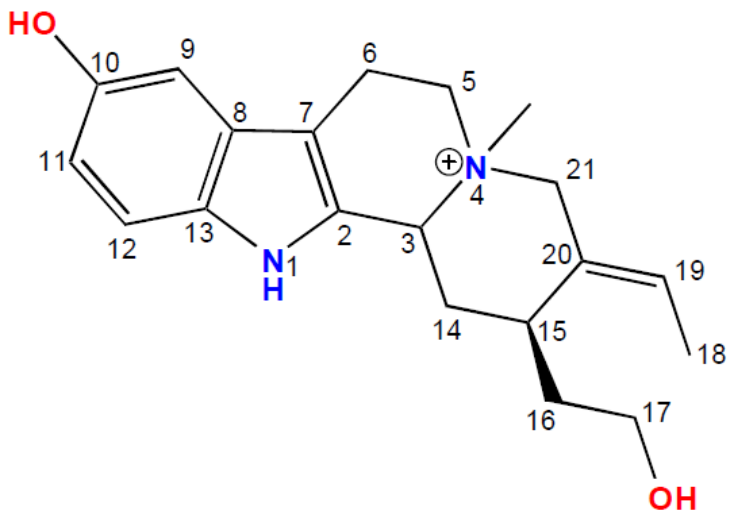

Fig. 29: Compound 5: 4-methylhuntrabrineammonium ion (Borris *et al*, 1983), from the stem bark extract.

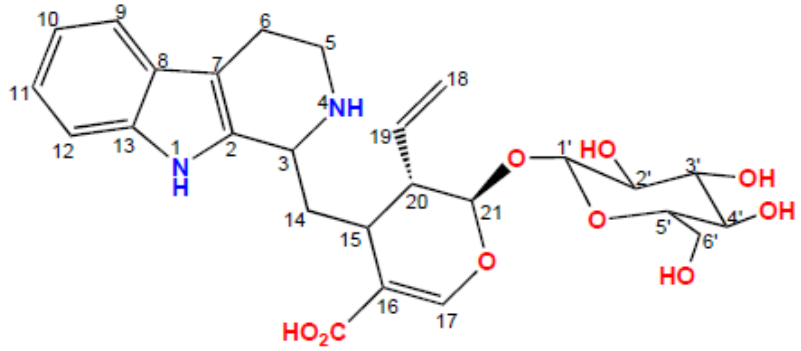

Fig. 30: Compound 6: Strictosidinic acid (do Nascimento *et al.*, 2006), from the stem bark extract.

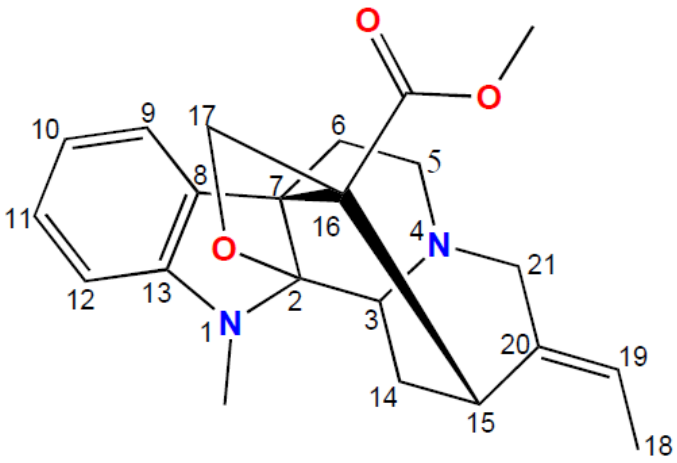

Fig. 31: Compound 7: Pseudoakuammigine (Ramirez and Garcia-Rubio, 2003), from the leaf extract.

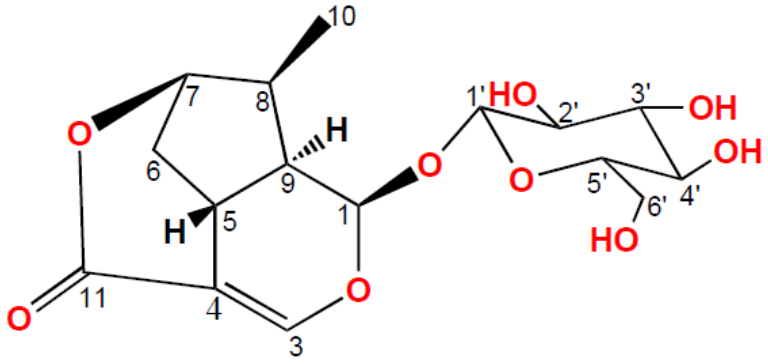

Fig. 32: Compound 8: 1-glucopyranosyl-8-methyliridan-3-en-4,7-carbolactone, from the stem bark extract.

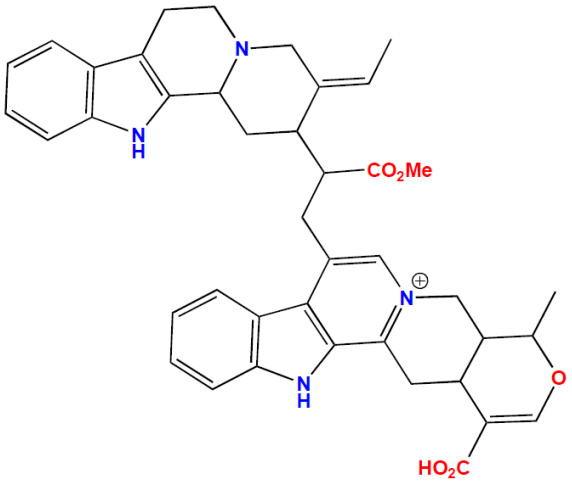

Fig. 33: Compound 9: desmethylserpentinine (Irie *et al.*, 1972), from the leaf extract.

4.3 Results of P-gp Inhibition Assay (section 3.8)

Table 9: Calcein accumulation in MDR cells, measured as Relative flouresence units (RFUs), following incubation with calcein AM in the presence of compounds 1-8 and the controls.

Compounds	**RFU±SD**			
	0.25µg/ml	**2.5µg/ml**	**25µg/ml**	**Controls**
1*	132473±2000	135125±4000	185456±5000	-
2	130434±0	136000±0	132134±1000	-
3	132000±0	129498±1240	130223±2500	-
4*	126097±500	137355±467	230089±5630	-
5	136000±980	135422±300	127000±3000	-
6	130455±321	135000±1000	138429±167	-
7	126466±2500	130568±1000	138541±130	-
8	125002±800	130000±564	135000±4985	-
PBS	-	-	-	126334±1021
MDR/DMSO	-	-	-	127000±490
MDR	-	-	-	126579±0
Verapamil	-	-	-	130269±4200

* Hits (section 3.8): 25 µg/ml compounds 1 and 4 ($P < 0.01$)

Table 10: Calcein accumulation in MDR cells, measured as Relative flouresence units (RFUs), following incubation with calcein AM in the presence of the compounds except comounds 1 and 4.

Compounds	RFU±SD			
	0.25µg/ml	**2.5µg/ml**	**25µg/ml**	**Controls**
2	185332±500	174126±5076	18087±65	-
3	175643±2500	183128±500	185721±4506	-
5	186089±4030	185316±1000	180090±3000	-
6*	174000±900	180000±50	225000±8540	-
7*	180452±500	177225±1040	215000±300	-
8	175432±300	176341±900	200220±3000	-
PBS	-	-	-	170389±2500
MDR/DMSO	-	-	-	175442±2530
MDR/PBS	-	-	-	176264±1500
Verapamil (800µM)	-	-	-	224000±1080

***** Hits (section 3.8): 25 µg/ml compounds 6 and 7 ($P < 0.01$)

A.

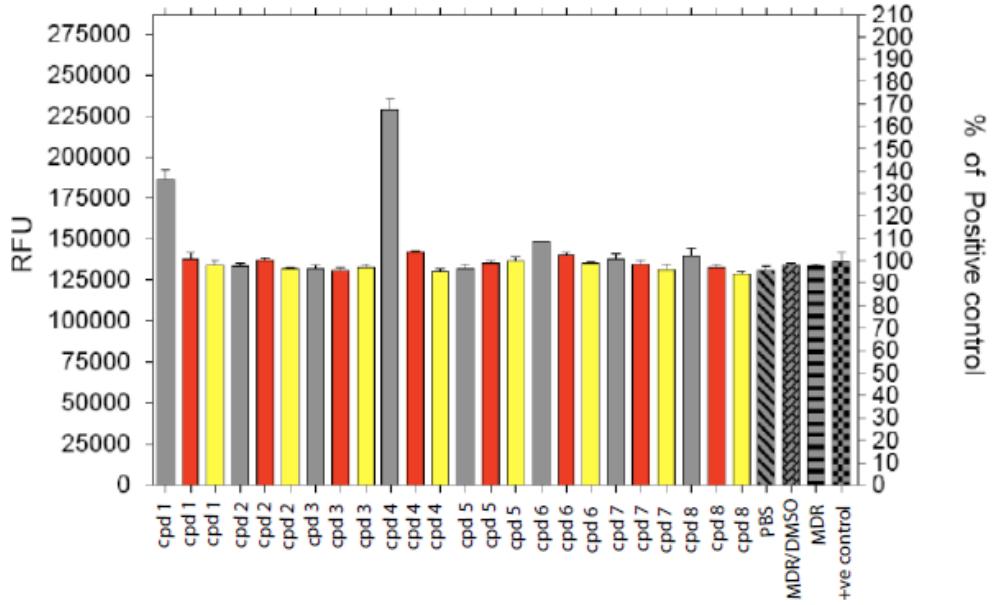

B.

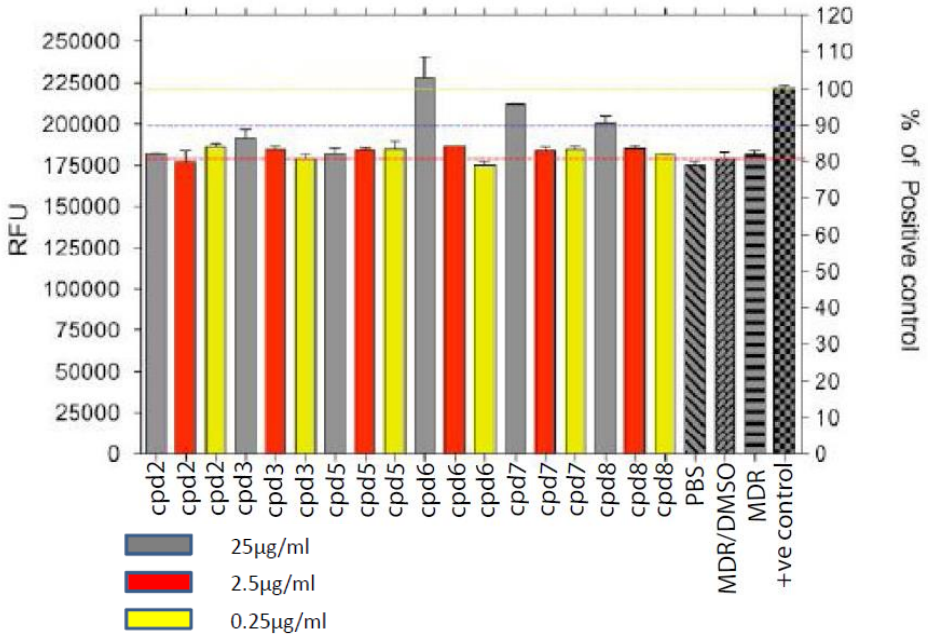

Fig. 34: Bar charts showing, A: RFUs due to 0.25, 2.5, and 25 µg/ml of compounds 1-8, and B: RFUs due to the same concentrations in the absence of compounds 1and 4.

CHAPTER FIVE
DISCUSSIONS

5.1 General

^{1}H NMR profiling as a structural guide to isolating predetermined chemical groups simply depends on the ability to identify characteristic proton NMR spectral signals of such groups in the spectra of fractions containing or suspected to be containing them. Identifying fractions containing indoles, therefore, was roughly based on the presence of characteristic aromatic signals in the spectra of nitrogenous fractions of the general fractionation procedure (Fig. 22). The complex overlapping upfield methylene proton signals characteristic of triterpenoids (Bhart *et al.*, 2005) was used to identify triterpenoid–containg fractions (Fig. 23). Iridoid-containing fractions were given out by their characteristic enolic proton singlet coupled with a cluster of hydroxylated methine/methylene proton resonances typical of sugars, bearing in mind that most iridoids are also glycosides (Fig. 24.) (Dewick, 2001). The structure-guided isolation of the afore-mentioned privileged structures from the leaf, seed and stem bark extracts of *Hunteria umbellata* afforded nine compounds; one triterpenoid, seven monoterpenoid indole alkaloids and one lactone iridoid glucoside. This ratio in a way confirms the earlier series of phytochemical investigations on various species of the genus *Hunteria* which show alkaloid–dominated chemistry (section 2.3). Four of these compounds (compounds 1, 3, 8 and 9) are new, compounds 1 and 8 being spectacularly new as they defined unprecedented scaffolds in their respective groups.

5.2 Structure Elucidations

The structure elucidation of each of the compounds was achieved by an integrative approach to the interpretation of 1D (^{1}H, ^{13}C), 2D homonuclear chemical shift correlation (^{1}H – ^{1}H gCOSY and ^{1}H – ^{1}H ROESY), and 2D heteronuclear chemical shift correlation (^{1}H – ^{13}C HSQC, and ^{1}H–^{13}C HMBC) NMR spectra (Breitmaier, 2002). This was, in almost all of the cases, aided by molecular formula information obtained from a prior analysis of the High Resolution Electrospray Ionization Mass Spectrum (HRESIMS) of the compound, the only exception being compound 8 whose pseudomolecular ion was inferred to be unstable despite the soft ionization mode of the electrospray ionization technique (appendices 56 and 57) (Mclaffety and Turecek, 1993).

The two homonuclear correlation experiments used, i.e., gCOSY and ROESY are both ^{1}H – ^{1}H chemical shift correlation experiments. But while gCOSY, the pulsed field gradient (PFG)-selected version of the traditional absolute-value ^{1}H – ^{1}H correlation spectroscopy (simply referred to as COSY), is a through-bond (or *J* coupling) correlation experiment, ROESY, the Rotational Overhauser Effect Correlation Spectroscopy, is a 2D experiment which measures the dipolar or through-space interaction of coupling nuclear spins in a spin system (Jacobsen, 2007).

The heteronuclear 2D chemical shift correlation experiments used [i.e. ^{1}H – ^{13}C Heteronuclear Single Quantum Coherence (HSQC) and ^{1}H–^{13}C Heteronuclear Multiple Bond Coherence (HMBC)] are the modern inverse or ^{1}H-detected versions of the traditional ^{13}C-detected ^{1}H–^{13}C Heteronuclear Correlation experiments, i.e., *CH* Heteronuclear Correlation (HETCOR) and CH Correlation Over Long range Coupling (*CH* –COLOC) respectively, which are today getting out-of-favour because of the considerably longer time required for their acquisition. Both HSQC and HMBC are used to correlate ^{1}H and ^{13}C

chemical shifts; but while the former shows direct (one-bond) *CH* or ^{1}J correlation, the latter is biased to showing long-range *CH* correlations which are *CH* correlations over two, three or at times four bonds i.e. ^{2}J, ^{3}J or ^{4}J (Simpson, 2008).

The Distortionless Enhancement Polarization Transfer (DEPT)-edited version of HSQC, which in addition to its single quantum coherence selection pulse sequence also incorporates pulse sequences that transform the information of *CH* signal multiplicity and of spin-spin coupling into phase relationships (i.e. positive and negative amplitudes) of the ^{1}H-^{13}C cross peaks was used throughout. This version of the HSQC experiment more or less combined two experiments in one, as two pieces of information were obtained simultaneously from each HSQC spectrum plotted: One, the correlation of ^{1}H and ^{13}C resonances and two, the multiplicity of each *CH* cross peak depicting methyl (CH_3) and methine (*CH*) signals as positive amplitudes (shown as blue cross peaks) and methylene (CH_2) signals as negative amplitudes (shown as red cross peaks) (Appendices 4a-4c, 11a-11b, 19a-19c, 27, 35, 43a-43b, 51, 60a-60b and 68).

The HMBC experiment used was the pulsed field gradient-selected version in which coherence selection was largely by field gradients as opposed to phase cycling in the phase-sensitive DEPT-edited HSQC (Jacobsen, 2007).

By and large, the first step in the process of translating the spectra of each of the compounds into its respective structure was the cross-matching and subsequent labelling of resonances in the ^{1}H and ^{13}C spectra using the cross peaks in the HSQC spectrum which, by virtue of being DEPT-edited, also served as a means of identification of the multiplicity of each carbon resonance as primary, secondary, tertiary, thus more or less identifying every carbon–hydrogen bond in the molecule as well as the number of hydrogens attached at such bonds. Moreover, quaternary carbons were identified by counting the number of carbon resonances

that did not show cross peaks in the 2D DEPT-edited HSQC spectrum, and when such quaternary carbons signals were so weak that they were lost in the background noise, as it was the case for compound 7, long-range correlations shown to them in the gHMBC spectra by hydrogens on neighbouring non-quaternary carbons often let them out (appendices 51, and 53) (Simpson, 2008). Both labelled 1D spectra (^{1}H and ^{13}C) were then thoroughly gleaned for as many structural fragments as they could possibly offer using chemical shifts, multiplicity, coupling constants (*J)* and integration/relative signal intensities as main instruments.

Analysis of the gCOSY spectrum almost always followed, primarily to elucidate the geminal or vicinal relationships of signals in the proton spectra, in the process generating substructures or confirming those structural fragments earlier deciphered by the 1D ^{1}H and ^{13}C spectral analyses.

Piecing the fragments together, to arrive at the gross structure of the compound, was a multifactorial step which relied on the consideration of the ^{1}H and ^{13}C shifts, muliplet patterns and coupling constants of the resonances at the joints, but much more on the analysis of long range *CH* correlations obtained from the gHMBC spectra.

Gross structures were in most of the cases double-checked with the molecular formulae and their attendant degrees of unsaturation. Where this was not applicable because the molecular formula could not be determined by the High Resolution Electrospray Ionization Mass Spectrum (HRESIMS), molecular weight information from the Low Resolution ESIMS was very informative, e.g. compound 8 (section 5.2.8).

Finally, ^{1}H-^{1}H ROESY was used in conjunction with coupling constants analysis, where applicable, to assign relative configurations at points where geometric orientations of atoms or groups were consequential, particularly at chiral centres and isolated carbon-carbon double

bonds. In case the ^{1}H-^{1}H ROESY cross peaks were antiphase and were as such not in any way better than gCOSY cross peaks, making them unreliable for assigning such stereochemical orientations, coupling constants analysis alone was used and found to be as good as using a combination of the two methods, e.g., compound 4 (section 5.2.4).

The NMR Assignment Table for compound 9 could not be prepared because its set of NMR data acquired in CD_3OD were not sufficient to exclusively assign its proton and carbon-13 resonances, as there were a lot of overlaps in the proton spectrum that even the HSQC spectrum could not resolve, hence the conspicuous absence of its table of NMR data in the results. Acquiring the NMR spectra in other deuterated solvents like $CDCl_3$ and C_5D_5N would most probably have helped but time and financial constraints precluded this. Notwithstanding, a systematic (refined scifinder) data base search based on its molecular formula determined by HRESIMS analysis suggested its structure to be a monomethylester analogue of the dimethylester natural product serpentinine, the assignment of which carboxyl group was the methylester made easy with HMBC correlations analysis (appendix 69).

5.2.1 Structure Elucidation of Compound 1 (appendices 1-7).

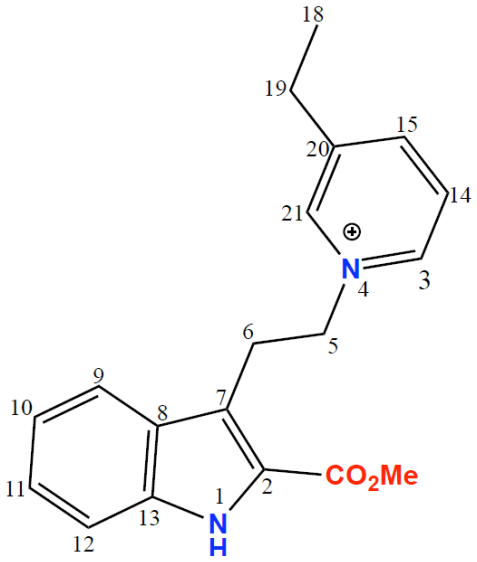

Compound 1: N- [2-(2-carbomethoxy-3-indolyl)ethyl]-3-ethylpyridinium (Fig. 25).

The molecular formula of Compound 1 was obtained on the basis of the analysis of the molecular ion $[M]^+$ peak at m/z 309.1607 in the positive mode of its HRESIMS (appendix 1) as $C_{19}H_{21}N_2O_2$. The calculated mass based on this formula was 309.1598 giving a ppm error of -2.9. The ^{13}C spectrum (appendix 3) showed 19 distinct resonances in agreement with the molecular formula. No spectrum was obtained in the negative mode of the HRESIMS probably for inability of the compound to form negative ions readily, more or less bringing suspicions of a positively charged compound. The suspicion that the compound was a positively charged compound was riveted by the non-integer degree of unsaturation (10.5) calculated from the molecular formula, a feature very commonly encountered with even electron cations (Mclaferty and Turecek, 1993).

The proton NMR spectrum (appendix 2) was perfectly first order. Analysis of coupling patterns, coupling constants, chemical shifts and relative integrals of this proton spectrum together with chemical shifts and relative intensities of the resonances in the ^{13}C spectrum(appendix 3) revealed five structural fragments namely; an ethyl – , a dimethylene chain – , a methoxy– , an ortho – disubstituted benzene ring and a pyridinium moiety.

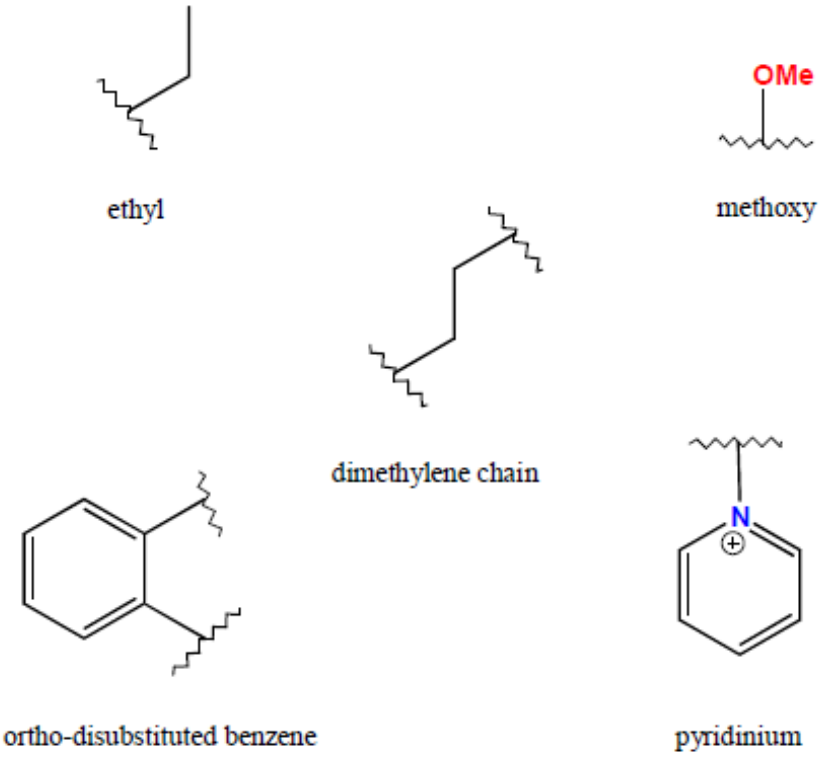

Fig. 35: Molecular fragments of compound 1.

The ethyl group was assigned based on the triplet at δ_H 0.88ppm (J = 7.6Hz) and quartet at δ_H 2.46ppm (J = 7.6Hz) with respective relative integrals of 3 and 2. The dimethylene chain was assigned based on the two triplets at δ_H 3.62ppm (J = 5.9 Hz) and 4.83ppm (J = 5.9 Hz), each with a relative integral of 2. The three-proton singlet at δ_H 3.62ppm was unequivocally a

methoxy group and was assigned as the methoxy of a carboxyl carbonyl resonance seen at δ_C 177.8ppm of the ^{13}C shift scale based on its distinct long range correlation to the latter in the gHMBC spectrum (appendix 6a), and thereby resulting in a carboxymethyl fragment.

The eight resonances in the aromatic region (of the proton spectrum) integrating to eight protons suggested that there were at least two aromatic rings in the molecule. The chemical shift (8.66ppm) and the coupling constant (5.6 Hz) of the doublet most down-field of these aromatic resonances are typical of the β – proton of the π – electron deficient heteroaromatic pyridine (Breitmaier, 2002). The aromatic resonances at δ_H = 7.68ppm, 8.10ppm, 8.47ppm, and 8.66ppm were thus ascribed to a pyridine ring, and analysis of their coupling patterns and coupling constants revealed that the pyridine ring was a meta – substituted one. The fact that the pyridine ring was attached to the molecule at some point placed the point of attachment on the ring nitrogen as there is no way it could have been at any other part of the ring without violating the coupling pattern seen in the proton spectrum. This of a necessity made the ring become positively charged, i.e., pyridinium, hence confirming the earlier suspicion that the molecule was positively charged. The coupling patterns and coupling constants of the remaining four aromatic resonances up-field to the pyridinium protons resonances i.e. the two doublets at δ_H6.61ppm (J = 7.9Hz) and δ_H 7.22ppm (J = 8.0 Hz), and the two pseudotriplets at δ_H 6.67ppm (J = 7.6 Hz) and δ_H 6.91ppm (J = 7.4 Hz) were certainly typical of an *ortho* – disubstituted benzene ring, one of the substituents being a +M electron-donating species, most likely an O– or N– heteroatom. The fact that the total number of oxygen atoms in the molecular formula had been accounted for in the carboxymethyl group and that there was yet one nitrogen to be accounted for, unequivocally made this substituent a nitrogen atom, and since the UV spectrum (appendix 7) showed a characteristic indole absorption maxima, all this put together were enough evidence that second aromatic ring was actually a 2, 3 –

disubstituted indole ring. Coming back to the *meta*– substituted pyridinium ring, the substituent at the *meta*– position was assigned as the ethyl group as the chemical shift of the protons of the methylene end of the ethyl group (δ_H 2.46ppm) showed that it was attached to an sp^2 carbon: The indole and pyridinium moieties were the only sources of sp^2 – hybridized carbon that the ethyl group could be attached to satisfy this chemical shift value, and since it couldn't have been on the indole without distrupting the coupling pattern already established, the only possible position of its attachment in the molecule was a *meta*– position on the pyridinium ring. The possibility of the dimethylene chain being the pyridinium *meta*– substituent was ruled out as the former's chemical shifts, δ_H 4.83ppm and δ_H 3.63ppm, fit that of a linker of the pyridinium ring at the ring nitrogen at one end and the indole at the other. The long range correlations shown by both the ethyl's methylene (δ_H 2.46ppm, q, J = 7.6 Hz, 2H) and methyl (δ_H 0.88ppm, t, J = 7.6 Hz, 3H) signals to the pyridine ring *meta*- carbon (δ_C = 145.9ppm) confirmed this.

All these put together reduced our working substructures to four: a 2, 3 – disubstituted indole group, a 3– ethylpyridinium moiety, a carboxymethyl group and a dimethylene chain. The 2D COSY spectrum confirmed these spin systems. Further analysis of the 2D gHMBC spectrum showed that the methylene protons at one end of the dimethylene chain, δ_H = 3.36ppm, t (5.9 Hz) 2H, showed long range correlations to the indole's 3– and 4– positions corresponding to positions 7 and 8 in the numbering order of the molecule (i.e. δ_C = 105.9ppm and δ_C = 130.0 repectively). In a like manner, the methylene protons at the other end of the chain, δ_H = 4.83ppm, t (5.9 Hz) 2H, showed long range correlations to the two β-carbons of the pyridine ring, i.e., δ_C = 143.2ppm and δ_C = 145.7ppm.

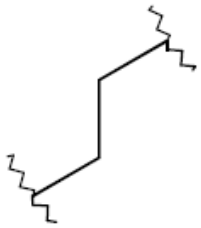

dimethylene chain

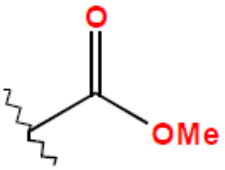

carboxymethyl

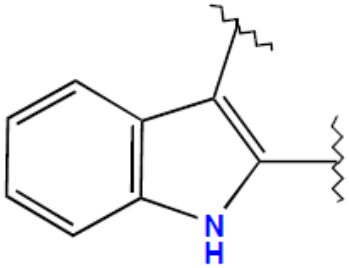

2, 3- disubstituted indole

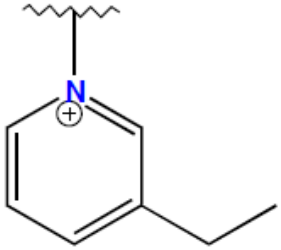

3- ethylpyridinium

Fig. 36: Further simplified molecular fragments or substructures of compound 1.

These correlations established the dimethylene chain as the linker of the indole and pyridine aromatic fragments of the molecule.

The ^{13}C chemical shift of the –OMe group which is more upfield than expected (δ_C = 36.5ppm as against 50 – 55ppm expected for such a carbon) (Breitmaier, 2002) can be explained by its spatial proximity to the lone pair on the indole ring nitrogen; its long range correlations to the carboxyl carbon (δ_C = 177.8ppm) as well as to the indole moiety's 2- and 3– positions corresponding to 2– and 7– positions in the numbering order of the molecule

(i.e. δ_C = 135.3ppm and 105.9ppm) confirmed not only that it was a carboxyl – OMe but also the point of attachment of the carboxymethyl group to the indole ring (Fig. 37).

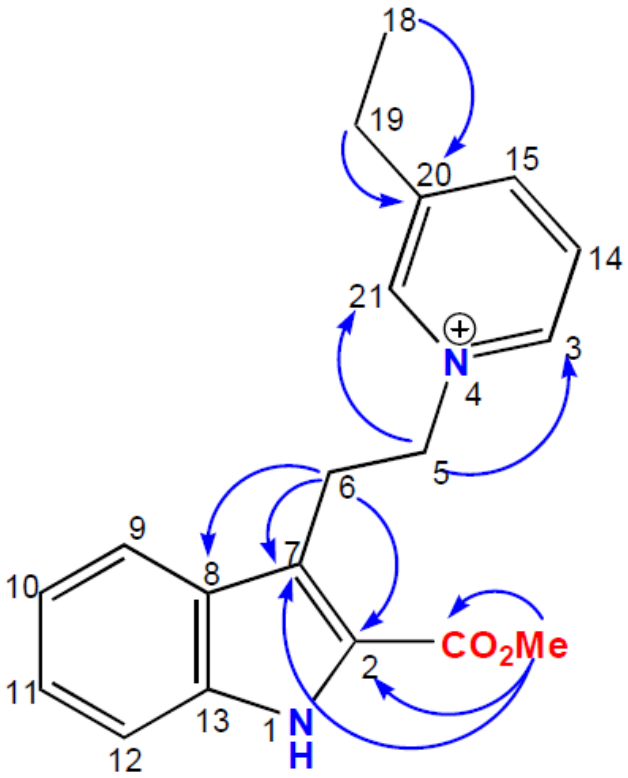

Fig. 37: Important ^{1}H-^{13}C HMBC correlations in compound 1.

5.2.2 **Structure Elucidation of Compound 2** (appendices 8-15)

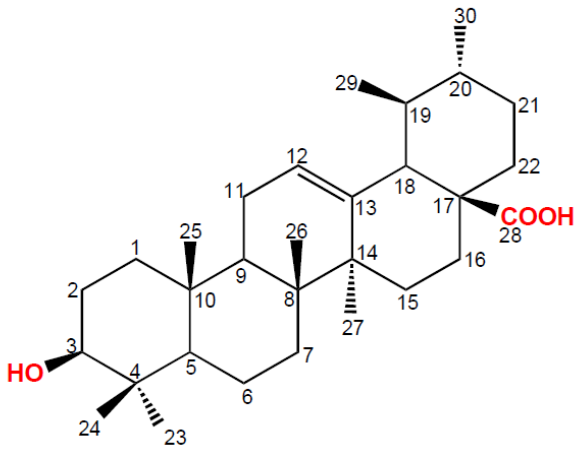

Compound 2: ursolic acid (Fig. 26).

Molecular formula was determined as $C_{30}H_{48}O_3$ based on the analysis of the $[M+Na]^+$ pseudomolecular ion at m/z 479.3475 in the positive High Resolution ElectroSpray Ionization Mass Spectrum (HRESIMS) of the compound. The calculated molecular mass based on this formula was 479.3496 giving a ppm error of 4.41. The ^{13}C spectrum at a glance showed 29 carbon resonances but after a careful analysis of the relative intensities of the resonances the accidental isochrony (Simpson, 2008) of two carbons resonating at δ_C = 48.4ppm became obvious, bringing the number of carbons to 30 and in agreement with the molecular formula, ruling out symmetry in the molecule. The molecular formula suggested seven degrees of unsaturation, two of which were easily accounted for by a C-C double bond (revealed by the signals at δ_H = 5.52ppm, br s; δ_C = 126.0ppm and δ_C = 139.6ppm of the ^1H and ^{13}C chemical shift scales) and a carboxyl double bond assigned to the resonance at δ_C = 180.3ppm in the ^{13}C spectrum. The remaining five unsaturations could only be accounted for by rings, and thus a molecule containing five rings was assumed.

The complicated nature of the proton spectrum upfield is typical of terpenoids and the identification of five tertiary methyl signals (also known as angular methyls in steroid and triterpenoid chemistry) (Bhart *et al*; 2005), coupled with the five rings earlier suggested by the molecular formula was a strong indication that the molecule was most probably a pentacyclic triterpenoid. So an initial assumption of a pentacyclic triterpenoid skeleton was made. The characteristic triterpenoid five tertiary methyls (δ_H = 0.90ppm, 1.05ppm, 1.08ppm, 1.25ppm, 1.26ppm) and two secondary methyl signals (δ_H = 0.91ppm and 1.02ppm) observed in the ^1H spectrum (appendix 9) confirmed that the molecule is a pentacyclic triterpenoid of the ursane skeleton. The assignments of these methyl groups were confimrmed by HMBC correlations (appendices 13a-13c). The position of the carboxylic acid group was assigned based on the HMBC correlations between Ha/b-16 (δ_H 2.14ppm, m, and 2.02ppm, m) and the carboxyl carbon, C-28 (δ_C 180.3ppm). In the same vein the position of the double bond was assigned based on the HMBC correlations H-12 showed to C-8, C-11, C-14 and C-18. The 3-OH group was assigned based on the HSQC correlation between a proton (H-3) (δ_H 3.48ppm, dd, *J* = 9.5, 5.8 Hz) and an oxygenated carbon (δ_C 78.4ppm), vis-a-vis the molecular formula. H-3 axial orientation was deduced by the large coupling constant (9.5Hz) it shows with one of the H-2 protons with which it is in a 1-2 diaxial trans coupling. This more or less confirmed the equatorial orientation of the 3-OH group and hence the β – orientation assignment of its relative configuration. The α-orientation assignments of H-23 (and hence the β-orientation of H-24), H-27 and H-30 were based on the strong ^1H-^1H ROESY correlation each of them showed to H-3 whose α-orientation had earlier been established.

Other relative configurations including that of the carboxyl group were largely assumed as the $[\alpha]_D$ agreed with literature value for ursolic acid (Thanakicharoenpath and Theanphong, 2007)

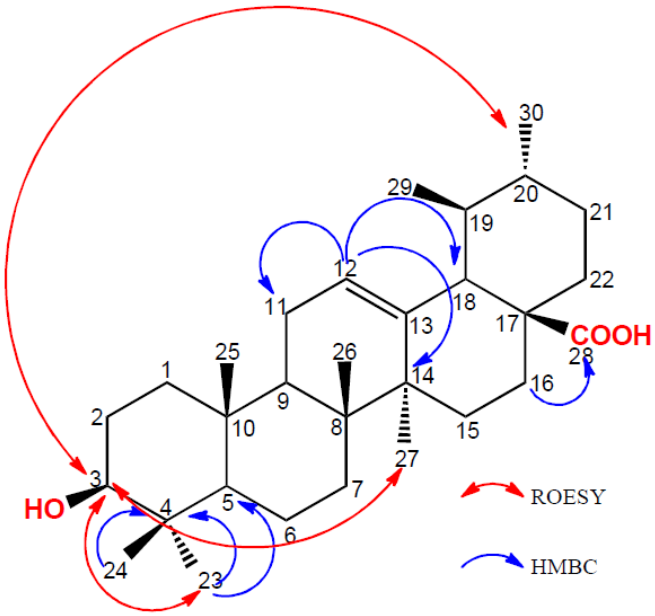

Fig. 38: Important ^{1}H-^{13}C HMBC and ^{1}H-^{1}H ROESY correlations in compound 2.

5.2.3 **Structure Elucidation of Compound 3** (appendices 16-23)

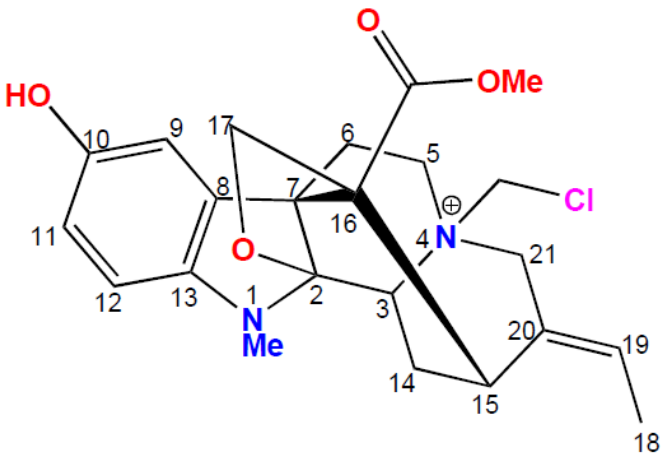

Compound 3: 4-chloromethylakuammineammonium ion (Fig. 27).

Analysis of the M^+ peak (suggestive of a positively charged compound) at m/z 431.1740 of the positive HRESIMS of compound 3 showed that it had an isotopic peak two atomic mass units heavier but one-third of its intensity, which was diagnostic of the presence of a covalently bonded chlorine atom in the molecule (McLafferty and Turecek, 1993). The molecular formula based on this peak, taking the presence of one chlorine atom into consideration, was $C_{23}H_{28}N_2O_4Cl$. The calculated mass based on this formula was 431.1732, giving a ppm error of -1.94. The $\{^1H\}$-^{13}C NMR spectrum showed 23 distinct resonances in agreement with this molecular formula, ruling out symmetry in the molecule. Further analysis of the ^{13}C spectrum showed a carboxyl carbonyl resonance, δ_C 171.9ppm, which was attributed to a carboxymethyl moiety (fragment **A**) based on the long range correlation peak an O – Me proton signal (δ_H = 3.80, s, 3H) showed to it in the gHMBC spectrum.

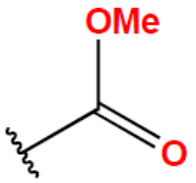

A

Fig. 39: Molecular fragment 'A' for compound 3.

The proton NMR spectrum revealed two resonances integrating to 3 protons in the aromatic region of the shift scale. A careful analysis of these rather shielded aromatic resonances revealed that they were two superimposed pseudotriplets (δ_H 6.65ppm) and a broad singlet (δ_H 6.68ppm) – a coupling pattern in agreement with a 1, 2, 4– tri– substituted benzene ring. Further analysis of the proton spectrum revealed an N –Me (δ_H = 2.82ppm, s, 3H) whose gHMBC long range *CH* correlation to a quaternary aromatic carbon-13 resonance (δ_C = 144.6ppm) showed that it was a substituent on the aromatic ring. Another quaternary aromatic ^{13}C resonance δ_C = 153.5ppm was unequivocally phenolic, and a further analysis of the gHMBC long range correlations of the aromatic protons established the *para* relative positioning of the OH and the N–Me aromatic substituents (table 3). The N-Me protons yet showed another HMBC correlation to a non-aromatic quaternary carbon (C-2) whose ^{13}C shift, δ_C=103.2ppm (in the range of sugar's anomeric cabon resonance) suggested it was sandwiched between two electron withdrawing heteroatoms, one of which has been established to be the N–Me nitrogen, the other being most likely oxygen as another nitrogen wouldn't have caused that much deshielding. The attachement of the Cl atom here was ruled out as there were other HMBC correlations to this carbon which wouldn't have been possible if the terminal Cl were the substituent. The partial structure (fragment **B**) emerging from the

aromatic ring was thus suggestive of an indoline ring in which the position-2 carbon is oxygenated. This suspicion was corroborated by the UV absorption pattern λmax (logε) 203nm (4.40), 241nm (3.80) 310nm (3.40) which quite supported the presence of an indoline chromophore (Wu *et al.*, 2010).

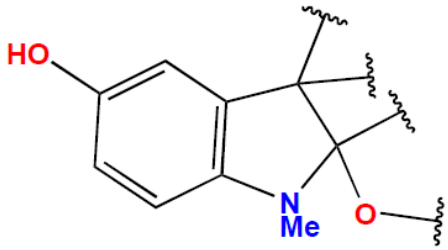

B

Fig. 40: Molecular fragment 'B' for compound 3.

The two doublets at δ_H 5.41 ppm (J = 9.8 Hz) and δ_H 5.33ppm (J = 9.8 Hz) were, on the bases of chemical shift and $^1H - ^1H$ coupling constants alone, erroneously suggestive of a cis double bond (appendix 17). A careful analysis of the DEPT-edited HSQC spectrum however showed them to be the resonances of a pair of heterotopic methylene protons with their carbon resonating at δ_C 72.8ppm on the ^{13}C shift scale. This ^{13}C shift initially suggested mono-oxygenation, but the fact that mono-oxygenated methylene protons would ordinarily not be deshielded to resonate as downfield as in the olefinic region of the proton shift scale gave room for the consideration of the possible attachment of the earlier spotted Cl atom (with a higher -I effect) at this point. However, because one chlorine atom also wouldn't have caused this much deshielding either, and there was a nitrogen yet to be accounted for in the molecular formula, this methylene was assigned as attached to nitrogen and to a chlorine

atom (fragment **C**), and thereby accounting for its highly deshielded protons and carbon as well as their very low ethane coupling constant referred to above. It also accounted for the improper phasing of their DEPT-edited HSQC cross peaks (appendix 19a), as the DEPT's transformation of *CH* multiplicities into a phase relationship, i.e., positive (blue cross peaks) for ethane and methyl carbons, and negative (red cross peaks) for methylene carbons, is also basically a *J* coupling affair (Breitmaier, 2002). Further analysis of the DEPT-edited HSQC spectrum revealed six more methylene groups (five of which were heterotopic pairs on the F_2 axis of the spectrum), and two methines in addition to the aromatic and ethylidene methines earlier established.

Further analysis of the proton spectrum revealed an ethylidene moiety based on the H-19 quartet at δ_H 5.83ppm (*J* = 7.1 Hz) integrating to 2 protons and the secondary methyl signal (H-18) at δ_H 1.66ppm (*J* = 7.1 Hz). The ethylidene (H-19) showed three ^4J COSY correlations; two, to the two heterotopic metylene protons Ha/b -21 (δ_H = 4.48ppm, d, *J* = 15.1Hz and δ_H = 4.06ppm, d, *J* = 15.1Hz) and the third, to H-15 (δ_H =3.80ppm, br s), which in turn showed strong COSY correlations to the Ha/b -14, δ_H = 2.69 ppm, d, (15.3 Hz), and δ_H 2.34 ppm, d, (15.3 Hz), which themselves showed strong COSY correlations to the H-3(ethane)signal, δ_H = 4.79, br s, leading to fragment **D**. Further analysis of the COSY spectrum revealed the isolated vicinal interactions of H-5 methylene protons, δ_H = 4.42ppm, ψt, (13.2 Hz), δ_H = 3.40, dd, (12.0, 5.4 Hz), and H-6 methylene protons, δ_H = 3.37ppm, dd, (15.5, 5.8 Hz), δ_H=1.88ppm, dd, 15.5, 5.4 Hz), i.e., fragment **E**. The ^{13}C shift of 17–methylene group (δ_C 74.9ppm) revealed oxygenation and the fact that its protons showed no COSY correlations outside the ethane interactions they showed to each other pointed to the fact that it was attached to an oxygen atom and a quaternary carbon, hence fragment **F**. The

structural interpretation of all these HSQC and COSY correlations are as shown in the partial structures shown in fig. 41 below:

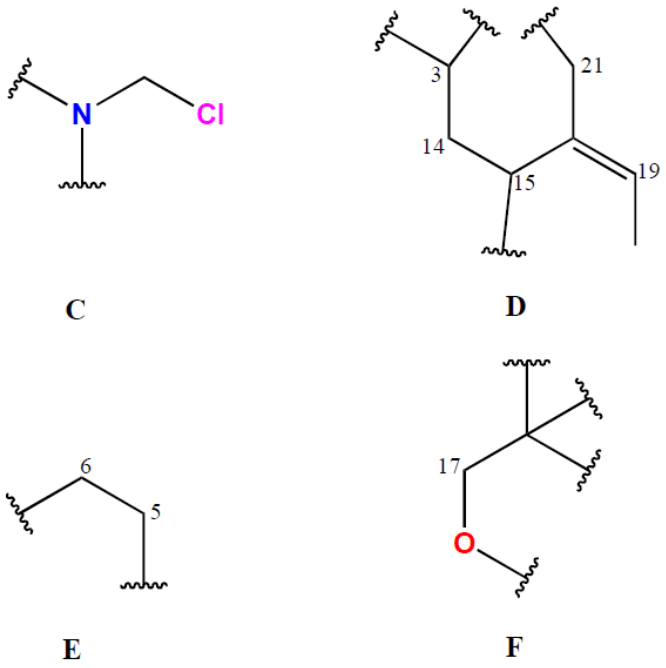

Fig. 41: Molecular fragments 'C', 'D', 'E' and 'F' of compound 3.

The ^{13}C shifts of C-3, C-5 and C-21 (δ_C 64.9ppm, 58.1ppm snf 62.4ppm respectively) suggested attachment to strong –I heteroatoms. The fact that all the heteroatoms in the molecular formula have however been accounted for strongly suggested the attachment of the trio to a common heteroatom and the only heteroatom that could satisfy this condition was the fragment B nitrogen which became essentially quaternized hence accounting for the more deshielded chemical shifts of the attached carbons than would have ordinarily been expected for non-quaternary nitrogen attachment. This also in principles explained the suspicion of a

positively charged molecule from the HRESIMS. Thus putting fragments C, D and E together in this fashion gave fragment **G**.

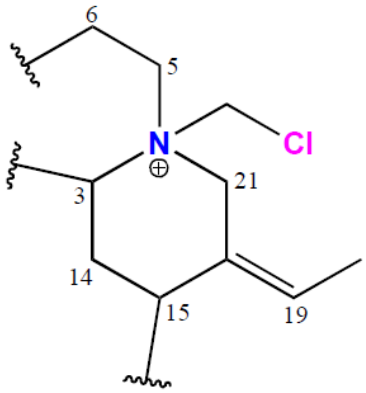

G

Fig. 42: Substructure resulting from piecing fragments 'C', 'D' and 'E' of compound 3 together.

The HMBC correlations of the ethane H-3, methylene H-6 and ethane H-15 (see table 3, and appendices 21a-c) supported piecing fragments A, F, and G together to arrive at the suggested gross structure. The α-orientation of H-15 was assumed for biosynthetic reasons (Wachsmuth, *et. al*., 2002), and the α-orientation of H-3 based on the correlation of H-15 to H-3 in the ^{1}H-^{1}H ROESY spectrum. The geometry of the ethylidene side chain was assigned as (E) based on the ROESY correlation between the ethylidene (H-19) and the axial methylene proton at position -6 (i.e. Hb-6), which could not have been possible with (Z) configuration. All these spectral data show that Compound 3 is an N_4-chloromethyl analogue of the known natural product akuammine (Ramirez and Garcia-Rubio, 2003).

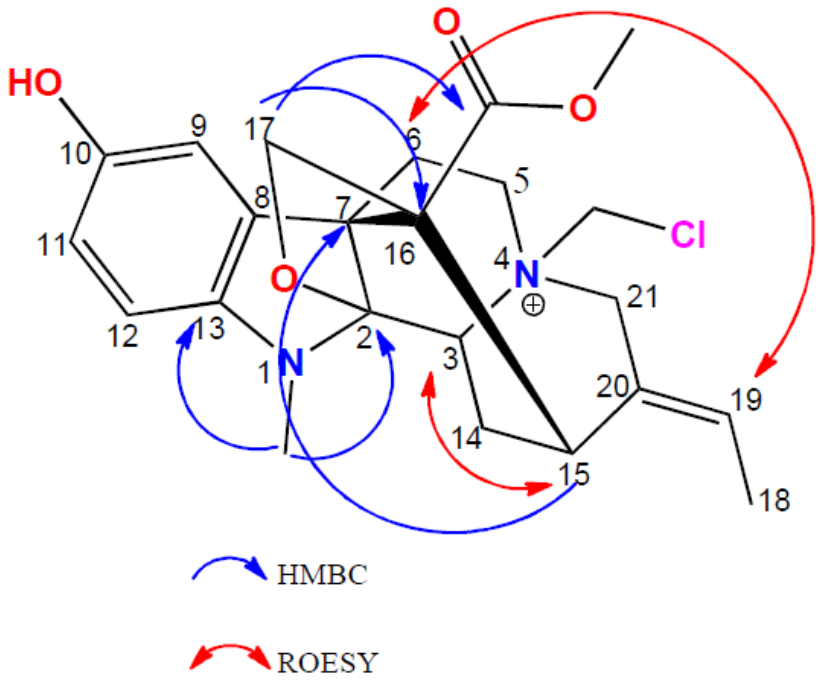

Fig. 43: Important ^{1}H-^{13}C HMBC and ^{1}H-^{1}H ROESY correlations in compound 3.

5.2.4 **Structure Elucidation of Compound 4** (appendices 24-31)

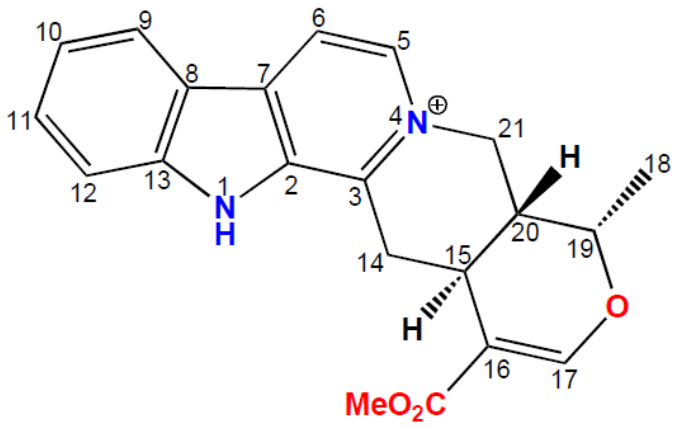

Compound 4: serpentine (Fig. 28).

The molecular formula of compound 4 was determined as $C_{21}H_{21}N_2O_3$ based on the analysis of the molecular ion $[M]^+$ peak at m/z 349.1557 of its HRESIMS (appendix 24). The calculated mass based on this formula was 349.1547, giving a ppm error of -3.09. The ^{13}C spectrum (appendix 26) showed 21 distinct resonances in agreement with the molecular formula, indicating lack of symmetry. Analysis of the aromatic region of the proton spectrum (appendix 25) revealed seven resonances integrating to seven protons. The carbon – 13 shift (δ_C 157.3ppm) corresponding to of one of these protons (δ_H7.74ppm) in the DEPT-edited HSQC spectrum (appendix 27) was quite too downfield for such an unsubstituted aromatic carbon: A phenolic carbon that could probably be as deshielded would essentially be quaternary, casting doubt on the aromatic nature of this proton but strongly suggesting an enol or enol ether double bond proton. (Fragment **A**). Lack of characteristic vinyl ABM system or any coupling partner in the olefinic region of the proton spectrum strongly suggested the quaternary nature of the second double bond carbon.

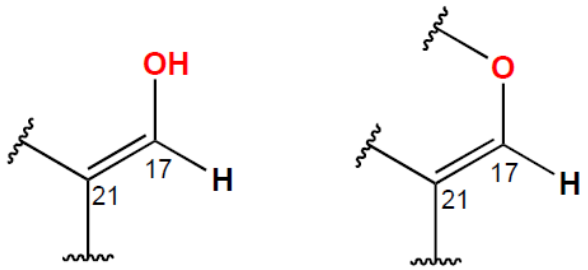

A: enol or enol ether

Fig. 44: Molecular fragment 'A' of compound 4.

Further analysis of the aromatic region of the proton shift scale revealed coupling patterns and coupling constants (δ_H 8.39, ddd, ppm,d, J = 8.2, 2.0, 1.1 Hz, δ_H 7.80ppm, ddd, J = 7.2, 5.8, 1.0 Hz, δ_H 7.76ppm, ddd, J = 8.2, 2.0, 1.0 Hz, and δ_H 7.47ppm, d, J = 7.0, 5.8, 1.0) that agreed with an ortho-disubstituted benzene ring, which together with the characteristic aromatic AB spin system (δ_H 8.53ppm, d, J = 6.5, δ_H 8.47ppm, d, J = 6.5) is typical of the β-carbolinium ring system of which the UV spectral data [UV (MeOH) λ_{max} (logε) 206nm (4.480), 251nm (4.38), 308nm (4.21), 364nm (3.54)] was also characteristic (Wachsmuth *et. al.*, 2002), and hence the arrival at fragment **B**.

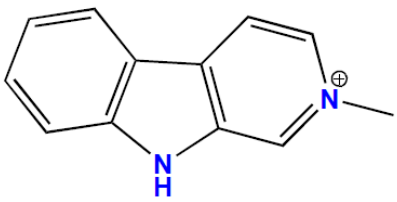

B: β – carbolinium

Fig. 45: Molecular fragment 'B' of compound 4.

The gCOSY spectrum revealed the methyl doublet at δ_H 1.49ppm (H-18) as showing a strong COSY correlation to the H-19 methine (δ_H 4.03, qd, *J* = 6.0, 2.0Hz). The latter showed correlation to the H-20 methine proton (δ_H 2.57ppm, m) which in turn showed three distinct strong correlations; two to the H-21 heterotopic methylene protons (δ_H 5.04, dd, *J* = 14.3, 5.9 Hz; δ_H 4.70, dd, *J* = 14.3, 5.2 Hz) and the third to the H-15 methine proton (δ_H 3.22, m) which on another hand showed strong geminal correlations to the heterotopic H-14 pair (δ_H 4.17, dd, *J* = 14.3, 6.3 Hz; δ_H 3.38, dd, *J* = 17.7, 9.3). The chemical shift (δ_H 1.49ppm) of the H-18 methyl doublet was indicative of attachment to an oxygenated carbon. This suspicion was confirmed by both the ^{13}C and ^{1}H shifts (72.6ppm and 4.03ppm respectively) of the 19-methine group to which it is attached. This series of COSY correlations were thus structurally translated into the partial structure (fragment **C**) in fig.46.

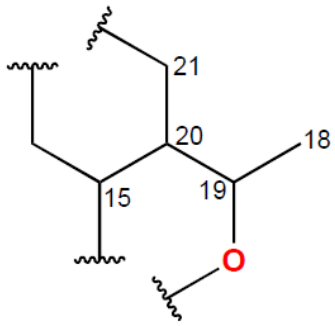

C

Fig. 46: Molecular fragment 'C' of compound 4.

Further analysis of the proton spectrum revealed an unequivocal O-Me signal (δ_H = 3.80ppm, s, 3H) which was attributed to a carboxymethyl group (fragment **D**), based on the carboxyl

carbonyl resonance, δ_C 169.0ppm, in the broad band proton-decoupled ^{13}C spectrum, and the long range correlation the methyl signal in question showed to it in the gHMBC spectrum.

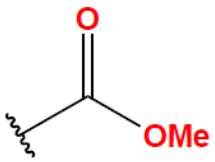

D: carboxymethyl

Fig. 47: Molecular fragment 'D' of compound 4.

Further analysis of the gHMBC spectrum revealed the long range correlations of H-15 to a quaternary carbon (δ_C 109.4ppm) in the aromatic/olefinic region of the ^{13}C shift scale, which without doubt was the quaternary double bond carbon of the earlier mentioned enol/enol ether fragment; another H-15 HMBC correlation to the enol carbon C-17 (δ_C 157.3ppm) confirmed this, while the remaining H-15 HMBC correlations to C-19 (δ_C 72.6ppm) and C-20 (δ_C 37.3ppm) confirmed a ring system ruling out the possibility fragment **A** being an enol. The HMBC correlations of Ha/b -21 to C-6 (δ_C 134.1ppm) and Ha/b-14 to C-2 (δ_C 141.6ppm) confirmed the attachment position of fragment **C** to the β-carbolinium fragment. And hence the suggested gross structure of compound 4.

The α-orientation of H-15 was assumed for biosynthetic reasons (Wachsmuth, *et. al.*, 2002). Two large coupling constants observed for each of the axial proton resonances of H-14 and H-21 (δ_H 17.7, 9.3Hz and 14.3, 10.3Hz respectively) showed their 1, 2 diaxial trans coupling with H-15 and H-20 respecitively which in turn showed that H-15 and H-20 are co-axial and hence mutually trans.

The small coupling constant (2.0Hz) of H-19 must be due to its coupling to H-20 (its larger coupling constant, 6.0Hz, haven been ascribed to its *J*-coupling to the H-18 methyl). This implies an equatorial-cis orientation of H-19 relative to H-20 which is axial, and hence the relative configuration of H-18 methyl. This could not be corroborated by the ROESY correlation between H-19 and H-20 which was antiphase (appendix 30a). The entire spectra data conformed to those of the known MTIA – serpentine (Wachsmuth *et. al.*, 2002).

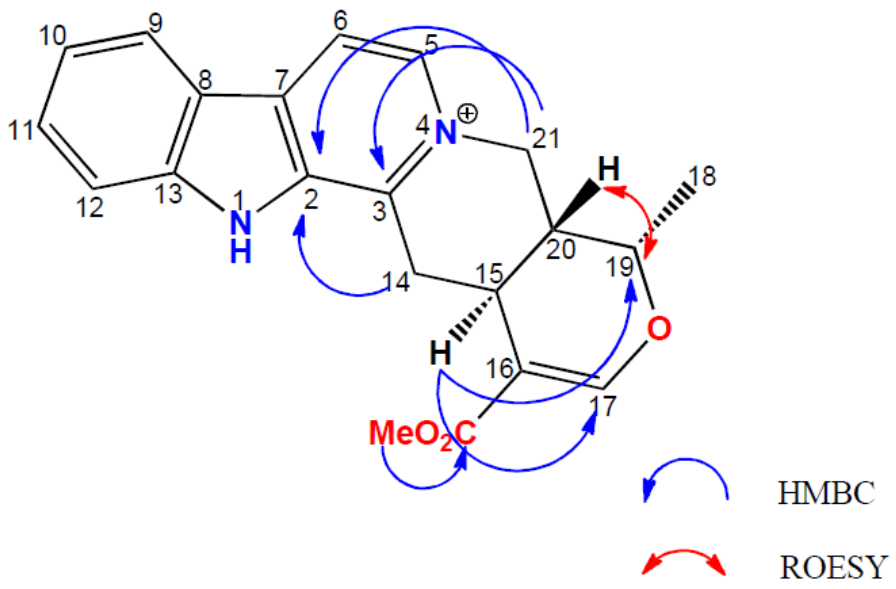

Fig. 48: Important ^{1}H-^{13}C HMBC and ^{1}H-^{1}H ROESY correlations in compound 4.

5.2.5 **Structure Elucidation of Compound 5** (appendices 32-39).

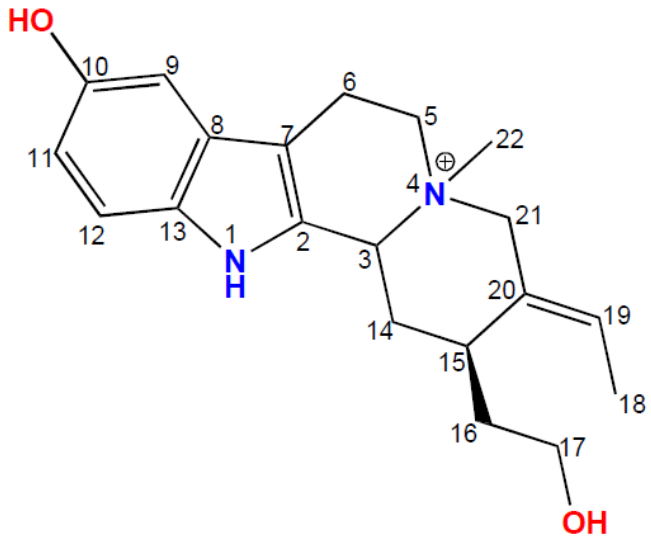

Compound 5: 4-methylhuntrabrineammonium ion (Fig. 29).

Molecular formula was determined on the basis of the molecular ion, $[M]^+$, peak at m/z 327.2070 of the High Resolution Electro-Spray Ionization Mass Spectrum (HRESIMS) as $C_{20}H_{27}N_2O_2$. The calculated molecular mass based on this formula was 327.2067, giving a ppm error of -0.92. Analysis of the ^{13}C spectrum revealed 17 conspicuous resonances, three carbons short of the number of carbons in the molecular formula. A closer look at the ^{13}C spectrum and the DEPT-edited HSQC spectrum accounted for the missing carbons as follows: C-13 and C-20 resonances were seen to be accidentally isochronous, resonating at δ_C 131.8ppm in the ^{13}C shift scale; C-21 (which though not a quaternary carbon, but nevertheless had its ^{13}C resonance lost in the background noise for reasons not unconnected to relaxation issues) was revealed by the HSQC spectrum to resonate at δ_C = 62.5ppm; an N–Me carbon whose resonance was effectively overlapped by the solvent (MeOH) signal was

also revealed by the HSQC spectrum. The coupling patterns of the aromatic signals of the ^{1}H NMR spectrum were reminiscent of a 1, 2, 4– trisubstituted benzene. This aromatic substitution pattern coupled with the UV absorption pattern [UV spectrum (UV (MeOH) λ_{max} (logε) 209nm (4.84), 272nm (3.99), 308nm (3.54)] which is approximately that of a tetrahydro-β-carboline chromophore (Wachsmuth, *et. al.*, 2002) suggested the presence of 10-substituted tetrahydro-β-carboline skeleton in the compound.

The aromatic/olefinic carbon-13 resonance at δ_C=150.8ppm of the broad band proton decoupled ^{13}C NMR spectrum was identified as phenolic, thus suggesting that the substituent on the aromatic ring of the tetrahydro-β-carboline ring system was a hydroxyl group**.**

Further nalysis of the HSQC spectrum revealed two methine signals, two methyl signals (one of which was the N–Me mentioned above) and six methylene signals, five of which were heterotopic pairs. The gCOSY spectrum analysis showed two of the methylene groups (Ha/b-5 and Ha/b-6) in an isolated spin system, a feature corroborating the presence of the tetrahydro-β-carboline ring system (Structural fragment **A**), and confirmed by the long range correlations of both the H-5 (δ_H 3.88ppm, m, δ_H 3.86ppm, m) and H-6 (δ_H 3.16ppm, m, δ_H 3.08ppm, m) methylene proton pairs to C-3 (δ_C 29.7ppm) and C-7 (δ_C 103.4ppm).

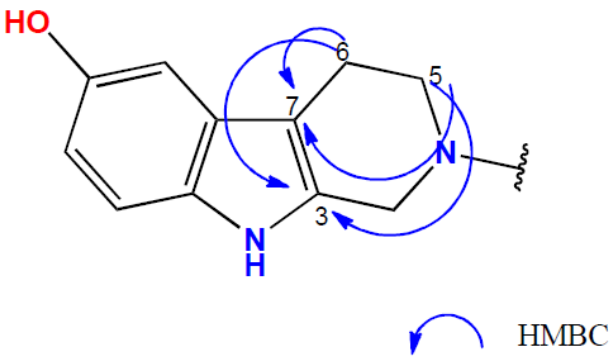

A: tetrahydro-β-carboline scaffold

Fig. 49: Molecular fragment 'A' of compound 5.

Analysis of the gCOSY spectrum showed H-3 methine (δ_H 4.65ppm, br s) in strong COSY correlations to the H-14 heterotopic pair (Ha-14 δ_H 2.64 ppm, m, and Hb-14 δ_H 2.30 ppm, m,) which in turn showed strong correlations to the H-15 methine (δ_H 3.24 ppm dd, J = 14.5, 7.2 Hz) which also showed strong COSY correlations to Ha/b-16 methylene protons (δ_H 1.60ppm, m, and δ_H 1.43ppm, m, respectively), the latter also observed to be in vicinal correlations to the homotopic H-17 methylene protons (δ_H 3.51ppm, m), the ^{13}C shift (δ_C 58.6ppm) of which implied oxygenation most likely by a hydroxyl group, more or less accounting for the second oxygen in the molecular formula. On another hand, further analysis of the proton spectrum revealed an ethylidene moiety based on the H-19 olefinic quartet (δ_H 5.98ppm, J = 7.0 Hz) and the H-18 methyl double doublet (δ_H 1.84ppm, J = 7.0, 1.4 Hz) signals. The ethylidene methyl was found to show a strong COSY correlation to the olefinic quartet and a weaker ^5J (long range COSY) correlation to Ha-21 (δ_H 4.36ppm, m). Structural translation of these series of COSY correlations resulted in the structural fragments **B** and **C** shown in fig. 50.

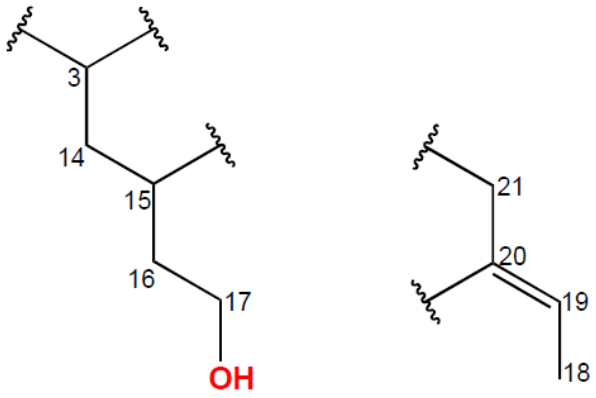

B **C**

Fig. 50: Molecular fragments 'B' and 'C' of compound 5.

The gHMBC spectrum analysis revealed the C-3 carbon to be the isolated carbon of the C-ring of fragment A, on the basis of the long range *HC* correlations between Ha/b-5 and Ha/b-6 and C-3, and C-21 was shown to be attached to the tetrahydro- β- carboline fragment at the ring C nitrogen based on the long range correlations of Hb-21 to C-3 and the quaternary aromatic carbon, C-2(δ_C 131.8ppm). Positions 15 and 20 respectively on fragments B and C were also fused based on the long range correlations of Hb-21 (δ_H 3.69ppm, m) to C-20 (δ_C 127.8ppm) and C-15 (δ_C 30.2ppm), while the N-Me was assigned as on N-4 based on its protons' long range correlation with C-3, C-5, and C-21, and hence the gross structure of compound 5. The α-orientation of H-15 was assumed for biosynthetic reasons.

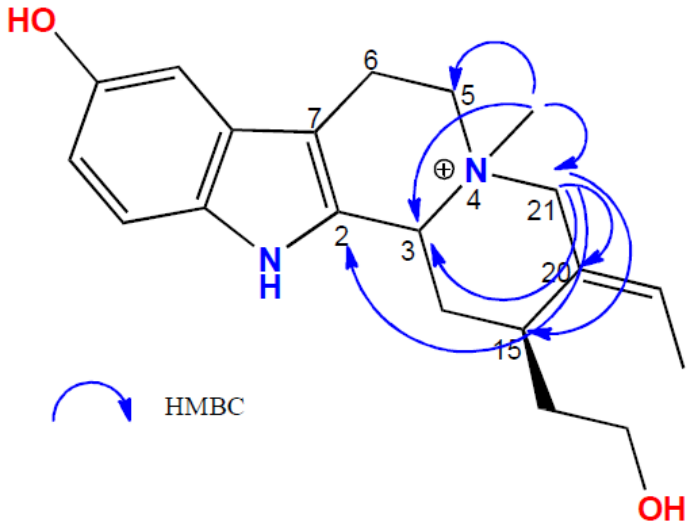

Fig. 51: Important ^{1}H-^{13}C HMBC correlations in compound 5.

5.2.6 Structure Elucidation of Compound 6 (appendices 40-47)

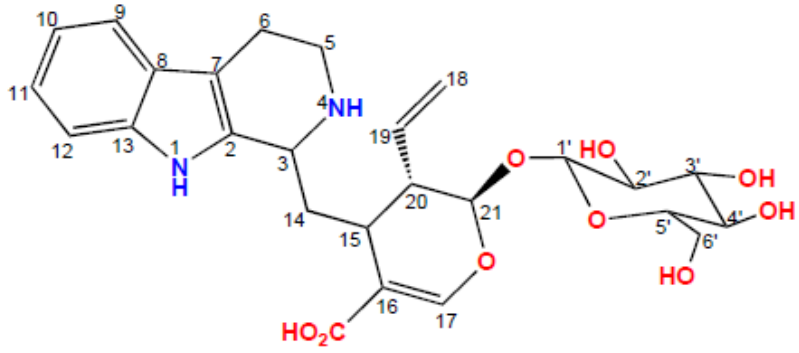

Compound 6: Strictosidinic acid (Fig. 30).

Obtained as a yellow crystalline substance, $[\alpha]_D$ -177.7 (c 0.067, MeOH), compound 6 had the molecular formula $C_{26}H_{32}N_2O_9$ (calcd mass = 517.2181, err -1.32ppm), determined on the basis of the pseudomolecular ion $[M+H]^+$ peak at m/z 517.2187 of its positive High

Resolution ESI Mass Spectrum. Analysis of the DEPT-edited HSQC spectrum showed that the compound contained fifteen methine and five methylene groups. In addition the proton broad band decoupled ^{13}C spectrum revealed six quaternary carbons, including a carboxyl carbonyl carbon (COO–), all of which showed no correlations in the HSQC spectrum.

The UV spectrum exhibited characteristic absorption maxima (λ_{max}) at 273nm (logε = 3.9) and 208nm, (logε = 4.9) typical of the tetrahydro – β – carboline chromophore (Wachsmuth *et al*., 2002). The presence in the proton spectrum of four aromatic resonances (H-9 δ_H 7.32ppm, d, *J* = 7.0Hz; H-10 δ_H 7.14 ppm, dd *J* = 8.0, 7.0Hz; H-11 δ_H 7.05 ppm, dd, *J* = 8.0, 7.0Hz; H-12 δ_H 7.47ppm, d, *J* = 8.0Hz) assignable to an *ortho*-disubstituted benzene, coupled with two heterotopic pairs of methylene protons (Hα-5 δ_H 33.75ppm *J* = 9.7, 5.6, 4.1 Hz, Hβ-5 δ_H 3.41ppm, m; and Hα-6 δ_H 3.05 ppm, m; Hβ-6 δ_H 3.04ppm, m) which the gCOSY spectrum showed to be in an isolated vicinal coupling, and the methine (H-3 δ_H 3.05ppm, m) confirmed the presence of a tetrahydro-β-carboline ring system substituted at the 3- position (Fig. 52) .

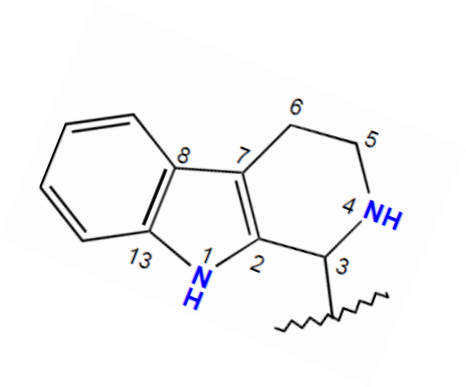

A

Fig. 52: Molecular fragment 'A' of compound 6.

The ^{13}C shift (δ_C 157.3 ppm) of the remaining aromatic resonance in the proton spectrum was too downfield for an unsubstituted aromatic carbon, more or less ruling out the possibility of

the signal being aromatic. Only a phenolic carbon could give a ^{13}C aromatic resonance as deshielded, and at any rate it must essentially be quaternary. The signal must have therefore resulted from a proton attached to an oxygenated double bond carbon, thus suggesting the presence of an enol or enol ether fragment in the molecule. The fact that the enol methine proton was an isolated singlet and had no *J* coupling relationship especially to any signal in the olefinic region of the proton shift scale showed that its carbon was doubly bonded to a quaternary carbon thereby resulting in the fragment B (Fig. 53) below:

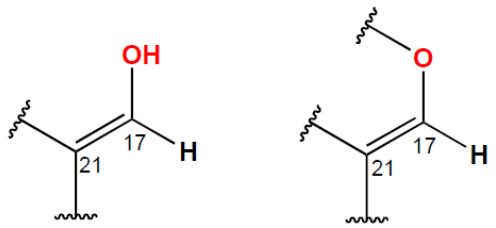

B : enol or enol ether

Fig. 53: Molecular fragment 'B' of compound 6.

Moving up-field from the aromatic region of the proton shift scale were two superimposed methine signals (a doublet, *J* = 9.0Hz and a triple doublet, *J* = 17.5, 11.0, 7.0 Hz), resonating at δ_H = 5.86ppm. Analysis of the gCOSY spectrum revealed the triple doublet as resulting from the olefinic methine proton (H-19) of a vinyl ($-CH=CH_2$) ABM spin system, the two triple doublets at δ_H 5.36ppm (*J* = 17.4, 2.4, 1.3 Hz) and δ_H 5.27ppm (*J* = 17.4, 2.4, 1.3 Hz) (Ha-18 and Hb-18 respectively) being the AB part of the system. The fact that there were three resolvable coupling constants in each of the three signals of the vinyl ABM spin system indicated that the vinyl group was attached to a methine carbon. This suspicion was confirmed by a futher analysis of the gCOSY spectrum which showed the vinyl methine proton in a strong correlation to another methine, H-20, (δ_H 2.76 ppm, m), which in spite of

its unresolvable coupling constants, was shown to have two additional COSY correlations: one to the H-15 methine (δ_H 3.05ppm, m) and the other to the H-21 methine doublet (δ_H 5.86ppm, *J* = 9.0Hz) superimposed on the vinyl methine signal, and whose ^{13}C shift (δ_C 97.2ppm) indicated it to be most probably an acetal carbon (Breitmaier, 2002) thus accounting for two out of the yet seven outstanding oxygens, and giving a new outstanding of H_5O_5. The strong COSY correlations between H-15 methine and the Ha/b-14(δ_H 2.36ppm, dddd, *J* = 17.7, 15.1, 12.5, 3.0 Hz, and δ_H 2.22ppm, dddd, *J* = 18.0, 15.4, 12.1, 3.8 Hz) revealed the vicinal relationship of the H-15 with the H-14 geminal pair. The above series of COSY correlations were structurally translated into the fragment **C** as seen in fig. 54.

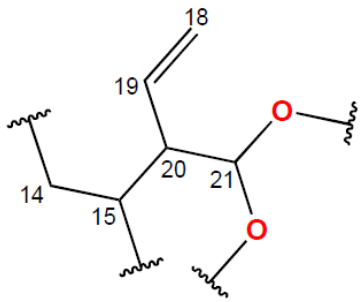

C

Fig. 54: Molecular fragment 'C' of compound 6.

Further analysis of the COSY spectrum which revealed the strong COSY correlations between H-3 and the H-14 pair established the link between fragments A and C via C-3 and C-14. Analysis of the gHMBC spectrum revealed that fragment B was the link between C-15 and C-21 positions on fragment C via one of the acetal oxygens on the basis of the

strong long range *HC* correlations of H-17 to C-15, C-16, C20, C-21, which also confirmed that fragment A was an enol ether, ruling out a terminal enol. In addition, H-17 showed another long range correlation to the carboxyl carbonyl carbon (16 –COO–), establishing the attachment of the latter to C-16. There was no other HMBC correlations to the carboxyl carbonyl, neither was there any O–Me or O– alkyl spin systems decipherable in the proton and/or ^{13}C spectra to suggest an ester linkage to it, thereby confirming the carboxyl group as carboxylic acid. A further analysis of the proton spectrum showed that the methine resonance at δ_H 4.82ppm, br d, J = 11.2 Hz whose ^{13}C shift (δ_C 100.6ppm) also indicated acetal linkage was typical of a sugar molecule anomeric proton. This was confirmed by tracing the coupling partner to an oxygenated methine multiplet at δ_H 3.02ppm using an expansion of the gCOSY spectrum. All the remaining resonances to be assigned were in the region of the shift scale characteristic of typical sugars' hydroxylated methines and methylenes and the outstanding formula suggested a hexose sugar, the anomeric proton resonance exhibition of which confirmed it to be an aldopyranose. The large coupling constant of the anomeric proton signal pointed to a 1, 2 – diaxial trans relationship of the anomeric proton to the sugar's H-2' proton, more or less confirming that the O – glucopyranosyl linkage was β as well as confirming the equatorial orientation of all the pyranose ring substituents – the hydroxyls and the 5' – hydroxymethyl (Jacobsen, 2007). Position C-21 as the glucopyranosyl linkage point was confirmed by the *HC* long correlation of the glucopyranose anomeric proton (H-1') to C-21(δ_C 97.4ppm).

The α-orientation of the H-15 methine was assumed for biosynthetic reasons. The large coupling constant (9 Hz) of H-21, a 1, 2- diaxial trans coupling constant in chair-locked cyclohexane /cyclohexene system, revealed that H-21 and H-20 were coaxial. That H-15 was co-axial with them was revealed by the ^1H – ^1H ROESY correlation between H-21 and H-15,

confirming that H-15 was trans relative to H-20 but cis with respect to H-21. H-3 also was assigned an α-orientation (i.e. cis to H-15) based on its correlation to H-15 in the ^{1}H – ^{1}H ROESY spectrum. The deduced structure is that of the known MTIA – strictosidinic acid (do Nacimento *et al.*, 2006).

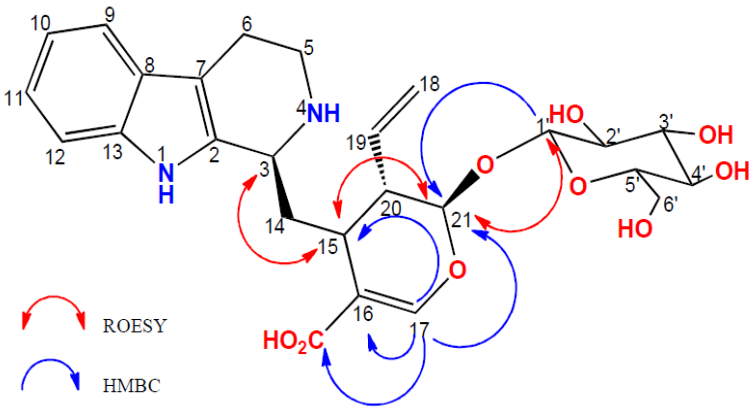

Fig. 55: Important ^{1}H-^{13}C HMBC and ^{1}H-^{1}H ROESY correlations in compound 6.

5.2.7 **Structure elucidation of compound 7** (appendices 48-55).

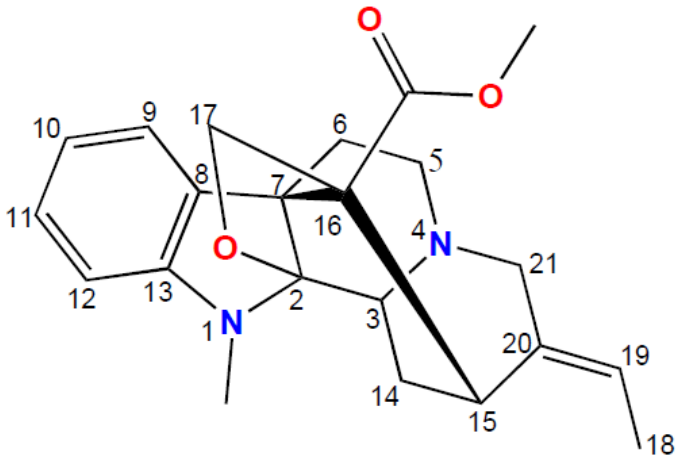

Compound 7: Pseudoakuammigine (Fig. 31).

The molecular formula of compound 7 was determined as $C_{22}H_{26}N_2O_3$ by the analysis of the $[M+H]^+$ pseudomolecular ion peak in its positive High Resolution Electro–Spray Ionization Mass Spectrum (HRESIMS). The proton broad band- decoupled ^{13}C NMR spectrum had a low signal to noise ratio raising the suspicion of possible loss of Some signals in the back ground noise of the spectrum which was observed to show only 15 distinct signals compared to the 22 suggested by the molecular formula. This suspicion was confirmed by a careful inspection of the gHMBC spectrum which showed six correlation peaks at F_1 co-ordinates (δ_C = 59 ppm, 101 ppm, 132ppm, 139ppm, 153ppm and 172ppm) with no visible ^{13}C signals. These were assigned to six (C-16, C-2, C-20, C-8, C-16 and COO respectively) of the seven quaternary carbons in the compound on the basis of their chemical shifts and HMBC correlations to neighbouring

hydrogens. The seventh quaternary carbon, C-7, was shown to be accidentally isochronous with the C-21 ^{13}C resonance to which Ha-17 appeared to be showing long range correlation: A careful inspection of this cross peak showed that it was too intense for such a ^{5}J *HC* correlation: Such an intense cross peak could have only resulted from a ^{3}J correlation to C-7, showing that C-7 and C-21 were isochronous. The ^{1}H NMR spectrum showed four aromatic resonances (δ_H 7.21ppm, td J = 7.7, 1.2 Hz; δ_H 7.14ppm, J = 7.7 Hz; δ_H 6.86ppm, td J = 7.7, 1.2 Hz; δ_H 6.81ppm, d J = 7.7 Hz) assignable to an *ortho* di – substituted benzene ring, indicating that the suspect indoline ring system was unsubstituted at the benzene ring component part .

Further analysis of the ^{1}H and gHMBC spectra revealed the following fragments: An ethylidene moiety based on the olefinic quartet (H-19) at δ_H 5.81ppm, J = 7.0 Hz and the methyl double doublet (C-18) at δ_H 1.66ppm, J = 7.0, 2.7 Hz; an N–Me (δ_H 2.86, s, 3H) ascribed to N-1 based on HMBC correlations shown to C-13; and an O–Me (δ_H 3.80ppm, s, 3H) ascribed to a carboxymethyl based on HMBC correlation shown to the carboxyl carbonyl resonance at δ_C 172.3ppm. The gCOSY spectrum showed the ethylidene's double bond proton (H-19) in long range (^{4}J) correlations(made possible by the intervening double bond) to Ha-21(δ_H 4.73, d, J = 15.6 Hz) and H-15 methine (δ_H 3.80ppm, br s) which on another hand showed strong correlations to the two H-14 heterotopic pair (δ_H 2.64, dd, J = 16.8, 5.0 Hz , and δ_H 2.31, ddd, J = 16.5, 3.5, 1.6 Hz) ,and which in turn showed strong correlations to the H-3 methine (δ_H 4.62ppm, br s). The isolated vicinal correlations of two pairs of heterotopic methylene protons, Ha/b -5 and Ha/b -6, was also revealed by the gCOSY spectrum analysis. With the consideration of one more nitrogen to be accounted for, having ascribed the third oxygen in the formula to an ether linkage between C-17 and C-2, and considering the heteroatom attachment suggestion of both the proton and ^{13}C shifts of

positions 3, 5, and 21, linking the fragments to yield an akuammine skeleton (see Fig. 27) was proposed and confirmed by HMBC correlations between Ha-5 and C-3 on the one hand, and Ha-5 and C-21 on the other.

The α-orientation of H-15 which has always been assumed for biosynthetic reasons set the pivot for the relative configurations around the stereogenic centres at C-15, C-16 and C-7. The ethylidene side chain double bond geometry was assigned as (E) on the basis of the $^{1}H - {}^{1}H$ ROESY cross peak between H-19 and Ha-21 which couldn't have been possible if the geometry were (Z). This showed compounds 7 to be the known natural product pseudoakuammigine (Ramirez and Garcia-Rubio, 2003), and to be geometrically isomeric to compound 3 with respect to the ethylidene side chain orientation.

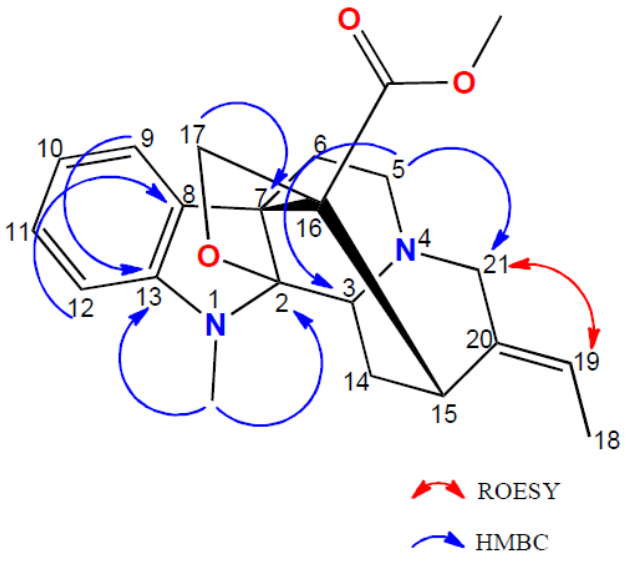

Fig. 56: Important ^{1}H- ^{13}C HMBC and ^{1}H-^{1}HROESY correlations in compound 7.

5.2.8 Structure Elucidation of Compound 8. (appendices 56-64)

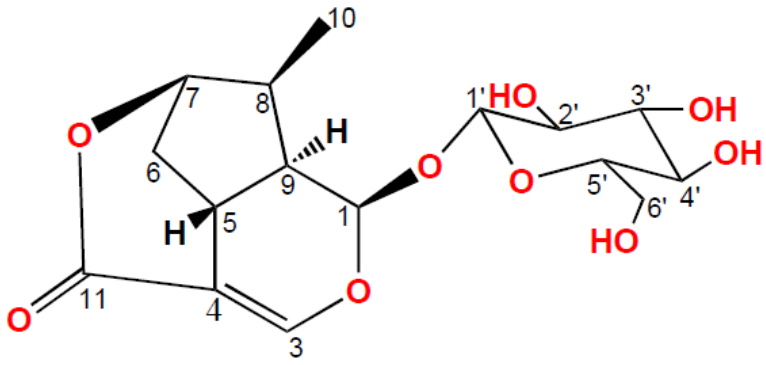

Compound 8: 1-glucopyranosyl-8-methyliridan-3-en-4, 7-carbolactone (Fig. 32).

The low resolusion ESI mass spectrum showed low intensity $[M+H]^+$ and $[M+MeOH+H]^+$ psuedomolecular ion peaks at m/z 359.1 and 394.1 respectively, portending unstable molecular ion which as a matter of fact failed to show up at high resolution. The molecular formula of the compound could therefore not be determined by HRESIMS as done for the preceeding compounds.

The $\{^1H\}$ – ^{13}C spectrum showed16 resonances two of which are quaternary – due to an olefinic carbon and a carboxyl carbon resonating at δ_C 114.3ppm and 171.0ppm respectively. Analysis of the DEPT-edited HSQC spectrum revealed that one of the remaining 14 ^{13}C resonances was methyl, two were methylenes while 11 were methine carbons including the one at δ_C 152.3ppm which was quite unusual for an unsubstitued aromatic carbon as its corresponding proton (δ_H 7.39 ppm) resonance would have ordinarily suggested: Phenolic aromatic carbons that could resonate that downfield must essentially be quaternary,

suggesting this methine carbon to be enolic and thereby indicating an enol or enol ether fragment in the molecule. The fact that the enol methine proton was a singlet also implied that the second double bond carbon of the enol fragment was essentially quaternary as shown Fig. **57**.

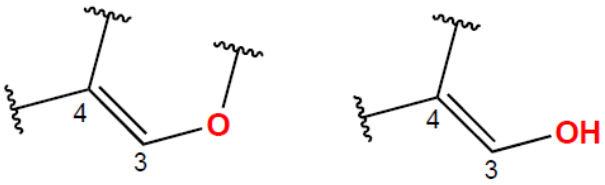

A: enol ether or enol

Fig. 57: Molecular fragment 'A' of compound 8.

The weak ^{13}C signal at δ_C 40.5ppm which the DEPT–edited HSQC spectrum showed to correlate to an intense proton signal integrating to 3.5 in the proton spectrum was considered spurious, based on the fact that it was not in the proton spectrum of the immediate parental sample purified to yield compound 8, and the 2D spectra did not show it to be connected to the molecule anyway. It would most likely be due to a solvent contaminant e.g. acetone.

The ^{13}C shifs (δ_C 100.2ppm, 97.7ppm) of the two proton signals respectively at δ_H 5.27ppm and 4.65ppm were suggestive of the presence of two acetal linkages in the molecule (Fig. 38).

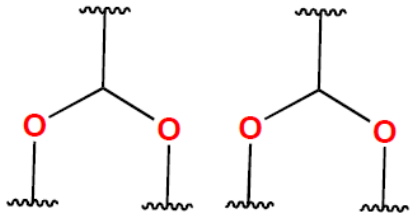

B **C**

Two acetal moieties

Fig. 58: Molecular fragment 'B' and 'C' of compound 8.

The acetal proton at δ_H 4.65ppm was deciphered to be the anomeric proton of a sugar moiety on the basis of its COSY correlation to one resonance (δ_H 3.20ppm) in a cluster of oxygenated methine resonances in the region typical of sugar methines/methylenes. This was further confirmed by the analysis of an expanded gCOSY spectrum of this region which clearly revealed a glucopyranose fragment (fig. 59).

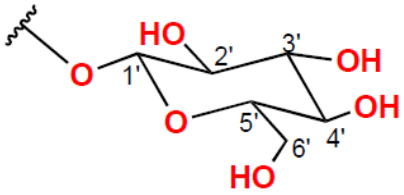

D

Fig. 59: Molecular fragment 'D' of compound 8.

Further analysis of the complete gCOSY spectrum revealed a tetra-substituted cyclopentane ring (fragment E), one of the substituents being unequivocally revealed as the methyl doublet at δ_H 1.10ppm, and another as the second acetal carbon. The chemical shifts of the two other substituted positions revealed attachments to some sort of electron withdrawing substituents.

Both the proton and the carbon-13 shifts (δ_H = 4.04 ppm and δ_C =75.2 ppm) of one of them (C-7) clearly implied an oxygenated substituent, while the nature of the electron withdrawing substituent on the remaining substituted position could not be deciphered based merely on chemical shift arguments.

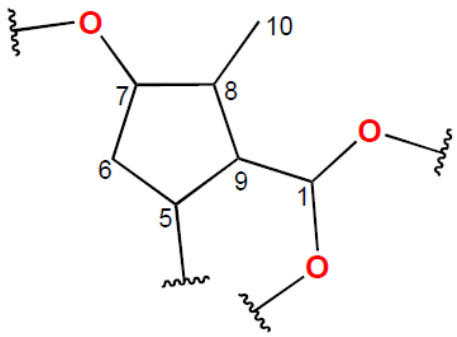

E: Tetrasubstituted cyclopentane ring fragment

Fig. 60: Molecular fragment 'E' of compound 8.

Analysis of the gHMBC spectrum showed that the cyclopentane ring was actually in fusion with a six-membered ring based on the long range correlation of the enolic methine proton to the acetal carbon substituent of the cyclohexane ring, and to the substituted carbon of the cyclopentane ring whose electron withdrawing substituent could not be deciphered earlier. This confirmed the attachement of the quaternary double bond carbon of the enol fragment as the unknown substituent on the cyclopentane ring as well as confirming an enol ether fragment instead of a terminal enol. Furthermore, the longrange correlation of the enol methine proton to the carboxyl carbon showed that the latter was attached to the quaternary carbon of the enol fragment, thereby reducing the working substructures to two main partial structures as shown in fig. 61 below:

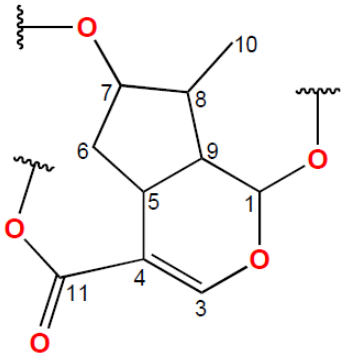

Iridoidyl substructure

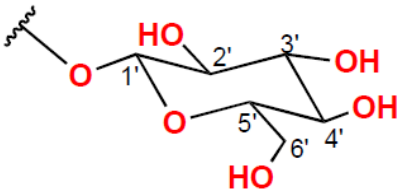

Glucopyranosyl substructure

Fig. 61: Two main partial structures from the various fragments of compound 8.

The long range correlation of the glucopyranosyl anomeric proton H-1' (δ_H 4.66ppm) to the iridoidyl's acetal carbon C-1 (δ_C 97.8ppm) established that the two acetal moieties shared one oxygen. Moreover, maintaining five oxygens on the iridoidyl fragment put an excess of 16 , the mass of one oxygen atom on the molecule, also more or less showing that the carboxyl carbon group (via its singly bonded oxygen) was actually the oxygenated substituent on the cyclopentane ring, returning the gross structure of compound 8 as a new lactone iridoid glucoside.

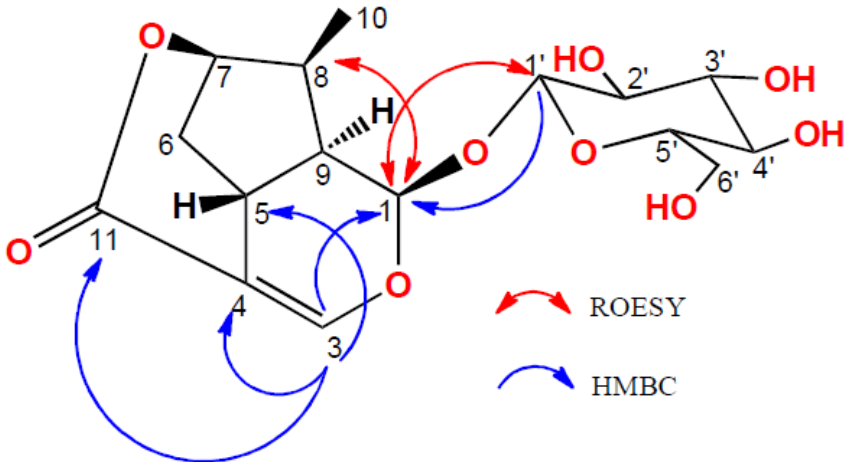

Fig. 62: Important ^{1}H-^{13}C HMBC and ^{1}H-^{1}H ROESY Correlations in Compound 8.

The large coupling constant (9.8Hz) of the glucopyranosyl anomeric proton showed its 1, 2 diaxial relationship with the sugar's C-2' carbon, and by convention assigned the pyranosyl–O bond β-equatorial making the anomeric proton (H-1') α-axial. The strong ROESY correlation between H-1'and the iridoidyl acetal proton (H-1) was the basis for the α-orientation of H-1 and hence the β-orientation of the glycosidic linkage to C-1. The α-orientation of H-9, and H-8 (with the consequent β –orientation of H-10) was based on the strong ROESY correlations H-1 showed to H-8 and H-9. In the same vein the α-orientation of H-7 was based on its distinct ROESY correlation to H-8; and finally H-5 was assigned β – orientation based on its ROESY correlation to Ha-6 and not Hb-6 to which α-oriented H-7 and H-8 showed distinct ROESY correlations. The small coupling constant of the iridoidyl's acetal proton wan indication that the neighbouring proton was *cis* to it.

5.2.9 **Structure Elucidation of Compound 9** (appendices 64-69)

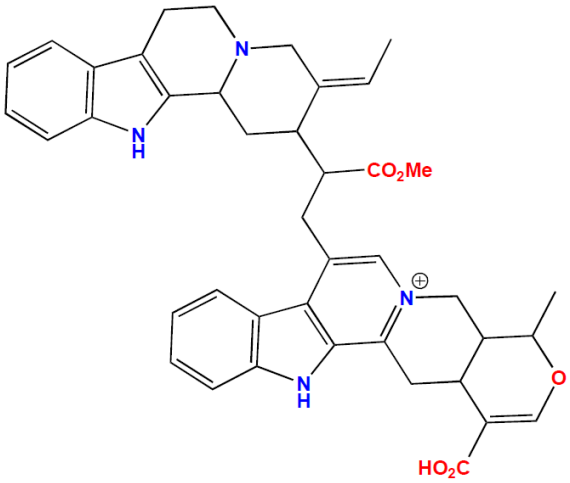

Compound 9: desmethylserpentinine (Fig. 33).

The HRESIMS analysis gave the molecular formula as $C_{41}H_{43}N_4O_5$ based on the M^+ peak at m/z 671.3248 of the spectrum. A systematic refined scifinder search based on this molecular mass suggested the above structure, a monomethylester analogue of the dimethylester natural product serpentinine. The set of NMR data acquired in CD_3OD for the compound were not sufficient to exclusively assign the proton and carbon-13 resonances as there were a lot of overlaps in the proton spectrum that even the HSQC spectrum could not resolve. Acquiring the NMR data in another deuterated solvent like $CDCl_3$ or C_5D_5N would most probably have helped but it was not done due to time constrains. Notwithstanding, the assignment of the methylester carboxyl group was quite easy with HMBC correlations analysis. P-gp inhibition activity of Compound 9 is yet to be evaluated as it was not available as at the time the preceeding 8 compounds were being submitted for the P-gp inhibition assay.

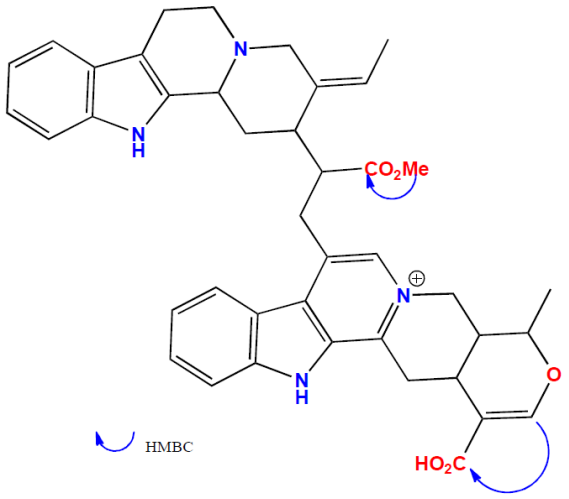

Fig. 63: Important ^{1}H-^{13}C HMBC correlations in compound 9.

5.3 Structural Uniqueness of Compound 1

Compound 1 is an indolopyridinium alkaloid with traces of evidence of having passed through the MTIA biosynthetic pathway: The triptamine-derived unit of the molecule is conspicuous. A careful examination of the remaining part of the molecule however shows subtle variations to the aspidosperma and iboga skeletons, the primary rearrangements that led to the current plethora of MTIAs with rearranged secologanin skeleton (Herbert, 1983; Ramirez and Garcia-Rubio, 2003). While it has structural relationship to dehydrosecodine(schemes 2 and 3), the biosynthetic precursor to all MTIAs with rearranged secologanin skeleton, the full dehydrogenation of the dihydropyridine ring of dehydrosecodine, the conspicuously missing C -16 and C-17 units of the typical MTIA, and the unusual attachment of the carboxymethyl group to the 2-position of the MTIA skeleton imply enzymatic activities in a biosynthetic route from dehydrosecodine quite different from those of the aspidosperma and iboga families of MTIAs (Scheme 2) (Herbert, 1983).

The probable biosynthetic route is hereby conjectured to most likely involve the following enzymatic steps: Full dehydrogenation of dehydrosecodine to secodine is mediated by reductases in the presence of $NADP^+$ leading to the formation of NADPH. Hydrolysis by esterases leads to the formation of free carboxylic acid upon which decarboxylases act to yield a terminal alkene one carbon less than dehydrosecodine. This alkene undergoes oxidative cleavage to yield a free carboxyl group which gets esterified under the influence of esterases (Scheme 3).

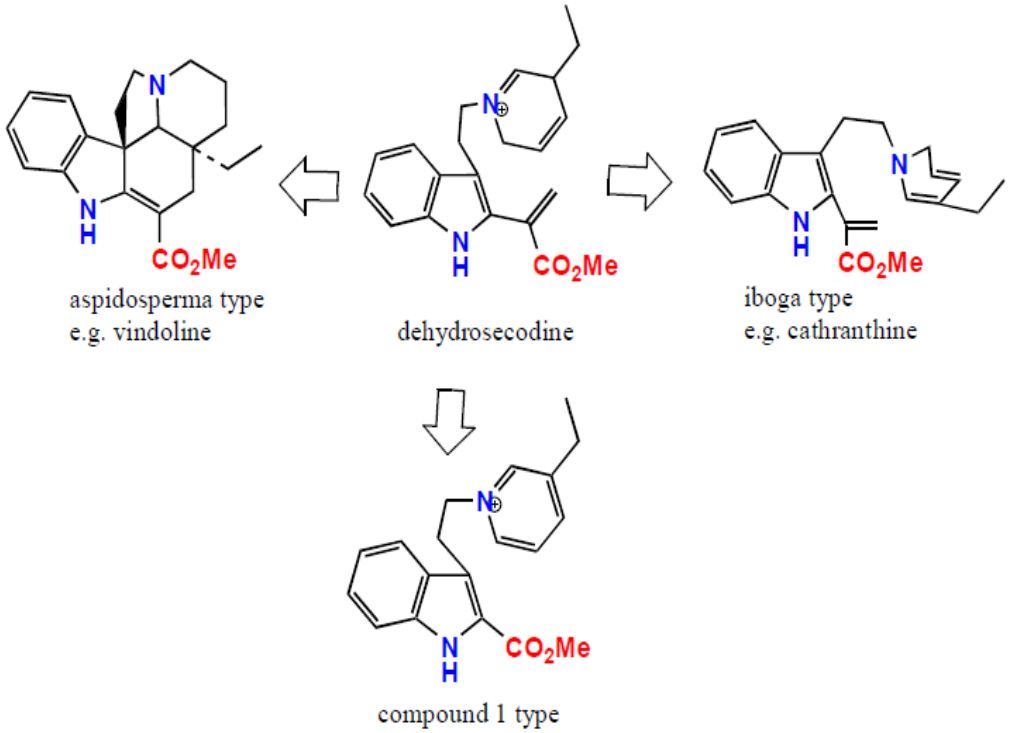

Scheme 2: compound 1 as a prototype of a possible biosynthetic terminus from dehydrosecodine.

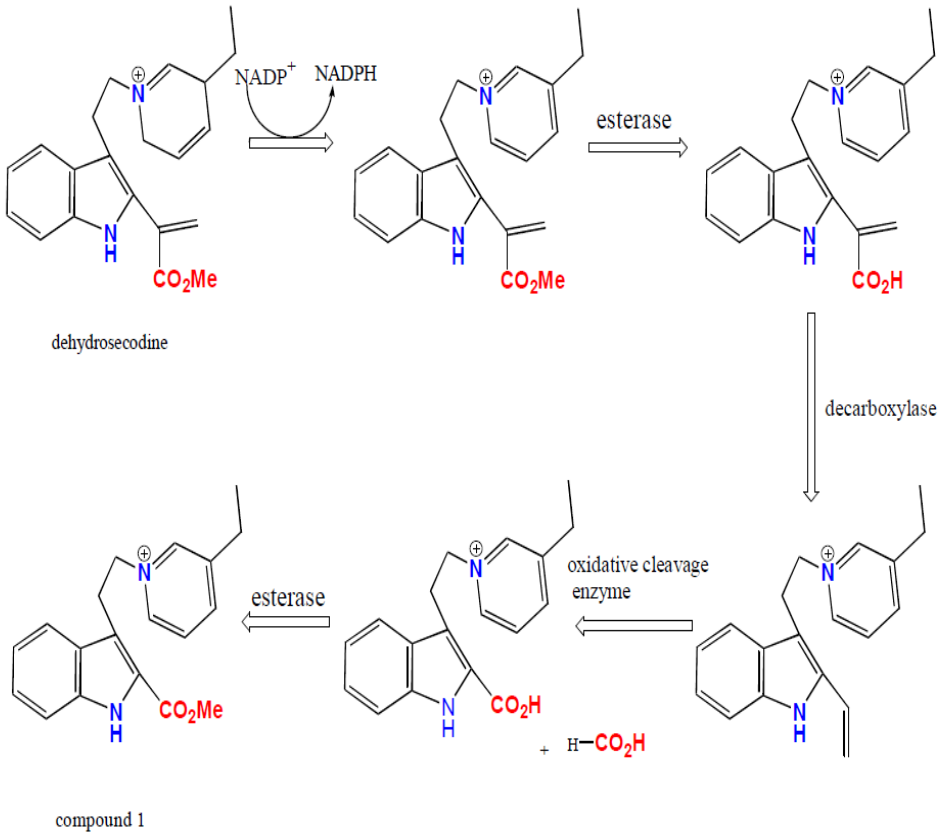

Scheme 3: **Possible biosynthetic pathway of compound 1 from dehydrosecodine.**

In addition to its biosynthetic uniqueness, compound 1 is a simple but unprecedented achiral indolopyridinium alkaloid with an excellent prospect for a simple chemical synthesis. Its common structural features to precursors of MTIAs with rearranged secologanin skeleton confers on it a biosynthetic heritage that cuts across historic therapeutic alkaloids – the antimalarial quinine, the anticancer vinca alkaloids, and the CNS toxin strychnine – and thus a high prospect of becoming a synthetic intermediate in the total synthesis of a number of drugs in various therapeutic categories.

5.4 P-gp Inhibition Assay.

P-gp inhibition is a measure of cancer multidrug resistance inhibition as P-gp has been highly implicated in the therapeutic failures of virtually all chemical classes of anticancer drugs via efflux from the cytoplasm (Gottesman, 1993; Gottesman, 2002).

The assay was based on the ability of the test compounds to cause accumulation of calcein, a flourigenic dye, in the cancer cells cytoplasm after incubation with non-flouresing calcein-AM which is an established P-gp substrate capable of librating calcein *in situ* courtesy of cytoplasmic esterases (Polli *et al.*, 2001, Schwab *et al.*, 2003). In the absence of an inhibitor P-gp efflux calcein AM as soon as it enters the cell via an ATP- dependent active transport process. Little or no fluorigenic calcein is thus formed producing little or no fluorescence.

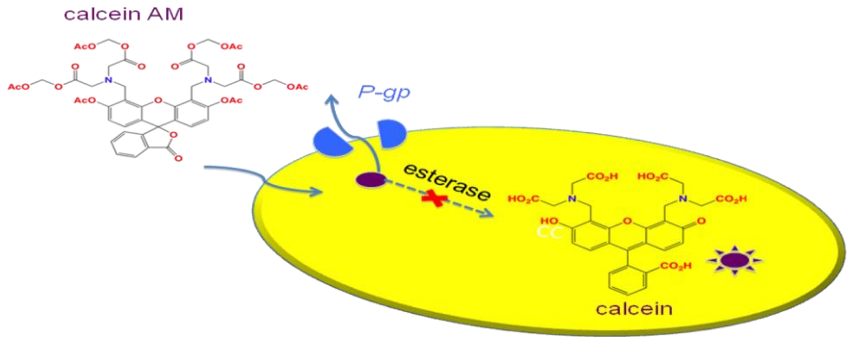

Fig. 64: Pictorial representation of an MDR cell, in the absence of a P-gp inhibitor.

In the presence of a P-gp- inhibiting test compound, however, the efflux of calcein AM out of the cytoplasm via the P-gp is significantly reduced, in the process enabling cytoplasmic esterases to act on calcein AM to liberate and accumulate calcein, a fluorescent compound, in the cytoplasm. Calcein fluoresces between 510 and 520 nm (Polli *et al*, 2001). Fluoresence (measured as relative fluorescence units or RFU) was therefore monitored at this wavelength

region as indicative of P-gp inhibition; and the higher the fluorescence the higher the P-gp inhibitory activity.

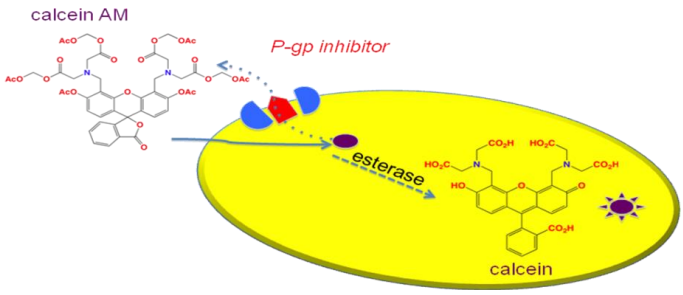

Fig. 65: Pictorial representation of a MDR cell following incubation with a P-gp inhibitor.

Two hits (compounds 1 and 4, at 25µg/ml) were found in the first experiment based on the set conditions (section 3.4). 25µg/ml Compound 4, and not the positive control, was set as pivot as the RFU of the latter was even below the 'hit' mark in the presence of this pivot to which compound 1's RFU was also comparable. This is what necessitated the second experiment in which compounds 1 and 4 were withdrawn. Two more hits (compounds 6 and 7, at 25 µg/ml) were discovered but this time around with comparable activities to that of the positive control (verapamil). The t-values for the comparison of the RFUs of these hits (i.e. 25 µg/ml of compounds 1, 4, 6, and 7) with those of their corresponding least-value negative controls in a student t-test were 23.17, 36.27, 12.27 and 22.85 respectively, the t- value in each case being far above 2.58 standard errors if a 99% confidence limit was assumed (McHugh, 2008), i.e., $P < 0.01$. In summary therefore, four compounds were found showing highly significant P-gp inhibitory activities.

CHAPTER 6

CONCLUSION

6.1 Summary of Findings.

Nine fractions were obtained per plant material from a pH differential-modified conventional alkaloid extraction of each of the leaf, seed and stem bark materials of *Hunteria umbellata*. It is worthy of note that the otherwise (conventionally) ignore alkaline aqueous left-over fraction of the alkaloidal extraction protocol incidentally yielded the two structurally most unique compounds; N-[2-(2-carbomethoxy-3-indolyl)ethyl]-3-ethylpyridinium and 1-glucopyranosyl-8-methyliridan-3-en-4,7-carbolactone (i.e. compounds 1 and 8) obtained from this project. This fraction was therefore an unconventional source of novel scaffolds.

^{1}H NMR profiling was successfully used as a structural guide to the identification of fractions rich in indoles, triterpenoids, and iridoids, three biosynthetically interdependent phytochemical groups that are either established or conjectured privileged structures which by definition have high propensities of interacting with the P-gp, the indoles in particular presenting with biochemical rationales for putative P-gp interactive abilities. This, in a way, showed that natural drug discovery should not necessarily be random and sagacity-dependent as its traditional activity-guided approach presupposes it to be. It can actually be based on some scientifically testable hypotheses, and hence a rational process as done here, thereby reducing its time involvement and capital intensiveness. Moreover, the successful simultaneous targeting of three phytochemical groups from a plant source, the chemistry of which literature establishes as dominated by only one, points to the fact that careful studies of the interdependence of various biosynthetic pathways *vis-a-vis* chemotaxonomy could lead

to the discovery of novel compounds, the chemical groups of which the source had never been noted for.

A total of nine compounds were isolated and purified from the fractions with the afore-mentioned interesting chemistries, four of which were found to be new, and two of the new being as spectacully new as patentable. It is also worthy of note that this is by all means a high turn- out of new compounds, a feat alludable to the effectiveness of the adopted structure guided approach with its attendant hypotheses. In the same vein four, out of the tested eight compounds in the P-gp inhibition assay, showed significant activities – another ratio indicating that the approach with its attendant hypotheses does not only have the potential for quick generation structurally novel compounds but actually those with inherent biological activities.

Compounds 1, 4, 6 and 7, each at 25µg/ml, were found to display highly significant P-gp inhibitory activities ($P < 0.01$). They could be employed as leads in the design/developmet of clinical P-gP inhibitors administered as adjuncts with anticancer agents for effective cancer chemotherapy.

6.2 Contributions to Knowledge.

1. The cancer multidrug resistance inhibition potentials, on the basis of P-gp inhibitory activities, of N-[2-(2-carbomethoxy-3-indolyl)ethyl]-3-ethylpyridinium (i.e.compound 1), and, to the best of our knowledge, of serpentine, strictosidinic acid and pseudoakuammigine (i.e. compounds 4,6 and 7) are being reported for the first time.

2. N-[2-(2-carbomethoxy-3-indolyl)ethyl]-3-ethylpyridinium, 4-chloromethylakuammineammonium ion, 1-β-glucopyranosyl-8-methyliridan-3-en-

4,7-carbolactone and desmethylserpentinine (i.e. compounds 1, 3, 8 and 9) are new compounds; their discovery, therefore, by this work is a definite expansion of the frontiers of natural product medicinal chemistry. In the same vein, this is the first time, to the best of our knowledge, that all the characterized compounds, with the exception of pseudoakuammigine (i.e. compound 7), would be isolated from the plant *Hunteria umbellata* and thus a definite expansion of the frontiers of the plant's chemistry.

3. The structural uniqueness of N-[2-(2-carbomethoxy-3-indolyl)ethyl]-3-ethylpyridinium, is suggestive of the existence of a yet –to-be reported biosynthetic subgroup terminus from the molecular junction that bifurcates to the two main arms of MTIAs with rearranged secologanin skeleton, making it the prototype of a new subclass of MTIAs.

4. Moreover, N-[2-(2-carbomethoxy-3-indolyl)ethyl]-3-ethylpyridinium, being an unprecedented achiral indolopyridinium alkaloid, has an excellent prospect for a simple chemical synthesis: Its biosynthetic heritage that cuts across historic therapeutic alkaloids – the antimalarial quinine, the anticancer vinca alkaloids, and the CNS toxin strychnine – bestows on it a high prospect of becoming a synthetic intermediate in the total synthesis of a number of drugs in various therapeutic categories.

REFERENCES

Adebamowo C. A. and Ajayi O. O. (2000). Breast cancer in Nigeria. *West African Journal of Medicine* **19** (part 3): 179-191.

Adegoke E. A. and Alo B. (1986). Abereamines, water-soluble alkaloids from *Hunteria umbellata*. *Phytochemistry*. **25** (6): 1461-1468.

Adeneye A. A. and Adeyemi O. O. (2009). Further evaluation of antihyperglycaemic activity of *Hunteria umbellata* (K. Schum) Hallier F. Seed extract in experimental diabetes. *Journal of Ethnopharmacology*. **126**: 238-243.

Adeneye A. A., Adeyemi O. O. and Agbaje E. O. (2010). Antiobesity and antihyperlipidaemic effects of Hunteria umbellata seed extract in experimental hyperlipidaemia. *Journal of ethnopharmacology*. **130**: 307-314.

Ambudkar S. V., Dey S. and Hrycyna C. A. (1999). Biochemichemical, cellular, and pharmacological aspects of the multidrug transporter. *Annu Rev Pharmacol Toxicol*. **39**: 361-398.

Ariens E. J., Beld A. J., Rodrigues de Miranda J. F. and Simonis A. M. (1979). In: O'Brien R.D. (ed.). The Receptors: A comprehensive Treatise. Plenum Press, New York Pp 33.

Bartlett M. F., Korzun B., Sklar R., Smith A. F. and Taylor W. I. (1963). The alkaloids of *Hunteria eburnea* Pichon II. The quaternary bases. *The Journal of Organic Chemistry* **28** (6): 1445-1449.

Batist G., Tulpule A. and Sinha B. J. (1996). Overexpresion of a novel anionic glutathione transferase in multidrug human breast cancer cells. *J Biol Chem*. **33**: 15544-15549.

Bemis G. W. and Murcko M. A. (1996). The properties of known drugs. .*J Med Chem*. **39** (15): 2887-2893.

Bemis G. W. and Murcko M. A. (1999). The properties of known drugs 2: Side chains. *J Med Chem*. **42** (25): 5095-5099.

Bevan C. W. L., Patel M. B., Reefs A. H. and Loudon A. G. (1967). The seed alkaloids of *Hunteria umbellata*. *Tetrahedron.* **23**: 3809-3821.

Bhart S. V., Nagasampagi B. A. and Sivakumar M. (2005). Chemistry of Natural Products. Narosa Publishing House, New Delhi. Pp 27, 268-284, 350-387.

Bouffard D. Y., Ohkawa T., Kijima H., Irie A., Suzuki T., Curcio L. D., Holm P. S., Sassani A. and Scanlon K. J. (1996). Oligonucleotide modulation of multidrug resistance. *Eur J Cancer*. **32A** (6): 1010-1018.

Boyd M. R. (1993). The future of new drug development. In: Neiderhuber J. E. (ed.). Current therapy in oncology. Decker, New York. Pp. 11-22.

Breitmaier E. (2002). Structure elucidation by NMR in organic chemistry, a practical guide. John Wiley and sons Inc. Hoboken. Pp13, 22.

Buss A. D. and Waigh R. D. (1995). Natural products as leads for New Pharmaceuticals. In: Wolff M. E. (ed.). Burger's medicinal chemistry and drug discovery. Fifth edition vol 1 John Wiley and sons Inc. New York. Pp 983-1033.

Buttler M. S. and Mark S. (2004). The role of Natural product chemistry in drug discovery. *J Nat Prod*. **67** (12): 2141-2153.

Buttler M. S. (2005). Natural products to drugs: Natural product compounds in clinical trials. *Nat Prod Rep*. **22**: 162-195.

Chen C. J., Chin J. E. and Ueda K. (1986). Internal duplication and homology with bacterial transport proteins in the mdr1 (P-glycoprotein) gene from multidrug-resistant human cells. *Cell*. **47**: 381-389.

Choi C. H. (2005). ABC transporters as multidrug resistance mechanisms and the development of chemosensetizers for their reversal. *Cancer Cell Int*. **5**: 30.

Choi H. K., Yang W. J., Roh S. H., Han C. Y. and Kang K. W. (2007). Induction of multidrug resistance-associated protein 2 in tamoxifen resistant breast cancer cells. *Endocrine-related Cancer*. **14**: 293-303.

Clark A. M. (1996). Natural products as a resource for new drugs. *Pharmaceutical Research*. **13** (8): 1133-1141.

Coiffier B. (2002) Rituximab in the treatment of diffuse large B-cell lymphomas. *Semin Oncol*. **29** (1suppl.2): 30-35.

Cohen N. C., Blaney J. M., Humblet C., Gund P. and Barry D. C. (1990). Molecular modelling software and methods for medicinal chemistry. *J Med Chem*. **33** (3): 883-894

Constanlino L. and Barlocco D. (2006). Privileged structures as leads in medicinal chemistry. *Current medicinal chemistry*. **13** (1): 65-85.

Cuschieri A., Fayers P. and Fielding J. (1996). Postoperative morbidity and mortality after D1 and D2 resections for gastric cancer .Preliminary results of the MRC randomised controlled surgical trial. *Lancet*. **347**: 995-997.

De Lange T. (2005). Shelterin: the protein complex that shapes and safeguards human telomeres. *Genes Dev*. **19**: 2100-2110.

Dell'Eva R., Pfeffer U. and Indraccolo S. (2002). Inhibition of tumour angiogenesis by angiostatin: from recombinant protein to gene therapy. *Endothelium*. **9**: 3-10.

Demain A. L. and Sanchez S. (2009). Microbial drug discovery: 80 years of progress. *The Journal of Antibiotics* **62**: 5-16.

Demant E. J., Shested M. and Jensen P. B. (1990). A model for computer simulation of P-glycoprotein and transmembrane delta pH-mediated anthracyline transport in multidrug–resistant tumour cells. *Biochim Biophys Acta*. **1055**: 117-125.

Desimone R. W., Currie K. S., Mitchell S. A., Darrow J. W. and Pippin D. A. (2004). Privileged structures: Applications in drug discovery. *Combinatorial Chemistry and High throughput screening*. **7** (5): 473-493.

Dewick P. M. (2001). Medicinal natural products, a biosynthetic approach. Second edition. John wiley and sons Ltd., Chichester. Pp 186-190: 350-358.

Dillman R. O. (2001). Monoclonal antibody therapy for lymphoma: an update. *Cancer Pract*. **9**: 71-80.

Dimarco A. (1967). Daunorubicin and related antibiotics. In Gottlieb D. and Shaw D. (eds.). Antibiotics I. Springer – Varlag, New York. Pp. 190-210.

do Nacimento C. A., Gomes M. S., Liao L. M., de Olivera C. M. A., KatoL., da Silva C. C. and Tanaka C. M. A. (2006). Alkaloids from *Palicourea coriacea* (Cham.) K. Schum. *Zeitschrift fuer Naturforschung/B*. **61** (11): 1443-1446.

Dzubak P. Hajduch M., Vydra D., Hustova A., kvasnica M., Biedermann D., Markova L., Urban M., and Sarek J. (2006). Pharmacological ativities of natural triterpenoids and their therapeutic implications. *Nat Prod Rep*. **23**: 394-411.

Evans B. E., Rittle K. E. Bock M. G., Diprardo R. M., Freidingar R. M., Whitter W. L., Lunell G. F., Veber V. J., Cerino D. J., Chen T. B., Wing P. J., Kunkel K. A., Springer J. P. and Hirshfield J. (1998). *J Med Chem*. **31**: 2235-2246.

Falodun A., Nworgu Z. A. M. and Ikponmwonsa M. O. (2006). Phytochemical components of *Hunteria umbellata* and its effect on isolated non-pregnant rat uterus *in oestrus*. *Pakistan Journal of Pharmaceutical Sciences*. **19**: 256-258.

Fardel O., Lecureur V. and Guillouzo A. (1996). The P-glycoprotein multidrug transporter . *Gen Phamacol*. **27**: 1283-1291.

Ferry D. R., Traunecker H. and Kerr D. J. (1996). Clinical trials of P-glycoprotein reversal in solid tumours. *Eur J Cancer*. **32A** (6): 1070-1087.

Folkman J. (1995). Clinical applications of research on angiogenesis. *New Engl J Med*. **333** (26): 1757-1763.

Folkman J. (2001). Angiogenesis-deependent diseases. *Semin Oncol*. **28** (6): 536-542.

Ganong W. F. (1999). Review of medical physiology. Appleton and Lange. Stamford, Connecticutt. Pp. 98-100.

Gaspar L. E. and Ding M. (2008). A review of intensity-modulated radiation therapy. *Current Oncology Reports* **10** (4): 294-299.

Goldkorn A. and Blackburn E. H. (2006). Assembly of a mutant-template telomerase RNA into catalytically active telomerase ribonucleoprotein that can act on telomeres is required for apoptosis and cell-cycle arrest in human cancers. *Cancer Res*. **56**: 5763-5771.

Gordon L. I., Witzig T. E. and Wiseman G. A. (2002). Ytfrium 90 ibritumobab tiuxetan radioimmunotherapy for relapsed or refractory low-grade non-Hodgkin's lymphoma. *Semin Oncol*. **29** (1suppl.2): 87-92.

Gottesman M. M. (2002). Mechanisms of cancer drug resistance. *Annu Rev Med*. **53**: 615-627.

Gottesman M. M., Fojo T. and Bates S. E. (2002). Multidrug resistance in cancer: role of ATP-dependent transporters. *Nat Rev Cancer*. **2**: 48-58.

Gottesman M. M. and Pastan I. (1993). Biochemistry of multidrug resistance mediated by the multidrug transporter. *Annu Rev Biochem*. **62**: 385-427.

Grabowski H. G. and Wang Y. R. (2006). The quantity and quality of world wide new drug introductions. *Health Aff. (Millwood)* **25**: 452-460.

Greider C. W. and Blackburn E. H. (1985). Identification of a specific telomere terminal transferase enzyme with two kinds of primer specificity. *Cell*. **51**: 405-413.

Grillo-Lopez A. J., Hedrick E. and Rashford M. (2002). Rituximab: an ongoing and future clinical development. *Semin Oncol*. **29** (1suppl.2): 105-112.

Harley C. B. (2008). Telomerase and therapeutic strategies. *Nature Reviews/Cancer*. **8**: 167-179.

Harvey A. L., Clark R. L., Mackay S. P. and Johnson B. F. (2010). Current strategies for drug discovery through natural products. *Expert Opin. Drug Discov*. **5** (6): 559-568.

Heidelberger C. (1975). Fluorinated pyrimidines and their nucleotides. In: Sartorelli A. C. and John D. J. (eds.). Handbook of experimental pharmacology. Vol 38, part 2. Springer-verlag, New York. Pp. 193.

Herbert R. B. (1983). Structural and biosynthetic relationships In: Edwin J. (ed). Indoles part four: The monoterpenoid indole alkaloids. Indoles, the chemistry of heterocyclic compounds. Vol 25 Pt 4. John wiley and sons Inc. New York Pp 2 -45.

Higgins C. F. (1992). ABC transporters: from microorganisms to man. *Annu Rev Cell Biol*. **8**: 67-113.

Hornung A. Bertazzo M., Dziarnowski A., Schneider K., Welzel K., Wohlert S., Holzenkampfer M., Nicholson G. J., Bechthold A., Sussmuth R. D., Vente A. and Pelzer S. (2007). A genomic screening approach to the structure-guided identification of drug candidates from natural sources. *ChemBiochem* **8**: 757-766.

Jacobsen N. E. (2007). NMR spectroscopy explained: simplified theory, application and examples for organic chemistry and structural biology. John wiley and sons Inc. Hoboken, New Jersey. Pp. 14-15, 353-538.

Juliano R. L. and Ling V. (1976). A surface glycoprotein modulating drug permeability in Chinese harmster ovary cell mutants. *Biochim Biophys Acta*. **455**: 152-162.

Karp G. C. (1996). Cell and molecular biology: concepts and experiments. 2nd edition. John Wiley and Sons Inc. New York. Pp. 700-723.

Kristiansen J. E., Hendricks O., Dlvin T., Butterworth T. S., Aagaard L., Christensen J. B., Flores V. C. and Hendrik K. (2007). Reversal of resistance in microorganism by help of non-antibiotics. *Journal ofAntimicrobial Chemotherapy*. **59**: 1271-1279.

Lage H. (2008). An overview of cancer multidrug resistance: a still unsolved problem. *Cell Mol Life Sci*. **65** (20): 3145-3167.

Lai G. M., ChenY. N., Mickley L. A., Fojo A. T. and Bates S. E. (1991). P-glycoprotein expression and schedule dependence of Adriamycin cytotoxicity in human colon carcinoma cell lines. *Int J Cancer*. **49**: 696-703.

Lawrence T. A., Ten Haken R. K. and Giaccia A. (2008). Principles of Radiation Oncology. In: Devita V. T. Jr., Lawrence T. S., Rosengerge S. A. (eds). Cancer: Principles and Practice of Oncology. 8th edition, Lippincott Williams and Wilkins, Philadelphia. Pp. 678-721.

Leonard G. D., Fojo T. and Bates S. E. (2003). The role of ABC transporters in clinical practice. *Oncologist*. **8**: 411-424.

Levy S. B. (1992). Active efflux mechanism for antimicrobial resistance. *Antimicrob Agents Chemother*. **36**: 695-703.

Li J. W. H. et al. (2009). Drug discovery and natural products: End of an era or an endless frontier? *Science* **325**: 161-165.

Lipinski C. A., Lombardo F., Domry B. W. and Feeney P. J. (1997). Computational approaches to estimate solubility and permeability in drug discovery and development settings. *Adv Drug Del Rev*. **23**: 3-25.

Liu D., O'Connor M. S., Qin J. and Songyang Z. (2004). Telosome, a mammalian telomere-associated complex formed by multiple telomeric proteins. *J. Biol. Chem*. **279**: 51338-51342.

Liu J., Shimizu K., Konishi F., Noda K., Kumamoto S., Kurashiki K. and Kondo R. (2006). Anti-androgenic activities of the triterpenoids fraction of *Ganoderma lucidum*. *Food Chemistry*. **100** (4): 1691-1696.

Loo T. W. and Clarke D. M. (2001). Defining the drug-binding site in the human multidrug resistance P-glycoprotein using a methanesulfonate analog of verapamil, MTS-verapamil *J Biol Chem*. **276**: 14972-14979.

Mahamoud A., Chevalier J., Albert-Franco S., Kern W. V. and Pages J. (2007). Antibiotic efflux pumps in gram-negative bacteria: the inhibitor response strategy. *Journal of Antimicrobial Chemotherapy*. **59**: 1223-1229.

McLafferty F. W. and Turecek F. (1993). Interpretation of mass spectra. Fourth edition. University science books, California. Pp 19-34.

Mendel D. B., Laird A. D. and Smolich B. D. (2000). Development of SU5416, a selective small molecule inhibitor of VEGF receptor tyrosine kinase activity, as an anti- angiogensis agent. *Anticancer Drug Des.* **15**: 29-41.

Mi Y., Liang Y., Huang H., Zhao H., Wu C., Wang F., Tao L., Zhang C., Dai C., Tiwan A. K., Ma X., To K., Ambudkar S. V., Chem Z. and Fu L. (2010) Apatinib (YN968D1) reverses multidrug resistance by inhibiting the exflux function of multiple ATP-binding cassette transporters . *Cancer Res.* **70** (20): 7981-7991.

Morrell J. (1996). Mining information from databases for drug discovery. Book of Abstracts, 211th ACS national meeting, New Orleans.

Munoz-Bellido J. L., Munoz-Criado S., Garcia–Rodriguez J. A. (2000). Antimicrobial activity of psychotropic drugs: Selective serotonin reuptake inhibitors. *Journal of antimicrobial agents* **14** (3): 177-180.

Newman D. J. and Cragg G. M. (2007). Natural products as sources of new drugs over the last 25 years. *J Nat Prod*. **70**: 461-477.

Nicolaoaou K. C., Pfefferkorn J. A., Roecker A. J., Cao G. Q., Barluenga S. and Mitchell H. J. (2000). Natural Product-like combinatorial libraries based on privileged structures . General principles and solid phase synthesis of Benzopyrans. *J Am Chem Soc.* **122**: 9939-9953.

Oh K., Mar W., Kim S., Kim J., Lee T., Kim G., Shin D., Sim C. J. and Shin J. (2006). Antimicrobial activity and cytotoxicity of Bis (indole) alkaloids from the sponge *Spongosorites Sp Biol Pharm Bull*. **29** (3): 570-573.

Olaniyi A. A. (1989). Essential medicinal chemistry. Shaneson C. I. Ltd., Ibadan. Pp. 355.

Patchett A. A. and Nargund R. P. (2000). Privileged structures-an update. *Annual Reports in Medicinal Chemistry*. **35**: 289-298.

Pierre A., Leonce S., Perez V. and Atass G. (1998). Circumvention of P-glycoprotein-mediated multidrug resistance by S16020-2: Kinetics of uptake and efflux in sensitive and resistant cell lines. *Cancer Chemother Pharmacol*. **42** (6): 454-460.

Polli J. W., Wring S. A., Humphreys J. E., Huang L., Morgan J. B., Webster L. O. and Serabjit-Singh C. S. (2001). Rational use of in vitro P-glycoprotein assays in drug discovery . *J Pharmacol Exp Ther*. **299**: 620-628.

Porter P. (1989). The synthesis of navelbine prototype of a new series of vinblastine derivarives. *Sem Oncol* **16**: 2-4.

Posner B. A. (2005). High-throughput Screening-driven lead discovery: Meeting the challenges of finding new therapeutics. *Current Opinions in Drug Discovery and Development*. **8**: 487-494.

Price R. N., Uhlemann A. C, Brockman A., Mcgrady R., Ashley E., Phaipun L., Laing K., Looareesuwan S., White N. J., Nosten F. and Krishna S. (2004). Mefloquine resistance in *Plasmodium falciparum* and increased *pfmdr1* gene copy number. *Lancet*. **364**: 438-447.

Ramirez A. and Garcia–Rubio S. (2003). Current progress in the chemistry and pharmacology of akuammiline alkaloids. *Current Medicinal Chemistry*. **10**: 1891-1915.

Rapaka R., and Sadee W. (2006). Drug Discovery from Natural sources. *The APIPS Journal*. **8** (2): E239-E253.

Rautio J., Humphrey J. E., Webster L. O., Balakrishnan A., Keogh J. P., Kunta J. R., Serabjit-Singh C. J. and Polli J. W. (2006). *In vitro* P-glycoprotein inhibition assays for assessment of clinical drug interaction potential of new drug candidates: A recommendation for probe substrates. *The American Journal for Pharmacology and Experimental Therapeutics*. **34**: 786-792.

Remers W. A. and Iyengar B. S. (1995). Antitumour antibiotics. In: Foye W. W. (ed.). Cancer Chemotherapeutic agents. American Chemical Society, Washington D.C. Pp. 620.

Remers W. A. (1998). Antineoplastic agents. In Delgado J. N. and Remers W. A. (eds.). Wilson and Gisvold's textbook of organic medicinal and pharmaceutical chemistry. 10th edition. Lippincott Williams and Wilkins, Philadelphia. Pp. 343-401.

Riordan J. R., Deuchars K. and Kartener N. (1985). Amplification of P-glycoprotein genes in multidrug-resistant mammalian cell lines. *Nature*. **316**: 817-819.

Rishton G. M. (2008). Natural products as a robust source of new drugs and drug leads: Past success and present day issues. *The American Journal of Cardiology*. **101** (10A): 43D 49D.

Rollinger J. M., Langer T. and Stuppner H. (2006). Strategies for efficient lead structure discovery from natural products. *Current Medicinal Chemistry*. **13**: 1491-1507.

Rosenberg M. F., Callaghan R., Ford R. C. and Higgins C. F. (1997). Structure of the multidrug resistance P-glycoprotein to 2.5 nm resolution determined by electron microscopy and image analysis. *J Biol Chem*. **272**: 10685-10694.

Ross J. S., Schenkan D. P., Pietrusko R., Rolfe M., Linette G. P., Stec J., Staghano N. E., Ginsburg G. S., Symans W. F., Pusztai L. and Hortobagyi G. N. (2004). Targeted therapies for cancer. *Am J Clin Pathol*. **122**: 598-609.

Sadowski J. and Kubinyi H. (1998). A scoring scheme fro discriminating between drugs and non-drugs. *J Med Chem*. **41** (18): 3325-3329.

Sahelin H. and Von Wartburg A. (1991). The chemical and biological route from podophyllotoxin glucoside to etoposide: Ninth Cain Memorial award lecture. *Cancer Research*. **51**: 5-15.

Sasako M. (2003). Principles of surgical treatment of curable gastric cancer. *Journal of Clinical Oncology*. **21** (23s): 274s-275s.

Schiff P. B., Fant F. and Horwitz B. (1979). Microtublule assembly *in vitro* by Taxol. *Nature*. **227**: 665-667.

Schwab D., Fischer H., Tabatabaei A., Poli S. and Huwyler J. (2003). Comparison of *in vitro* P-glycoprotein screening assays: Recomendations for their use in drug discovery. *J Med Chem*. **46**: 1716-1725.

Siemiatycki J., Krewski D., Franco E. and Kaiserman M. (1995). Associations between cigarette smoking and each of 21 types of cancer: A multiple case-control study. *International Journal of Epidemiology*. **24** (3): 504-514.

Silverman R. B. (2004). The organic chemistry of drug design and drug action.second edition, Elsevier academic press, Oxford. Pp. 8-120, 144, 323-403.

Simon S. M. and Schindler M. (1994). Cell biological mechanism of multidrug resistance in tumours. *Proc. Natl. Acacd. Sci*. **91**: 3497-3504.

Simpson J. H. (2008). Organic structure determination using 2D NMR spectroscopy, a problem-based approach. Academic press, Elsevier Inc., Burlington MA. Pp. 95-99, 137-148.

Skou J. C. (1988). Overview: Sodium-potassium pump. *Methods Enzymol*. **156**: 1-25.

Sonneveld P. and Wiemer E. (1997). Inhibitors of multidrug resistance. *Curr Opin Oncol*. **9** (6): 543-548.

Sweeney K. (2005). Angiogenesis inhibitors: An upcoming therapy for cancer and wet age – related macular degeneration. *Drug Discovery Today*. **10** (20): 1346-1348.

Takara K. Sakaeda T. and Okumura K. (2006). An update on overcoming MDR-mediated multidrug resistance in cancer chemotherapy. *Current Pharmaceutical Design*. **12** (3): 273-286.

Tamaki H., Satoh H., Jori S., Ohtani H. and Sawada Y. (2010). Inhibitory effects of herbal extracts on breast cancer resistance protein (BCRP) and structure-inhibitory potency relationship of isoflavonoids. *Drug Metab. Pharmacokinet*. **25** (2): 170-179.

Taylor A. and Powell M. E. (2004). Intensity-modulated radiotherapy-what is it? *Cancer Imaging*. **4** (2): 68-73.

Thanakicharoenpath W. and Theanphong O. (2007). Triterpenoids from the stem of *Diospyros glandulosa*. *Thai J Pharm Sci*. **31**: 1-8.

Thomas D. A. and Kantarjian H. M. (2000). Current role of thalidomide in cancer treatment. *Curr Opin Oncol*. **12**: 564-753.

Thomas G. (2003). Fundamentals of medicinal chemistry. John wiley and sons Ltd, Chichester. Pp 57-70.

Thomson A. J., Lochner M. and Lummis S. C. R. (2009). The antimalarial drugs quinine, chloroquine and mefloquine are antagonists at 5-HT_3 receptors. *British Journal of Pharmacology*. **151** (5): 666-667.

Tsuruo T., Lida H., Tsukagoshi S. and Sakuari Y. (1981). Overcoming of vincristine resistance in P388 leukemia *in vivo* and *in vitro* through enhanced cytotoxicity of vincristine and vinblstine by verapamil. *Cancer Res*. **41** (5): 1967-1972.

Tundis R., Loizzo M. R., Menichini F. and Statti G. A. (2008). Biological and Pharmacological activities of iridoids: Recent developments. *Mini Rev Med Chem*. **8** (4): 399-420.

Ullah M. F. (2008). Cancer multidrug resistance (MDR): A major impediment to effective chemotherapy. *Asian Pacific Journal of Cancer Prevention*. **9**: 1-5.

Umezawa H. (1976). Bleomycin: discovery, chemistry, and action. In Umeawa H. (ed). Bleomycin, fundamental and clinical studies. Cancer Res. Tokyo. Pp. 3.

Van Zuylen L., Nooter k., Spareboom A., and Verweij J. (2000). Development of multidrug-resistance converters: Sense or nonsense? *Invest New Drugs*. **18** (3): 205-220.

Wachsmuth O. and Matusch R. (2002). Anhydronium bases from *Rauwolfia serpentina*. *Phytochemistry*. **61**: 705-709.

Wall M. E., Wani M. C., Cook C. E., Palmer K. H., Mcphail A. T. and Sim G. A. (1996). Plant antitumour agents 1. The isolation and structure of camptothecin, a novel alkaloidal leukemia and tumour inhibitor from camptottheca acuminata. *J Am Chem Soc*. **88**: 3888-3890.

Wall M. E. (1993). Camptothecin and Taxol. In: Lednicer D. (ed.). Chronicles of drug discovery. Vol.3. American Chemical Society, Washington DC. Pp. 327-348.

Wang H. X. and Ng T. B. (1999). Natural products with hypoglycaemic, hypotensive, hypocholesterolemic and antithrombic activities. *Life Sciences* **65** (25): 2663-2677.

Wu Y., Kitajima M., Kogure N., Wang Y., Zhang R. and Takayama H. (2010). Two new aspidosperma indole alkaloids from Yunnan kopsia arborea. *Chem Pharm Bull*. **58** (7): 961-963.

Zogakis T. G. and Libutti S. K. (2001). General aspects of anti-angiogenesis and cancer therapy. *Expert Opin Bio Ther*. **1**: 253-275.

APPENDICES

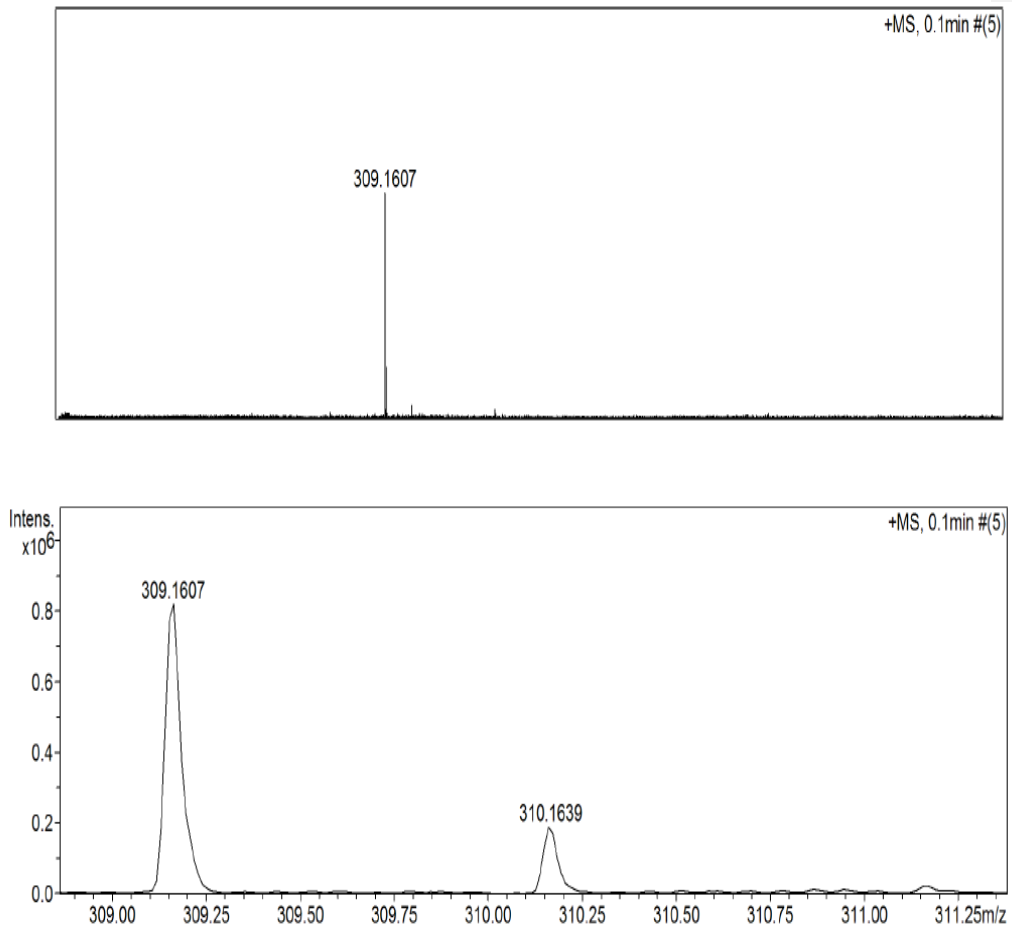

m/z 309.1607 $[M]^+$(calcd. For $C_{19}H_{21}N_2O_2$, 305.1598). Err.(ppm) 3.03

Appendix 1: High Resolution ESI(+)MS of compound 1.

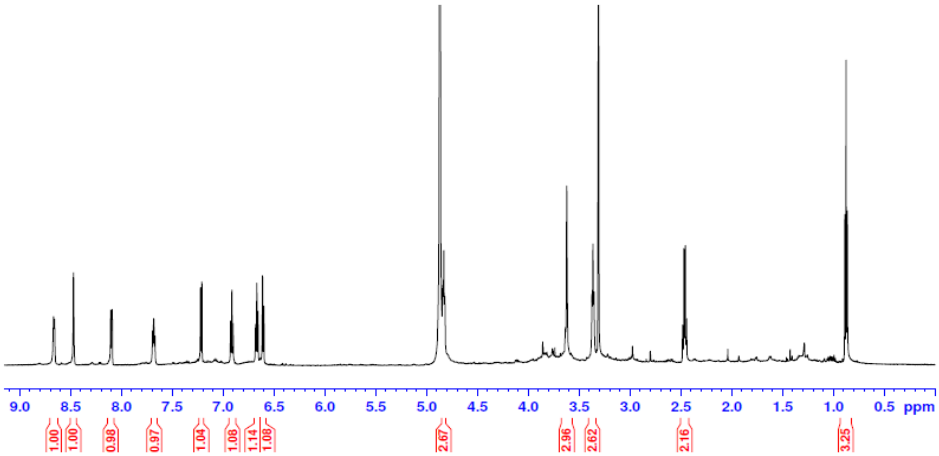

Appendix 2: ^{1}H NMR spectrum (600MHz, CD_3OD) of compound 1.

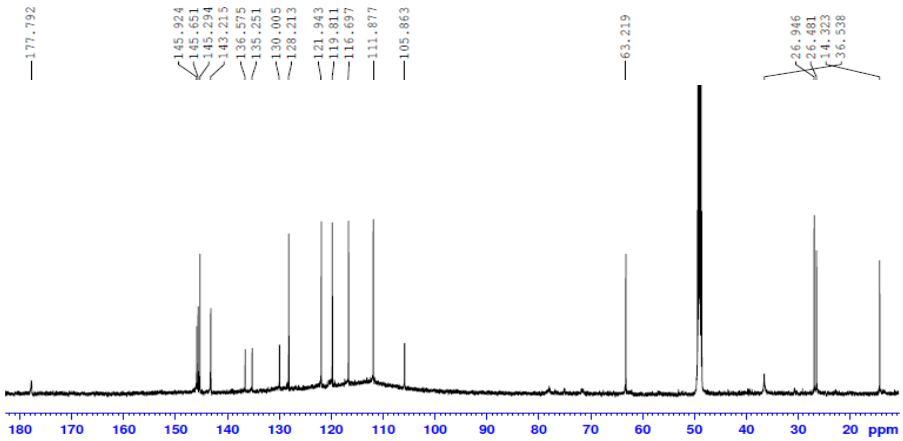

Appendix 3: $\{^{1}H\}$-^{13}C NMR spectrum (150MHz, CD_3OD) of compound 1.

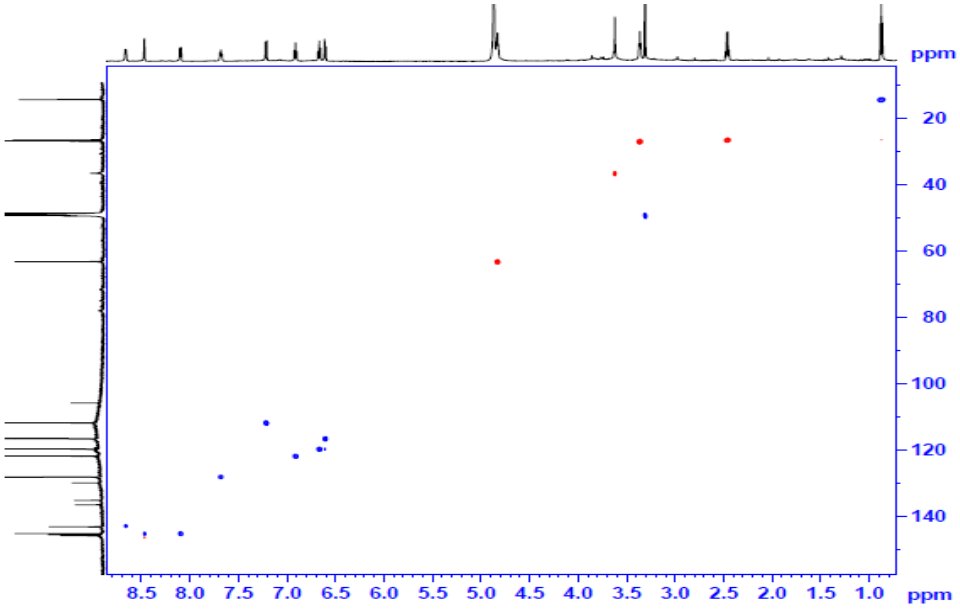

Appendix 4a: DEPT-edited ^{1}H-^{13}C HSQC spectrum (600MHz, CD_3OD) of compound 1

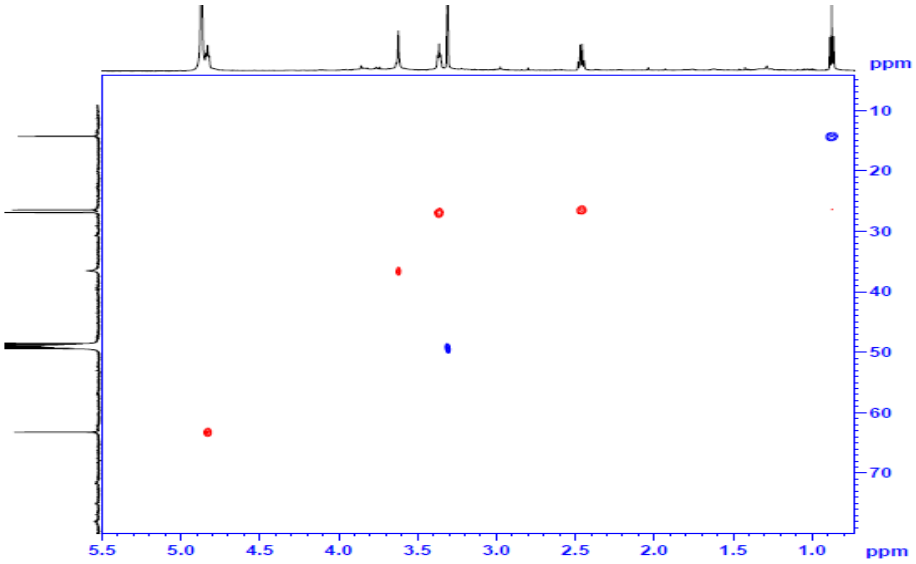

Appendix 4b: DEPT-edited ^{1}H-^{13}C HSQC spectrum (600MHz, CD_3OD) of compound 1 (expansion 1)

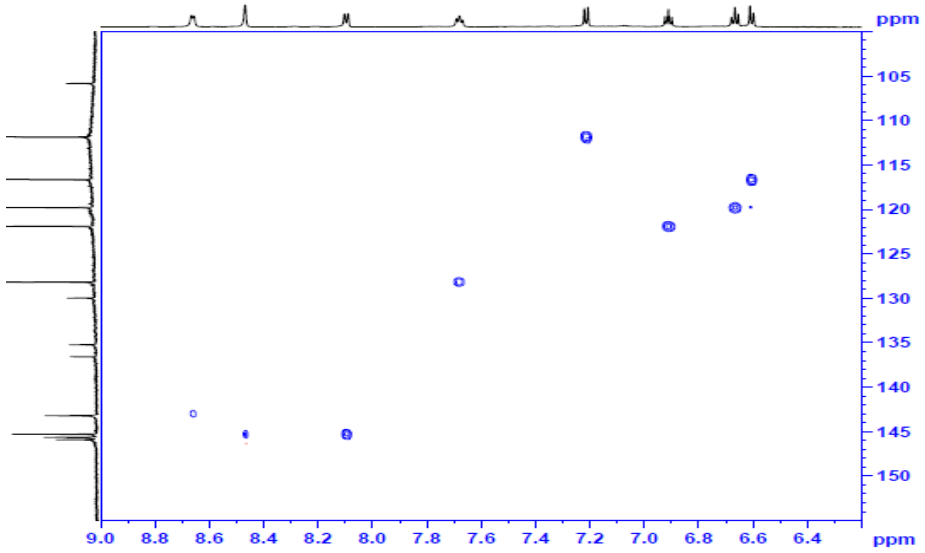

Appendix 4c : DEPT-edited ^{1}H-^{13}C HSQC spectrum (600MHz, CD_3OD) of compound 1 (expansion 2)

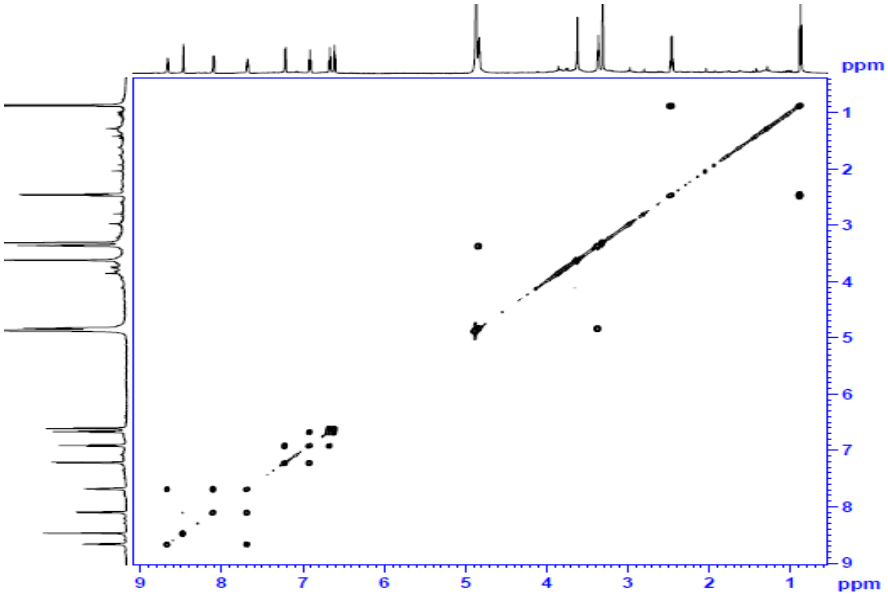

Appendix 5a: ^{1}H- ^{1}H gCOSY spectrum (600MHz, CD_3OD) of compound 1

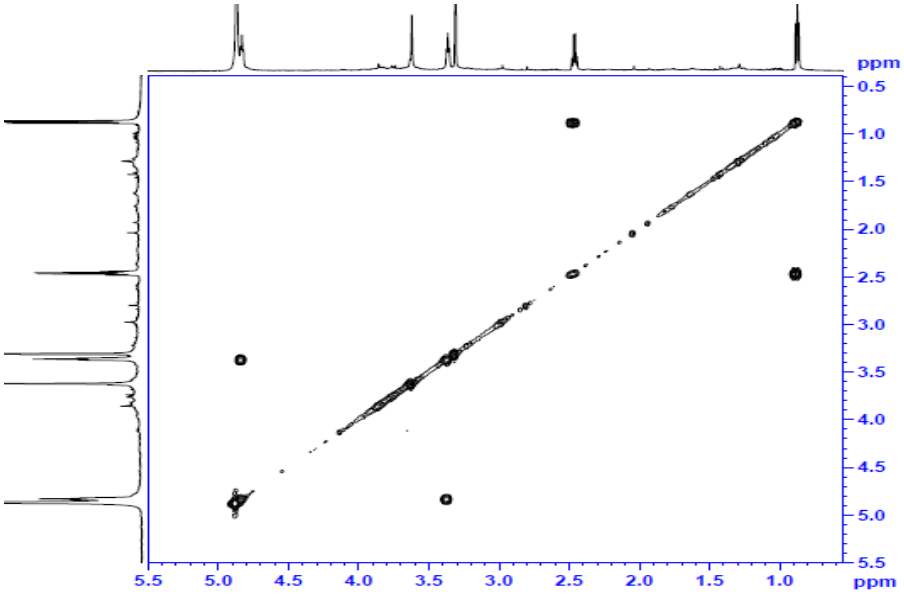

Appendix 5b: ^{1}H- ^{1}H gCOSY spectrum (600MHz, CD_3OD) of compound 1 (Upfield expansion)

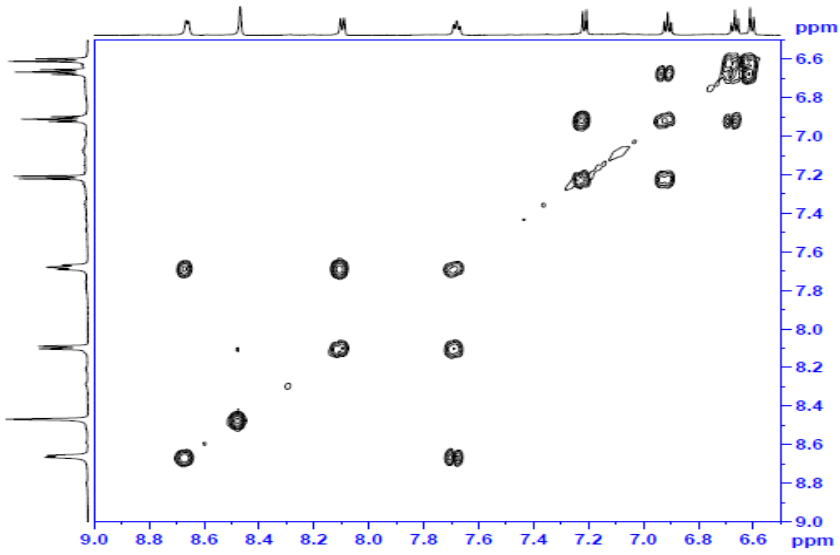

Appendix 5c: ^{1}H- ^{1}H gCOSY spectrum (600MHz, CD_3OD) of compound 1 (downfield expansion).

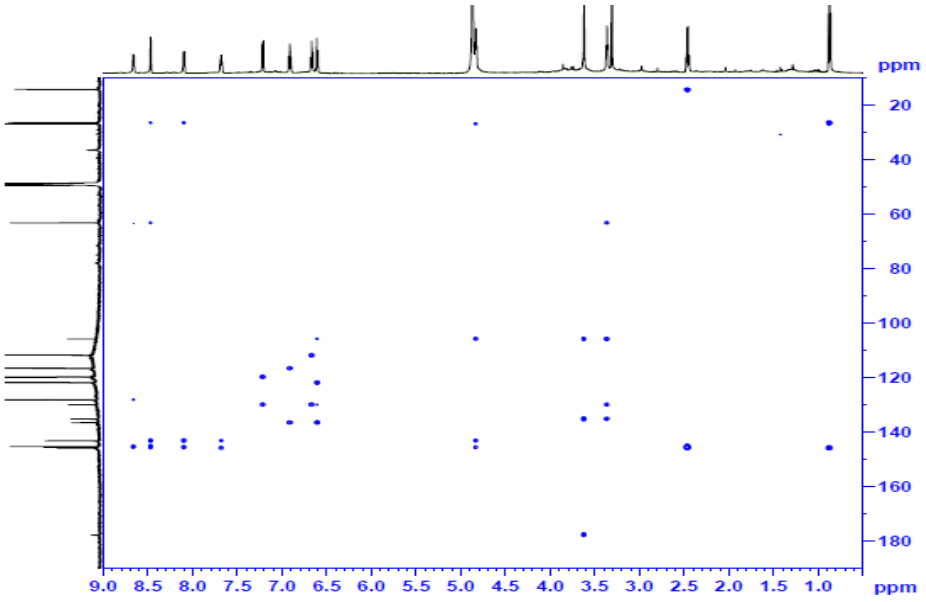

Appendix 6a: ^{1}H- ^{13}C gHMBC spectrum (600MHz, CD_3OD) of compound 1

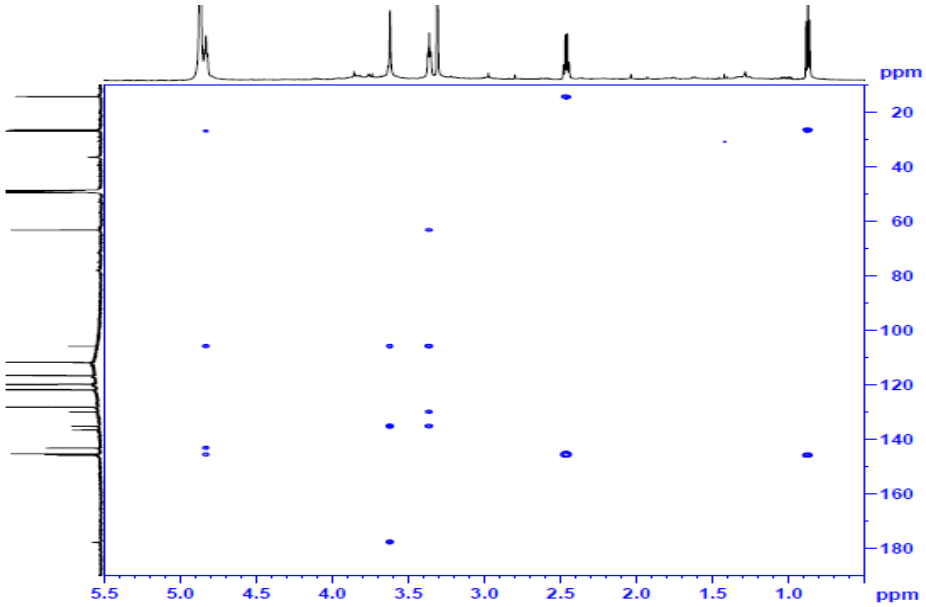

Appendix 6b: ^{1}H- ^{13}C gHMBC spectrum (600MHz, CD_3OD) of compound 1 (Upfield expansion).

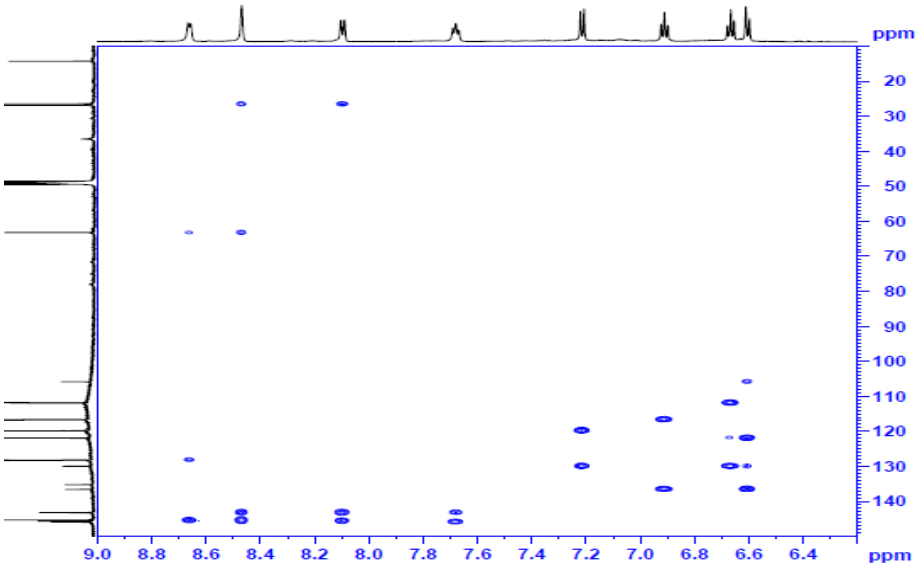

Appendix 6c: ^{1}H- ^{13}C gHMBC spectrum (600MHz, CD_3OD) of compound 1 (Downfield expansion)

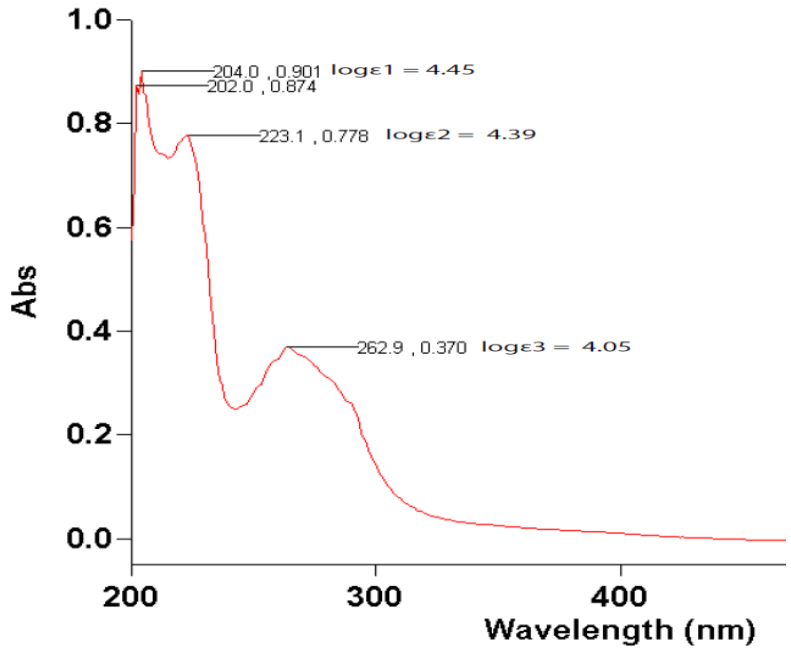

Appendix 7: UV spectrum (3.24 x 10^{-5}M, MeOH) of compound 1

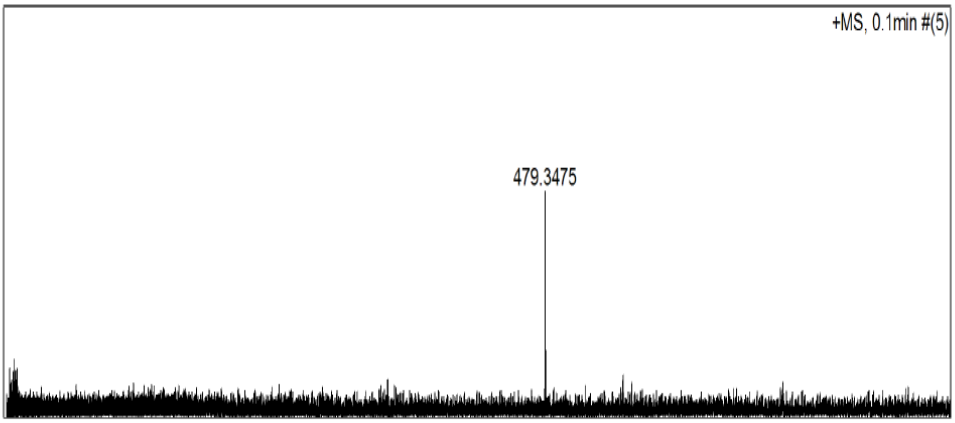

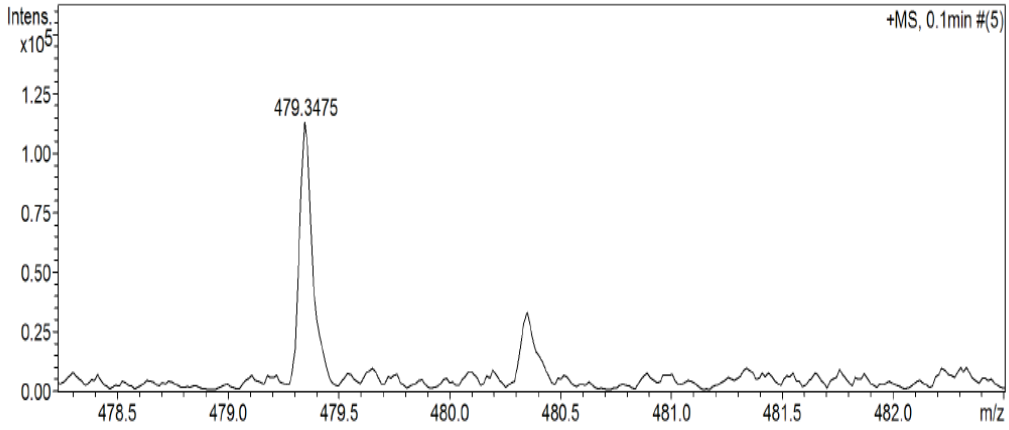

m/z 479.3475 $[M+Na]^+$ (calcd. for $C_{30}H_{48}NaO_3$, 479.3496). Err.(ppm) 4.41

Appendix 8: High Resolution ESI (+) MS of compound 2

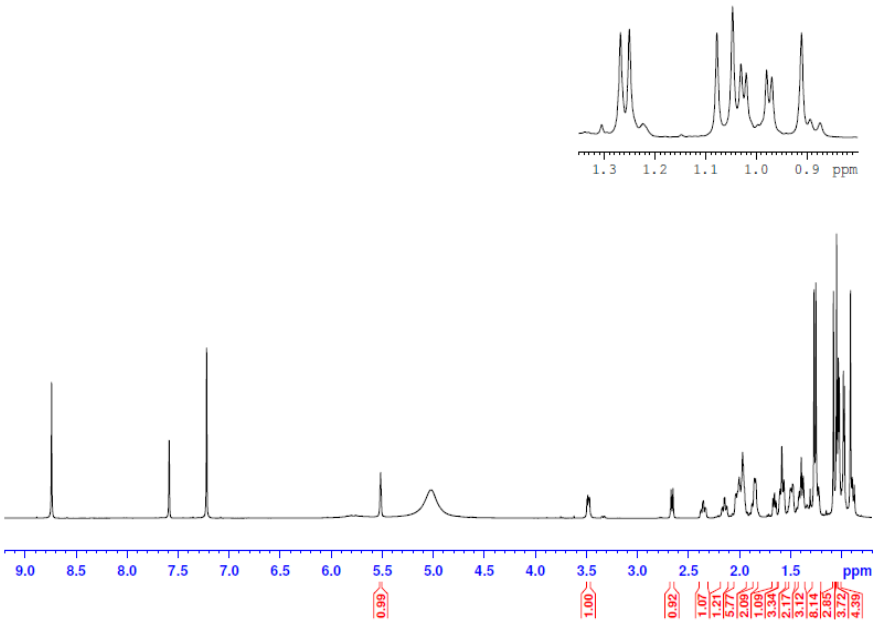

Appendix 9: ^{1}H NMR spectrum (600MHz, pyridine-d_5) of compound 2

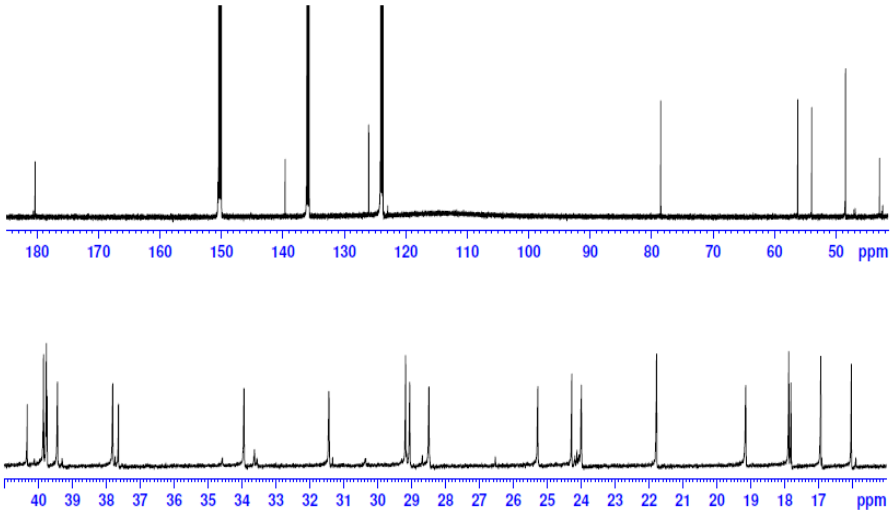

Appendix 10: {^{1}H}-^{13}C NMR spectrum (150MHz, pyridine-d_5) of compound 2

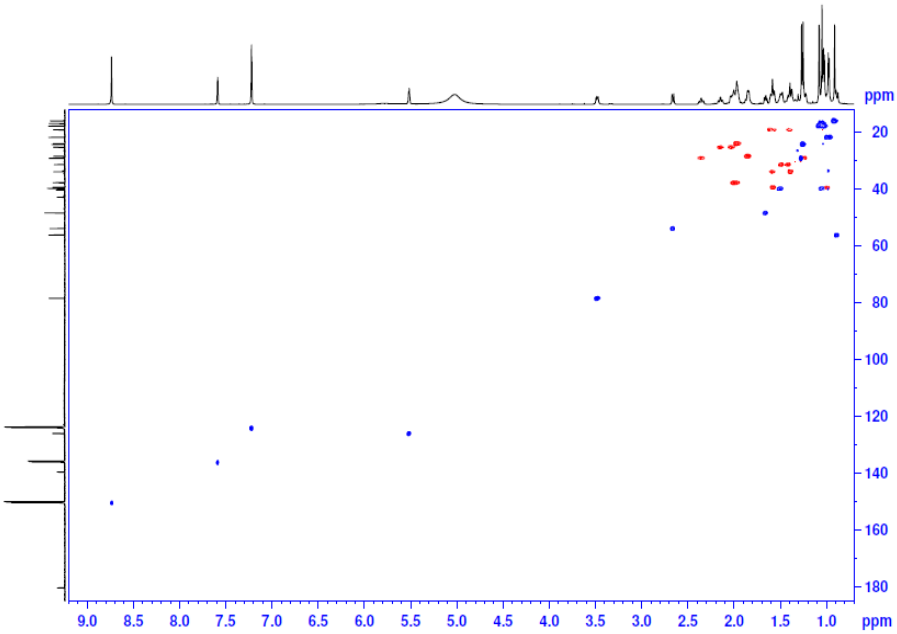

Appendix 11a : DEPT-edited ^{1}H-^{13}C HSQC spectrum (600MHz, pyridine d_5) of compound 2

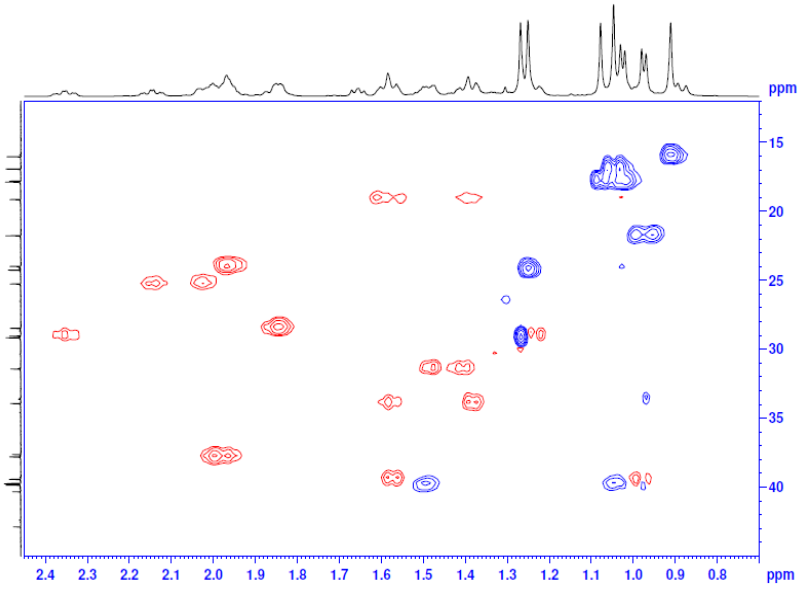

Appendix 11b: DEPT-edited ^{1}H-^{13}C HSQC spectrum (600MHz, pyridine d_5) of compound 2 (upfield expansion)

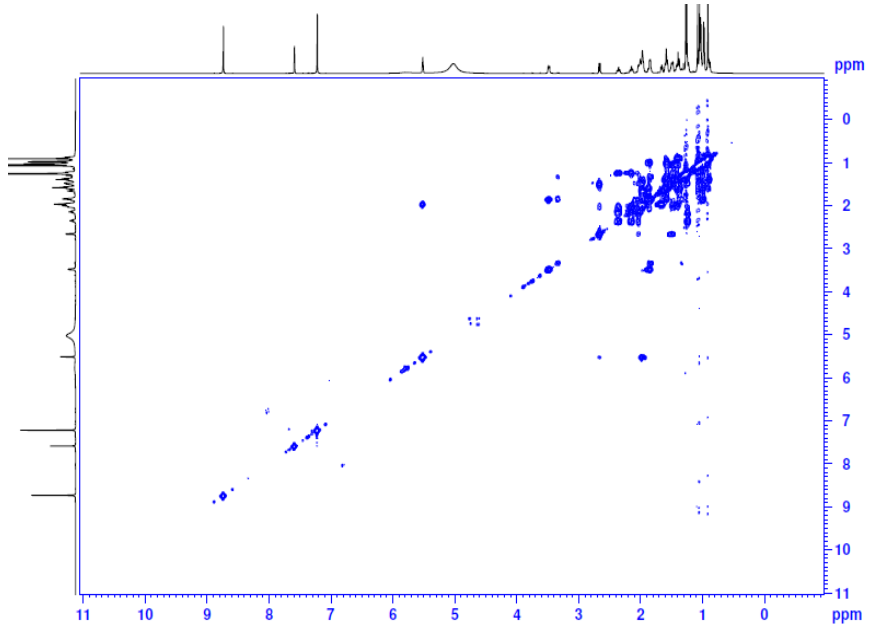

Appendix 12a: ^{1}H-^{1}H gCOSY spectrum (600MHz, pyridine d_5) of compound 2

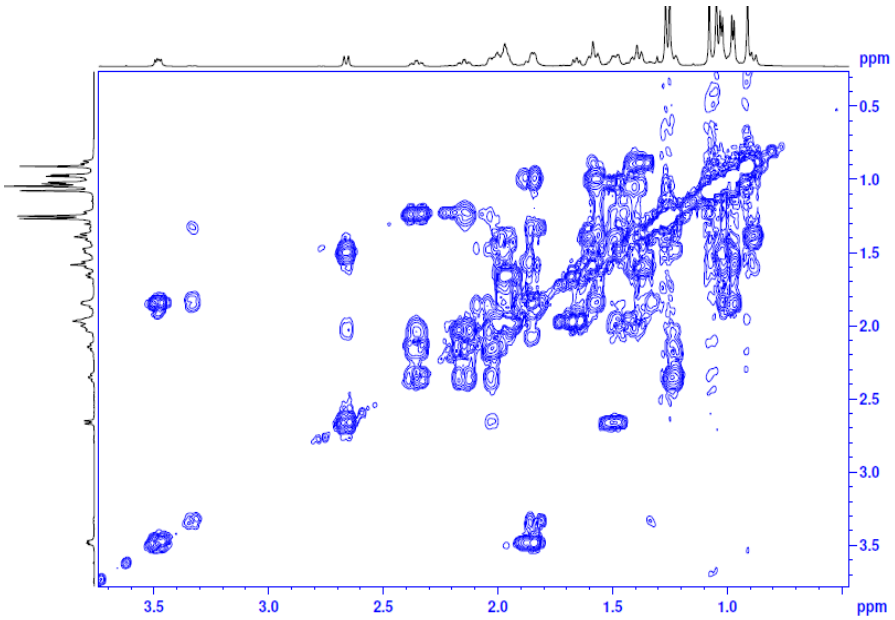

Appendix 12b: ^{1}H-^{1}H gCOSY spectrum (600MHz, pyridine d_5) of compound 2 (upfield expansion)

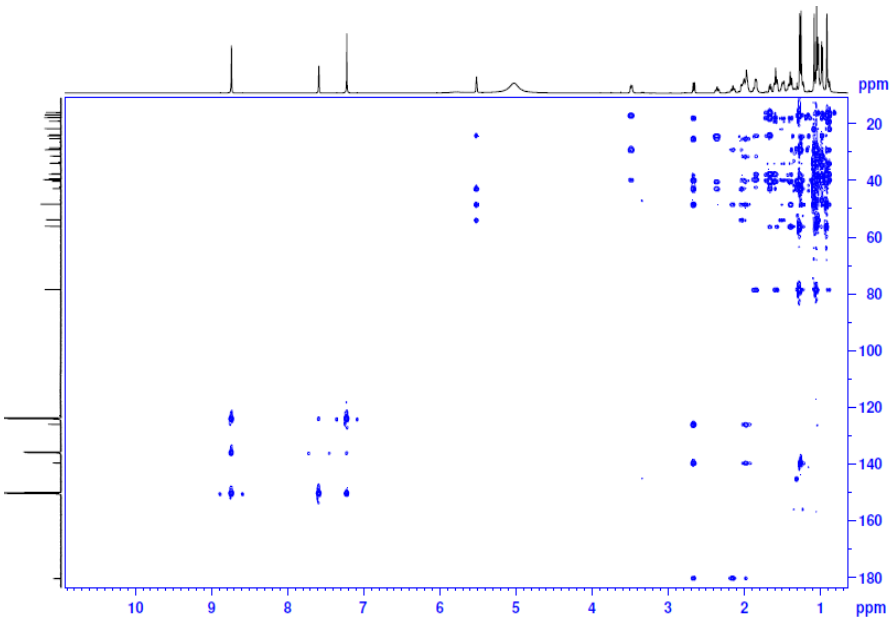

Appendix 13a: ^{1}H-^{13}C gHMBC spectrum (600MHz, pyridine d_5) of compound 2

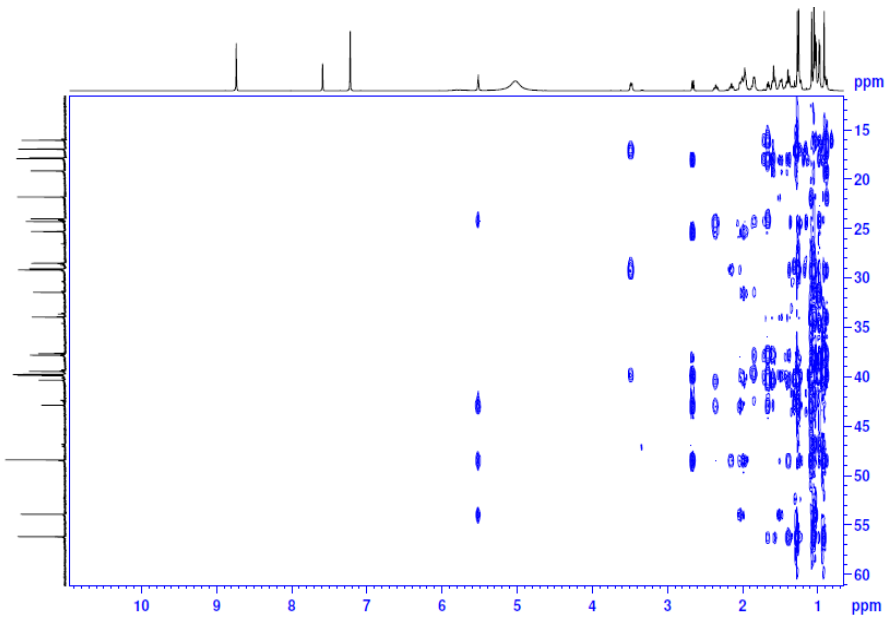

Appendix 13b: ^{1}H-^{13}C gHMBC spectrum (600MHz, pyridine d_5) of compound 2 (upfield expansion 1)

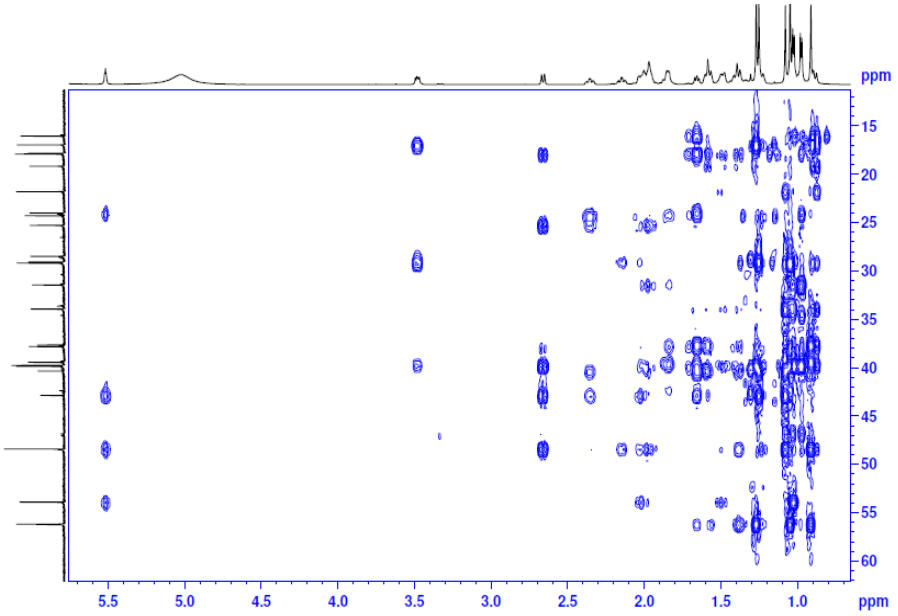

Appendix 13c: ^{1}H-^{13}C gHMBC spectrum (600MHz, pyridine d_5) of compound 2 (upfield expansion 2)

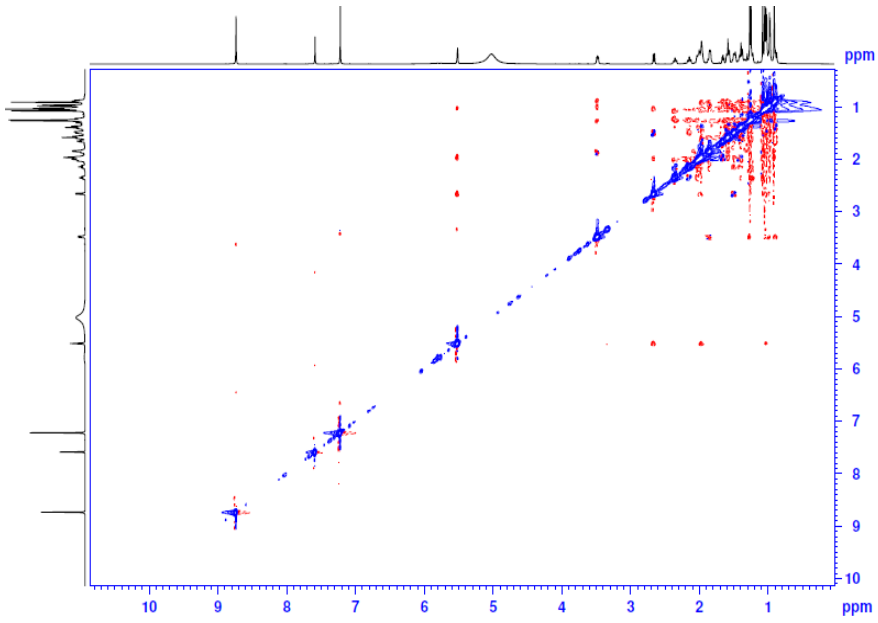

Appendix 14a : ^{1}H -^{1}H ROESY spectrum (pyridine-d_5, 600MHz) of compound 2

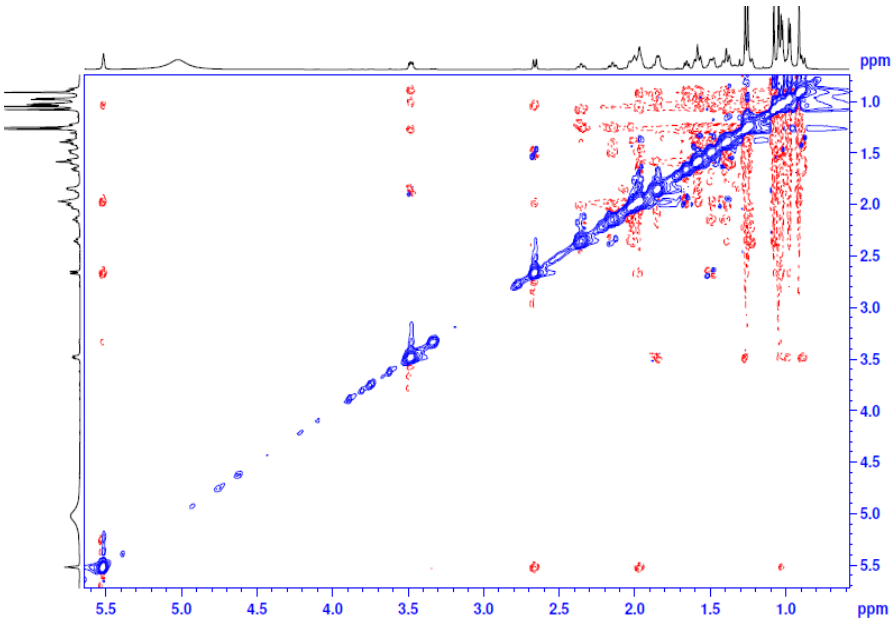

Appendix 14b : ^{1}H -^{1}H ROESY spectrum (pyridine-d_5, 600MHz) of compound 2 (upfield expansion)

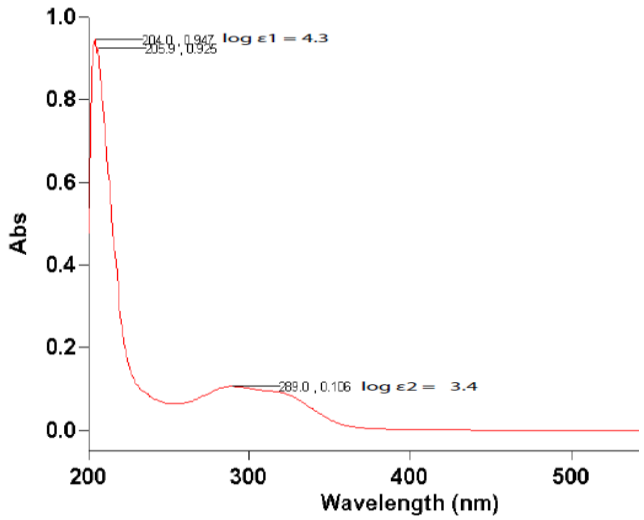

Appendix 15: UV spectrum (4.39 x 10^{-5}M, MeOH) of compound 2

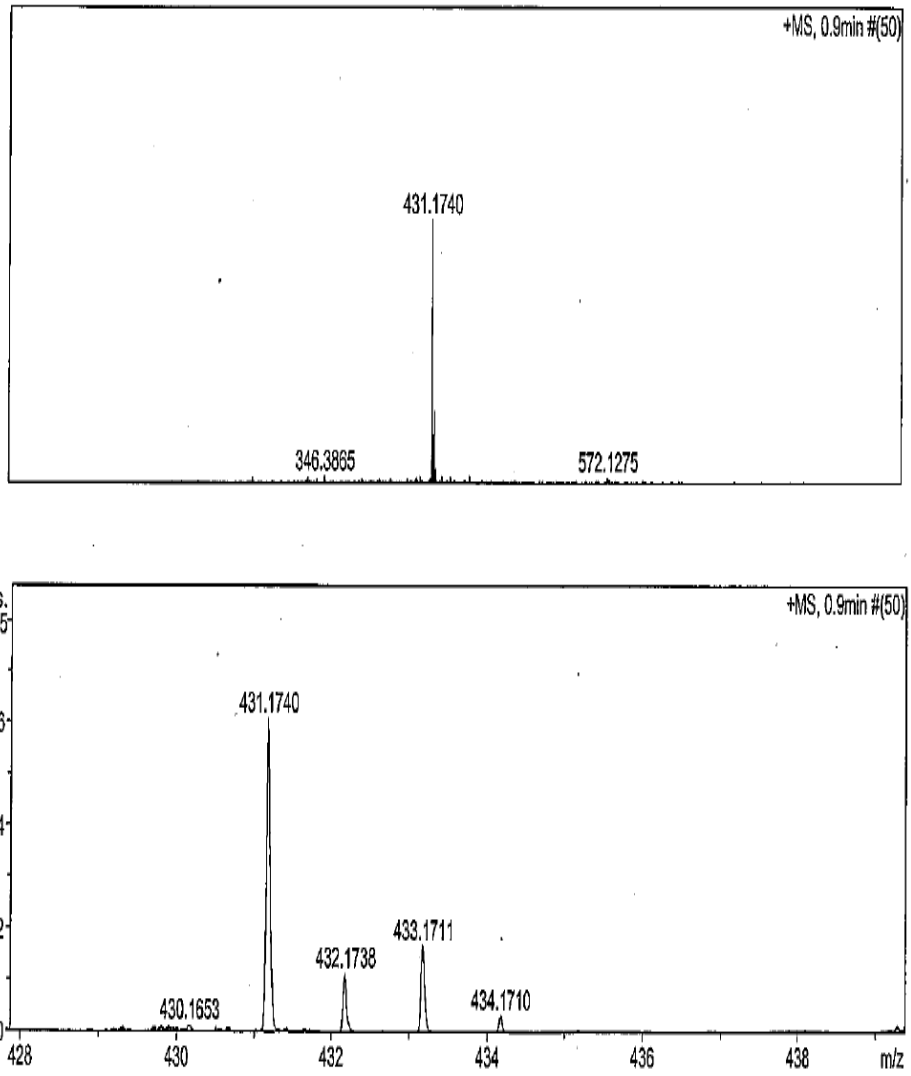

m/z 431.1740 $[M]^+$ (calcd. For $C_{23}H_{28}ClN_2O_4$, 431.1732). Err. (ppm) -1.94

Appendix 16: High Resolution ESI (+) MS of compound 3

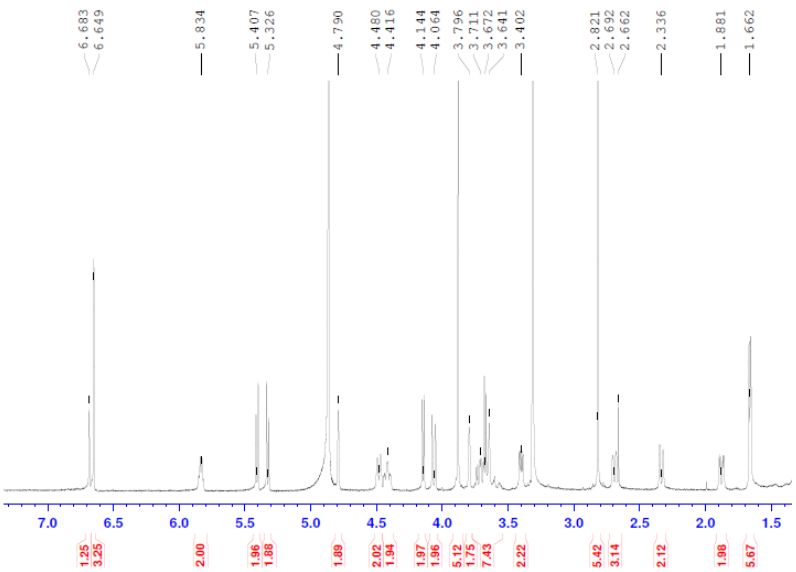

Appendix 17: ^{1}H NMR spectrum (600MHz, CD_3OD) of compound 3

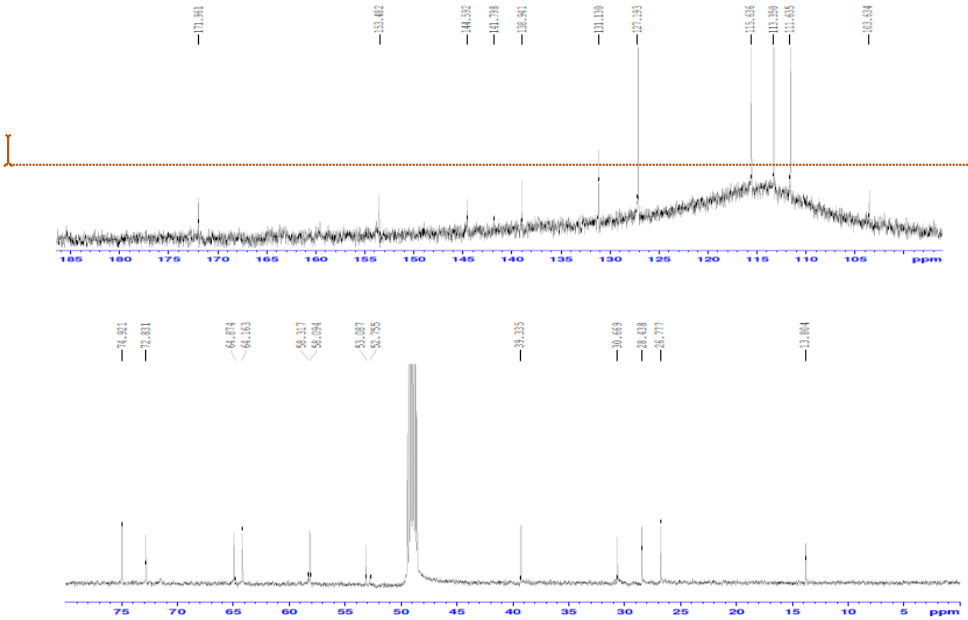

Comment [O1]:

Comment [O2]:

Comment [O3]:

Appendix 18: {^{1}H}- ^{13}C NMR spectrum (150MHz, CD_3OD) of compound 3

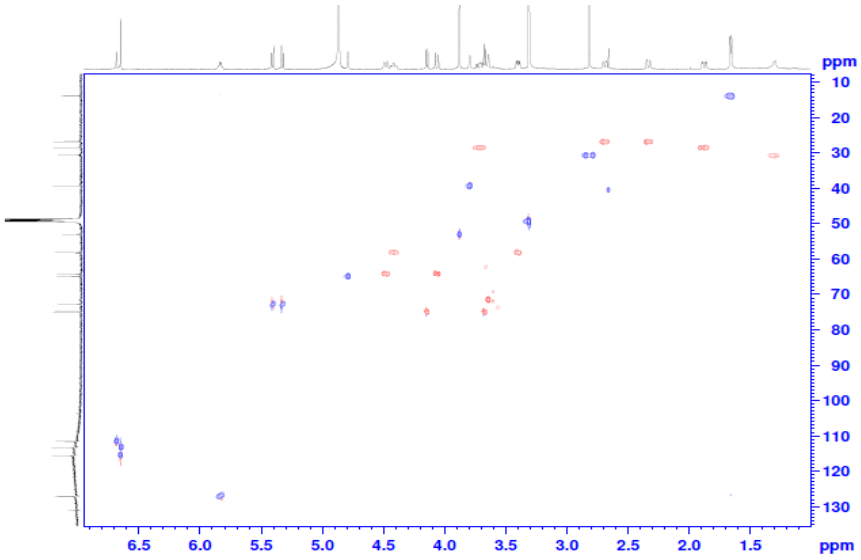

Appendix 19a: DEPT- edited ^{1}H-^{13}C HSQC spectrum (600MHz, CD_3OD) of compound 3

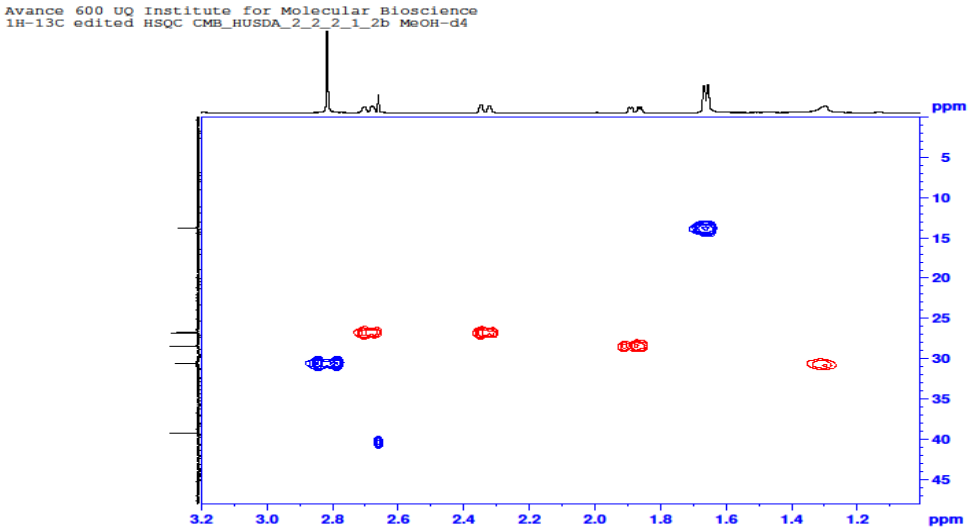

Appendix 19b: DEPT- edited ^{1}H-^{13}C HSQC spectrum (CD_3OD , 600MHz) of compound 3 (expansion 1)

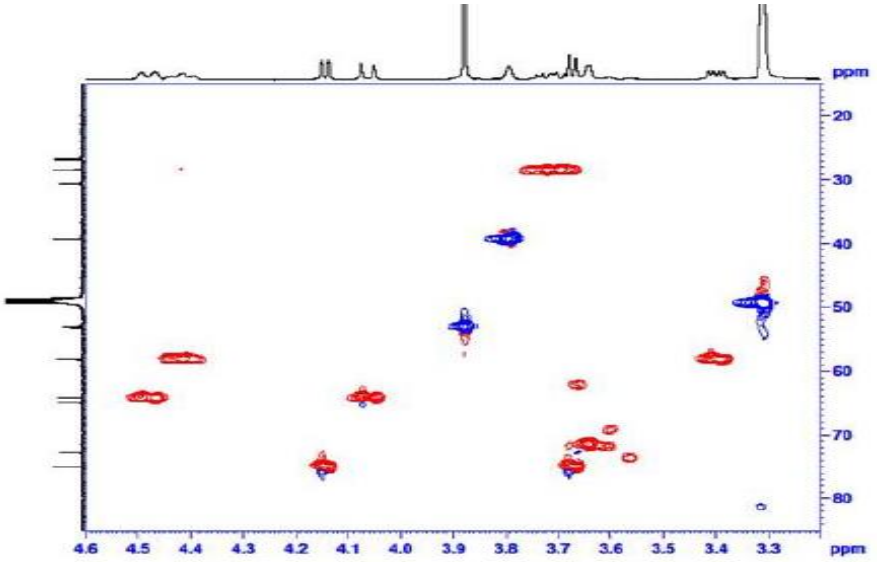

Appendix 19c: DEPT- edited ^{1}H-^{13}C HSQC spectrum(CD_3OD, 600MHz) of compound 3 (expansion 2)

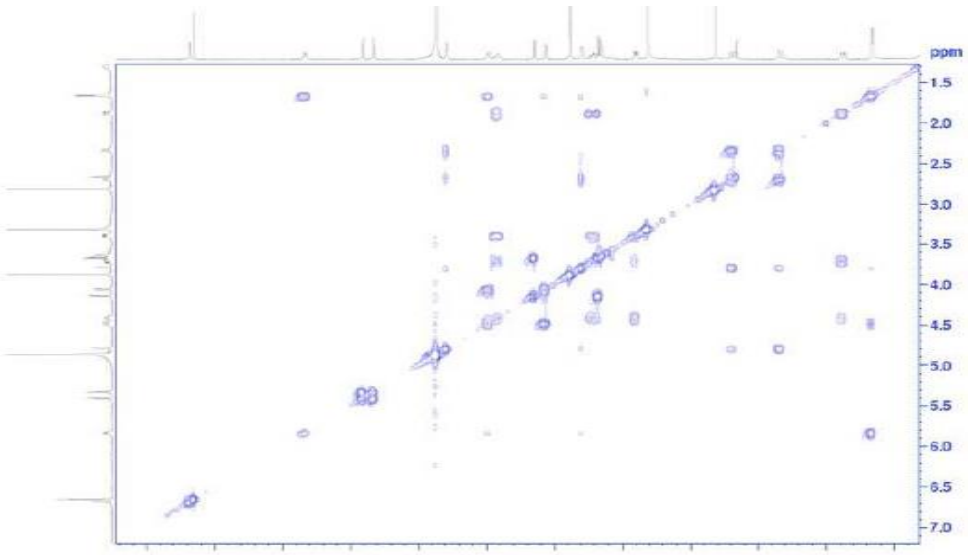

Appendix 20: ^{1}H-^{1}H gCOSY spectrum (600MHz, CD_3OD) of compound 3.

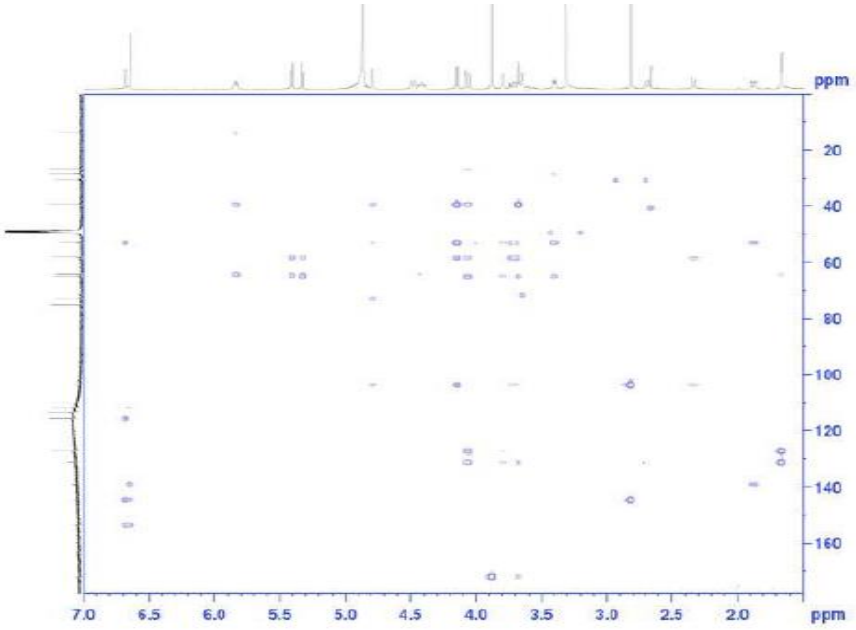

Appendix 21a: ^{1}H-^{13}C gHMBC spectrum (600MHz, CD_3OD))of compound 3.

Comment [O4]:

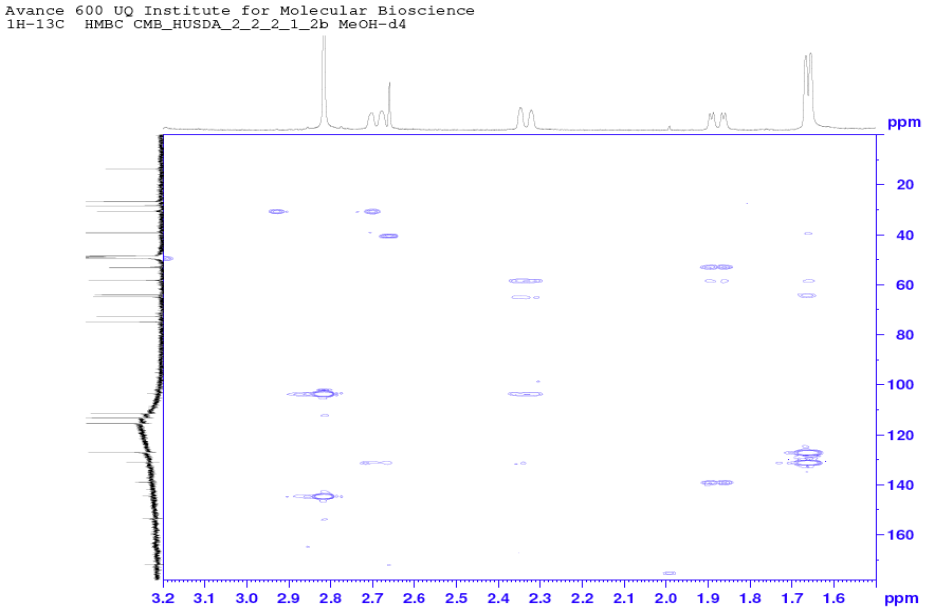

Appendix 21b: ^{1}H-^{13}C gHMBCspectrum (600MHz, CD_3OD) of compound 3.

(expansion 1)

Comment [O5]:

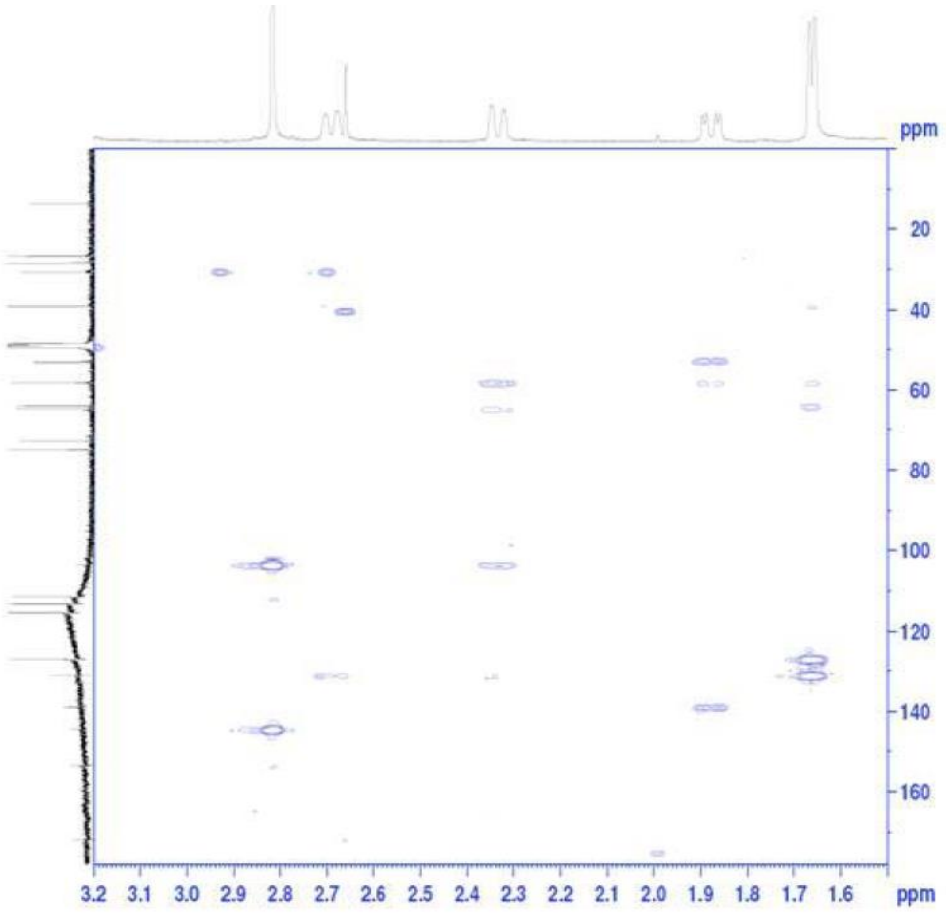

Appendix 21c: ^{1}H-^{13}C gHMBC spectrum (600MHz, CD_3OD) of compound 3 (expansion 2).

Comment [O6]:

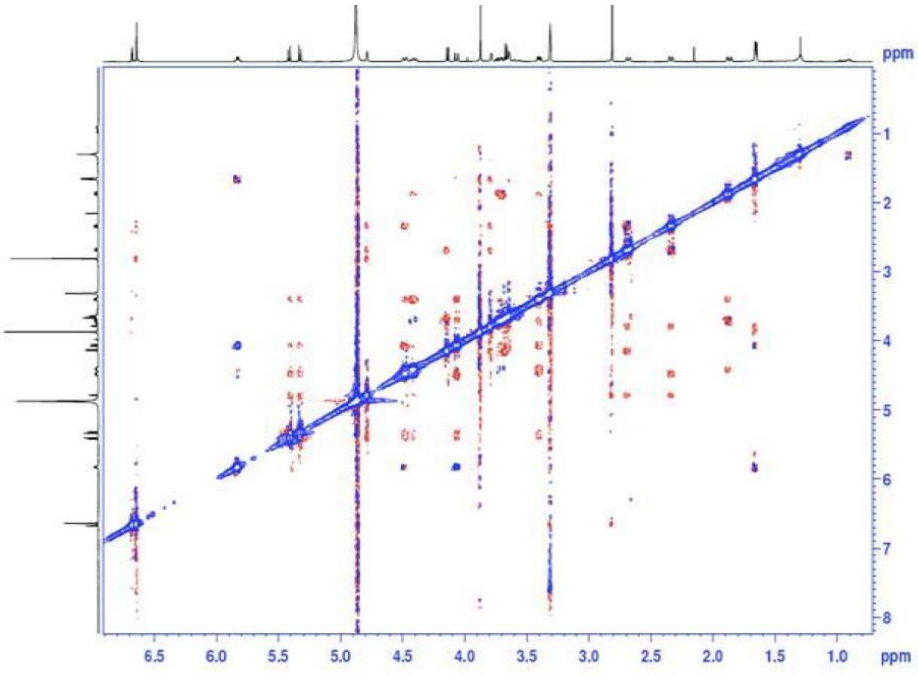

Appendix 22: ^{1}H-^{1}H ROESY spectrum (600MHz, CD3OD) of compound 3.

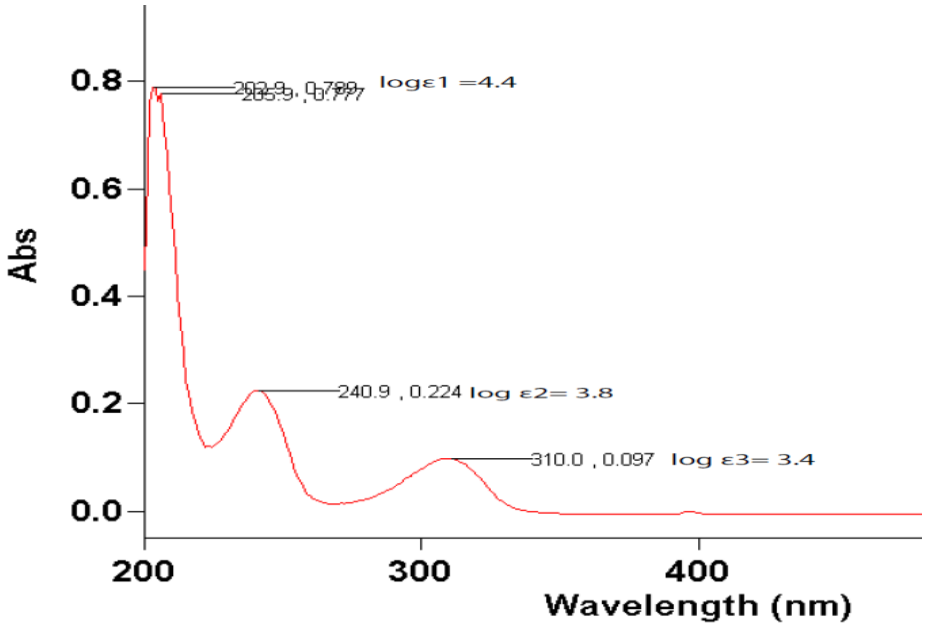

Appendix 23: UV spectrum (3.48 x10^{-5} M, MeOH) of compound 3.

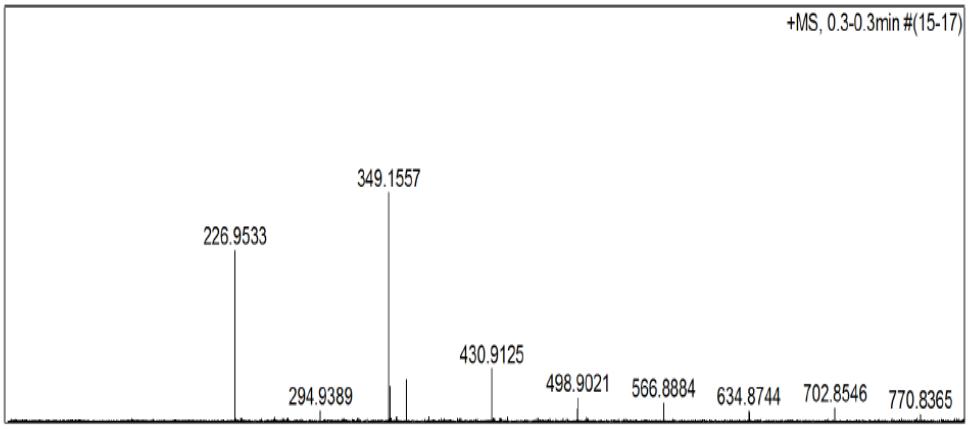

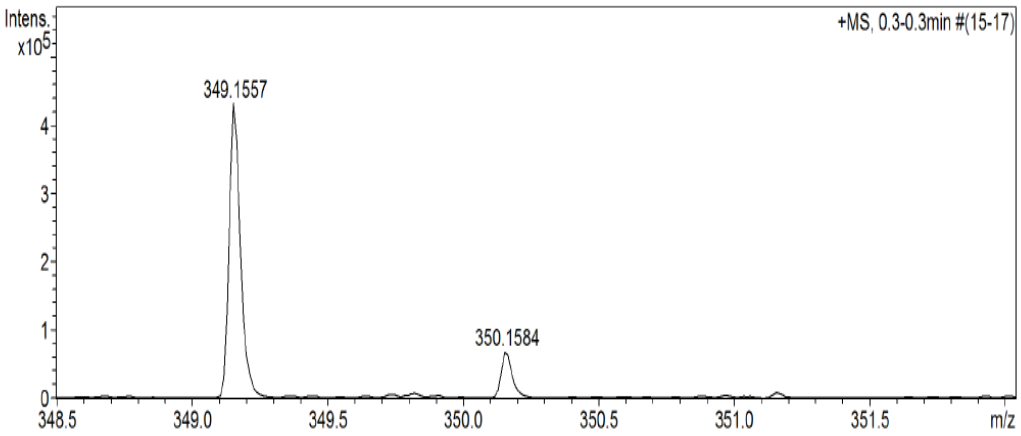

m/z 349.1557 M^+ (calcd. For $C_{21}H_{21}N_2O_3$, 349.1547) Err.(ppm) -3.09.

Appendix 24: High Resolution ESI (+) MS of compound 4.

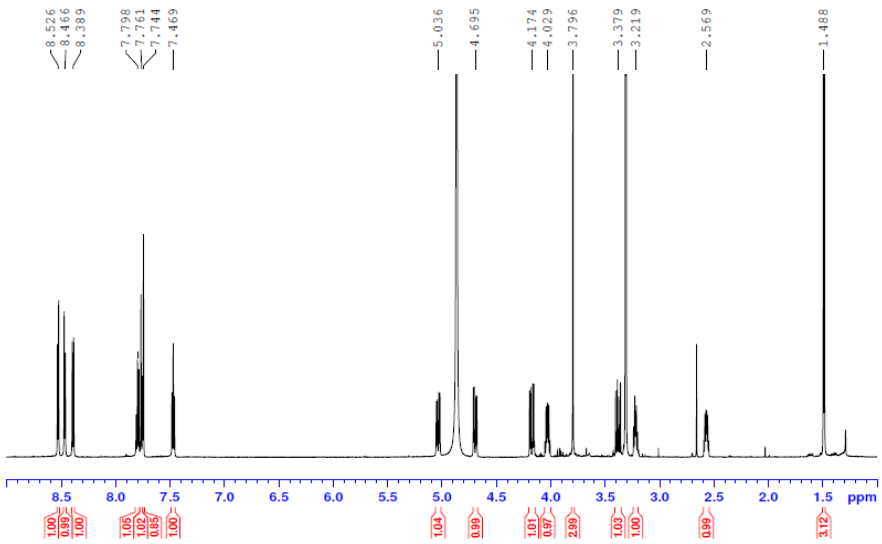

Appendix 25: ^{1}H NMR spectrum(600MHz, CD_3OD) of compound 4.

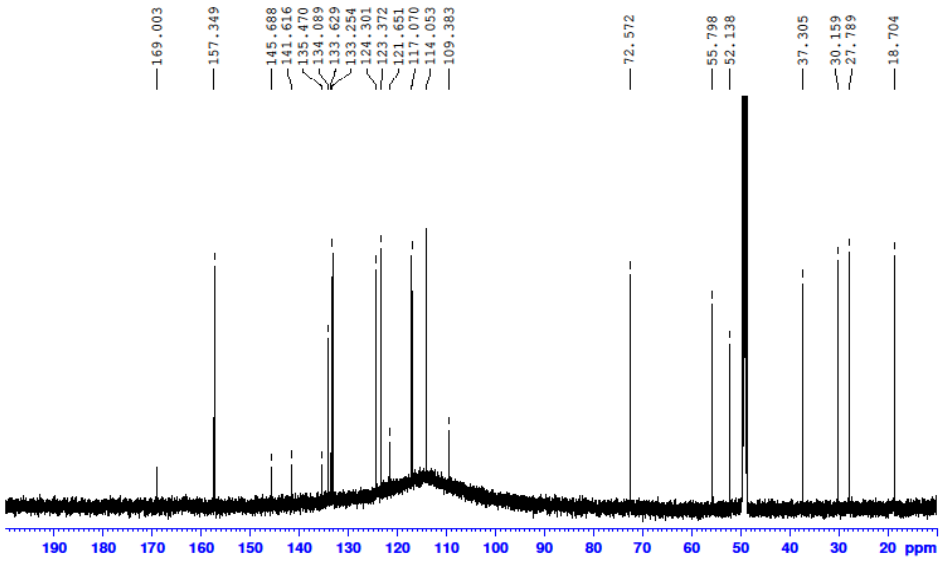

Appendix 26: {^{1}H}-^{13}C NMR spectrum (150MHz, CD_3OD) of compound 4.

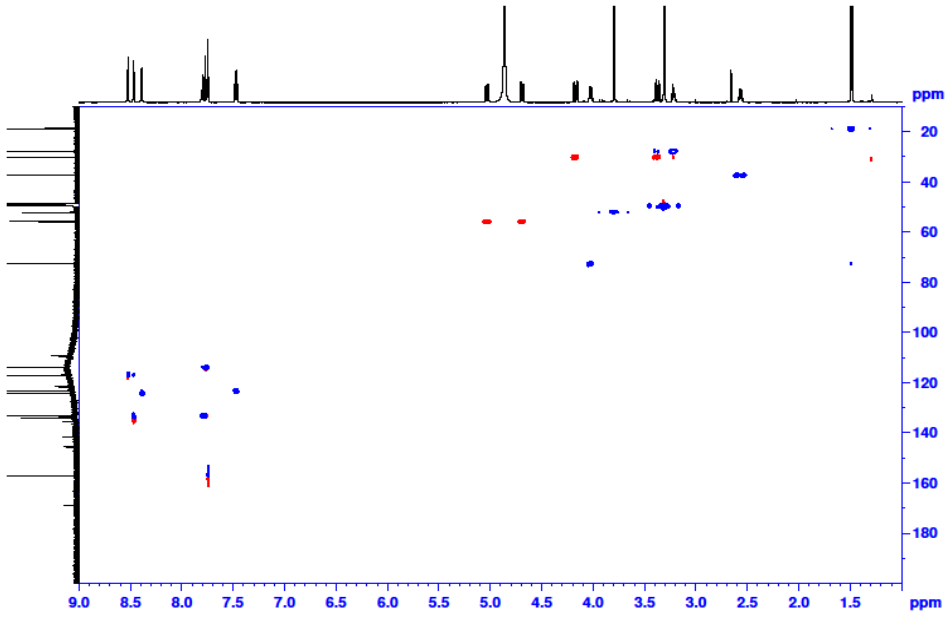

Appendix 27: DEPT- edited ^{1}H-^{13}C HSQC spectrum (600MHz, CD_3OD)) of compound 4

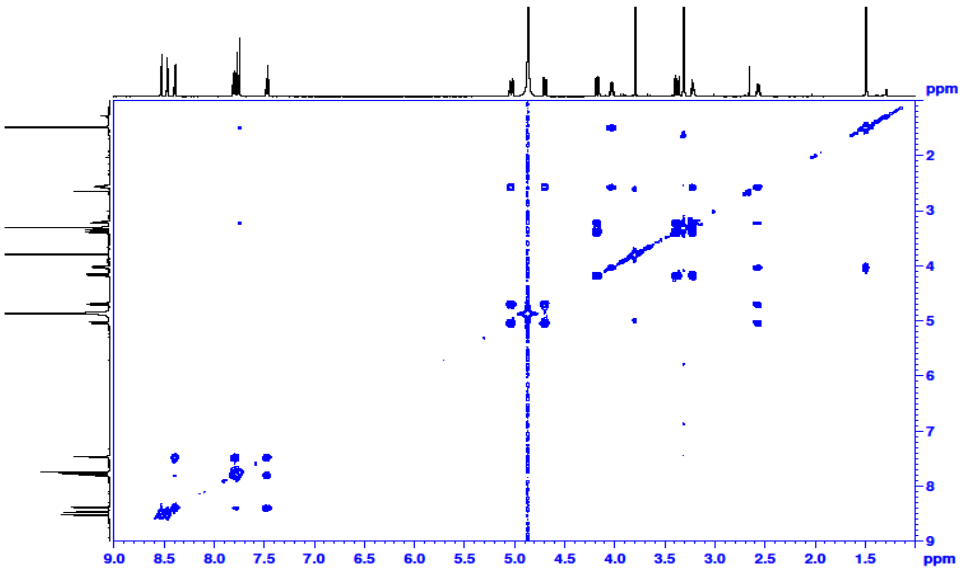

Appendix 28a: ^{1}H-^{1}H gCOSY spectrum (600MHz, CD_3OD) of compound 4

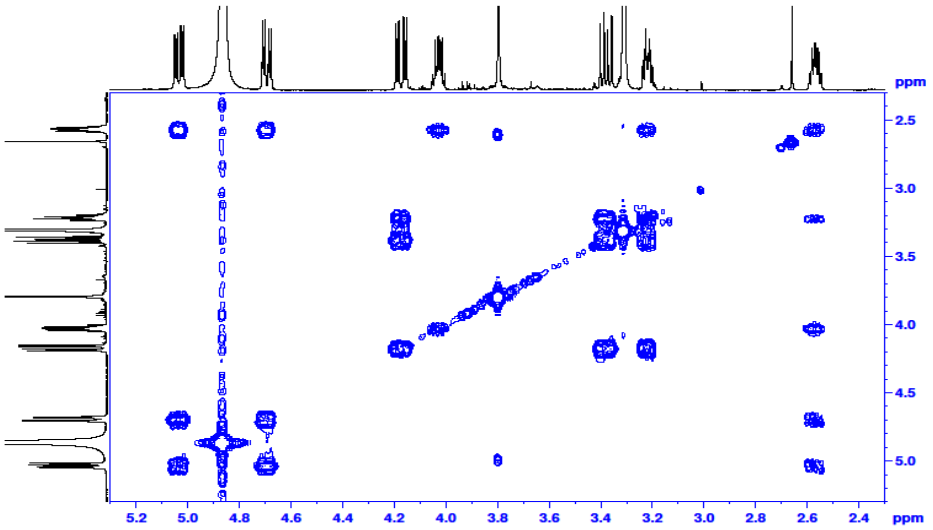

Appendix 28b: ^{1}H-^{1}H gCOSY spectrum (600MHz, CD_3OD) of compound 4 (expansion).

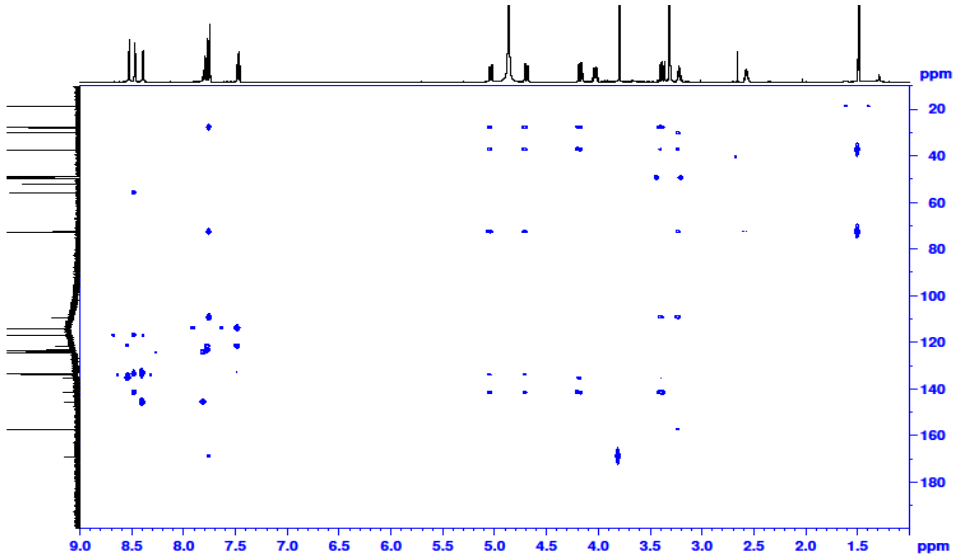

Appendix 29a: ^{1}H-^{13}C gHMBC spectrum (600MHz, CD_3OD) of compound 4.

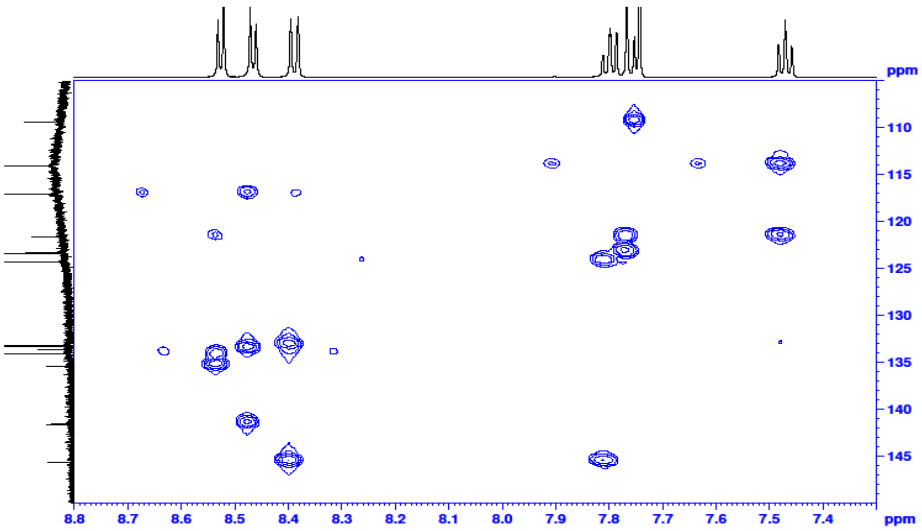

Appendix 29b: ^{1}H-^{13}C gHMBC spectrum (600MHz, CD_3OD) of compound 4 (expansion).

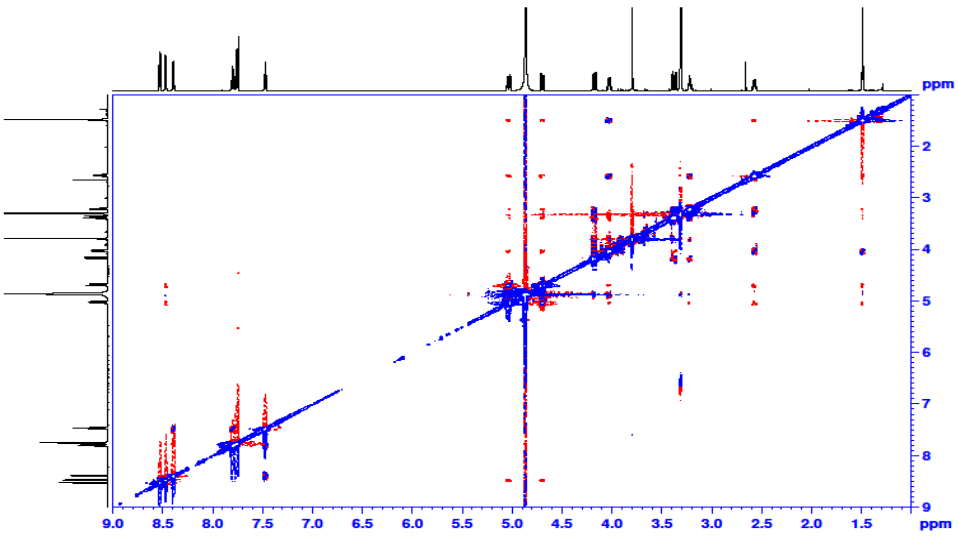

Appendix 30a ^{1}H-^{1}H ROESY spectrum (600MHz, CD_3OD) of compound 4.

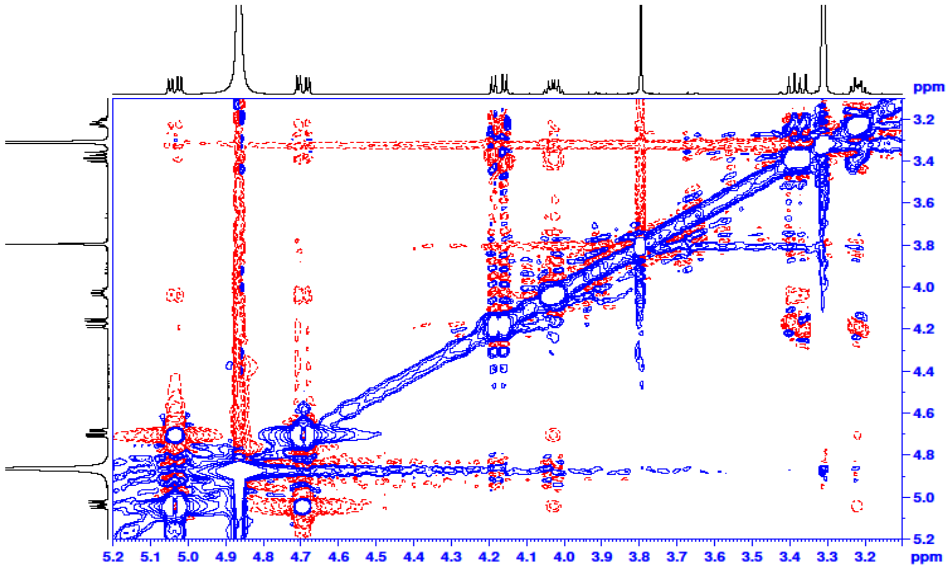

Appendix 30b: ^{1}H-^{1}H ROESY spectrum (600MHz, CD_3OD) of compound 4 (expansion).

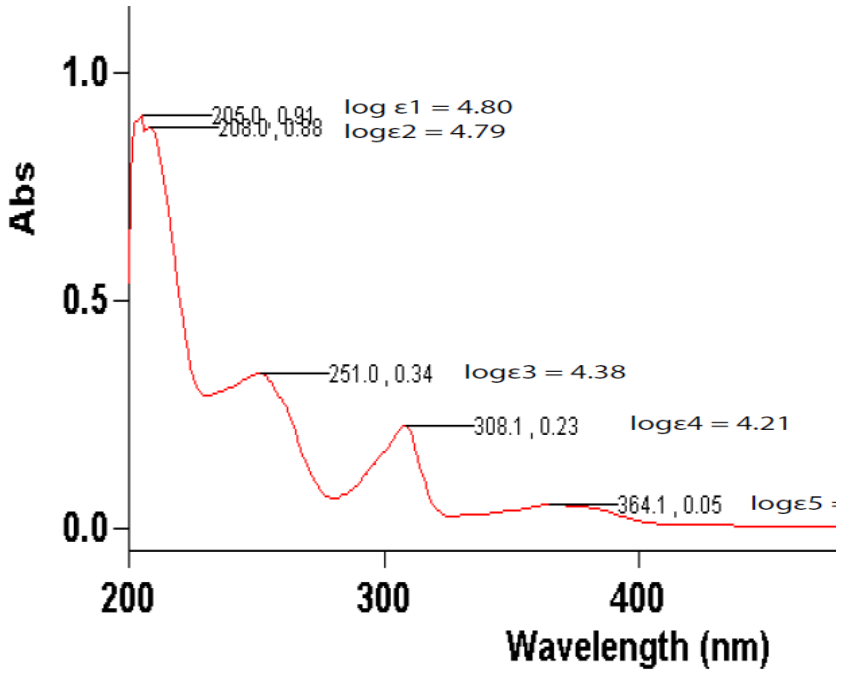

Appendix 31: UV spectrum (1.43 x 10^{-5}M, MeOH) of compound 4.

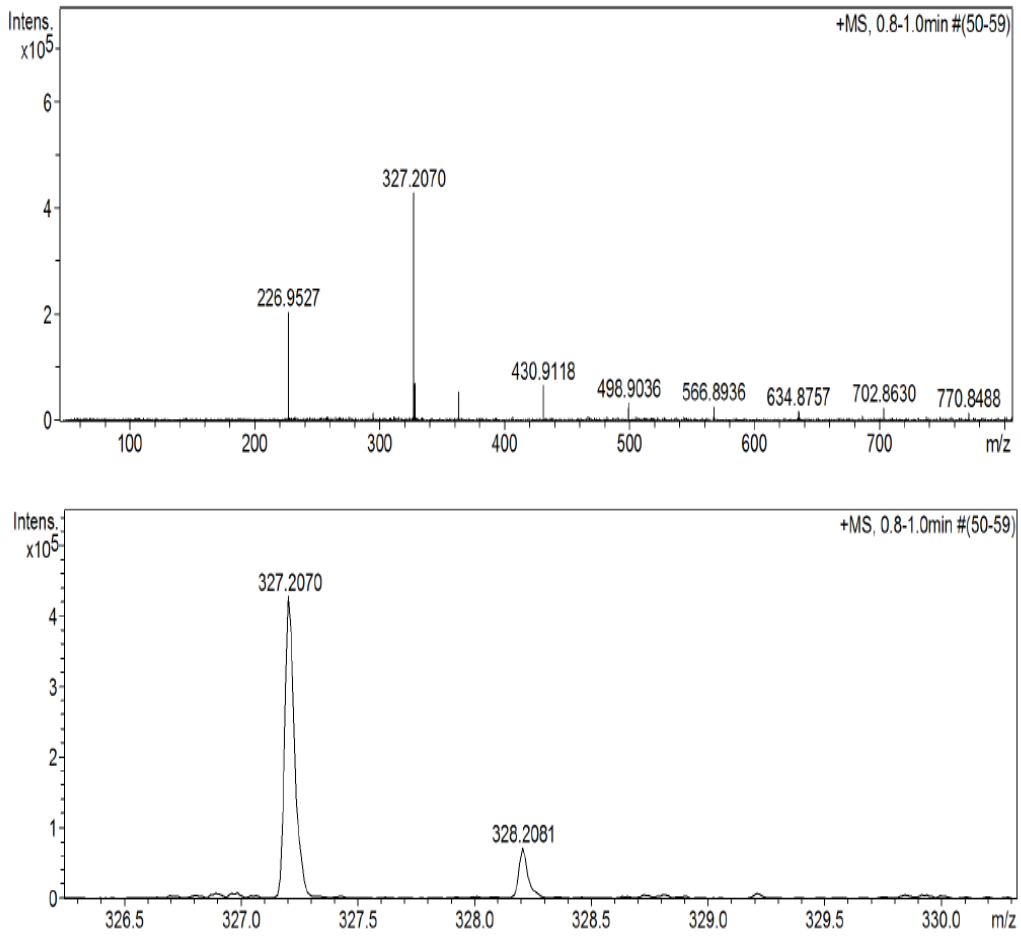

m/z 327.2070 M^+ (calcd. For $C_{20}H_{27}N_2O_2$, 327.2067) Err. (ppm), -0.92

Appendix 32: High Resolution ESI(+)MS of compound 5.

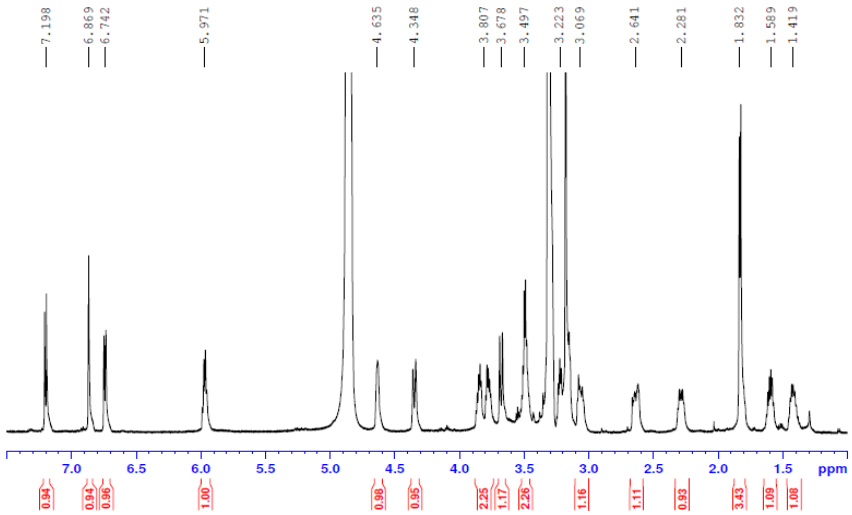

Appendix 33: ^{1}H NMR spectrum(600MHz, CD_3OD) of compound 5.

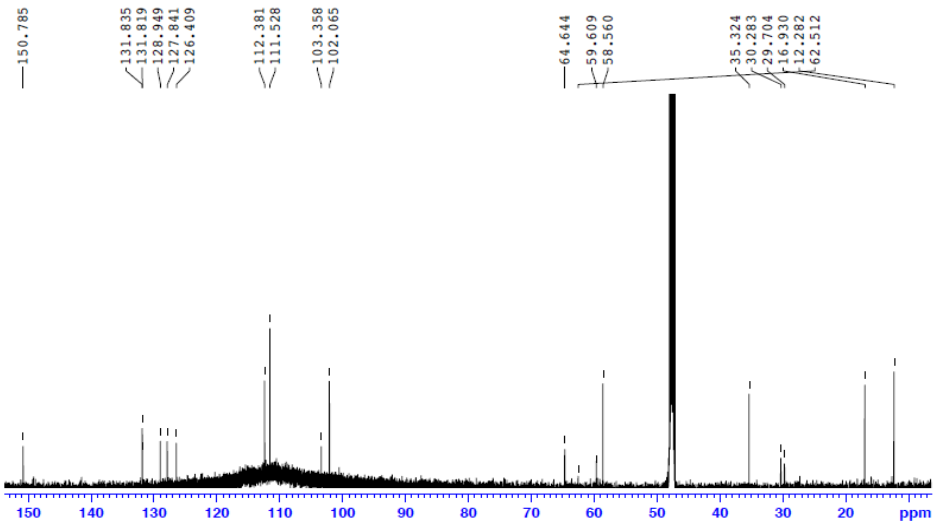

Appendix 34: {1H}-^{13}C NMR spectrum(150MHz, CD_3OD) of compound 5.

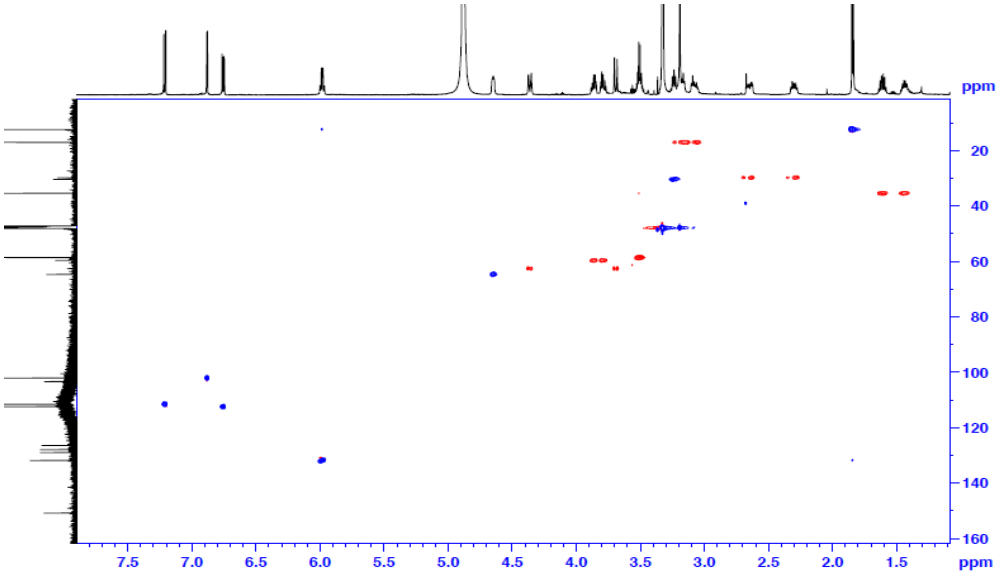

Appendix 35: DEPT-edited ^{1}H-^{13}C HSQC spectrum(600MHz, CD_3OD) of compound 5.

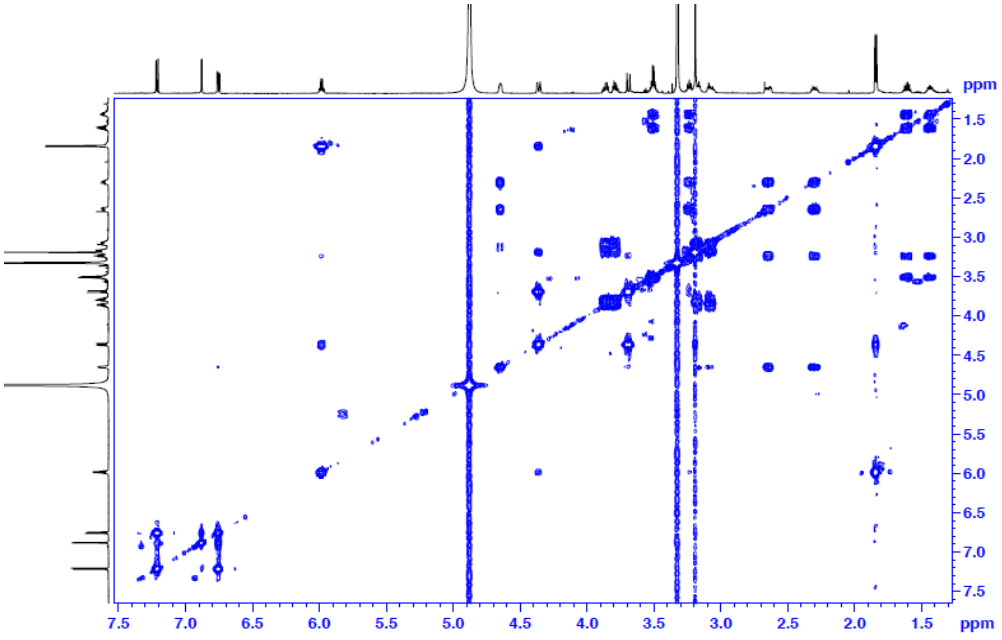

Appendix 36: ^{1}H-^{1}H gCOSY spectrum (600MHz, CD_3OD) of compound 5.

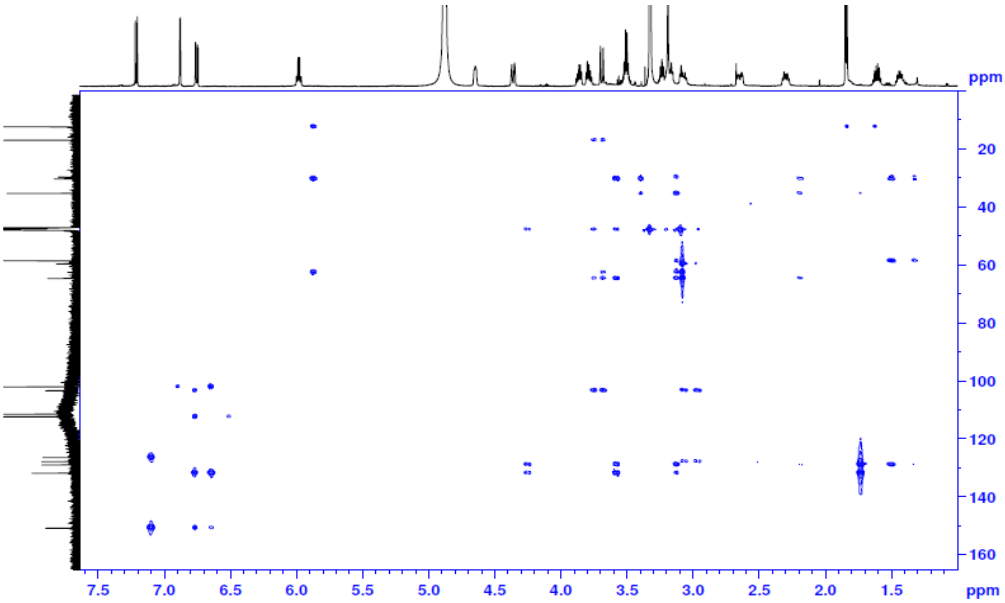

Appendix 37: ^{1}H-^{13}C gHMBC spectrum (600MHz, CD_3OD) of compound 5.

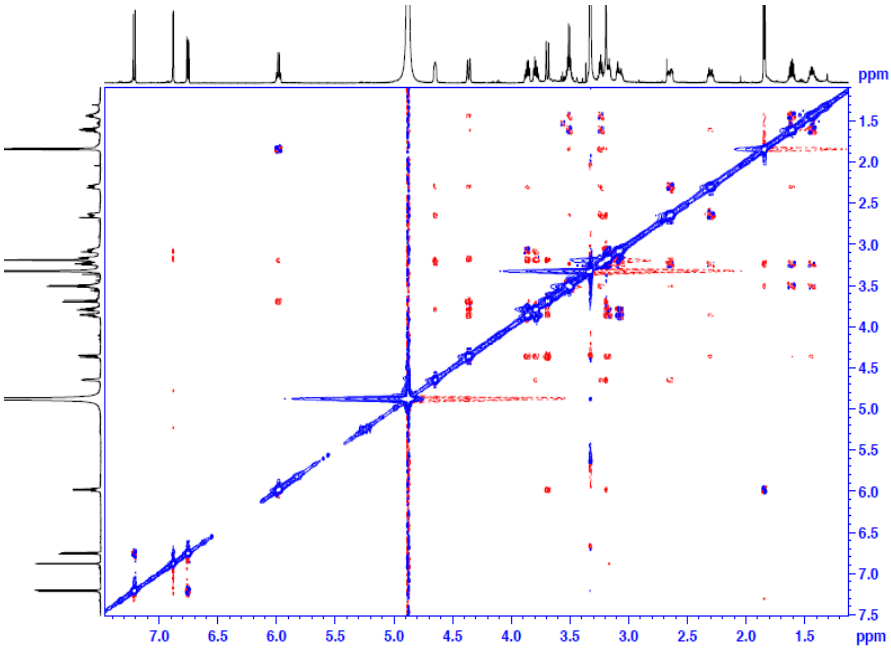

Appendix 38: ^{1}H-^{1}H ROESY spectrum (600MHz, CD_3OD) of compound 5.

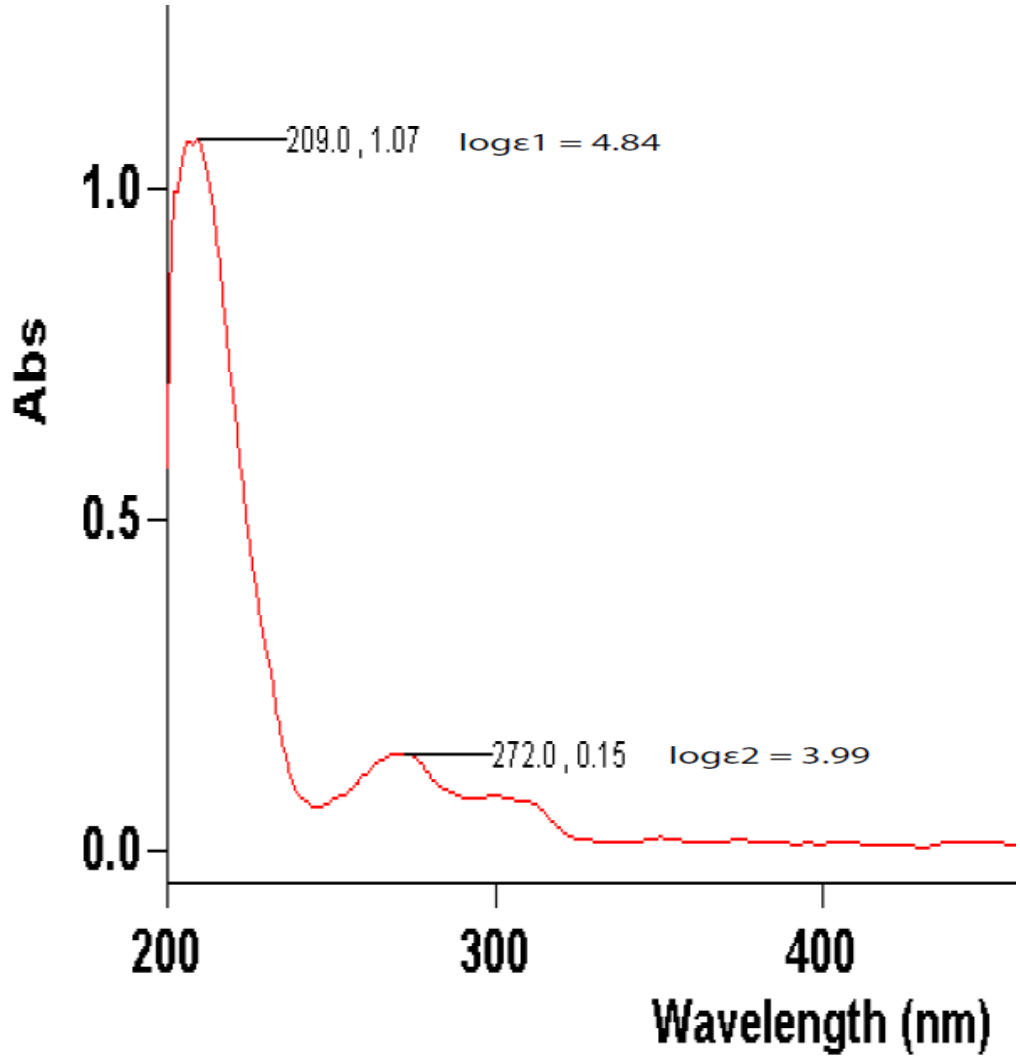

Appendix 39: UV spectrum (1.53 x^{10-5} M, MeOH) of compound 5.

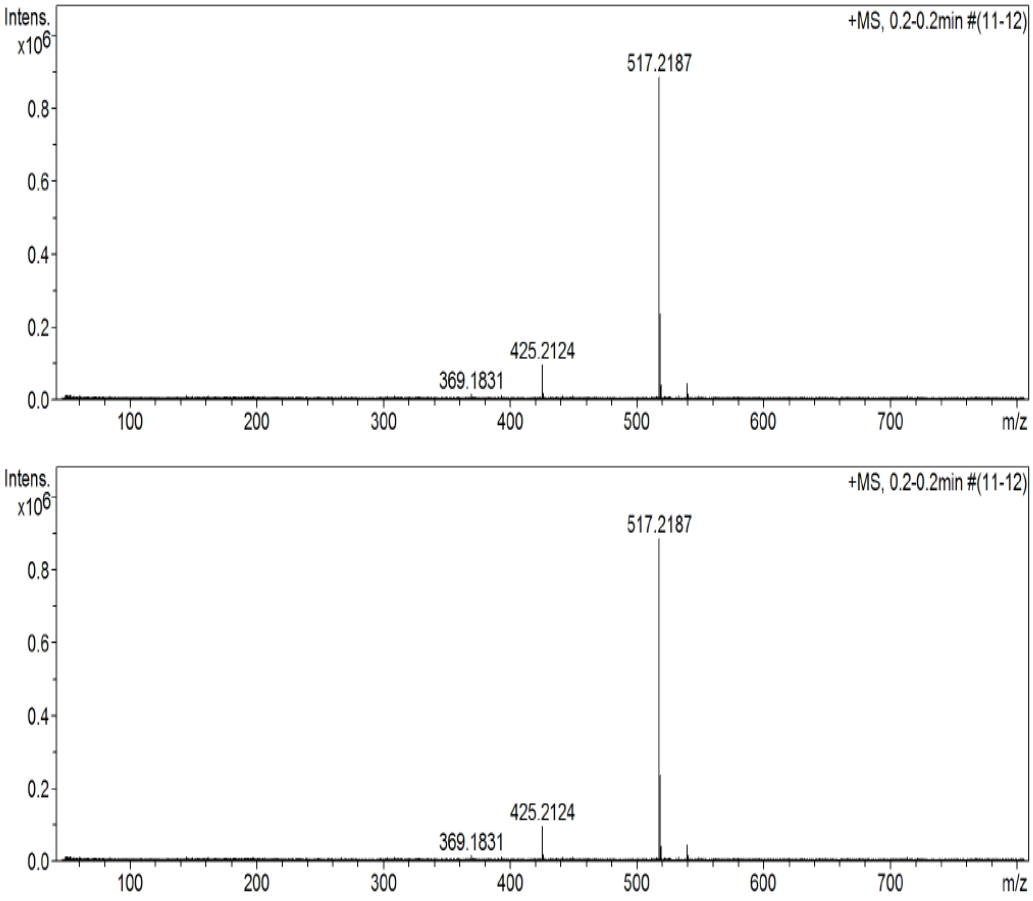

m/z 517.2187[M+H]$^+$ (calcd. for $C_{26}H_{33}N_2O_9$, 517.2181) Err.(ppm) -1.32

Appendix 40: High Resolution ESI(+)MS of compound 6.

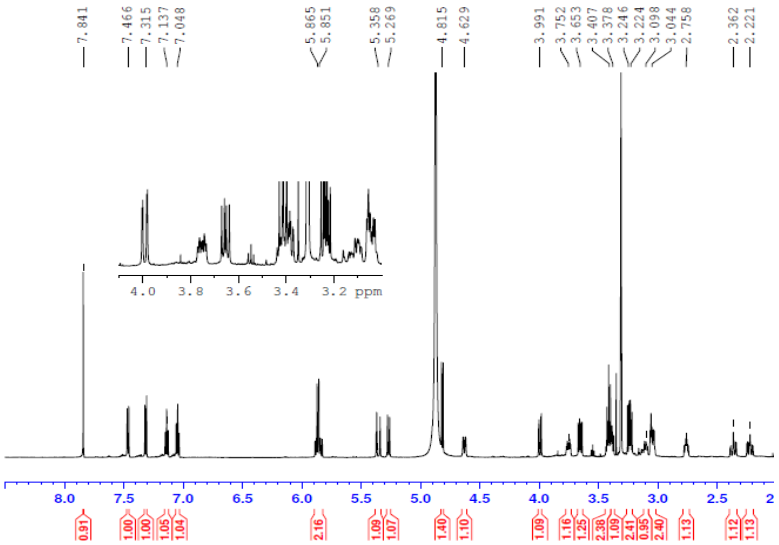

Appendix 41: ^{1}H NMR spectrum(600MHz, CD_3OD) of compound 6.

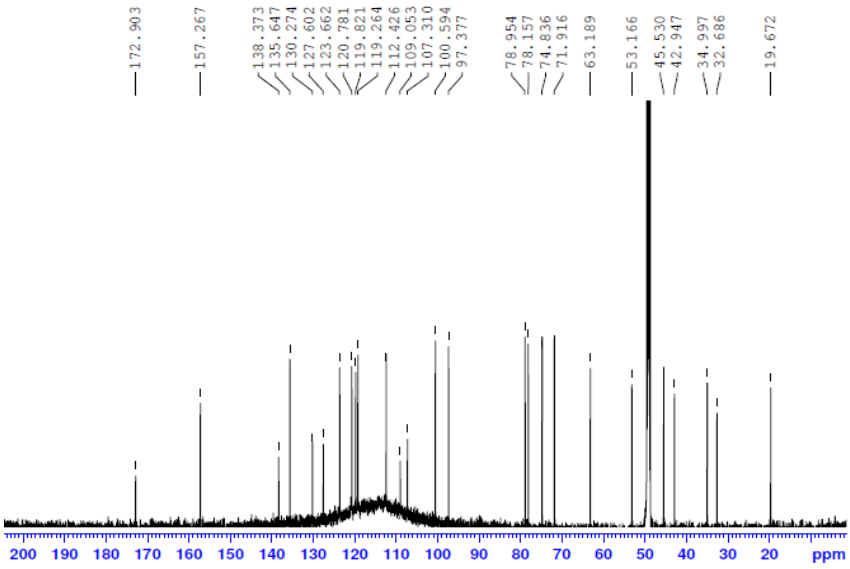

Appendix 42: $\{^{1}H\}$-^{13}C NMR spectrum(150MHz, CD_3OD) of compound 6.

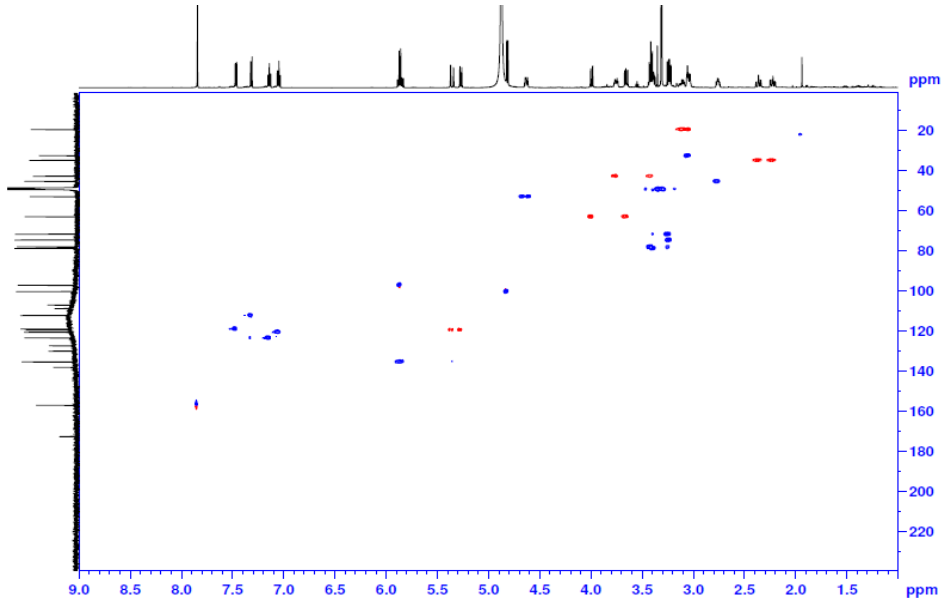

Appendix 43a: DEPT-edited ^{1}H-^{13}C HSQC spectrum (600MHz, CD_3OD) of compound 6.

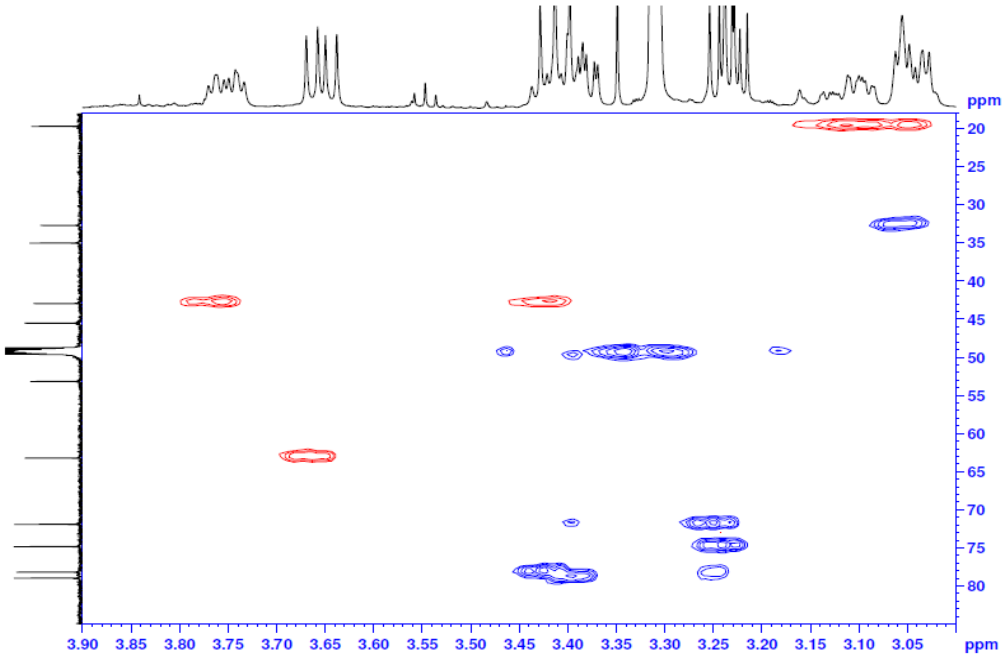

Appendix 43b: DEPT-edited ^{1}H-^{13}C HSQC spectrum expansion (600MHz, CD_3OD) of compound 6.

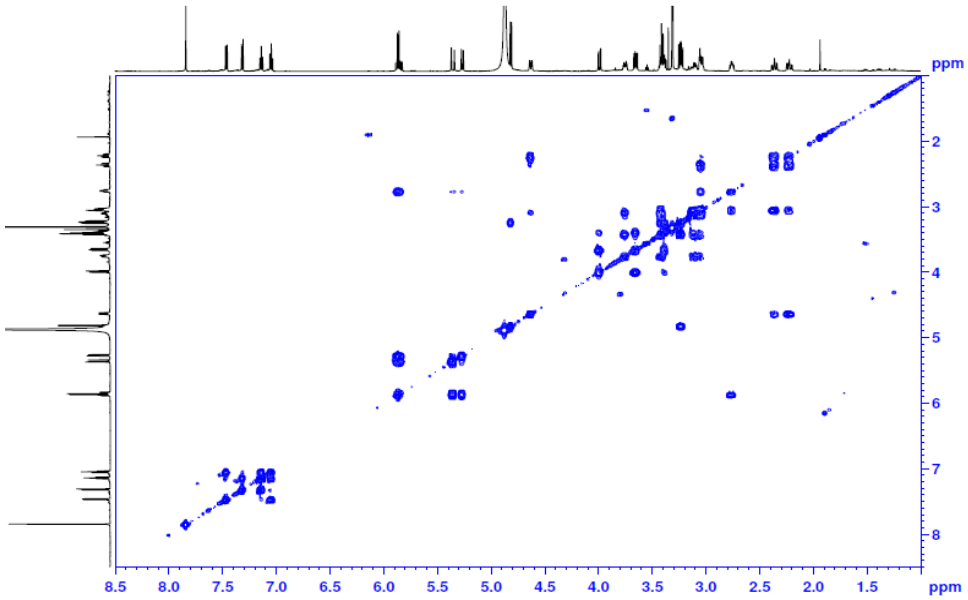

Appendix 44a: ^{1}H-^{1}H gCOSY spectrum (600MHz, CD_3OD) of compound 6.

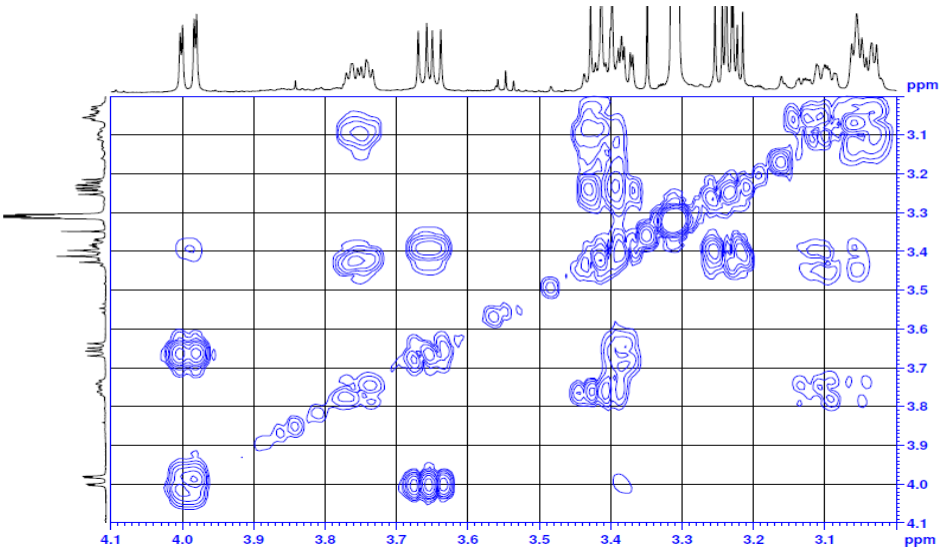

Appendix 44b: ^{1}H-^{1}H gCOSY spectrum expansion (600MHz, CD_3OD) of compound 6.

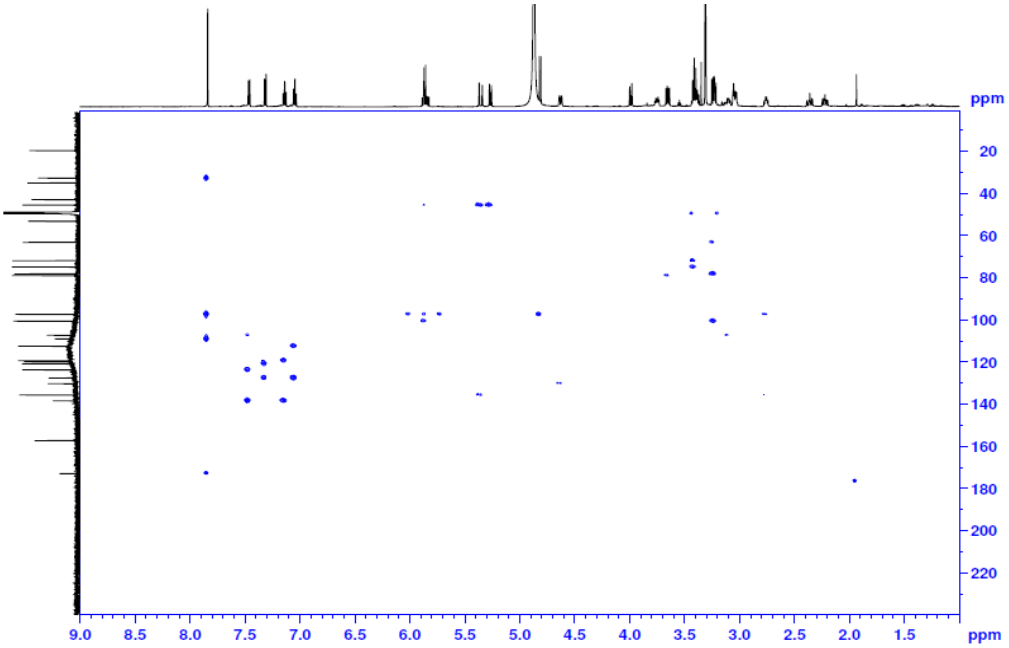

Appendix 45a: ^{1}H-^{13}C gHMBC spectrum (600MHz, CD_3OD) of compound 6.

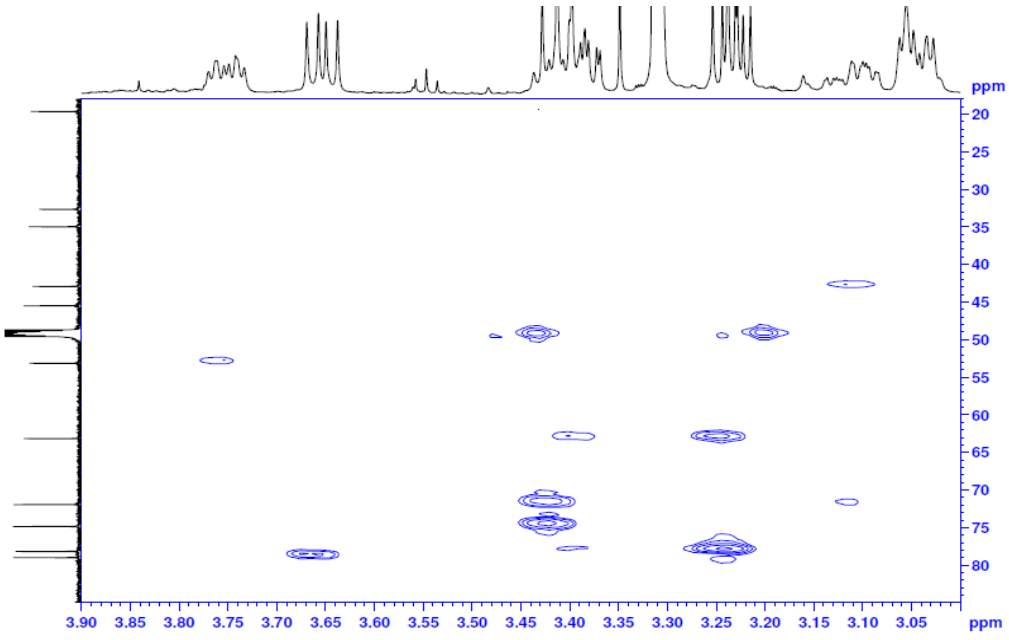

Appendix 45b: ^{1}H-^{13}C gHMBC spectrum expansion (600MHz, CD_3OD) of compound 6.

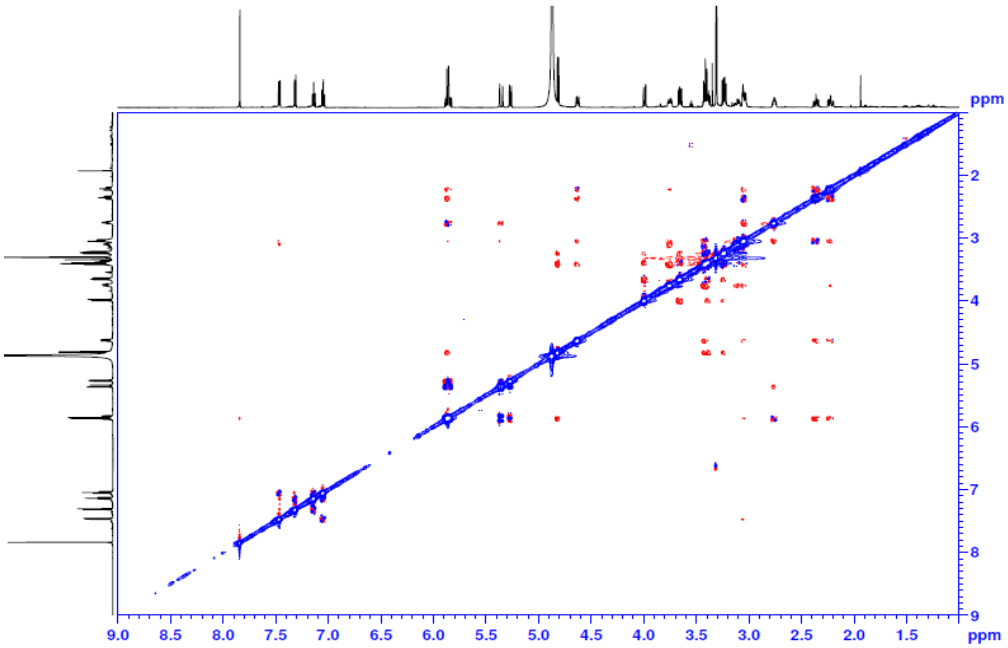

Appendix 46a: ^{1}H-^{1}H ROESY spectrum (600MHz, CD_3OD) of compound 6.

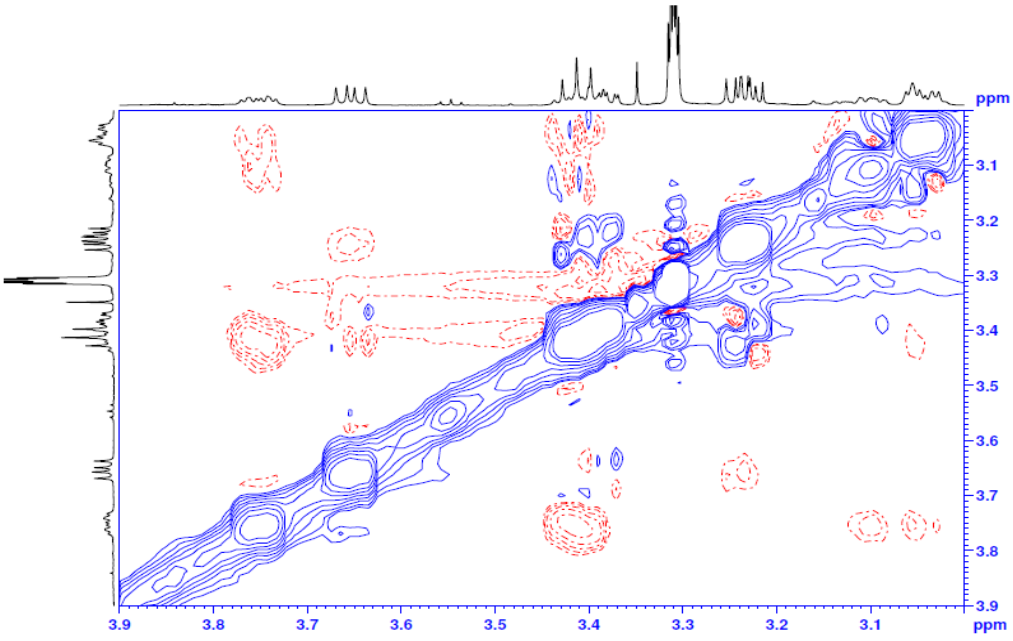

Appendix 46b: ^{1}H-^{1}H ROESY spectrum expansion (600MHz, CD_3OD) of compound 6.

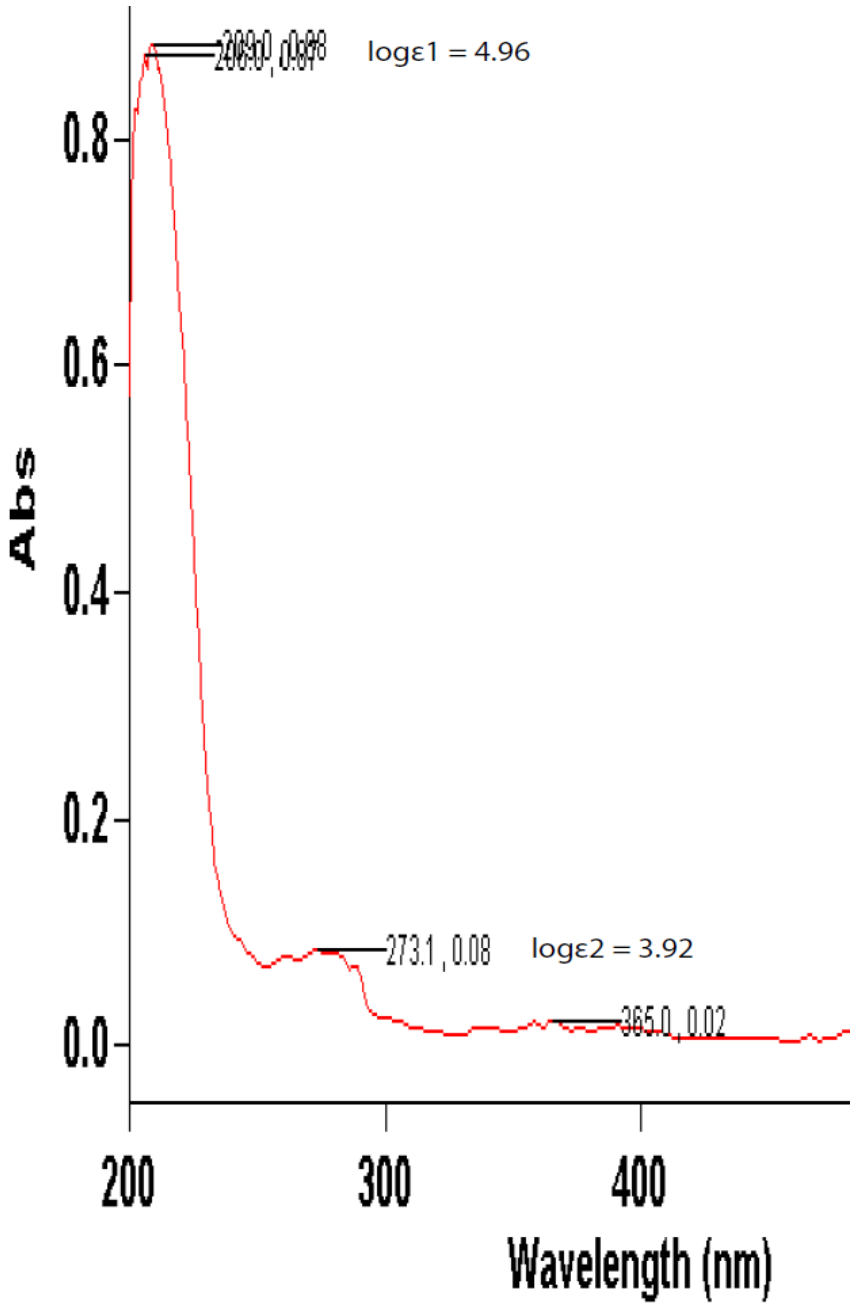

Appendix 47: UV spectrum (1.42 x 10^{-5} M, MeOH) of compound 6.

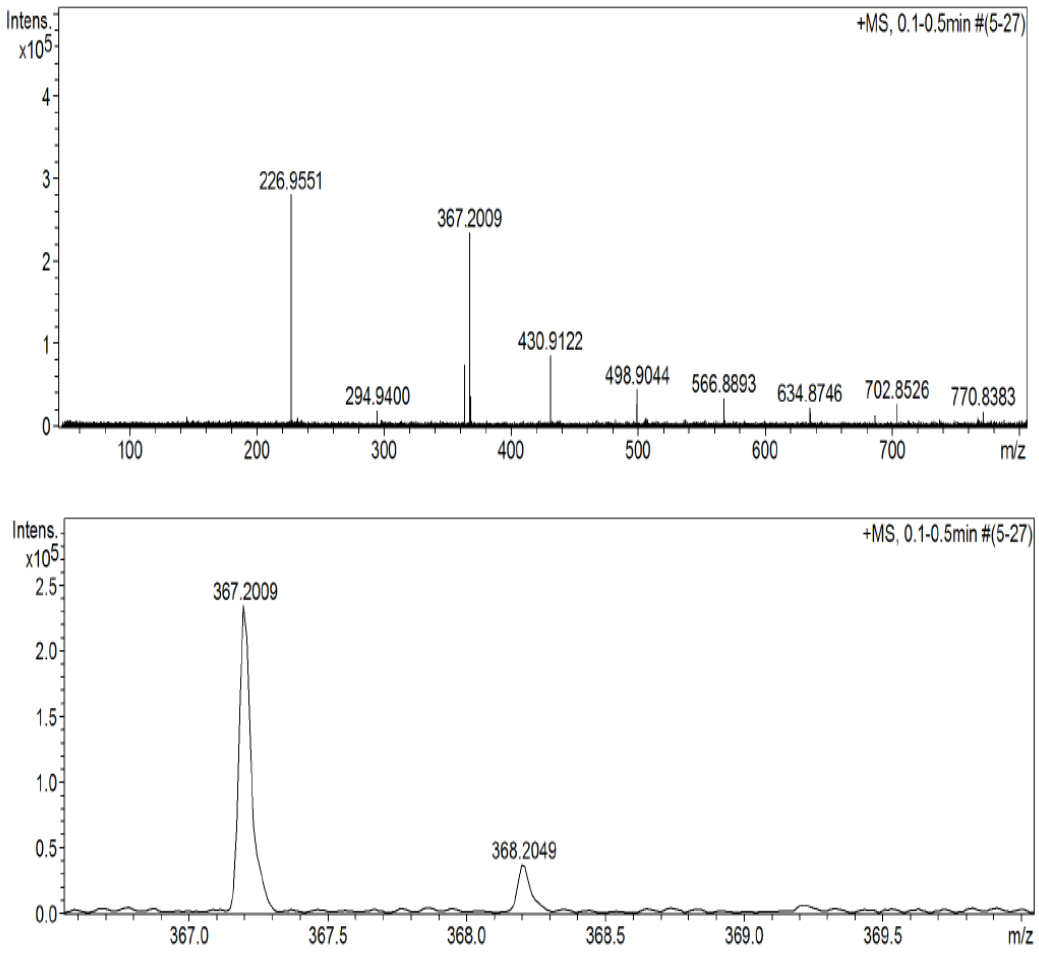

m/z 367.2009 $[M+H]^+$ (calcd. for $C_{22}H_{27}N_2O_3$, 367.2017), Err.(ppm) 1.82.

Appendix 48: High Resolution ESI(+)MS of compound 7.

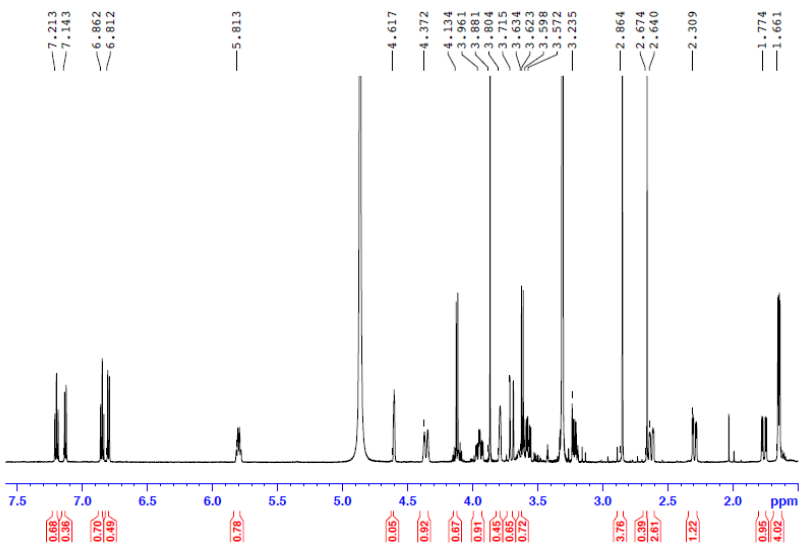

Appendix 49: ^{1}H NMR spectrum(600MHz, CD_3OD) of compound 7.

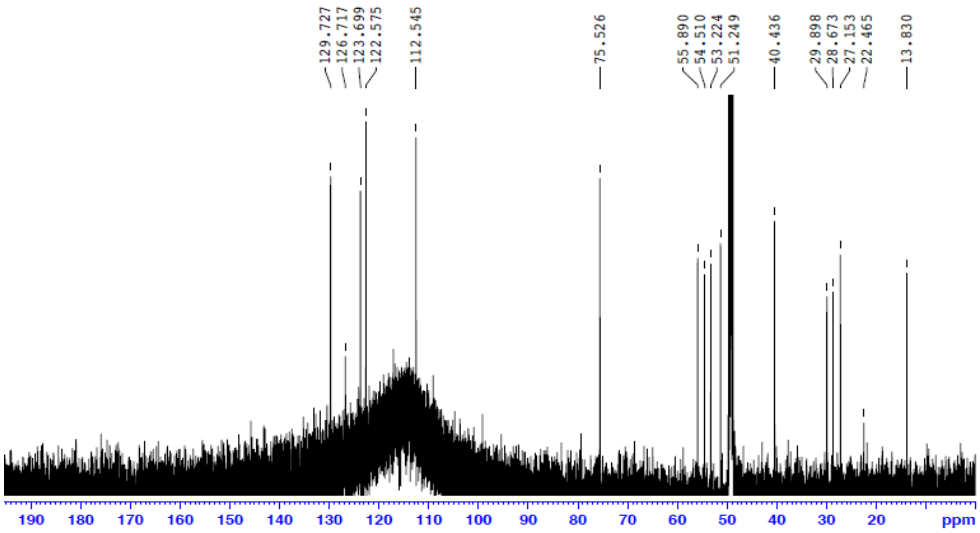

Appendix 50: {^{1}H}-^{13}C NMR spectrum (150MHz, CD_3OD) of compound 7.

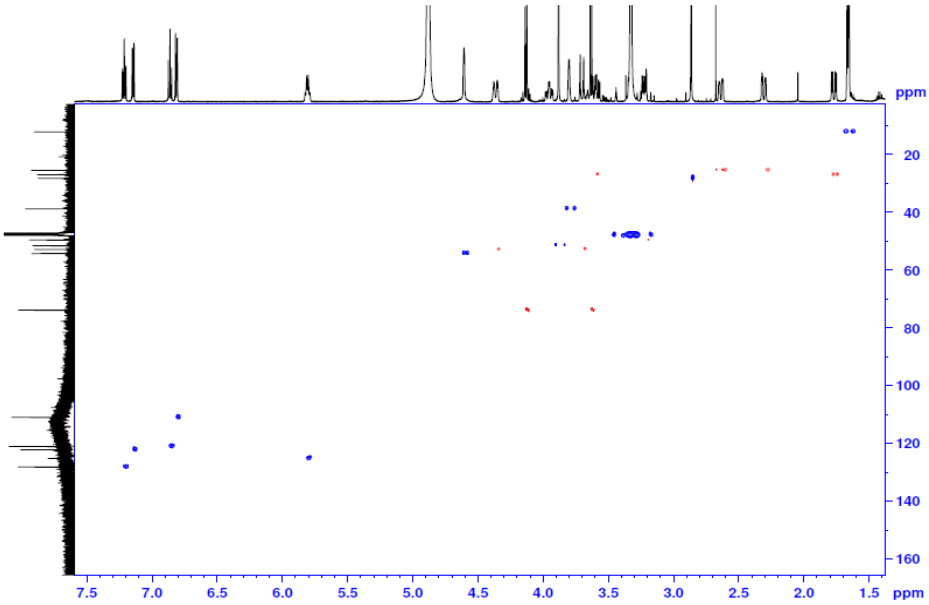

Appendix 51: DEPT-edited ^{1}H-^{13}C HSQC spectrum (600MHz, CD_3OD) of compound 7.

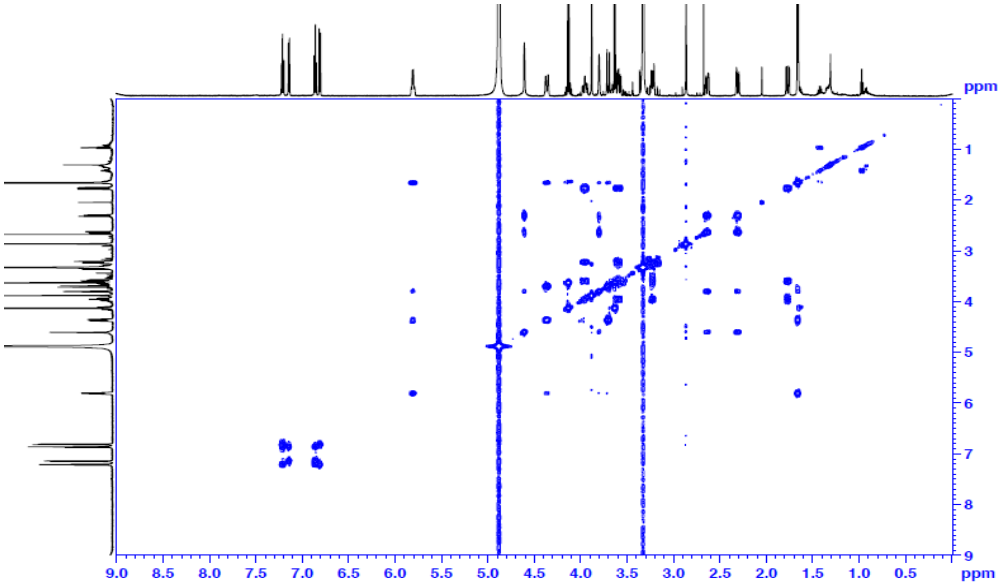

Appendix 52: ^{1}H-^{1}H gCOSY spectrum (600MHz, CD_3OD) of compound 7.

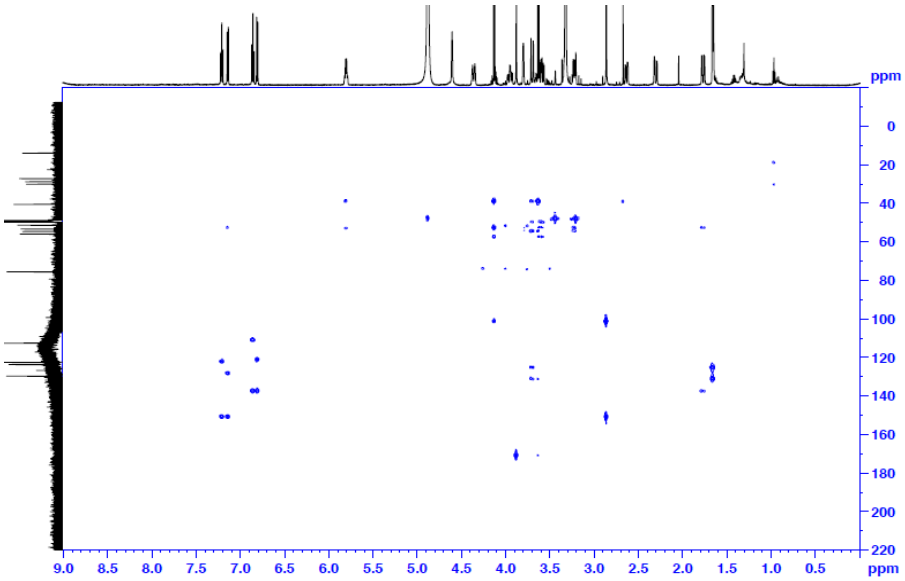

Appendix 53: ^{1}H-^{13}C gHMBC spectrum (600MHz, CD_3OD) of compound 7.

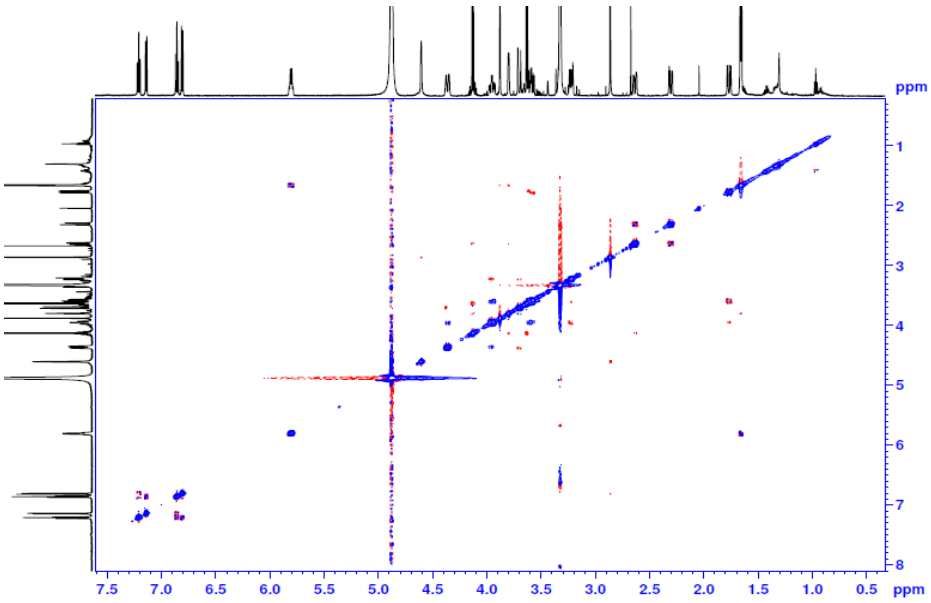

Appendix 54: ^{1}H-^{1}H ROESY spectrum (600MHz, CD_3OD) of compound 7.

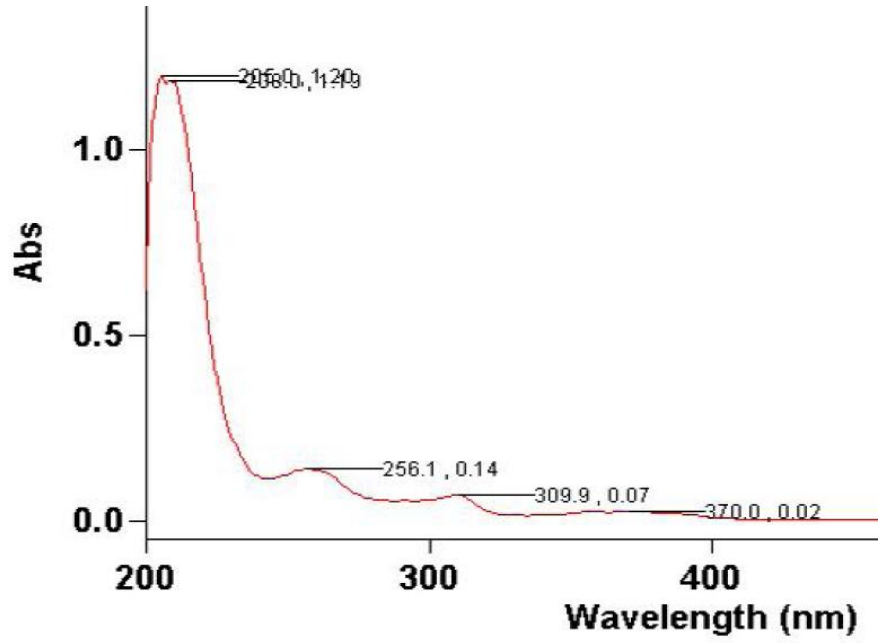

Appendix 55: UV spectrum (2.0 x 10^{-5} M, MeOH) of compound 7.

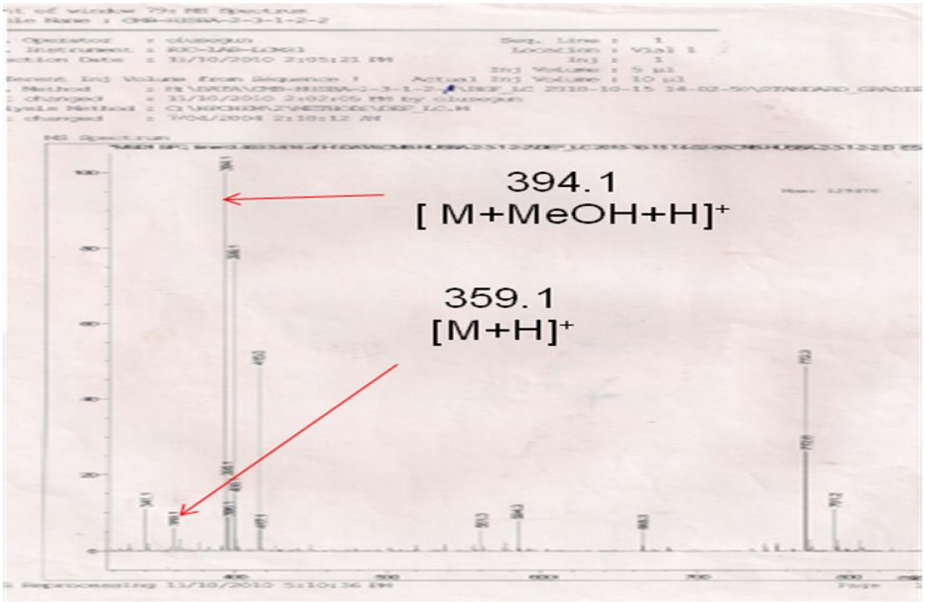

Appendix 56: Low Resolution ESI(+)MS of compound 8.

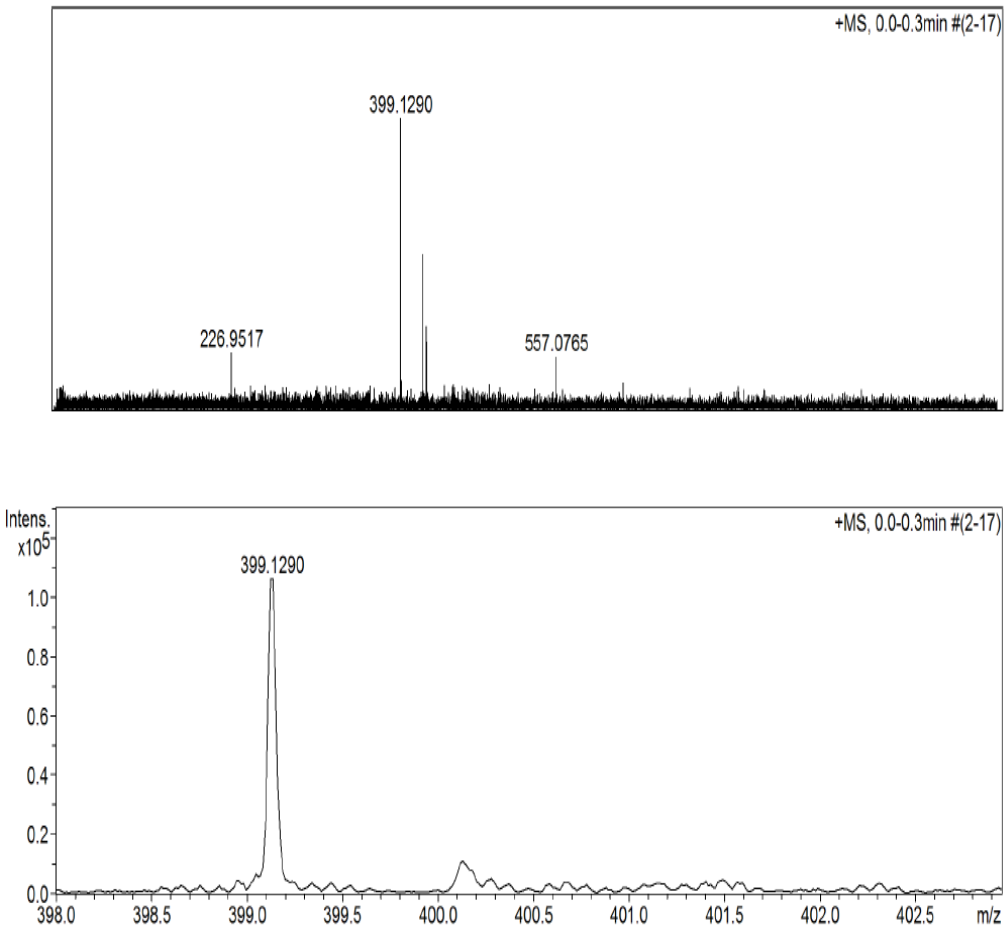

$[M+H]^+$ pseudomolecular ion conspicuously absent (ref. Appendix 56)

Appendix 57: High Resolution ESI(+)MS of compound 8.

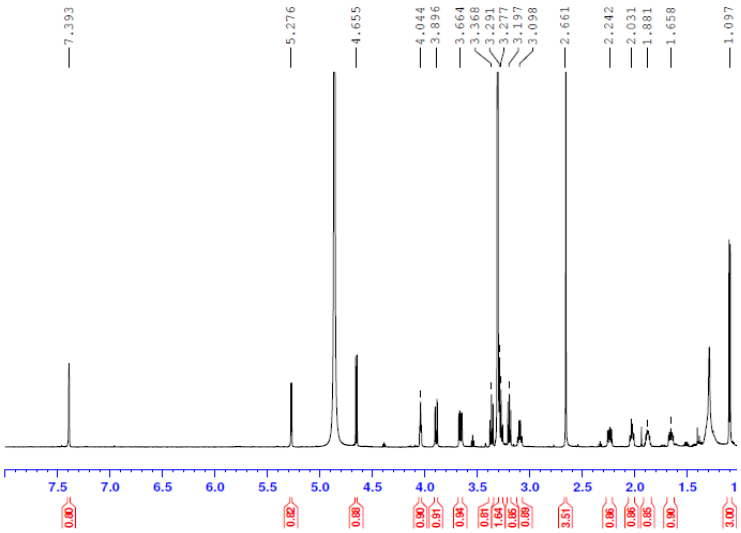

Appendix 58: ^{1}H NMR spectrum(600MHz, CD_3OD) of compound 8.

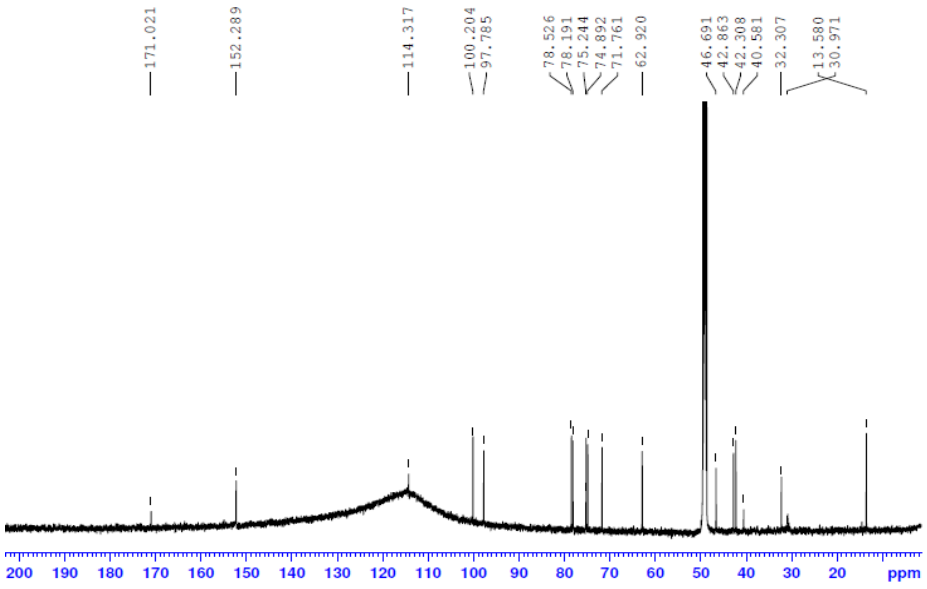

Appendix 59: $\{^{1}H\}$-^{13}C NMR spectrum (150MHz, CD_3OD) compound 8.

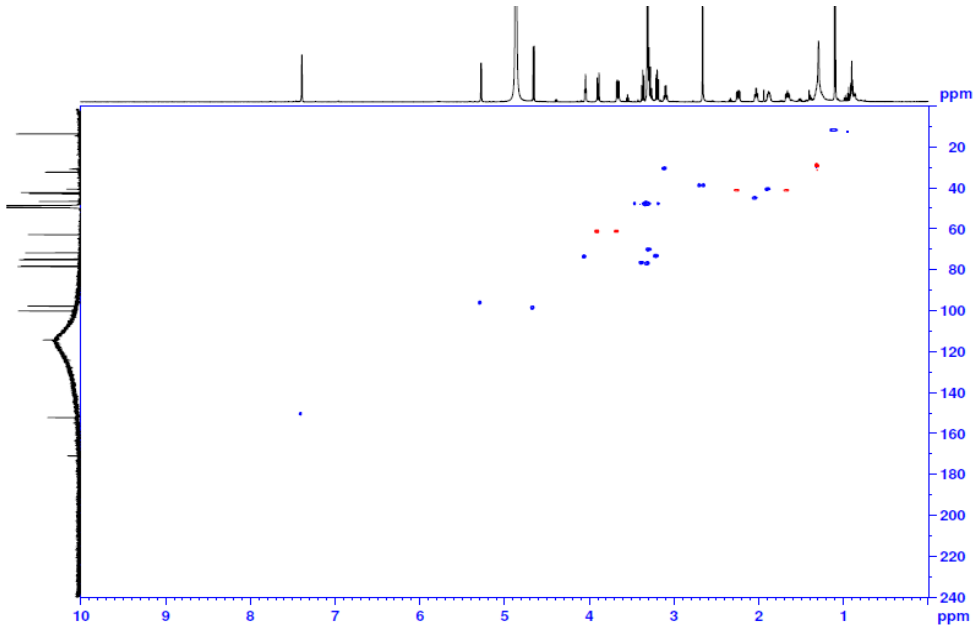

Appendix 60a: DEPT-edited ^{1}H-^{13}C HSQC spectrum (600MHz, CD_3OD) of compound 8.

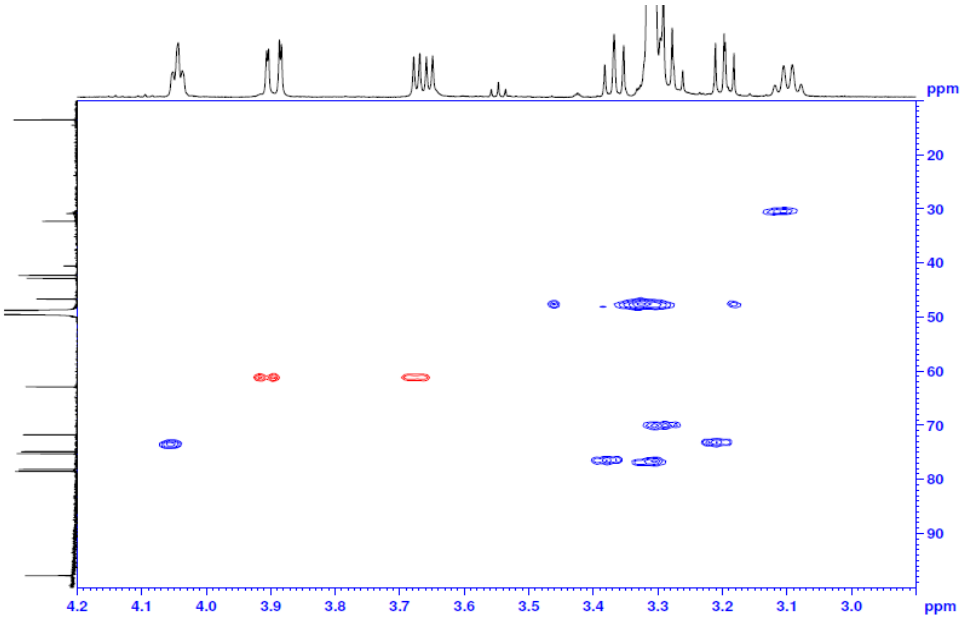

Appendix 60b: DEPT-edited ^{1}H-^{13}C HSQC spectrum expansion (600MHz, CD_3OD) of compound 8.

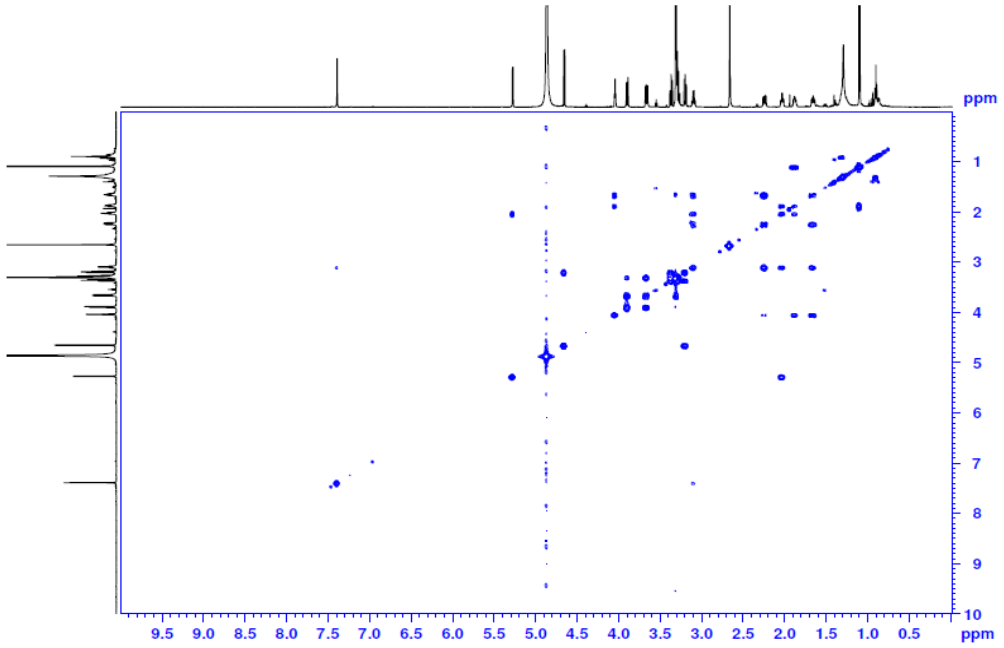

Appendix 61a: ^{1}H-^{1}H gCOSY spectrum (600MHz, CD_3OD) of compound 8.

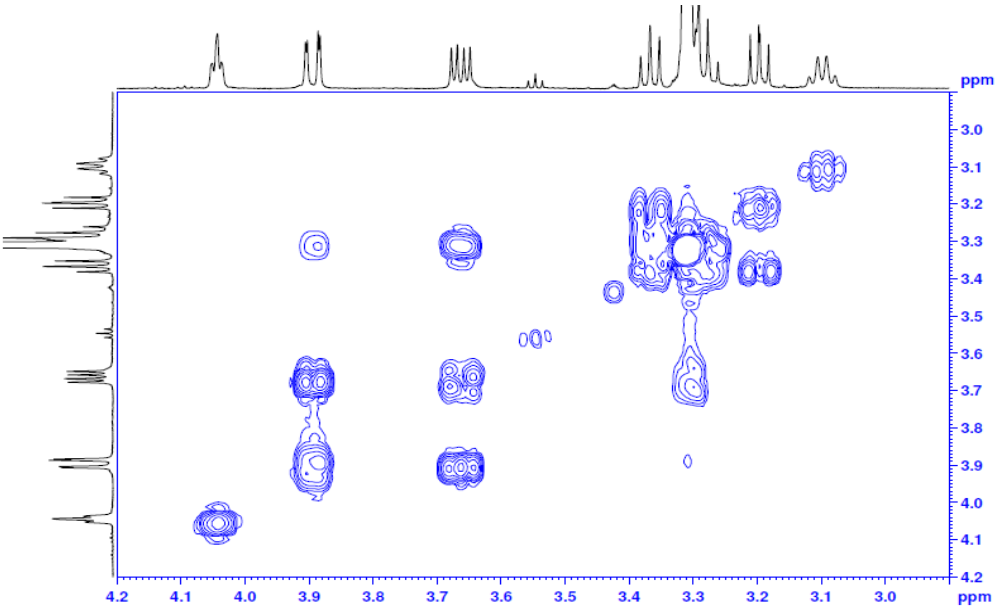

Appendix 61b: ^{1}H-^{1}H gCOSY spectrum expansion (600MHz, CD_3OD) of compound 8.

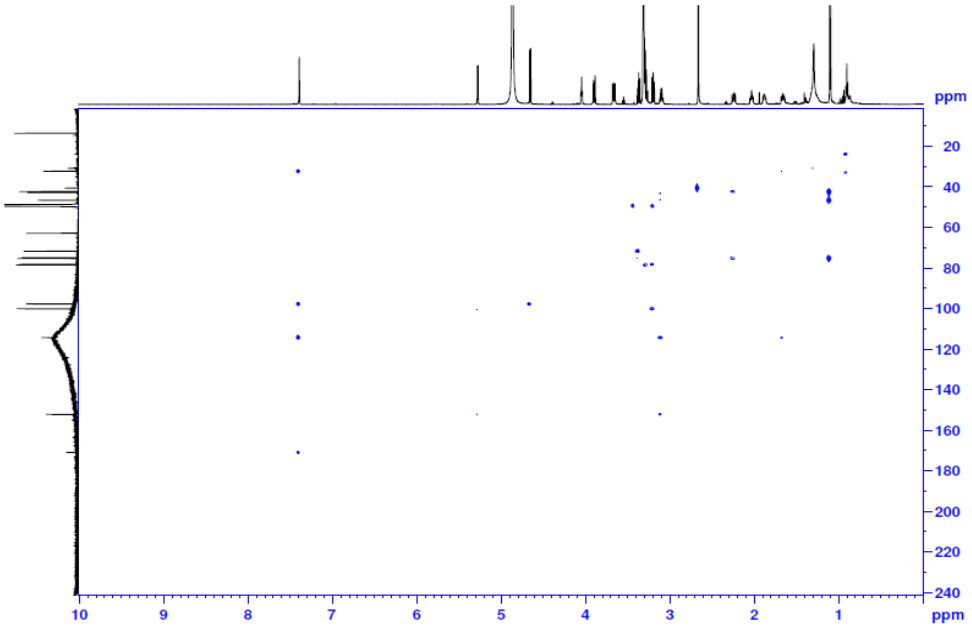

Appendix 62: ^{1}H-^{13}C gHMBCspectrum (600MHz, CD_3OD) of compound 8.

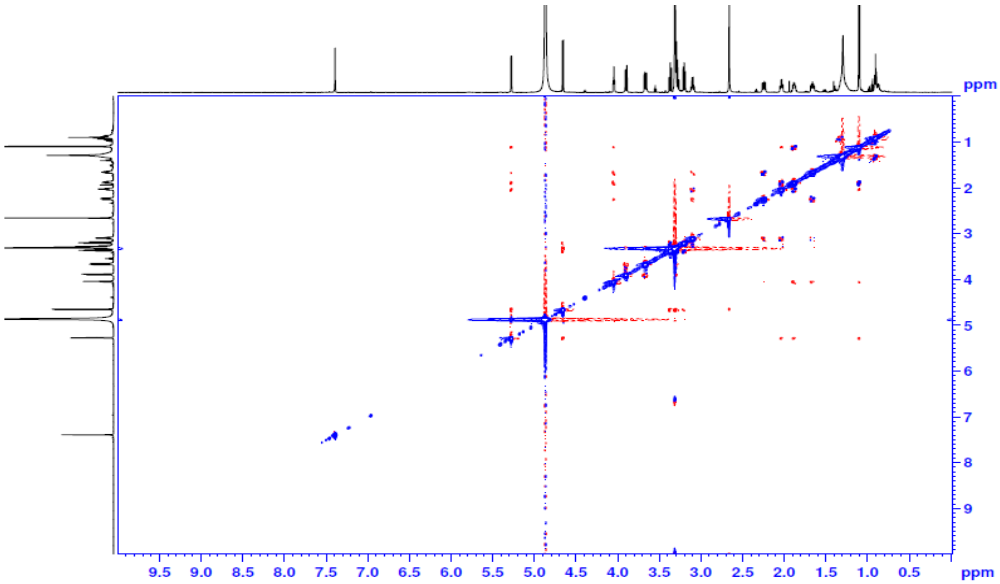

Appendix 63: ^{1}H-^{1}H ROESY spectrum (600MHz, CD_3OD) of compound 8.

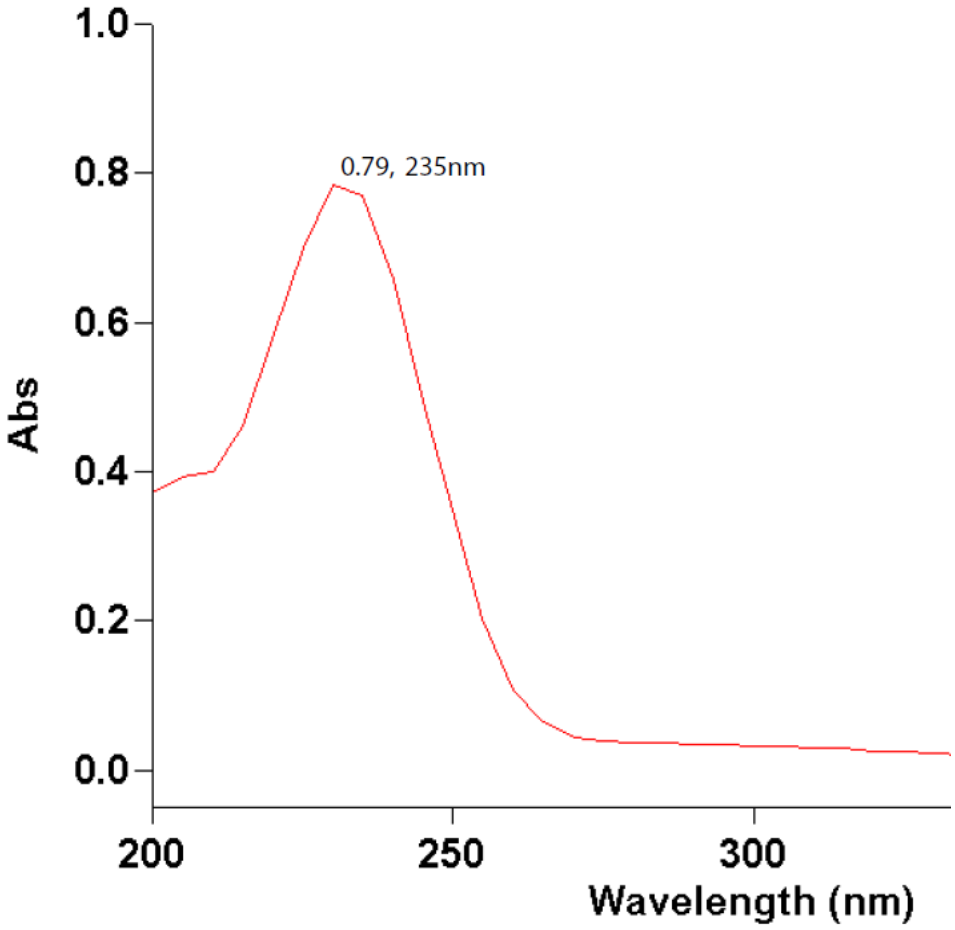

Appendix 64: UV spectrum (1.60×10^{-5} M, MeOH) of compound 8.

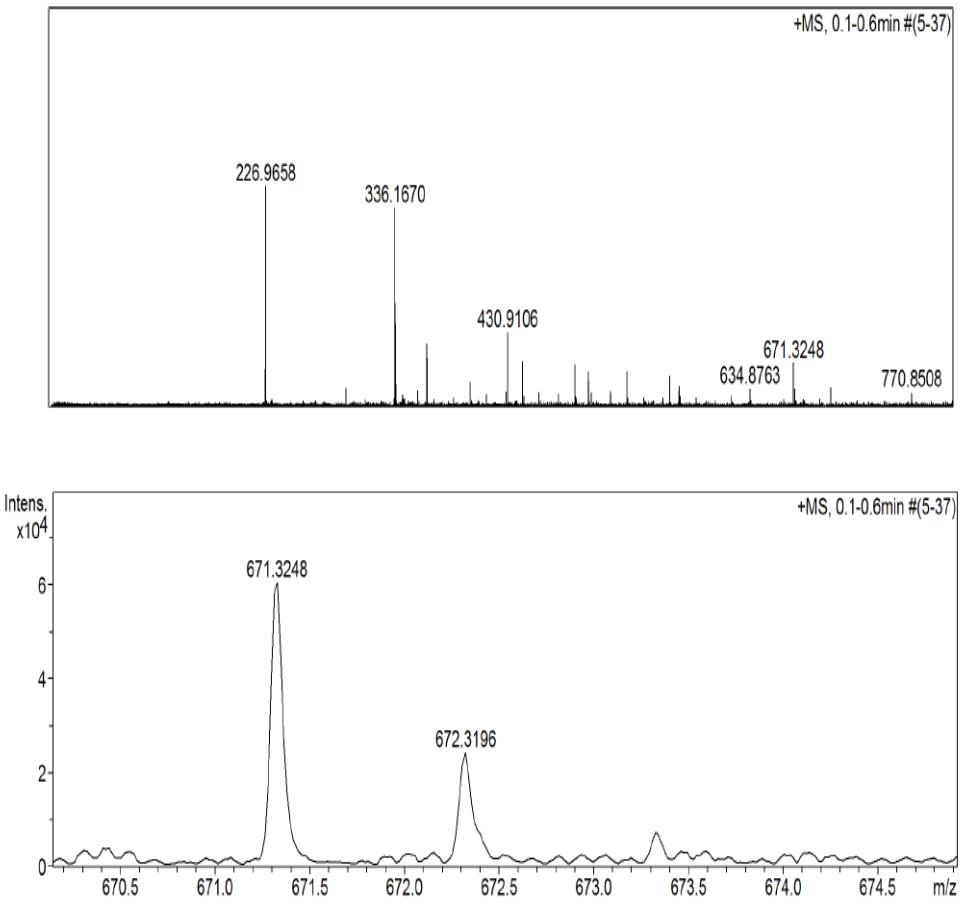

m/z 671.3248[M+H]$^+$ (calcd. for $C_{41}H_{43}N_4O_5$) Err.(ppm) -2.93

Appendix 65: High Resolution ESI(+)MS of compound 9.

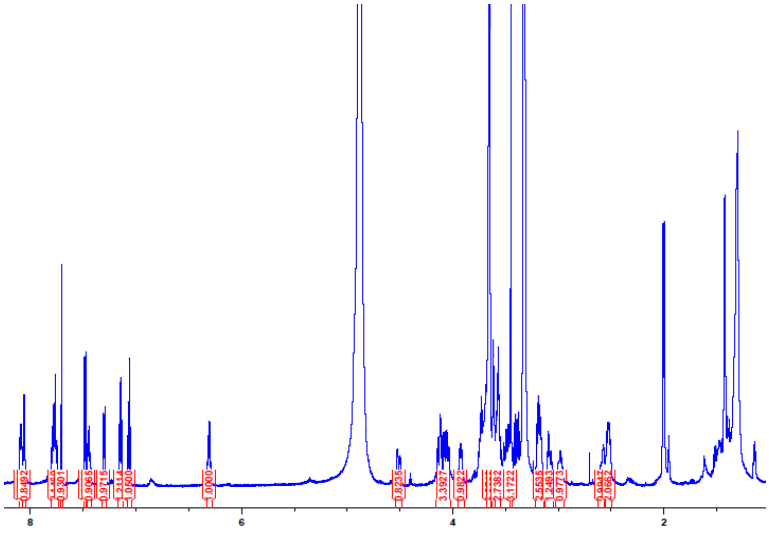

Appendix 66: ^{1}H NMR spectrum(600MHz, CD_3OD) of compound 9.

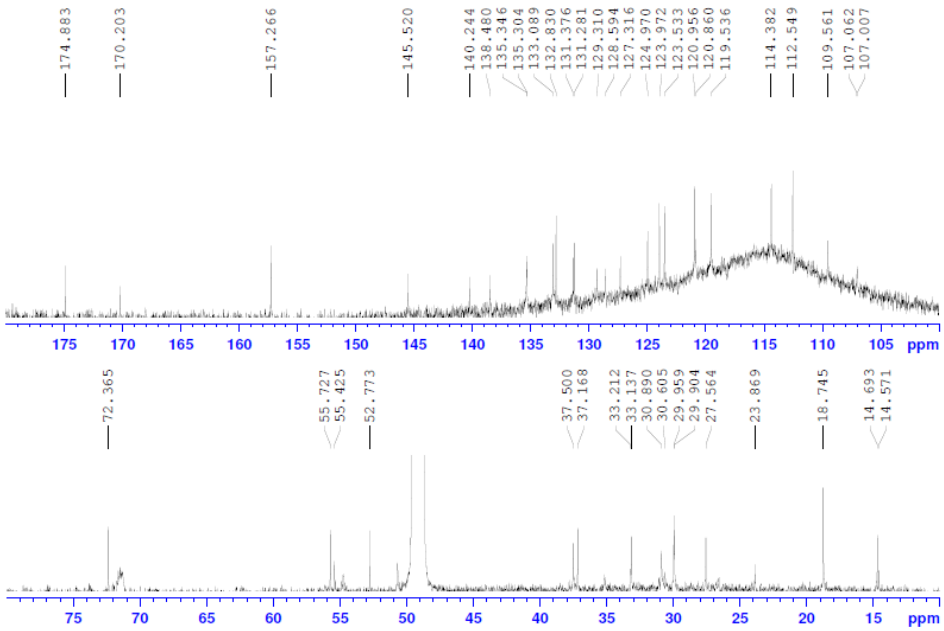

Appendix 67: {^{1}H}- ^{13}C NMR spectrum (150MHz, CD_3OD) of compound 9.

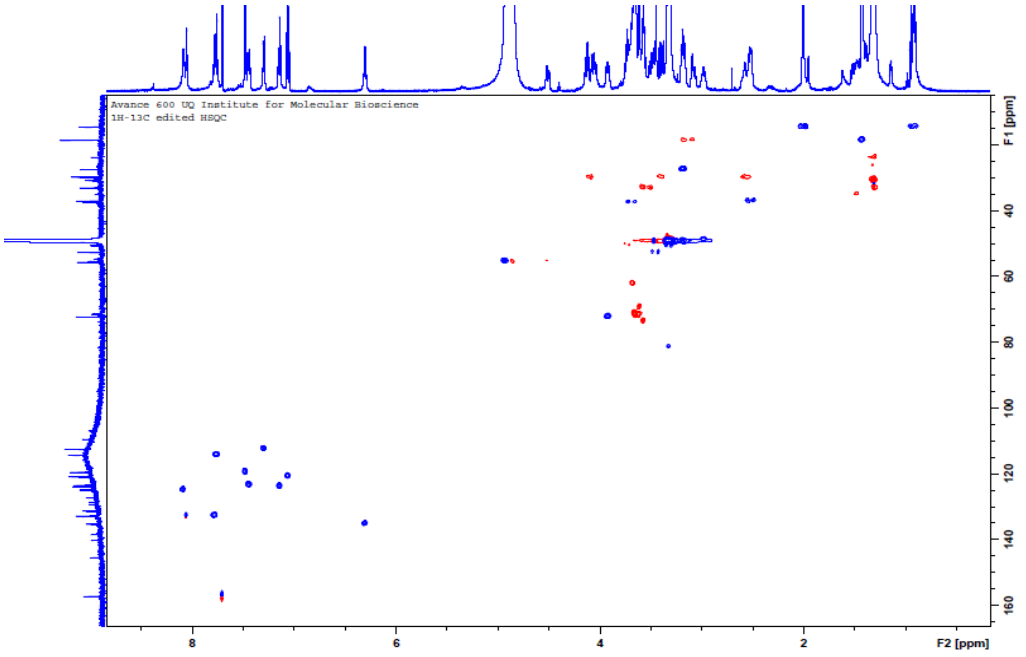

Appendix 68 : DEPT-edited ^{1}H-^{13}C HSQC spectrum (600MHz, CD_3OD) of compound 9.

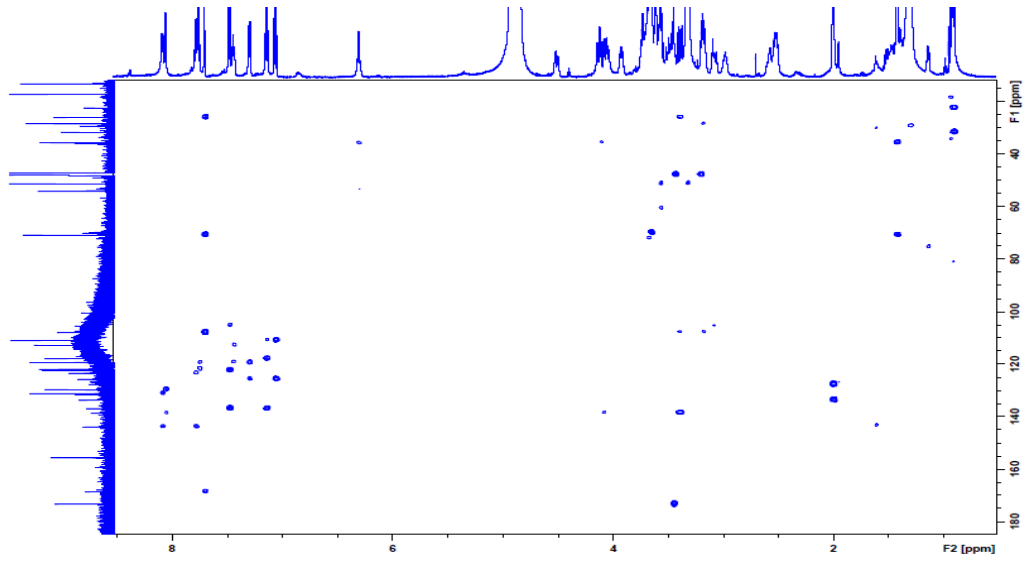

Appendix 69: ^{1}H-^{13}C gHMBC spectrum (600MHz, CD_3OD) of compound 9.